2004

The effect of baseplate flexibility on the fatigue performance of welded socket connections in cantilevered sign structures

John H. (Henry) Hall III
Lehigh University

Hall, John H., III

The Effect of Baseplate Flexibility on the Fatigue Performance of Welded ...

January 2005

The Effect of Baseplate Flexibility on the Fatigue Performance of Welded Socket Connections in Cantilevered Sign Structures

By

John H. Hall III

A Thesis

Presented to the Graduate and Research Committee

of Lehigh University

in Candidacy for the Degree of Master of Science

in

Civil Engineering

Lehigh University

January 2005

This thesis is accepted and approved in partial fulfillment of the requirements for the Master of Science.

NOVEMBER 23, 2004

Date

Thesis Advisor

Co-Advisor

Chairperson of Department

Acknowledgements

I would like to thank the several individuals who have helped me in course of this research:

Dr. Robert Connor: Thank you for the technical direction and expertise you have supplied throughout this project. The lessons I have learned in this project, I know will be of great benefit to me in my future endeavors.

John, Carl, Dave, Joe, and all of the laboratory technicians who were always available when I needed their help.

And thank you to my family and friends whose support allowed me to still have as normal of a life as possible over the last two and half years.

Table of Contents

Table of Contents (Continued)

List of Tables

List of Tables (Continued)

List of Figures

List of Figures (Continued)

List of Figures (Continued)

Abstract

Recently a considerable amount of research interest has been focused on the fatigue performance of cantilevered sign structures. NCHRP Report 412 and extensive fatigue testing performed at the University of Texas are examples of this recent focus on the fatigue of cantilevered sign structures, and were dictated by the fatigue related problems facing many state departments of transportation and urban municipalities (Kaczinski, Dexter, Van Dien 1998) (Koenigs 2003). Field investigations performed by Lehigh University determined that the flexibility of the baseplate has a very drastic effect on the stress behavior in the pole adjacent to the socket welded connection (Connor and Hodgson 2004).

This study investigates the effect baseplate flexibility has on the stress behavior and hence fatigue performance of welded socket connections in cantilevered sign structures. The results of a three specimen static load testing program and extensive finite element analysis, calibration, and parametric study are discussed. The study found that baseplate flexibility, primarily baseplate thickness, has a drastic influence on the stress behavior in the pole tubewall adjacent to the socket welded connection. Increasing baseplate thickness is shown to drastically reduce stresses at the fatigue critical vertical weld toe. Based on this trend, a simple procedure that incorporates the influence of baseplate flexibility into the nominal stress approach to fatigue design is proposed.

Section 1.1: Executive Summary

Recently a considerable amount of research interest has been focused on the fatigue performance of cantilevered sign structures. NCHRP Report 412 and extensive fatigue testing performed at the University of Texas are examples of this recent focus on the fatigue of cantilevered sign structures, and were dictated by the fatigue related problems facing many state departments of transportation and urban municipalities (Kaczinski, Dexter, Van Dien 1998) (Koenigs 2003). The results of a field testing investigation performed by the Lehigh University Infrastructure Monitoring Program made critical observations regarding the behavior of socket welded connections in cantilevered sign structures. The field research observed that stress behavior adjacent to the baseplate socket welded connection does not follow nominally calculated simple beam theory distribution. Field testing showed that stresses in line with the anchor rods had the maximum outer stress, as compared to the stresses at locations parallel with the mast-arm axis. The researchers correctly explained this unusual stress behavior to be induced by the flexibility of the baseplate (Connor and Hodgson 2004). The effects of baseplate flexibility were not fully understood and not included in major research or the AASHTO specifications (AASHTO 2001).

To better understand the influence of baseplate flexibility on the fatigue performance of welded socket connections in cantilevered sign structures, extensive finite element study and experimental testing of three different baseplate specimens was performed. The data provided from the experimental testing program was used to

calibrate the finite element modeling techniques used (Chapter 3). Given the experimental data and the analytical results of the calibrated finite element models, trends in baseplate flexibility were observed (Chapter 4). These trends were then expanded in a finite element parametric study, which allowed for fatigue design recommendations to be made (Chapter 5).

The results of the research show that increasing baseplate flexibility drastically alters the stress behavior in the tubewall adjacent to the baseplate, increasing maximum stresses and altering the stress distribution such that the maximum stress in the pole occurs in line with the anchor rods. The results of the calibration study show that relatively simple finite element modeling techniques are able to provide reasonable results, when compared to experimental data. The parametric study shows that baseplate thickness is the most efficient parameter of the baseplate geometry to alter in order to improve the fatigue performance of the welded socket connection. Given the benefits in stress reduction due to increasing baseplate thickness, a simple ratio method utilizing the infinite life design requirement of the nominal stress approach to fatigue design is proposed to incorporate the effects of baseplate flexibility.

Section 1.2 Background

Introduction

The focus of the research is to investigate the influence of baseplate flexibility on the fatigue performance of socket welded connections in cantilevered sign structures. Cantilever signs structures, are just one of many different types of sign

structures and are commonly used at intersections to support traffic signals. Historically speaking cantilevered sign structures have been in use for over a half century. Union Metal claims to have supplied the first traffic mast arm pole in 1923 (Union Metal Website 2004). As roadways and safety clearance distances increase, so have the lengths of mast-arms, and thus the size of cantilevered sign structures. Some state departments of transportation allow cantilevered sign structures to extend up to 85 feet. Recently due to several fatigue failures, there has been additional research and testing on the subject (Kaczinski, Dexter, and Van Dien 1998) (Koenigs 2003). Very little work, however has been done to understand the influence of baseplate flexibility on the tubewall stresses, and hence fatigue performance of the structures.

Sign structures in general can be divided into three categories based on member geometry and configuration. Span wire sign structures utilize two tubular poles to suspend a wire or pair of wires, from which traffic signals and signs are suspended. Bridge sign structures, which may utilize vertical tubular poles or trusses to support a horizontal truss are also used to support traffic signals. Cantilevered sign structures, the subject of this research, are often the most appealing type of sign structure. Typically the structures are considered to be the most aesthetically pleasing and are by far the most common. There single pole design limits the crash hazard to motorists as well as reduces the number of poles blocking visibility. Both of which, are very important at busy intersections. In addition they are typically a very inexpensive solution, with minimal impacts on traffic during installation. The common theme of these three different types of structures is that they provide a long

and light weight span as dictated by their function, to put the signals within the view of motorists.

Sign structures, especially cantilever sign structures are very unique structures, in purpose and their structural characteristics. Their main purpose, to allow for the orderly flow of traffic at busy intersections, is not absolutely necessary to travel. For a structure which influences daily life and has the potential to be dangerous, cantilevered sign structures are often unnoticed. Structurally their unique purpose, to cover large spans results in the necessity that their dead weight be minimized. This minimized deadweight requires very thin tubewall cross-sections, which are very flexible. This flexibility combined with the fact that the structure possesses little natural damping causes fatigue problems, as the structure has a very short natural period. Thus an excitation to the structure may produce many stress cycles in a short period of time (Kaczinski, Dexter, Van Dien 1998).

Basic Cantilevered Sign Structure Features

Figure 1.1.1 shows a typical cantilevered sign structure. Though designs vary from state to state and different connection details were used at different periods of time, all cantilevered sign structures have a tubular vertical pole member and horizontal tubular member. Sign structure nomenclature is fairly broad, but for the purpose of this research the vertical member will be referred to as the "pole", and the horizontal member as the "mast-arm". The base of the pole is almost always connected to a plate which is supported by leveling nuts. Under the scope of this

project "socketed" welded connections are to be studied. This type of connection is commonly used to connect the pole to the baseplate, as will be discussed shortly.

Different connections are used to connect the mast-arm to the pole. One of the more common connection methods utilizes a similar welded socket connection, in which the mast-arm essentially takes the form of a pole, with longer and reduced diameter tubular member sizes. The plate welded to the mast-arm is then described as an endplate, and is bolted onto the pole as will be discussed below. This type of a connection is referred to as a built-up-box detail.

The term socket refers to the way that the baseplate is cut-out to allow the pole to fit inside of it. Two fillet welds connect the baseplate to the pole. The first and most structurally significant is applied at the top of the baseplate. Several different fillet weld leg geometries are used, though typically an unequal leg fillet weld is used. The second fillet weld is applied inside the cut-out of the baseplate, between the bottom surface of the pole the sides of the cut-out in the baseplate. This weld is much smaller, and in general much more irregular. The lower weld serves a significantly lesser structural role and primarily serves to prevent corrosive materials from entering the gap between the tubewall and the baseplate cut-out hole. Figure 1.1.2 shows a schematic diagram of this welded connection, and Figure 1.1.3 shows a photograph of a typical baseplate to pole welded socket connection. The remainder of this section lists the common geometric features of a cantilevered sign structure, giving descriptions, typical dimensions, photographs, as well as the specific nomenclature used in this project.

- Hand access hole: The hand access hole allows access to the electrical wiring of the lights. A typical hand access hole is shown in Figure 1.1.4. Typical dimensions are approximately 12" by 4" and are located about one foot above the top of the baseplate. The hand access hole is reinforced with a rounded cornered rectangular tube, usually of a similar thickness as the pole tubewall. The reinforcement tube is connected to pole by a continuous wrap around fillet weld on the outside.
- Leveling nuts and anchor rods: Typically a four anchor rod pattern is used to secure the structure to the concrete foundation below. Several different sizes, grades of steel, and arrangements of anchor rods are used depending on the size of the structure. Pairs of leveling nuts (an upper and lower leveling nut) are used to support and connect the baseplate to the anchor rods. In addition some structures have a grout pad below the baseplate, hiding the anchor rods. A typical anchor rod and leveling nut assembly is shown in Figure 1.1.5.
- Built-up box and flange plate: As discussed the built-up box, flange plate style mast-arm to pole connection is not always used, but is one of the most common connections. As shown in Figure 1.1.6, the built-up box is constructed by welding thinner plates onto the sides of the pole. A thicker flange plate is then welded onto these side plates. The endplate of the mast-arm is then bolted to the flange plate.

Section 1.3 Wind Loading

Mast-arm cantilevered sign structures are primarily designed for wind loading and dead load. The fatigue design requirements of cantilevered sign structures almost always controls the design. Design wind loading, as it relates to cantilevered sign structures has been fairly well researched. One of the primary sources regarding wind loading for fatigue design of cantilevered sign structures is NCHRP Report 412 (Kaczinski, Dexter, and Van Dien 1998). Wind loading as it relates to the fatigue design of cantilevered sign structures can be broken into four specific types. These four wind loading phenomena are galloping, vortex shedding, natural wind gusts, and truck induced wind gusts. The following section briefly discusses these four wind phenomena and their relation to the fatigue design of cantilevered structures.

Galloping and vortex shedding are the two predominant wind phenomena which affect cantilevered sign structures. They can be described as the condition of large vertical resonant oscillation caused by constant wind flow normal to the axis of the mast-arm. Truck induced wind gusts and natural wind gusts have a lesser effect on cantilevered sign structures. As their names imply, in both wind phenomena a gust of wind causes the oscillation, similar to a pulse loading.

Galloping, also known as Den Hartog instability, is a wind phenomenon which causes oscillation in flexible and lightly damped structures with non symmetric cross sections. Galloping is typically the leading cause of wind induced vibration in cantilevered sign structures. A key component in galloping, is a periodic variation in the angle of attack that the wind takes against the structure. The Den Hartog stability criterion highly simplified, reduces to, galloping occurs when the negative

aerodynamic damping of the structures is greater than the actual mechanical damping. Galloping in cantilevered sign structures is characterized by a sudden onsét of large amplitude oscillation under a wind flow running perpendicular to the mast-arm axis. This oscillation increases with increasing wind velocity and is at the natural frequency of the structure. Thus in a short period of time many stress cycles occur as the natural period of cantilever sign structures typically is about a single second. As mentioned above galloping only occurs in structures with non-symmetric cross-sections, thus the presence of signal lights and signs are necessary for galloping to occur. Wind tunnel test confirm this, and showed that certain sign configurations are more susceptible to galloping (Kaczinski, Dexter, and Van Dien 1998).

Vortex shedding is a wind phenomenon similar to galloping. Like galloping vortex shedding induced vibration commonly occurs in flexible and lightly damped structures. It occurs during steady and uniform wind flow and produces resonant vibration in the plane normal to the wind flow. Vortex shedding induced oscillation is caused by a regular alternating pattern of vortice shedding and occurs in structures with symmetric cross-section, especially those that are round and smooth. Vortex shedding commonly occurs in un-tapered structural members, which may prevent it from occurring in many sign structures. The Strouhal relation governs vortex shedding, where fs is the frequency at which vortices are shed, S is the Strouhal number a unit less variable, V is the wind velocity, and D is the dimension of the cross section perpendicular to the direction of the wind.

$$fs = SV/D$$

When the frequency in which the vortices are shed at reaches the natural frequency (fn) of the structure resonant vibrations occur, this condition is known as "lock-in". The corresponding critical wind velocity (Vcr) is then simply equal to the natural frequency of the structure times the ratio of the cross-section dimension D divided by the Strouhal number, S. Resonant vibration of the structure then occurs for a range of increasing wind velocity, until the amplitude of the vibration becomes great enough to disrupt the alternating pattern of vortice shedding. Typically for cantilevered sign structures the range of wind speed in which vortice shedding induced vibration can occur is 10 to 35 mph.

Mitigation of galloping and vortice shedding follows two different approaches: Altering the aerodynamic properties of the structure and sign attachments to create additional positive aerodynamic damping. The second approach to mitigation is altering the mechanical vibration properties of the structure to better resist vibration, and improve the damping to reduce the number of stress cycles produced under wind loading events.

Natural wind gust induced oscillations involve wind phenomena absent of steady wind conditions, as the name would imply. As wind speeds increase and decrease pressure applied to the cantilever sign structure fluctuates resulting in vibration. Unlike vortex shedding and galloping, the displacement response of the structure includes many different excitation frequencies, but is dominated by the resonant frequency of the structure. In addition the amplitude of oscillation due to natural wind gusts is much more irregular than the case of galloping and vortex

shedding. Thus, stress ranges due to minor natural wind gust excitation often only reach a critical level on an infrequent basis as opposed to galloping and vortex shedding in which wind induced vibration, can produce many repeated critical stress ranges in a short period of time. However structures that are exposed to large natural wind gusts, such as structures in open areas, can acquire many critical stress cycles per severe wind event as the structure has very little damping and a high natural frequency.

Truck induced wind gusts, the last wind phenomena to be discussed, has the least effect on cantilevered sign structures. Truck induced wind gusts apply a pressure to cantilevered sign structures which is much less than natural wind gusts. Truck induced wind gusts primarily is more of a concern for highway signs and in particular variable message signs, which have a large horizontal surface area. The uplift pressures, and hence forces on the bottom face of variable message signs has been shown to be greater than forces due to galloping at times. But for cantilevered sign structures truck induced wind gusts cause lesser vibration than natural wind gusts (Kaczinski, Dexter, and Van Dien 1998).

Section 1.4 Overview of Fatigue

As discussed previously in Chapter 1 the design of cantilevered sign structures is typically controlled by fatigue. In NCHRP Report 412 the authors clearly indicate that cantilevered sign structures perform well under intense wind events as result of AASHTO's conservative gust factor. Fatigue is the only likely cause of failure in

cantilevered sign structures. The following section provides an overview of fatigue as it relates to cantilevered sign structures (Kaczinski, Dexter, and Van Dien 1998).

Fatigue is a general term describing the process of repetitive damage and the formation of a crack due to a fluctuating tensile stress, most commonly associated with welded steel structures. The problem of fatigue occurs separately from the design for ultimate strength of the structure. Fatigue only occurs in locations of highly localized plastic deformation. However even structures that have been sufficiently designed to remain elastic under fluctuating load have locations where stress raisers increase the nominal stress above the elastic limit of the material. The higher the stress concentration and hence the local stresses, the faster the growth of fatigue cracks. Welded structures which, typically have high tensile residual stresses and some initial weld flaws, are especially susceptible to fatigue cracking. Residual stresses due to the rapid contraction of hot weld metal, typically reach the tensile yield limit of the material. Considering these high residual stresses fatigue damage can occur with the application of even compressive stresses. In addition to high residual stresses, welding also unavoidably produces flaws which further intensifies the formation of fatigue crack growth. These flaws are typically the result of incomplete penetration of weld metal into the root of fillet welded connections and lack of fusion between weld and base metal. These flaws typically have the most undesirable possible geometry, as they typically form a sharp tip, just like the tip of a crack. The sharp tips of these flaws become locations of very high stress and become initiation points for the formation of fatigue cracks.

Typically in the fatigue design of bridges, fatigue is considered a serviceability limit state as fatigue of one member in such a highly redundant system does not cause failure. In the case of cantilevered sign structures in particular, the welded connections have no redundancy. Any visible sign of a fatigue crack noted during inspection requires the immediate replacement of the structure.

Fatigue can be broken down into three stages, initiation, propagation, and fracture. The first stage marks the initiation of a fatigue crack and the corresponding number of cycles is noted as Ni. In the propagation stage, the total number of cycles required for the crack to increase in size to a critical size is Np. Thus the total fatigue life is the sum the initiation and propagation cycles, Nt=Ni+Np. The end of the fatigue life marks the beginning of fracture. Fracture is the rapid extension of the crack in tension causing collapse or excessive deformation. The most important factor affecting fatigue is the magnitude of the fluctuating local stress at the stress raiser. The most effective way to lessen the rate of fatigue damage and to increase the design life of a structure is to decrease the magnitude of the localized stress. There are two different approaches to reducing the localized stress. Most commonly the localized stress can be decreased by decreasing the nominal stress. Also it can be reduced by decreasing the severity of the stress concentration, by improving the weld quality in order to minimize flaws, or the geometry of the detail.

The other factors that influence fatigue can be divided into those related to the stress pattern, the physical attributes of the structure, and the environment. The loading pattern primarily the number of cycles, N applied to the weld detail affects

fatigue. Several important quantities are typically used to describe the fluctuating stress load pattern. Fatigue loading can be first be divided into two categories, constant amplitude fatigue loading and variable amplitude fatigue loading. Constant amplitude loading is typically how fatigue test specimens are loaded and is typically mathematically equivalent to the cosine function. Variable amplitude loading as the name implies is a random sequence of stress typical of wind or truck loading. Several parameters are commonly used to quantify the magnitude of these two loading types and directly affect the fatigue performance of a structure: The maximum and minimum stresses and the range between the two values of stress. As well as the stress ratio R, the ratio of the minimum stress to the maximum stress. The physical attributes of the structure also influence fatigue performance. These physical attributes include the nominal stress, the geometry of the stress raiser causing the stress concentration, the adjacent stress field, and the metallurgical properties of the particular material. Finally the environment, both temperature and the presence of corrosive substances also affects fatigue performance (Barsom and Rolfe 1987).

As discussed in NCHRP Report 412, the fatigue resistance of welded details primarily depends on the nominal stress range and the notch severity. By this description notch severity broadly includes all of the effects for the practical range of structure configuration and welded geometry of the particular detail. Nominal stress refers to the calculated stress at the structural level using simple bending and axial stress relationships and neglecting the presence of geometrical stress concentration and welds. The long accepted approach to fatigue design in the United States, as

governed by AASHTO specifications utilizes this concept of nominal stress range and notch severity. Over time AASHTO has established a series of seven weld detail categories through fatigue testing. These categories, known by the alphabetical letters A through E and E' (in alphabetical order with decreasing fatigue resistance) individually represent the safe performance of many different types of welded connections. The process of categorizing a new weld detail begins with fatigue testing of the particular detail. The results of the fatigue testing are statistically analyzed to provide a 95 percent confidence limit of excedence over the newly assigned category. It is important to note that due to the high cost of performing a fatigue test, sometimes it is not possible to test all of the different possible geometries of a weld detail (AASHTO 2001). In fatigue testing it is critical to mimic as closely as possible the actual geometries and boundary conditions of the weld detail found in service. (Boundary conditions will be discussed shortly.) In the nominal stress approach several different factors that affect the fatigue performance of a particular welded detail are lumped together. Thus it is important to ensure the geometrical limits imposed upon the designer in the specifications and the geometry of the specimens in the fatigue test program are in agreement.

Section 1.5: Design

The design of cantilevered signal structures follows the AASHTO Standard Specifications for Structural Supports for Highway Signs, Luminaires and Traffic Signals (AASHTO 2001). The design procedure for sign structures is identical to that for highway bridges, both using a nominal stress approach for fatigue design.

AASHTO's 4th edition in 2001 for sign structures, is the most recent specification and included additional and more stringent fatigue design requirements. As a result of this new edition the fatigue design began to control the design of the structures. Much of the new specification is based on research conducted as part of NCHRP report 412, which was discussed previously in Section 1.2. The following section will discuss several of the key issues related to the design of cantilevered signal structures, especially the design for fatigue. The section will first briefly discuss the state of the industry, discussing some of the issues faced by municipalities regarding the design and maintenance of cantilevered structures. Next the non-fatigue design specifications of cantilevered structures will be briefly discussed, followed by an in-depth discussion of fatigue design.

Fatigue design

The 4th edition of AASHTO's Standard Specification for Highway Signs, Luminaires and Traffic Signals (2001) addresses the fatigue design of sign structures according to the research of NCHRP Report 412. The specification sets fatigue design requirements for overhead cantilever sign and signal structures as well as high-level lighting. Not included in the specifications are fatigue design requirements for common overhead lighting poles and regular highway signs, as no fatigue design is required for these structures. AASHTO's highway sign, luminaire, and traffic signal specifications for fatigue design are based on an infinite life nominal stress fatigue design approach. This approach follows a typical design philosophy incorporating importance factors, specified limit state wind loading, and maximum allowable stress

ranges for the various weld details. AASHTO's fatigue design provisions can be broken down into three main components or design steps: The first component of the specification is the importance factor table which determines the appropriate importance factor to be applied to the different wind loading cases. The second component outlined in the specification is the required equivalent static wind loading for each of the various types of wind loading discussed in Section 1.2. The final component is a listing of the fatigue categories of the various weld details commonly found on sign structures (AASHTO 2001).

The 4th edition highway sign, luminaire, and traffic signal specifications includes a table which lists the respective fatigue categories of all various sign structure details, both welded and non-welded. The table is broken down into the different types of construction used and the particular structure type of the particular detail. The specification also includes example figures for all of the details. AASHTO requires that sign structures (excluding sign structures deemed non fatigue sensitive) be designed for infinite life, requiring that nominal stresses at fatigue details be less than the respective constant amplitude fatigue limits. AASHTO's sign structure specifications require an infinite life design approach due to the unpredictability of wind loading. Thus in the iterative process of fatigue design, the designer must first establish what types of fatigue details will be used and their respective CAFL. After calculating nominal stresses that are above the CAFL at these locations based on the AASHTO specified wind loading limit states and importance

factors the designer can revise the design with either more fatigue resistant details or by increasing the cross section (AASHTO 2001).

The 4th edition AASHTO highway sign, luminaire, and traffic signal specifications gives fatigue importance factors (I_f's) in tabular format. These importance factors are similar to those found in seismic design and relate the severity of the consequences of a fatigue failure to a percentage of the design loading. Fatigue importance factor category I, which corresponds to the whole percentage of the wind loading (I_f=1.0), applies to cantilevered sign and signal structures as well as high level lighting poles adjacent to major highways in which the vehicle speed is great enough to cause severe danger in the case of a failure. Fatigue importance factor category I is also intended for those structures with large cantilevers and high level lighting poles exceeding 30 meters as well as variable message sign structures. Fatigue importance factors for Category II and III structures are less than one, thus the structures are designed to resist lesser factored fatigue wind loads (AASHTO 2001). Structures in Category II and III are not considered to receive lesser fatigue wind loading, but are expected to experience fatigue damage. Fatigue importance factor II corresponds to the previous AASHTO edition's most stringent fatigue loading. By the recommendation of NCHRP report 412, fatigue design loading was increased in the fourth edition specification. Under typical design conditions structures designed with the 3rd edition code correspond to the 4th edition's fatigue importance factor II (Kaczinski, Dexter, and Van Dien 1998).

AASHTO's 4th edition sign structure specification prescribes equivalent static loads, to be applied to the structure along with the appropriate importance factor. The basis for these prescribed static loadings is the experimental research conducted in NCHRP Report 412 (discussed in Section 1.2). Four different types of wind loading are considered, galloping, vortex shedding, natural wind gusts, and truck induced wind gusts. Note that as discussed in Section 1.2, several of these wind phenomena do not apply to certain structures. Thus the effects of the particular wind phenomena do not have to be considered in the fatigue design, essentially the particular importance factor is equal to zero. An example of this is that galloping induced vibration doesn't occur in high-mast lighting poles, this is indicated in the importance factor table and would not be included in the design. These four limit state wind loads are intended to produce the stress ranges that the structure would experience in the occurrence of the respective wind loading phenomena. The designer must analyze the structure, calculating stresses due to the wind loading phenomena that apply to the structure, which are clearly indicated in the importance factor chart. The stresses calculated conservatively represent the stress ranges that the actual structure would experience in the field, and can be calculated by simple beam theory. The designer then must apply the appropriate importance factors to these nominal stresses and verify that these various factored stress ranges are all below the CAFL. The prescribed loadings of the four wind loading limit states specified by AASHTO are omitted (AASHTO 2001).

General Design

As discussed in the introductory remarks, cantilever sign structures are very unique structures both in their purpose and structural geometry. Another unique aspect of the structures is the absence of structural engineering inspection throughout much of the structures lifecycle. Initial design and possibly inspection are typically the only two times in which an engineer with a structural background is involved with the structures. For example in the process of obtaining experimental specimens, the author was able to witness a small cross section of the industry, gaining insight to the sign structure management departments of two medium sized municipalities. While this information is not the result of large scale survey, it is likely to be reasonably representative of the industry as a whole. Although the information is very much secondary in the scope and objectives of the project, it is felt that it is worthy of inclusion, as it provides a background for the type of construction imperfection loading which may adversely affect delicate weld treatments, as will be discussed later in Section 2.2.

Even in fairly large municipalities, it is common that the responsibility of managing sign structures to fall under the town head electrician or utility expert. These individual managing sign structures often have very little or no background in structures. Funding for sign structure maintenance is typically not abundant, so it is unlikely that the management of the structures would be outsourced to an actual structural engineer. In addition to other duties, it is the job of the town electrician to purchase new structures and to make important decisions regarding the replacement and maintenance of the structures. Prior to fabrication a professional engineer

develops design specifications for several different mast-arm lengths based on wind loading values specific to a certain region. Thus the town electrician must only know what mast-arm length is required, and the appropriately designed structure will be shipped to the maintenance facility.

Cantilevered sign structures are very frequently "nudged" by large trucks, making wide turns in intersections. The problem of a limited budget for sign structures is made worse when in the case of a minor collision, in which the truck driver does not report the accident. Thus, no insurance claim is able to be made, and the municipality must bear the cost of the replacement. For this reason it is fairly common for municipalities to save older structures that have been replaced due to the widening of a road or "lightly" damaged structures. Thus in the case that funding for a replacement structure is not available, an out of service structure may be used as a temporary replacement.

In addition to maintenance issues the supervision of a structures engineer would also be beneficial in the erection process. There are a several potential problem areas that a trained engineer could quickly check to ensure that needless construction imperfection induced stresses are not being applied to the critical fatigue details. Common construction imperfections such as bolts that have been loosened, visible signs of out of straightness in the baseplate, or signs that anchor rods had been bent to fit into the baseplate anchor rod holes. Fortunately the sign structures can be erected fairly safely without the supervision or inspection of an engineer. Typically any construction imperfection induced problem is most likely the result of severely

negligent practice. However as will be discussed in Section 2.2 delicate weld treatments may in the future, be used to improve fatigue details. In this case it is important to understand the conditions of sign structure erection and management. The true cost of complex solutions should also include additional funds for implementation.

Section 1.6: Related Research

In the last ten years several national and state agencies have conducted research on the fatigue performance of cantilevered sign structures. The following section briefly discusses a few of the most relevant research related to the fatigue behavior of cantilevered sign structures.

One of the first major research studies on the fatigue of sign structures was conducted at Lehigh University in the late 70's, by Dr. John Fisher for the California Department of Transportation and the Federal Highway Administration. This work provided the first fatigue test data for the socket welded details used in cantilever signal structures, a fatigue category. The primary result of Fisher's research was that though there was some variation in the fatigue results especially over the slight differences in specimens tested, the fillet weld connection detail overall failed in correspondence with an E to E' fatigue category. The socket welded connection was recommended to be a Category E' detail. The number of test specimens was somewhat limited, especially considering that there were some small inconsistencies between the specimens. Fatigue cracking occurred at almost all mast-arm and pole socket welded connections of the specimens tested. All fatigue cracks formed at the

fillet weld toe adjacent to the tube wall and not on the baseplate or endplate side (Fisher, Slutter, and Miki 1981).

Several failures and fatigue related problems triggered additional studies. NCHRP Report 412, published in 1998, which updated the AASHTO Standard Specifications for Structural Supports for Highway Signs, Luminaires, and Traffic Signals, increasing fatigue loading. The results of the research primarily pertain to wind loading and the fatigue design process, and have been discussed in Section 1.3 and Section 1.5 of this report (Kaczinski, Dexter, and Van Dien 1998).

Recently an extensive cantilevered sign structure fatigue testing program was conducted at the University of Texas, and presented in Mark Koenigs' Masters' Thesis. A total of 55 mast-arm specimens were tested. Ultrasonic Impact Treatment (UIT) and various welded stiffener details were the primary focus of research. Comparing the fatigue resistance of welded socket connections with different baseplate flexibilities was not the main concern and only two specimens were tested with thicker endplate specimens. The results of the fatigue testing again showed that fatigue cracks always form at the vertical weld toe above the endplate (or baseplate) of the socket connection, as was shown in Fisher's research. The results of the two specimens with 2" thick endplates showed very considerable improvements in fatigue resistance, compared to the standard 1.5" endplate thickness specimens. Table 1.6.1 shows Koenigs' fatigue test results for the 2" endplate thickness specimen compared to the average data for the 1.5" thick endplate welded socket specimen. The drastic improvement in fatigue resistance will later be discussed in Chapter 5 (Koenigs 2003).

In New York State Department of Transportation Special Report 131 Hag-Elsafi, Alampalli, and Owens discuss a new analysis method for baseplate design. This report is one of several published works by the New York State Department of Transportation. For the purpose of this limited literature review, a brief discussion of the authors' method will follow. Later in Chapter 5 in the discussion of the parametric study a similar concept will be applied. The work primarily focuses on the baseplate stresses, primarily for the purpose of design. Which is opposite of this research study which primarily focuses on the tubewall stresses. However in the process of determining an improved design method, the authors do use the concept of baseplate flexibility, specifically treating the baseplate as a beam. To summarize the procedure developed for the New York State Department of Transportation, the authors using past experimental and analytical data, develop a method which would allow a designer to effectively treat the design of a baseplate (including thickness, side length, and pole outer diameter), as the design of a beam. The procedure begins by determining the forces in the anchor rods. Given these forces applied to the baseplate, several different design cases must be checked. One design case is bending, which would correspond to the uplift side of the baseplate. Given their experimental and analytical data the authors develop equations to determine the maximum stress of a particular baseplate geometry and loading, based on a simple bending equation (Hag-Elsafi, Alampalli, and Owens 1999).

Endplate Thickness [in]	Specimen Name	Number of Cycles	Stress Range [ksi]	A	A average	Fatigue Category average
1.5	VALNu (average)				5.46	E`
2	VALNu 2 A	5,144,528	11.9	86.69	57.17	C
2	VALNu 2 A	1,683,127	11.8	27.65		

Table 1.6.1: University of Texas Fatigue Test Results for Baseplate Thickness
Courtesy of Mark Koenigs (Koenigs 2003)

$$\text{Where } A = \frac{N * S_R^{\,3}}{10^{\,8}}$$

Figure 1.1.1: Typical Cantilevered Sign Structure

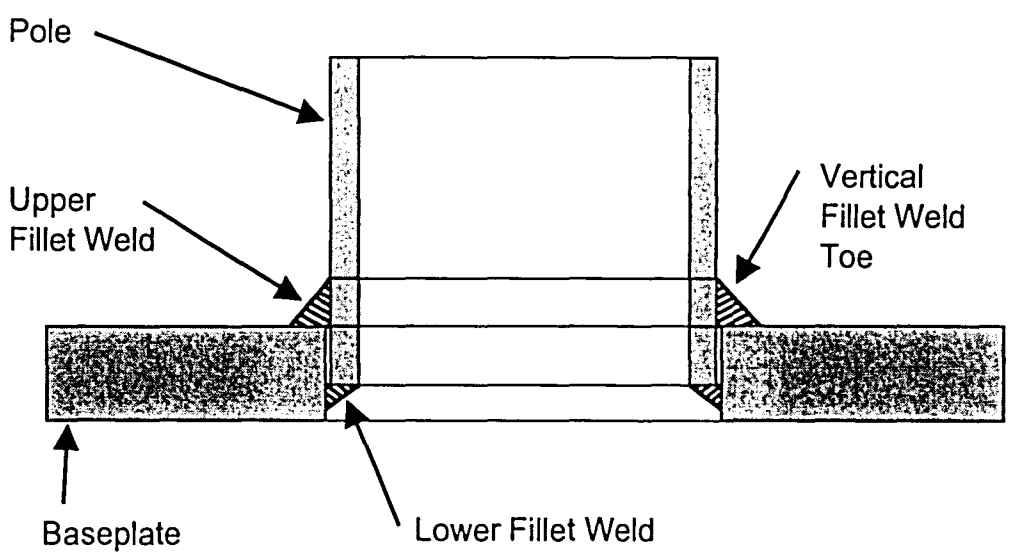

Figure 1.1.2. Schematic Cross Section Through Socket Welded Connection

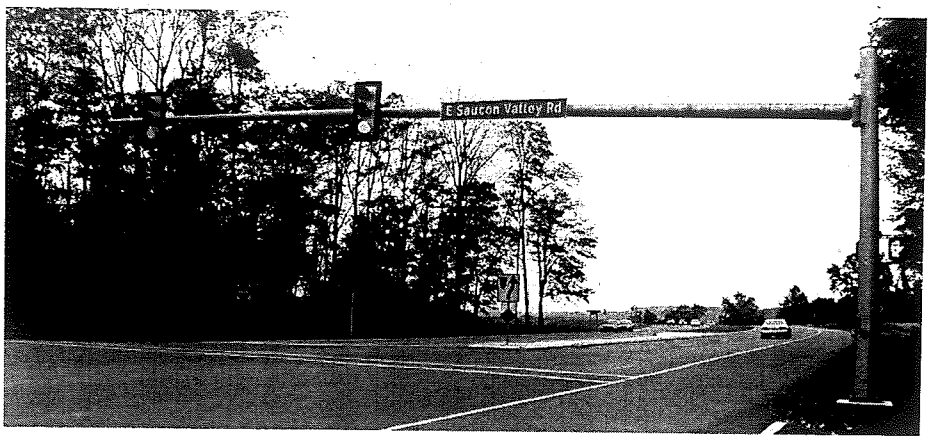

Figure 1.1.1: Typical Cantilevered Sign Structure

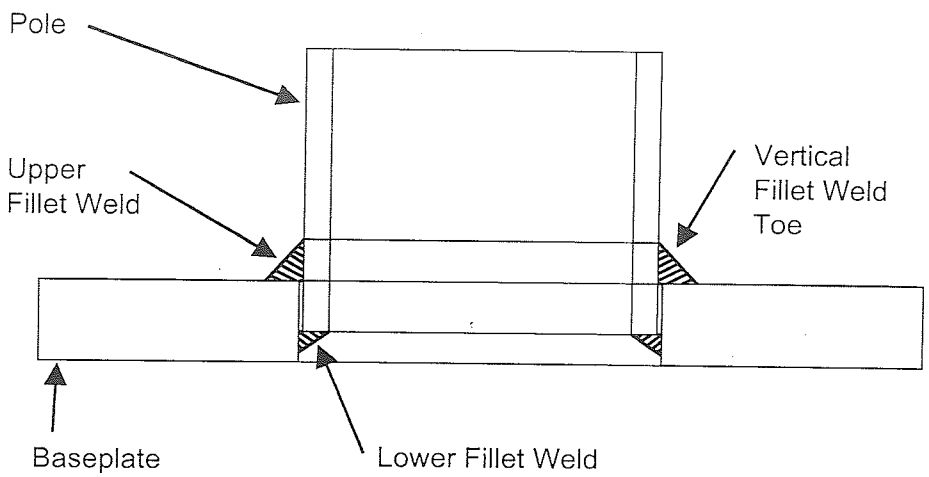

Figure 1.1.2. Schematic Cross Section Through Socket Welded Connection

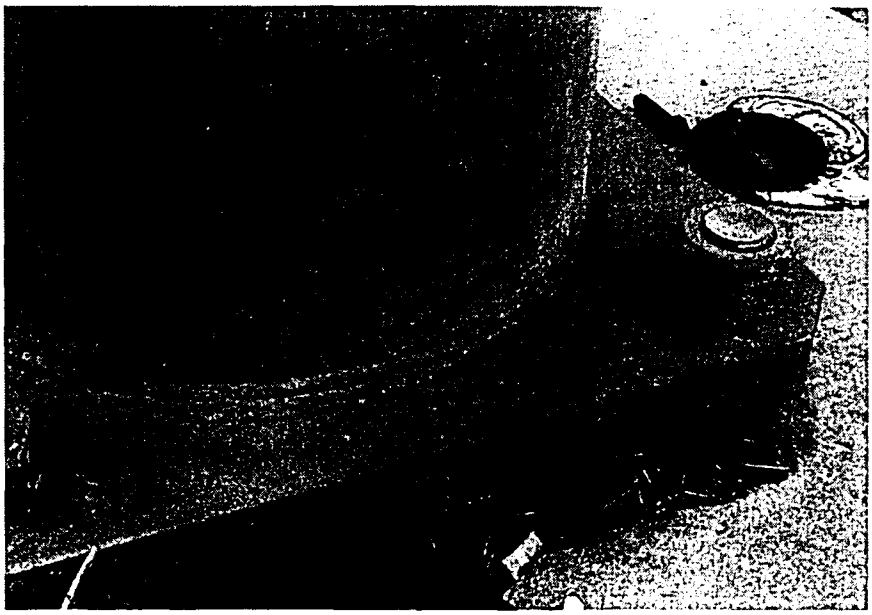

Figure 1.1.3: Close-up of Welded Socket Connection

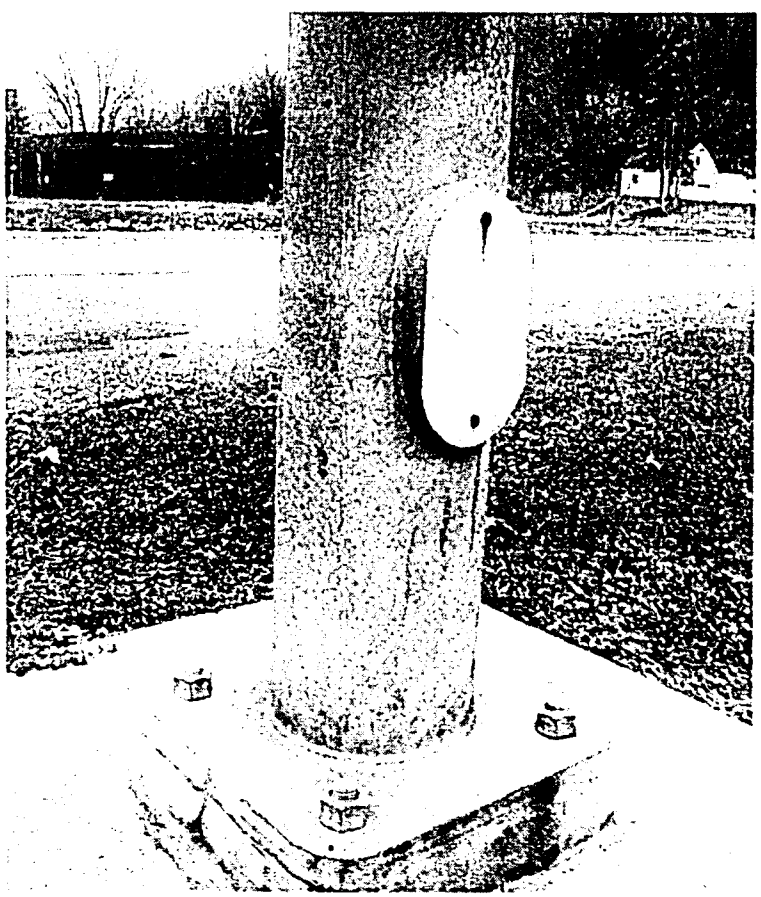

Figure 1.1.4: Typical Hand-Access Hole

Figure 1.1.5: Typical Anchor Rod and Leveling Nut Geometry. Note bottom leveling nuts can not be seen in this view.

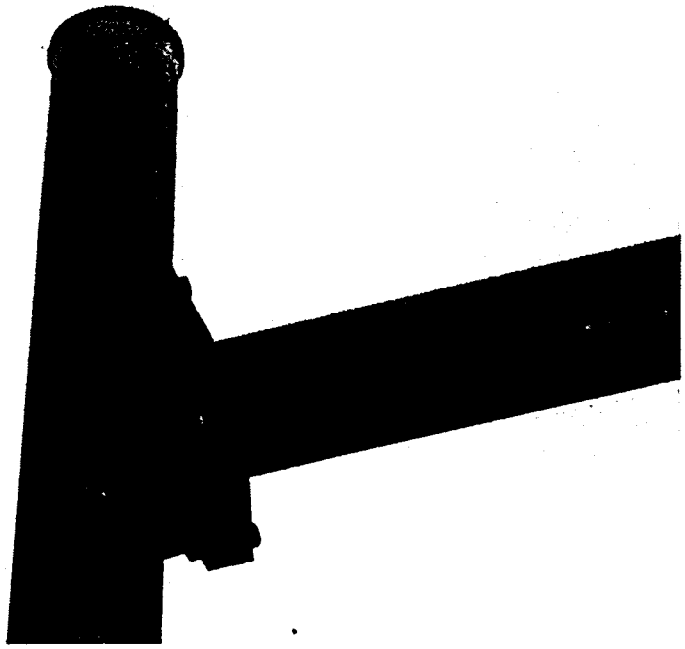

Figure 1.1.6: Typical Built-up Box and Endplate Geometry.

Section 2.1: Description of Specimens

In order to investigate the influence of baseplate flexibility on the fatigue performance of cantilevered sign structures, three pole specimens were obtained. Each pole specimen had a different baseplate thickness. The three pole specimens and a 44' long mast-arm were manufactured by Valmont Industries of Valley, Nebraska. The baseplate geometry, including baseplate thickness of the first specimen was selected based on PennDot standards for the 44' long mast arm considering typical signal weights and distribution. PennDot's standards require a 1 1/2" thick baseplate for this particular geometry. The baseplate thicknesses of the remaining two specimens were chosen to represent the two opposite extremes in baseplate thickness and thus baseplate flexibility. The second specimen's baseplate thickness was ¾", representing an extremely flexible baseplate. The third specimen had a baseplate thickness of 3", representing an extremely stiff baseplate. The other dimensions of the three pole specimens were identical, with the exception of slight differences in the weld geometries. There was some minor variation of the size of fillet welds between the baseplate and the tube wall between the three different baseplate specimens. The difference in the weld geometries of the three pole specimens was not prevalent enough to affect the intended comparison of baseplate flexibility, and was consistent with normal fabrication tolerance.

Figure 2.1.1 shows the measured dimensions of the three pole specimens and the mast arm. The mast-arm length was measured as 44'-0" from the mast-arm tip to the endplate. The three pole specimens measured 17'-6" from the baseplate to the

centerline of the mast-arm. The square baseplate of all of the three pole specimens, measured between a range of 17" and 16 15/16". Note that as shown in the plan approximately an inch by one inch isosceles triangle was cut out at the corners. The anchor rod holes of the three baseplates consistently measured 1 ½". The anchor rod hole spacing was measured at a range of 14 ¼" to 14 3/16", centerline to centerline. Outer diameter pole dimensions were measured at several different locations along the length, thus providing an outer diameter dimension above the weld toe and tube taper. The resulting pole diameters and tapers are presented in Table 2.1.1.

The weld geometry was the geometric feature that varied the most between the three pole specimens. Typical values for the outer fillet weld of the three specimens were: The vertical fillet weld leg was approximately ½" and the horizontal filet weld leg was approximately 3/8". The inner fillet weld was slightly less regular than the outer fillet weld. Dimensions were taken as closely as possible and averaged at several locations if necessary. All of the welded geometries possessed some minor variability as different locations had different lengths of vertical and horizontal fillet weld legs. In addition there was some variability in the shape of the fillet weld, as the fillet weld was made with multiple passes of the weld metal. Valmont industries uses a mechanical rotation device to apply a very consistent weld around the pole base, but there is still some small variability in the weld profile. The vertical and horizontal fillet weld leg lengths are also presented in Table 2.1.1 for each of the three baseplate thickness specimens.

The most difficult geometric property of the three pole specimens to measure was the tube wall thickness. Tube wall thickness measurements could not be made near the pole base with a regular digital caliper, because the baseplate would get in the way. The only location where the tube wall could be measured was at the top of the pole. Due to the rolling process used to fabricate the pole tubes the actual thickness near the base of the pole could be different than that at the top of the pole. This small difference could make a very considerable difference in the stresses local to the baseplate. Due to the high degree of stress concentration and high stress gradient small differences in the tube wall thickness local to the baseplate could make a severe difference in the finite element stress data. In order to measure these critical tubewall thicknesses an ultrasonic thickness meter was used and the tubewall thicknesses were measured fairly consistently at a thickness of 0.23".

Section 2.2: Test Set-up

The objective of the experimental test fixture is only to provide a static constraint for the mast-arm sign structure. In the field the structures are typically supported by a reinforced concrete foundation which extends below ground. The stiffness of the soil has little effect on the static response to the structure in the field, but plays a more significant role in the dynamic properties of the structure. Since the experimental investigation was not directly concerned with the dynamic properties of the structures, it was sufficient to neglect the soil interactions and create a concrete foundation that would bear directly on the concrete lab floor. Another option considered was to mount the cantilevered sign structure by the anchor rods directly to

a stiff steel plate fixture. However the concrete foundation bearing pad had the advantage that it would provide the most realistic boundary conditions. The high degree of variability in the concrete to anchor rod interaction is influenced by many factors including: air voids, the placement of large aggregate, uneven concrete heights, shrinkage, and creep.

The concrete foundation bearing pad was designed to prevent overturning in all directions, considering experimental static loads, construction loads including forces from ladders and tightening mast-arm bolts. Since overturning along the direction of the mast-arm drastically controlled the design a non rectangular "L" shape was used to reduce the amount of materials needed. The designed foundation provided very conservative factors of safety for overturning, while being relatively inexpensive in material costs. The length of the bearing pad foundation measured approximately 10' long by 4' wide, with 42" of depth adjacent to the anchor rods. Number 4 rebar was used to prevent cracking and to allow for the concrete foundation to be moved by crane.

Because all three pole specimens had the same baseplate geometry only one anchor rod spacing configuration was needed. As discussed in Section 2.1, the anchor rod hole diameter was 1.5" and the nominal diameter of the anchor rods was 1.25". Due to this small margin, care was taken to ensure that the spacing of the anchor rods matched the spacing of the anchor rod holes. Care was also taking to ensure that the anchor rods remained in place and perfectly vertical during the pouring of the foundation. The concrete was allowed to cure for approximately one month before the

first pole specimen was erected. Laboratory technicians erected all the pole specimens and the mast arm using an overhead crane. All baseplate leveling nuts and mast-arm bolts were hand tightened using pipe wrenches, except for the mast-arm static load tests in which an air hammer gun was used. The particular air hammer gun provided a sufficient torque to provide full preload for the mast-arm 1" diameter bolt. All leveling of baseplate was measured with a simple levels, which had some limitation, especially when compared to more sophisticated equipment available in a laboratory setting. The leveling of the baseplate as well as the tightening of the leveling nuts was accomplished using a three and a half foot long pipe wrench, which also had its limitations in delivering the torque required to fully tighten the leveling nut. This simple approach was justified as it is typical of the erection procedures of the structure used in the field.

Loading was accomplished by simply hanging a series of different weights from the tip of the mast-arm. This loading type was chosen as it was very simple to perform in the laboratory. The decision as to which manner the test specimens were loaded was actually arbitrary for the scope of the investigation. Because the study was only concerned with the elastic behavior of the structure, the theory of superposition can convert the findings for a cantilever end load to other desired loading conditions. Section 2.3 discusses how elastic loading and behavior can be related to the fatigue performance of the cantilevered sign structures. A steel cable was secured to a hook located just inside the tip and on the bottom of the mast arm. The hook was likely installed and used at some point during the fabrication process. Initially a load cell

was mounted on the steel wire to measure the load being applied to the structure. However, the load cell was later removed as the end loads used were repeated.

Two different types of displacement sensors were used in order to provide additional data to calibrate the experimental results with the finite element analysis. A string pot was installed 8" away from the tip of the mast-arm. The mast-arm tip deflection was measured 8" away to provide clearance for hanging weights. Unfortunately late in the experimental testing, the string pot was damaged while changing the position of the mast-arm, and a replacement string pot had to be used for the remainder of the mast-arm testing. Care was taken in checking the calibration of the new string pot and the data for corresponding tests of the two different string pots were carefully checked.

A linear variable differential transformer (LVDT) was used to measure the baseplate deflection on the compression (down lift) side. The LVDT bracket was mounted to powerful magnet which attached to a steel plate anchored to the top of the foundation. Thus the LVDT could measure the baseplate deflection anywhere on the downlift side with some limitations due to clearance. In some static load tests baseplate deflection data was taken at a series of locations, providing a plot of the deflected shape of the baseplate. The standard position that the LVDT measured the displacement was on the mast-arm centerline one inch in from the edge of the baseplate.

The main feature of the experimental test set-up was the extensive amount of strain gages used. A total of 202 gages were used on the three pole specimens and

mast-arm specimen. This large number of gages provides valuable experimental stress data which as mentioned previously is somewhat incomplete in other related research. Whenever possible, strain gages were applied in pairs, on both the outside and inside of the tube wall (or top and bottom of the baseplate). These pairs of gages measured the inner and outer axial stress, from which the local bending and mid-plane stress can be calculated. Experimental values for bending are significant because there is no simple way to accurately predict the different stress components in the tube wall near the socket joint. Obtaining experimental values of the stress components are also important as an un-calibrated finite element model can be somewhat unreliable in predicting what the actual values of stress are, especially near an area of concentrated stress. A discussion on the selection of gage locations follows.

Section 2.3: Gage Locations

Prior to developing a gage plan extensive finite element analysis was conducted. The finite element results were used to determine the number and location of gages needed to adequately capture the behavior of the structure. The behavior of socket welded joints in cantilevered sign structures is not fully discussed in many major fatigue testing oriented sign structure research. Thus the finite element analysis was the only data available to be used in the determination of a gage plan. As discussed in Section 1.1 the results of a previous field investigation also indicated that the distribution of stress adjacent to the socket connection, would need to be carefully monitored experimentally.

The results of finite element analysis showed two major trends in the stress distribution local to the fillet-welded socket joint between the pole and baseplate. The discussion of these two trends in stress distribution is only for the purpose of justifying the number of and placement of strain gages. The complex local behavior will be discussed in Chapter 4. The two trends in stress observed in the finite element analysis are shown in Figures 2.3.1 and Figure 2.3.2. Note that neither the vertical nor radial distribution of stress is consistent with the stress distributions assumed in design.

Figure 2.3.1 shows a typical vertical stress distribution. The distribution plot shows the various stress components: outer and inner stress, bending stress, mid-plane stress, and Simple Beam Theory outer stress verse the height above the baseplate. Many factors influence the distribution, especially the radial location the distribution is taken at, baseplate and weld geometry. It was noted that the vertical stress distribution profile always followed a similar pattern. Stresses were extremely high just above the tubewall connection to the baseplate. The stresses then decreased with increasing height above the baseplate until they reached a local maximum or minimum. Further increasing height above the baseplate resulted in bending stresses decreasing to zero, and the outer, inner, and mid-plane stresses eventually converge to Simple Beam Theory.

Figure 2.3.2 shows a typical radial plot of the absolute value of stresses in the tubewall ½" above the tubewall to baseplate connection. Again a more detailed explanation of the radial plot will follow in section 3.2. The radial distribution of the

stresses in the tube wall is dependent on several factors especially the height above the connection that the profile is taken at, the baseplate and weld geometry. However finite element analysis results showed that all radial stress profiles followed the same typical pattern. Figure 2.3.2 shows that all stresses are substantially higher than Simple Beam Theory derived stresses, as would be expected for such a high stress concentration. Contrary to the assumptions used in design, the outer stress is at a maximum value when roughly in line with the anchor rods, not when at a maximum distance away from the neutral axis.

Using the knowledge gained from finite element analysis a gage plan for each of the three pole specimens and mast-arm specimen was developed. The objective in determining the gage plan was not just to provide the most experimental data possible, but to provide the most useful experimental data possible. The number of strain gages used was obviously limited, by factors such as cost, labor time, and by equipment capabilities. Thus the challenge became measuring the complex three dimensional stress behavior, illustrated in the previous distribution plots by a minimum number of gages. It also was very important due to the many sources of error and variation, to provide duplicate experimental stress data when possible. Also the order that the three different specimens were tested also dictated the number of gages used on each specimen. As the experimental data of the first specimen agreed reasonably well with preliminary finite element analysis, fewer gages could be used on the later specimen.

A total of 202 strain gages were installed on the three pole specimens and one mast-arm specimen as shown in Table 2.3.1. The 1 ½" thick baseplate pole specimen

was the first of the specimens to be tested, followed by the testing of the ¾" thick baseplate specimen. The final specimens tested were the 3" thick baseplate specimen tested concurrently with the mast-arm specimen. The number of total gages per pole specimen was decreased after every pole specimen tested. Upon analyzing the data from the first specimen, several gages on the baseplate were eliminated from future tests. The gage plan for the mast-arm specimen was different than the first three pole specimens in that the gages on the mast-arm specimen were only on the outer surface of the tube wall and endplate. No interior gages were used on the mast-arm specimen as it would have been difficult to run wires to the data logger. Thus the mast-arm specimen utilized a similar gage plan as the 1 ½" and ¾" thick baseplate specimens, without having interior gages. It was estimated that due to the slightly more complex contact condition between the endplate and the flange plate, the stress distribution could be different from that of the baseplate in the pole specimens.

Baseplate and Endplate gages:

Strain gages on the pole and mast-arm specimen were subdivided into two groups: gages on the pole or mast-arm tubewall and those on the baseplate or endplate. The decision as to the number and location of the gages on the baseplate was fairly simple. Because one of the primary objectives in the investigation is to determine the extent baseplate flexibility plays on the stress local to the socket joint it was imperative to measure the amount of baseplate bending. Baseplate bending is at a maximum in the centerline locations, directly in between the two compression anchor rods, and the two tension rods, as shown in Figure 2.3.3. In these areas, uplift occurs

on the tension side of the pole and down-lift occurs on the compression side. The maximum bending, top, and bottom stresses occur in a direction perpendicular to the mast-arm axis. Since the LVDT was mounted on the down-lift portion of the baseplate it was only possible to measure strain at the uplift regions of the baseplate.

In all three pole specimens tests, the uplift stresses at both the top and bottom of the baseplate were measured perpendicular to the mast-arm axis. The gage numbers are 66 and 67 (top and bottom) for the 1 ½" specimen, 28 and 29 for the ¾" specimen, and 32 and 33 for the 3" specimen. Because there was no LVDT on the endplate, the mast-arm specimen had both its uplift and down-lift stresses measured, but only on the top surface as discussed previously. The gage numbers for the uplift and down-lift stress were 56 and 57 respectively.

Tubewall gages:

The primary concern in determining the location of the gages along the tubewall was to provide enough gages along the height above the baseplate to accurately capture the stress profile discussed previously. The complex shape and curvature of the profile and the stress behavior local to the socket joint obviously can not be described by a single gage. Obtaining experimental values throughout the whole profile allows for an improved calibration with the finite element model data. This is very important because finite element data can be extremely sensitive to mesh size adjacent to the weld toe, and therefore will provide inconclusive results. Minimally it is important to obtain enough experimental data to define the linear portion of the vertical stress profile directly above the socket joint. Thus at least two

gages are necessary, one above the weld toe and the other approximately an inch away. As mentioned earlier, it also important to provide duplicate gages and data at locations directly above the weld toe, as the large stress gradient can be greatly magnified by human error.

In order to capture the vertical and radial stress profile in the tubewall local to the socket joint, while minimizing the number of gages and maintaining an orderly system of gage locations that could be repeated on all specimens tested, a series of three gage configurations were used at prescribed radial locations. Gage numbers were always numbered from the outside of the tubewall to the inside, and pairs of gages were numbered with decreasing height above the baseplate or endplate. The first gage configuration was a series of 10 gages, 5 gages on the outside of the tubewall and 5 gages on the inside of the tubewall. The pairs of gages were at heights of 8", 5", 3", 2", and ¾" above the top of the baseplate. This first gage configuration provides an extensive discretization of the vertical stress profile. The second gage configuration used 6 gages in total with pairs of gages at heights of 5", 2", and ¾" above the top of the baseplate. With a reduction in the number of gages, the second gage configuration still allows experimental data describing the stress and stress gradient near the socket joint and a point in the valley of stress above the peak. In addition to the two gage configurations, single pairs of gages were applied at ¾" above the top of the baseplate. These single pairs were used to verify duplicate or symmetric stress data. Using only two gage configurations allowed for easy comparison of the experimental stress data between different specimens and finite

element models. The two gage configurations were placed at various radial locations on the specimens with additional pairs of gages when needed. The radial locations were primarily at multiples of 45° away from the mast arm axis.

Prior to discussing particular gage locations of the specimens tested, it is necessary to first discuss the gage location notation. It was necessary to have a standard gage location notation for the tubewall gages that would indicate: whether the gage was applied to the inner or outer tubewall surface, the radial location, and the height. The simplified gage location notation will be seen in future tables in the following chapters.

The radial location is described first by either Tension, Compression, or Neutral Axis according to simple beam theory. The radial location is next described by the angle of skew, measured from the gage location to the nearest side of the mast-arm axis, such that skew angle will never exceed 90 degrees. The last part of the radial location notation is the Left or Right, as in the left or right hand side while standing facing the pole and looking towards the mast-arm cantilever tip. For example a gage location on the outside of the pole, 5" above the baseplate, in line with the left compression anchor rod would be notated as C 45 L, and would be indicated by O four outside and 5 for 5" above the baseplate.

Section 2.4 Testing Procedure

The objective of the research is to study the fatigue performance of socket welded connection of cantilevered sign structures. The fatigue performance was investigated utilizing extensive finite element analysis and experimental data. As

briefly discussed in the discussion of the data collection system, the experimental testing program was only concerned with elastic static displacement and elastic static strain data. As related to the testing procedure used, the term static refers to the physical condition when the applied load has no acceleration. There was some difficulty in applying the load with out causing the flexible structure to oscillate, and hence accelerate the load. Thus true static loads were measured when the natural damping in the cantilevered sign structure had damped out all of the motion induced in the application of the load. Using a linear elastic fracture mechanics approach fatigue resistance can be compared and be determined according to the elastic stresses applied in the tubewall adjacent to the weld. Thus fatigue performance can be determined with static experimental data, without performing an actual fatigue test.

The static load testing performed can be broken down into two primary tests. The first and most important static testing was the static cantilever load tests. The other major static testing conducted, the baseplate leveling tests involved examining the effects of forcing the baseplate to be out of level. These leveling conditions were used to examine the role of construction imperfections, in the leveling process. In addition to these two major tests, similar static cantilever testing was performed on the mast-arm. Also various other tests were performed with different leveling nuts missing to simulate the effects of a fractured anchor rod. The following section discusses the procedure used in and justification for these different static tests. Also included in the discussion is the simple numeric procedure that was used to convert the collected time history data into static stress values.

Cantilever Load Testing

Cantilever load testing was one of the most critical components of the study. The experimental results provided a basis for finite element calibration. The calibrated finite element models then in turn can be used to investigate a wider range of geometric variable influencing the fatigue performance of welded baseplate socket joints. Static cantilever load testing was performed on all three pole specimens. (And as will be discussed later, on the mast-arm specimen as well) In general all three specimens were tested with three different cantilever end loads, 99 pounds, 149 pounds, and 193 pounds. By testing with three different cantilever weights it was possible to determine whether the structures response was linear. The experimental program was conducted the same way, as to examine the effect of different stand-off lengths. Though by the end of the testing program the 3" thick baseplate specimen was only tested at the base 1 5/8" stand-off length. Initially the first specimen, the 1 ½" thick baseplate specimen was tested at stand-off lengths of 1 5/8", 1 ¾", 2", and 2 ½". However the experimental results showed no considerable difference in stress data. The ¾" thick baseplate specimen was only tested at stand-off lengths of 1 5/8" and 2 ½", and again there was no considerable difference in stress between the two fixity conditions.

The general procedure used for the static cantilever end load tests was quite simple. The cantilever end load was accomplished by hanging weights from a steel cable that was attached to the tip of the mast-arm. In general the procedure involved slowly applying the weight to the structure, allowing the structure and weight to come

to rest, and slowly removing the weight. Data collection began prior to application of the weight and continued until after the weight had been removed, and the structure had come to rest. Prior to applying the weight the real-time stress and deflection was checked for errors and malfunction gages. The real time data also was very useful in determining just when the structure had come to rest, and the acceleration was zero.

Baseplate Leveling Tests

The particular objective in performing baseplate leveling tests was to examine how much construction erection imperfections affect tubewall stresses. Construction loading stresses applied to the tubewall are of very little consequence to the ultimate strength and fatigue design of the structure. However recently there has been an increased interest in the use of weld treatment to increase the fatigue resistance of welded socket joints. Ultrasonic impact treatments, UIT, is a newer technology, involving a plastically deforming the surface welded regions, to induce a compression field on weld defects within. The treatments have shown considerable gains in the fatigue lives of steel girders, with welded attachments. These treatments are very sensitive to the order in which loading and treatment is applied. For example, the treatment must be applied after the galvanization process, as it has been shown that the galvanization process diminishes the benefits of the weld treatment. Also the treatment must be applied with the structure under its' in-service dead load (Koenigs 2003). As it has also been shown that the treatment loses some of its effectiveness if not performed with the structures dead load applied. Thus the proposed method for treatment, is to apply treatment after the galvanization process, at the fabrication site

with the structure supporting its' deadweight. Then to transport the treated structures to their customers, where the structures may or may not be installed immediately (Koenigs 2003).

In the field erection process, it is very difficult to position all four bottom leveling nuts exactly level. Especially using simple tools, it is very likely that the top of the bottom leveling nut plane will not be perfectly level, and that one of the leveling nuts may be out of plane. As only three leveling nuts are required to establish this plane, the final leveling nut will likely be lower than this plane. Using simple leveling equipment, it was noted that it is possible to have as much as a 1/16" difference in height, between leveling nuts that would appear to be level. If the structure is erected without care towards these possible differences in leveling nut heights, essentially a condition of enforced baseplate displacement loading is applied to the structure. These stresses induced in the tubewall due to construction imperfection may negate the effectiveness of UIT. In the same way that the application of additional dead load after UIT, decreases the effectiveness of the treatment, the addition of construction imperfection induced stresses may also decrease the effectiveness.

In order to examine the magnitude of construction imperfection induced stresses a simple testing procedure was developed. Essentially the procedure began with the specimen initially at rest with the baseplate leveled. Then the one of the anchor rod leveling nut pairs was loosened. The upper (or lower) leveling nut was first raised (or lowered) away from the baseplate. Then the opposing leveling nut was raised (or lowered) forcing the baseplate, which was still restrained by the three other

anchor rods, to deflect. All leveling nut tightening was done using a 42" pipe wrench. Measuring from in line with the anchor rod adjacent to the baseplate deflection, the baseplate was forced to move 1/16" and then an additional 1/32". Data collection began with the structure at rest, and gave sufficient time for the structure to come to rest after both movements. Data collection continued as the baseplate was moved back to its' original position, and again the structure was allowed to come to rest.

Mast-Arm Testing

Mast-Arm static load testing is the final major static load testing performed, and was just a continuation of the cantilever end static load testing. The mast-arm was first tested with three different cantilever end loads, just as in the initial cantilever end load testing on the three baseplate specimens. One major difference between the mast-arm and pole static testing was that an air hammer wrench was used to sufficiently develop the preload tension force in the endplate bolts. At the time the primary motivation for developing the full preload in the bolts (And not in the anchor rod connection) was because it was believed the contact between the endplate and flange plate would influence stresses in the mast-arm tubewall, and thus it was important to ensure that this contact pressure was consistent. In addition, the mast-arm was also tested with washers separating the endplate and flange plate surfaces, as to allow for the study of the influence the contact has on mast-arm tubewall stresses. Thus for both of these tests, the air hammer allowed for consistency. In addition to these two mast-arm tests, the mast-arm was also tested with the absence of a tension

endplate bolt. Several tests were performed measuring the stresses induced when either the left or right tension endplate bolt was removed. Static cantilever end load tests were also performed with the tension bolt removed also.

Baseplate Thickness Specimen [in]	Average Measured Fillet Weld Leg Lengths [in]		Pole Outer Base Diameter [in]	Pole Taper [in/ft]
	Horiz.	Vert.		
3/4"	0.441	0.43	13	-0.132
1 1/2"	0.422	0.559	13.1	-0.144
3"	0.41	0.602	13.1	-0.141
Finite Element "BASE"	0.375	0.5	13.1	-0.144

Table 2.1.1: Measured Pole and Fillet Weld Geometry Per Pole Specimens

Specimen	# of Gages
1 1/2" Thick Baseplate Specimen	79
3/4" Thick Baseplate Specimen	50
3" Thick Baseplate Specimen	33
Mast-Arm Specimen	24
Anchor Rods	16
Total:	202

Table 2.3.1: Number of Gages used per Specimen

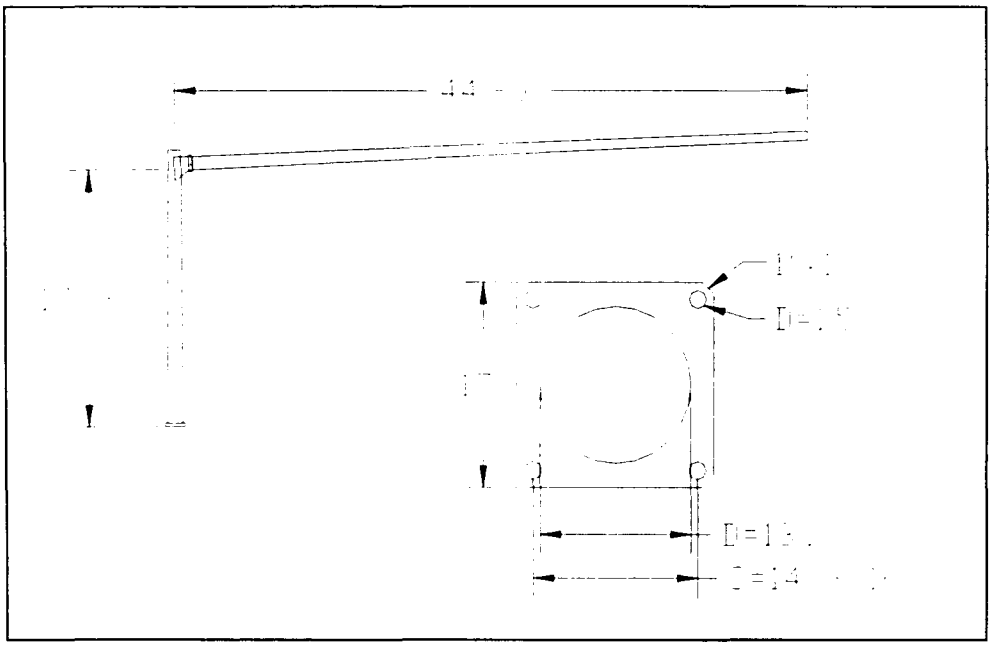

Figure 2.1.1: Typical Dimensions of Mast-arm and Pole Specimens

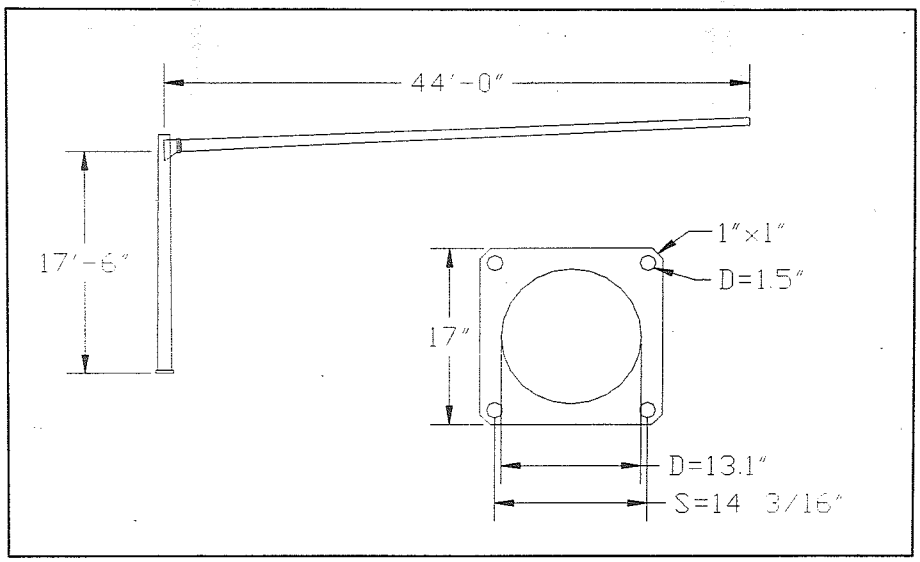

Figure 2.1.1: Typical Dimensions of Mast-arm and Pole Specimens

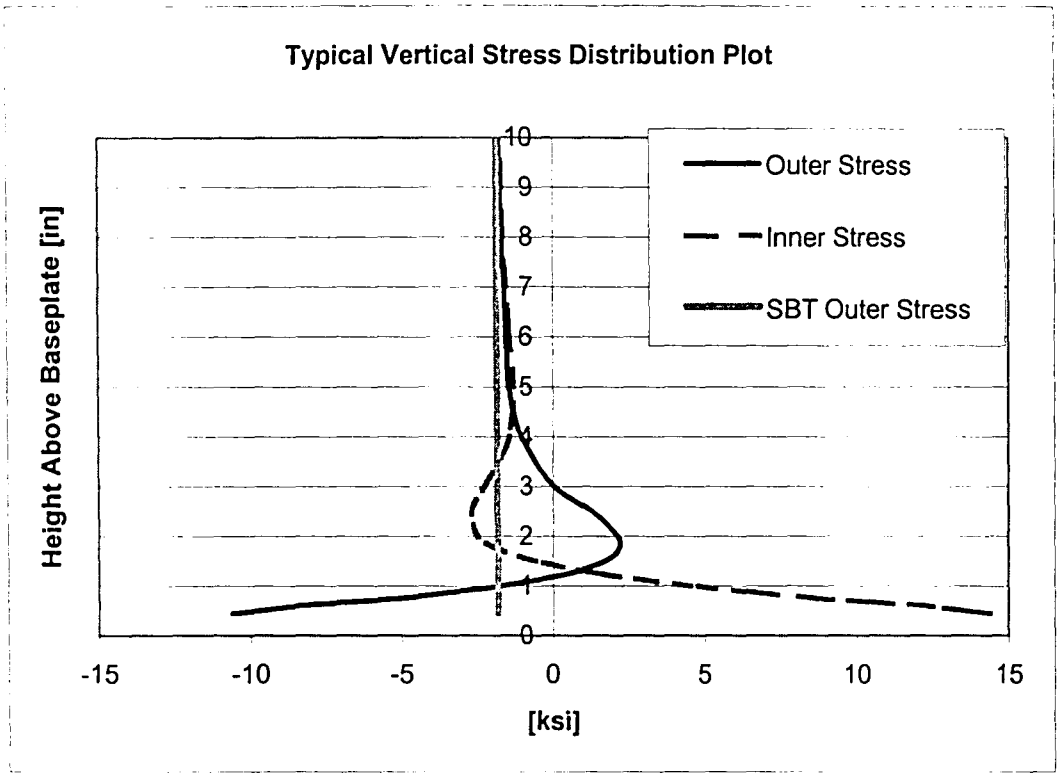

Figure 2.3.1: Typical Vertical Stress Distribution in Pole Tube Wall **

** Detailed description of behavior can be found in Chapter 4

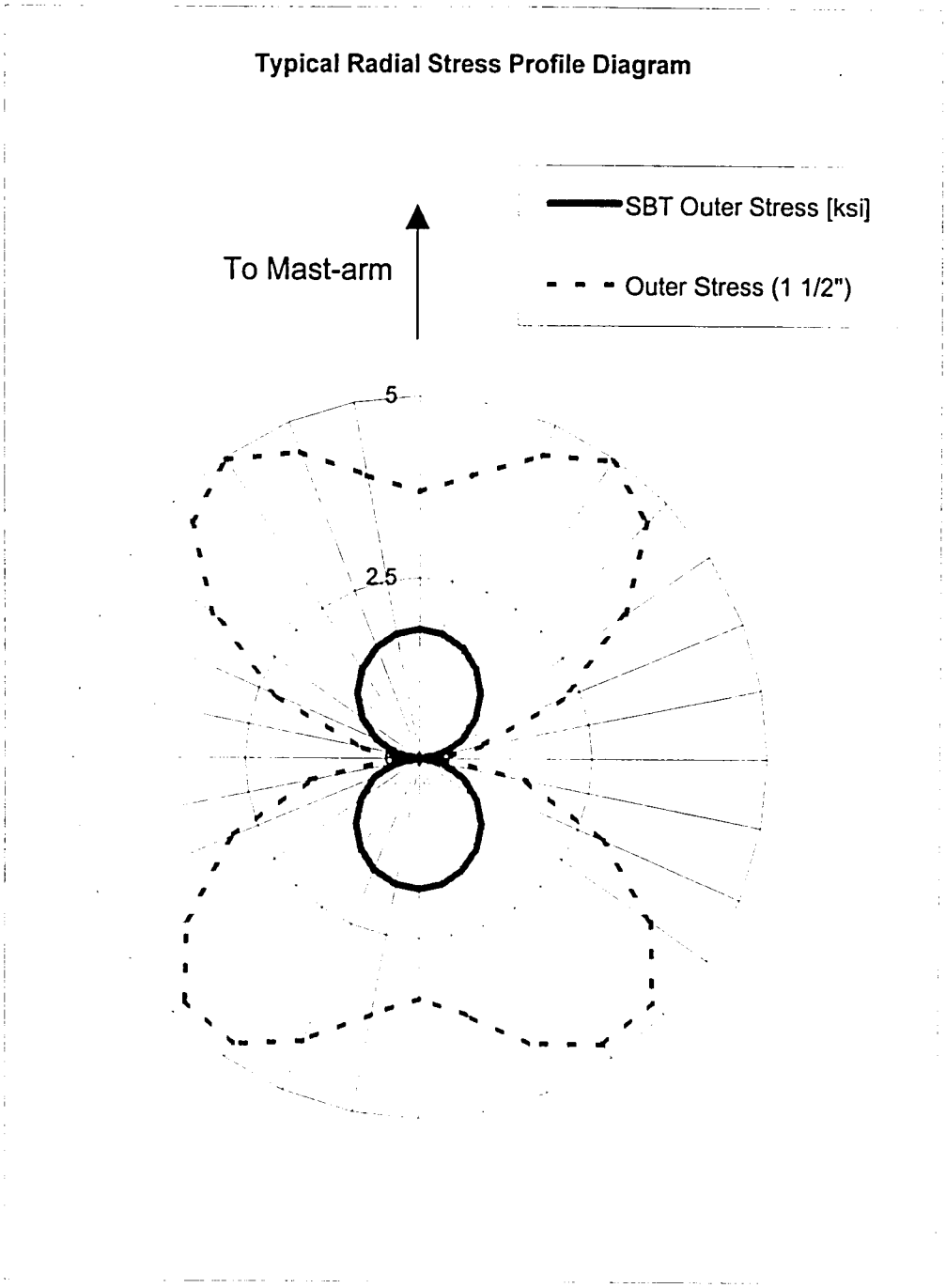

Figure 2.3.2: Typical Radial Stress Distribution in Pole Tube Wall **

** Detailed description of behavior can be found in Chapter 4

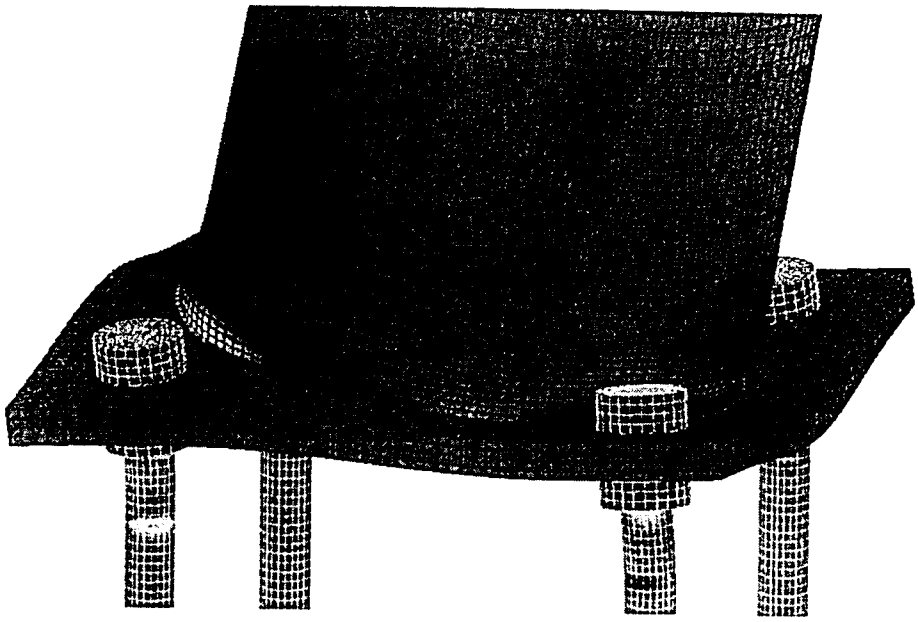

Figure 2.3.3: Deflected Shape of Baseplate Under Gravity Load

Chapter 3

Chapter 3 presents the results of the finite element modeling of the socket welded connections in cantilevered sign structures. A substantial effort was made to understand the relationship between the behavior of the actual test specimen structures (according to experimental data) and the analytical finite element models. This chapter documents the task of determining this relationship. Ultimately it was determined that it may not be possible to perfectly model the complicated structural detail, especially using relatively simple modeling techniques. Though agreement overall is good, the actual behavior of the structure is very difficult to simulate in a finite element model.

Chapter 3 first discusses the issues and specific structural aspects of the welded socket connection that the finite element model must be able to replicate, followed by a summary of the basic finite element modeling method, which was used for the BASE model (Section 3.1). Section 3.2 provides a quick discussion of the stresses that the study will be discussing. This section defines specifically how the finite element and experimental strain data were converted into stress data. Section 3.3 then discusses the problems seen in the comparison between the experimental data and the BASE series of finite element models. Section 3.4 then discusses the results of the calibration study, comparing the results to the BASE model results when helpful.

Chapter 4 will begin after performing this calibration study, the new analytical results will be quickly compared to the experimental data prior to the discussion of the structural behavior of the connection. In addition the problems with the data

agreement and the results of the calibration study will very briefly be summarized, early in Chapter 4, as to provide a complete summary of the finite element studies.

Section 3.1: Modeling Issues and Techniques

Section 3.1.1: Modeling Issues

The techniques used and issues related to the finite element modeling of cantilevered sign structures are very similar to that of the modeling of any typical structure. Upon initial inspection, the simple geometry of cantilevered sign structures appears to lend itself to simple finite element modeling techniques, using a fine mesh of solid elements to mathematically represent the structure's geometry. However there are several issues that complicate this simplified method, these issues are very similar to those encountered in modeling a typical structure, for example a multi-girder composite bridge. These primary issues, which influence the structural behavior of sign structures involve load path and flexibility, contact and friction, and stress concentrations. As with typical structures, it is extremely difficult to accurately model the effects of theses issues. The following section discusses these issues and then discusses the method used to model the basic geometry of the specimens, and finally discusses what steps were taken to correct and better understand the behavior related to these issues.

Issues affecting modeling

Load path and flexibility. The load path or mid-plane stress effect in tubewall stress distribution is dictated by the flexibility of the baseplate, just as diaphragms and the bridge deck distribute load amongst girders. To summarize the influence of baseplate

flexibility, it is helpful to remember that load is attracted towards the stiffest regions. The distribution of stress and load in cantilevered sign structures is primarily a function of baseplate flexibility, as the axial load in the tubewall is attracted to the stiffer connection at the anchor rods. This behavior will be discussed later in Section 4.2.1 and it will be shown that the greatest mid plane stresses are located in line with the anchor rods and dramatically decreases towards the locations of the expected maximum and minimum stress. Base plate flexibility also influences the distribution of stress through the tubewall as will also be discussed in Section 4.2.1. Due to local deformation in the baseplate, local deformations occur in the tubewall, thus creating a condition of local bending stress. Local bending stress increases with baseplate flexibility, and reaches a maximum at the radial locations directly in line with the anchor rods.

From the perspective of finite element modeling, flexibility is a serious concern. Given the simple exercise of modeling a cantilever beam with solid elements, it is evident that the number of (mesh refinement) and type of elements used is critical in accurately representing the flexibility of the beam. Also it is critical to be able reach a level of mesh refinement resulting in convergence of the solution, in which the further increase of mesh refinement produces consistent results. As shown by the simple example of the importance of mesh refinement, the mesh refinement and flexibility of the modeled structure must be carefully considered.

Contact and friction. The manner in which contact and friction is modeled in cantilevered sign structures is very significant to the results and difficult to quantify.

To continue the parallel, the difficulty in modeling the contact and friction in sign structures is similar to that of the shear interaction between the concrete deck and the girders. The areas of the structure that are sensitive to contact and friction in finite element modeling are primarily the two different bolted connections, which exist in the cantilevered sign structure. These two locations are the anchor rod, leveling nut to baseplate connection and the bolted endplate to built-up box flange plate connection. As discussed previously the scope of this project focuses primarily on the behavior of the baseplate connection, and only examines the mast-arm contact behavior through experimental data. The distribution of reactionary forces applied to the anchor rods by the concrete foundation is very much unknown. Contact and friction also determine the baseplate fixity due to the leveling nut connection to the baseplate. This fixity condition involves contact and friction and depends on the tightness of the leveling nuts and alters the baseplate flexibility and hence the deflected shape of the structure. Determining the level of fixity imposed by the contact and friction between incompletely tightened leveling nuts, anchor rods, and baseplate is very difficult, and is highly variable depending on local geometric imperfections. Though with the large amount of experimental data it was possible to verify different finite element modeling approaches to the issue of contact and friction.

Stress Concentration. As previously discussed in the section on fatigue design the most critical fatigue crack locations are located at points at the highest stress concentration. As discussed earlier, this approach combines many different factors that influence local stress, including the stress concentration at the tip of the weld

defect and the stress concentration due to the structure geometry. The first stress concentration or stress raiser relates to the microscopic local plastic stress at the tip of a crack or a weld defect. Under the scope of the project no experimental or finite element study will examine fatigue crack growth. The second stress concentration used in a general sense, is very applicable to the scope of the project. It relates to the way that a sharp discontinuity in the structure influences stress distribution. Primarily the stress concentration influence of the upper fillet weld on local tubewall stresses will be studied. Stress concentration is another issue that influences the modeling of cantilevered sign structures. Stress concentration with regards to modeling technique is a slightly different idea than the microscopic type of stress concentration (stress intensity) discussed earlier in Chapter 1. Stress concentrations at sharp corners and weld geometry are very important in finite element modeling, as the stress concentration can be greater than in the actual structure. Stress concentrations may be greater in finite element models as even very fine meshes are unable to geometrically model the minute curvature between welds, and corners.

Approach to issues

The individual effects of the issues discussed above, load path and flexibility, contact and friction, and stress concentration are difficult to quantify separately as the issues are strongly inter-related. For example, decreasing the vertical leg of the fillet weld between the outside of the tube wall and top of the baseplate would alter the stress concentration properties at the tubewall as well as the baseplate flexibility and load path. Both of these effects would alter hotspot stresses critical in determining

fatigue resistance. Also the manner in which contact and friction is modeled in the leveling nuts to baseplate connection also has a big influence on baseplate flexibility.

Thus in order to study the behavior of the structure, the approach must be to individually examine how particular modeling alterations influence the finite element stress data. Six major modeling alterations/calibrations were studied including: Tube wall thickness adjustments, leveling nut simplifications, weld profile alterations, standoff length adjustments, hand access hole reinforcing, and mesh refinement. All of these individual finite element studies were based on a single finite element model as will be discussed shortly. In each of these calibration studies in Section 3.4, this model, referred to as the BASE model, was altered allowing for comparison. This BASE model allowed for a constant comparison of the different modeled geometries. In each individual study a different aspect of the modeled geometry was altered. Thus the BASE model allows these effects of the variable modeled geometries to be isolated and compared.

Section 3.1.2: General Modeling Techniques Used in BASE Model

The BASE finite element model is shown in Figure 3.1.2.1. The BASE model can be subdivided into 3 portions which conveniently correspond to different element types. In every aspect of the BASE model the finite element model is based on the geometry measured in the 1 ½" thick baseplate test specimen. As shown, Portion 1 makes up the mast-arm and the upper pole. Portion 1 is composed of beam elements beginning at a vertical height of Y=108" and extends to the centerline to centerline intersection of the mast-arm and the pole at Y=210". Portion 2 consists entirely of

parabolic 8-noded shell elements, and begins at a height of Y=11" to Y=108". Portion 2 also contains the shell element hand access hole. Portion 3 consists of the anchor rods, baseplate, weld profile, and lower tubewall, and is entirely modeled with parabolic solid elements, 20-noded elements. Portion 3 begins at Y=-20" and extends to Y=11". The nodal constraints (boundary conditions) are entirely contained within Portion 3. As stated in the scope of the project, the main area of concern is the tubewall stresses adjacent to the fillet weld. In this critical region, both mesh refinement and sophistication of elements increases. The following section will discuss all aspects of the modeled geometry of the BASE model, and will be broken down by these three portions. The fourth section will discuss the rigid connections used to transition from one type of an element to another.

Portion1

The portion of the BASE model made up of beam elements, earlier referred to as Portion 1, is shown in Figure 3.1.2.2. As can be seen in the figure the tapered tube sections are made up of stepped element sections. The main purpose of this portion of the BASE Model is to provide the global geometry of the cantilevered signal support structure. The state of stress in the tubewall is very unique to the loading, as there is very little axial load or P/A type load. But due to the long mast-arm there are still large amounts of stress, due the large moment arm. Thus the primary purpose of the beam elements is to provide this moment arm geometry, while not requiring very much computational effort. Since not studying the local stresses in the mast-arm or upper pole is not part of the scope of the project, the use of beam elements is justified.

The procedure used to create the finite element mesh in the beam element portion of the BASE model began with measuring outer circumferences at various locations evenly spaced over the length of both the mast-arm and pole of the test specimens. Converting these circumferences to either outer diameters or radiuses, and plotting over the global X or Y coordinates allows for the precision of measurements to be verified. The pole circumference measurements of the 1 ½" thick baseplate pole specimen and the mast-arm measurements both showed good linear distribution as they should for tapered members. This linear distribution of the measurements verifies the precision and likely suggests the measurements are accurate. Using spreadsheet implementation and substituting the linear data with a linear curve outer radius values can be calculated at the mid element of each beam element. The upper portion of the pole is subdivided into (4) 25.5" long beam elements, and the mast-arm is subdivided into (6) 88" long beam elements. Since beam elements "B31" capture the exact static shear forces for cantilever end loading, the number of elements used to subdivide the mast-arm and pole only serve to capture the deflection of the mast-arm. The more subdivisions will provide a model that is a better approximation of the actual tapered structure. However, for cantilever concentrated end loading accurate deflection results are obtained with very few subdivisions. Certainly increasing the number of beam elements in the mast-arm above six elements can not be justified since using a more accurate tubewall thickness would have a much greater influence. The gain in accuracy from refining the beam element mesh is small in comparison to improving the accuracy of the measured thickness for such a large cantilever. The

tubewall thickness of the BASE finite element models was taken as 0.21875" according to measurements taken on the 1 ½" thick baseplate specimen. The accuracy of this value will later be discussed in Section 3.2. Another assumption made, of less consequence, was the angle of inclination of the mast-arm. The angle between the mast-arm and the horizontal was assumed to be 5 degrees thus giving the horizontal projection of the 528"mast-arm as 526" and vertical projection of 46". The spreadsheet implementation of this process, including pole and mast-arm measurements and beam element section properties can be seen in Figures 3.1.2.3 and 4.

Portion 2

The shell element portion of the BASE model is shown in Figure 3.1.2.5. Note the shell element portion begins at Y=11" (11" above the top of the baseplate) and extends to a height of Y=108". The portion consists of most of the lower half of the pole, and the hand access hole, all modeled with parabolic shell elements. The primary purpose of the portion is to properly distribute the moment loading applied by the beam elements to the solid elements below. The shell element portion must also model the load path altering effects of the hand access hole. The parabolic shell elements, though much more computationally strenuous than the beam elements discussed above, provide accurate stress results with less effort than solid elements. In addition to distributing stress to the critical solid elements below, the shell element mesh also serves another lesser purpose. The shell element portion is also very useful in providing stress results away from the baseplate. In order to illustrate the

comparison to Simple Beam Theory analysis results it is helpful to plot vertical stress profiles. These vertical stress profiles show that often the finite element stresses do not completely converge to the anticipated stresses until several feet above the baseplate, much past the limit of solid elements. Thus the shell elements must be able to capture theses stresses accurately, including at the location of mesh transitions. In discussing the shell element portion of the BASE model it must be noted that the refinement and the number of shell elements used may be excessive, especially at locations far away from the baseplate. As will be discussed, experience dictated the appropriate mesh refinement. However it certainly may have been appropriate to decrease the number of shell elements by replacing some of the length of the pole with beam elements.

As shown in Figure 3.1.2.5, only three different shell element sizes were used, (not considering the effects of the gradual pole taper). The size of the shell elements were increased with in increasing distance away from the critical tubewall to baseplate connection. The region utilizing the smallest element size was found at the bottom of the shell element portion at Y=11" extending to Y=27". The vertical element height was 0.25", with 160 elements around the circumference of the pole. At a height of 11" above the top of the baseplate this provides a radial element length of 0.25". As the pole diameter slowly decreases, with increasing height, this radial element length decreases slightly. The next element size region, from Y=27" to Y=54" increased the element height from 0.25" to 0.50". The number of elements around the circumference of the pole remained the same. Thus, a special element transition was

not needed between the two differently sized element regions. The final element size region from Y=54" to Y=108" consisted of elements with a vertical height of 1.00" and 80 elements around the pole circumference. The method used to transition between the two different sized element size regions was a simple incompatible node type transition. The other option in creating a geometric mesh transition would be to manually create mesh consisting of irregular quadrilateral and triangular elements, connecting the differently sized regions of elements. In addition to triangular and irregular shell elements this would also create modeled indentations in the tubewall, as maintaining a perfectly circular mesh would be very difficult. These indentations would locally increase bending stress through the P-Delta effect, and would produce a small spike in stress in the vertical stress profile plots discussed above. By experience it was found that it is very acceptable to transition the two differently sized elements by neglecting the mid-side nodes of the finer (lower) element size region, as shown in Figure 3.1.2.6. Note the incompatible nodes indicated in the inset view, are not shared by the larger element above. The effect of these incompatible nodes is minimal and can be justified by the exaggerated refinement of the mesh, even four and half feet away from the top of the baseplate.

Constructing the shell element portion of the base model begins with same steps in creating the beam element mesh. Referring back to Figures 3.1.2.4, the dimensions of the finite element model of the pole have been determined. Primarily the dimension of concern is the mid-thickness radius. Using some of the advanced capabilities of the pre and post processing software, and given the mid radius

dimensions at the top and bottom of the shell element portion the mesh can be created quickly and easily. Using plot only beam elements spaced with end nodes as desired, FeMap is able to revolve them into the pole geometry. The number of elements per circumference, and the element properties (including element thickness) are chosen and the pole shell element mesh is ready. The most difficult aspect of the shell element mesh creation was constructing the hand access hole mesh. Several of the modeling discussions pertaining to the shape, stiffness, element type, etc. of the hand access hole will be discussed in Section 3.2, as well as a comparison of the results of several different modeled hand access hole geometries. At the present time however, it suffices to say that the hand access hole will be modeled using a simple shell element to shell element nodal connection. The hand access hole reinforcement (thickness and depth) will be modeled strictly based on measurements taken. And the shape of the round hand access hole will be simplified as shown. The first step was to remove the existing whole shell elements, in the simplified hand access hole shape. The whole elements that were removed in the diagonal corners formed a stair case type pattern, and triangular shell elements were used to create the diagonal. A combination of different FeMap capabilities and manual determination were used to create the tricky hand access hole to tubewall connection. The resulting mesh is shown in multiple views in Figure 3.1.2.7.

Portion3

Portion 3, the solid element portion of the BASE finite element model is shown in Figure 3.1.2.8. The portion contains the most critical region of the model, as

the study of the tubewall stresses at the weld toe, as stated in the scope, are the main objective of the project. This critical region of the model, thus dictates the most refined mesh, and the most geometrically sophisticated elements, to model the physical behavior of the complex connection between the baseplate and the tubewall. Parabolic solid elements were selected to model the extreme lower section of pole, the baseplate, the fillet welded connection, the anchor rods and nuts. The element type selection decision was easily made based on the geometry of the structure. Simple two (shell) and one dimensional (beam) elements would not give reliable results for such a complicated geometry. Solid elements were extended up from the critical welded connection up the bottom of the tubewall as high as possible. The solid elements were extended in order to provide as much distance between the critical welded connection and the solid to shell element transition. Again this decision was also based on the creation of vertical stress profile plots. It is extremely difficult to create a mesh transition that does not locally raise bending stress. Thus the transition was positioned as far away from the critical weld toe as possible to minimize this effect.

The solid portion of the BASE finite element model is based on the exact measured geometry where possible. Baseplate dimensions for the most part appeared to be consistent with nominal values, though a small tolerance of about $1/32^{nd}$ of an inch was allowed, and baseplate side lengths and thicknesses were modeled as exactly 17" and 3/4", 1 ½", and 3". Weld profiles were simplified to be triangular with straight lines connecting the vertical and horizontal fillet weld legs. Anchor rods were

modeled by the root mean diameter as given by AISC, and leveling nuts were simplified to be circular.

As indicated in Figure 3.1.2.8, the solid portion of the model can be broken down into four subgroups including the anchor rods and nuts, the baseplate, the inner weld section, and the solid element tube wall section. The solid element portion of the BASE finite element model is most conveniently understood by examining the procedure used to create the solid mesh. Without the use of a fairly sophisticated pre and post processor the creation of the solid element portion of the BASE model may not have been possible. The capabilities of FeMap significantly decreased the time and difficulty in creating the large numbers of different models required in this project. In particular there were two mesh creation tools that were invaluable in creating the BASE finite element model. The first, the revolve function has already been described in the previous section. Previously it was used to create the shell element pole. The same function can be used with two dimensional plot only elements to revolve a series of concentric, solid elements, with a common axis of revolution. The second meshing tool used was an extrude function and is similar in concept. The function works the same exact way as the revolve function, but creates solid or shell elements by extruding plot only shell and beam elements. Between these two mesh creation function and with some careful planning prior to meshing, the BASE finite element model could be constructed with relative ease.

Figure 3.1.2.9 shows the two extrusion and revolution templates. Note that the different sub groups of the solid model as shown in Figure 3.1.2.8 are simply the result

of revolving or extruding different two dimensional elements. The solid element tubewall and the weld profile section are created by revolving the template shown in Figure 3.1.2.11. The baseplate, anchor rod, and anchor nuts are simply created by extruding the horizontal two dimensional element template shown in Figure 3.1.2.10. When using these two different techniques to build the separate sections of the model care must be taken to make sure that the end nodes and mid nodes of the different sub solid models align. In addition to modeling the complicated structural geometry these two solid meshing functions provided another benefit. It is well known that brick elements produced by the two techniques are much more desirable than tetrahedral solid elements created in automatic mesh generators. Using these two methods the user can control the element geometry and mesh refinement. It is also well known that solid brick elements are more reliable than similarly refined tetrahedral solid elements (Cook and others 2002).

A closer examination of the horizontal plane extrusion template in Figure 3.1.2.10, shows several significant features of the BASE model. First all elements are kept as close to a quarter inch cubic brick elements as possible. The mesh template is primarily constructed manually, and as can be seen it is not always possible to maintain perfect cubic elements. At some locations triangular and irregularly shaped elements are unavoidable. Also at some locations element size is larger or smaller than the intended element size. Symmetry was used about the diagonal plane, through the center of the pole to the center of the anchor rod, and about the mast-arm and perpendicular axis. A closer look at the revolved vertical template in Figure 3.1.2.11

shows several other critical features of the solid element portion of the BASE model. First the solid element tubewall portion of the model had only one element through the thickness, and subdivided the straight triangular upper fillet weld into 3 four sided (tapered bricks) elements. The lower fillet weld was simplified by clipping the corner of the lowest tubewall element. A gap was also modeled in all three specimen thicknesses, to capture the lack of fusion between the baseplate cut-out hole and the pole tubewall between the upper and lower fillet weld.

Another aspect of the solid model that needed to be simplified was the shape of the leveling nuts. It would not have been possible to record and model the exact orientation of the six sided leveling nuts, thus they were approximated by the average radius. The edge to edge distance of the leveling nuts was 2", and through geometry the average of the maximum and minimum radiuses was determined to be 2.16". The threaded anchor rods were modeled using the root minimum diameter by AISC as 1.08", which was verified. These and other pertinent leveling nut dimensions are shown in Figure 3.1.2.12. Figure 3.1.2.13 shows the anchor rod surface reactions. Note that the nodal reactions are located on the vertical surfaces of the anchor rods, providing reactionary forces in the horizontal plane. The nodal reactions on the bottom surfaces of the anchor rods provided a vertical reaction force. Stand off length is shown as the distance from the bottom of the leveling nut to the top line of applied reactions. Note also that the length of the anchor rods was maintained at 17" from the bottom of the lower leveling nut to bottom of anchor rod for all three specimens. The BASE model also used 1 5/8" for the stand-off length.

In Section 3.2, many different aspects of the solid model will be discussed in greater detail. Of the six modeling studies, only the hand access hole does not involve changes to the solid element finite element model. The other five modeling studies involve adjustments to the solid element portion of the BASE model, including: tube wall thickness adjustments, leveling nut simplifications, weld profile alterations, standoff length adjustments, and mesh refinement. The discussion of these studies follows in Section 3.2.

Portion 4 (Rigid Elements)

Providing continuity between solid and shell or shell and beam elements at the respective interfaces required rigid elements to be employed. Rigid Beam or specifically Abaqus's "MPC Beam" elements were used. These elements were able to transfer Axial, shear, and bending between the two elements, thus preventing discontinuities. At both interfaces in a time consuming manner, the rigid beam elements were applied at both corner and mid-side nodes. Figure 3.1.2.14 shows the solid element to shell element interface. Note the MPC beam elements create continuity between the lower solid element and shell element above it. A similar connection was made at the shell element to beam element interface using MPC beam rigid elements.

Section 3.2: Discussion of Experimental and Finite Element Stress

Prior to beginning the main objective of Chapter 3, to study and compare the experimental and finite element study results, the stress values and the methods used to determine these values must be discussed. This section briefly explains how the

experimental and finite element stresses that will be discussed, are determined, in addition to the assumptions made in determining these values. This section does not serve as a thorough discussion of experimental or finite element stress analysis. More advanced discussion on these topics can be found in Hetenyi's "Handbook of Experimental Stress Analysis" and the ABAQUS users' manual, as listed in the reference section (Hetenyi 1950) (Abaqus/Standard Users' Manual 2000).

Experimentally measured "stresses", don't refer to actual stresses directly measured by the gage. Rather, strains are measured and then converted into stress by Hook's Law. As mentioned in the Set-up section. Due to the moderate amount of hoop stress as determined in preliminary finite element models, the transverse sensitivity capabilities of the particular uni-axial strain gages are acceptable. Thus strain perpendicular to the primary gage axis will contribute negligible strain to the primary gage axis, as would be expected by Poisson's Law. Poisson's Law applies a strain to the primary gage axis equal to the negative of the perpendicular strain multiplied by the Poisson's ratio. Thus the tubewall gages which are positioned vertically on the inner and outer surfaces measure a pure axial strain. Considering the law of cosines, a small angular difference between the gage primary axis and true vertical will cause insignificant effect on the global Y or vertical strain measured. Using Hooke's Law these global vertical strains are converted into stress by multiplying by Young's Modulus, E. The stress units used in the study were ksi, unless noted otherwise.

Finite element stresses were obtained in a very similar manner. Nodal values of global Y or vertical strains were recorded and multiplied by Young's modulus E to obtain Normal Y stresses.

Section 3.3: Experimental and BASE Finite Element Results Comparison

Overall finite element data were in good agreement with experimental data. Considering the several factors that can affect the accuracy of the experimental data, the stresses calculated from the strains measured on the tube wall of the pole were quite good. Figure 3.3.1 illustrates the difficulties in the calibration and comparison of finite element data to experimental data. Experimental error can be broken down into two types. First experimental error is caused by variability in applying gages precisely to the intended gage location. In addition to this slight variation due to human error, the fact that the weld profile is constantly changing around the pole may also have some considerable effect on the data agreement. These two variations are magnified because the strains are measured in such severe strain gradients and thus a very high degree of precision is required. The second type of experimental error involves outlying data points, most likely the result of an improperly working gage. For example this type of experimental error could be caused by problems bonding the gages to the structure. Due to insufficient bond, the gage may measure the strain incompletely, but react as expected to the application and the removal of load. Given the number of gages used in the experimental test setup, there is a small chance that there will be some outlying experimental stress measurements. These outlying values though rare, may be considerably different than the expected values.

In addition to experimental error, similarly there is a level of modeling error that must be accepted. General modeling error may be result of something as simple as not modeling the structure with correct element types, insufficient mesh refinements, or using a modeled geometry that is not exactly the same as the dimensions of the actual structure. The other problem is that capturing the true behavior of the structure may be dependent on variable structure geometry (such as the slightly un-equal stand-off lengths of the anchor rods due to the roughness of the concrete), or complex contact and friction fixities. Modeling error also includes modeling these complex issues and random geometry with a simplified model. If the structural behavior is dependent on these complex and random conditions it may not be possible to simulate the exact behavior of the structure.

Due to experimental and modeling error it is unlikely to be able to have perfect data agreement. The objective of comparing the BASE finite element and experimental data is to better understand the insufficiencies of the model to improve the FINAL model comparison, and to better understand the structure behavior.

Finite element and experimental strain data from the anchor rods and base plate were (at gage locations previously discussed) were the exception to this good agreement. The likely role that several geometric irregularities in the actual structures, and anchor rod supports had on the experimental stresses in these locations will be discussed. Section 4.4 briefly discusses this problem with a focus on how the experimental test setup could have been improved. These irregularities are not the result of a negligent test set-up, but are rather most likely due to a set up process that

was not painstakingly meticulous, which is the case in the field, as will also be discussed. As defined in the scope, the objective of the research is focused on the fatigue performance of the welded socket joint, and the influence of baseplate flexibility, thus the somewhat irregular stresses in the anchor rods, and in the baseplate were not of paramount concern. The results show that the most drastic geometric and support irregularities will have a much more minor impact on stresses in the tubewall. For this reason, the experimental stresses in the anchor rods and baseplate gages, will not be discussed further and the paper will focus on the tubewall results.

Before beginning the discussion on the tubewall gage locations, comparing the trends in experimental and the finite element data from the base model BASE series for the three different baseplate thicknesses, it is important to note that the stress adjacent to the baseplate is highly localized and not easily generalized. As will be shown, trends in both the finite element and experimental data are different at different radial locations, as will be discussed in greater detail in Section 4.2.1. As preliminarily discussed in the experimental setup, the hotspot stress directly above the weld toe was not the only location that experimental stress was measured. To review the general gage plan and location nomenclature, strains were primarily measured at four different radial locations, C; 180, C; 45, T; 0, and T; 45. At these four locations strains were typically measured at heights above the baseplate of .75"(.875" for 3" thick baseplate specimen), 2", 3", 5", and 8", on both the outside and inside of the tubewall. Thus the complexity and number of different trends increases greatly. The following discussion compares the results of the BASE series finite element study

with the experimental results. The complex and multifaceted trends in the fit of the finite element data to the experimental data are discussed. The discussion primarily focuses on the hotspot stresses, measured just above the toe of the upper fillet weld. The following section will provide a concise discussion of the data agreement. The objective of the section is to briefly describe the shortcomings of the data agreement, which overall was good. Over analyzing the data agreement is not productive, due to the many different sources of error discussed in the beginning of this section. Additionally in order to fully understand the data agreement, it is important to compare the stress data not as an experimental verses an analytical value, but to examine the trends in stress data. In Section 4.2.1, the vertical distribution of axial stress is discussed, in which vertical stress profiles are displayed and discussed. In these profile plots both finite element and experimental stress values are shown. These plots clearly demonstrate the complexity and difficulty in obtaining perfect data agreement as the steep stress gradients and inflection zones are evident.

Tables 3.3.1-3.3.3 show a comparison of experimental and analytical BASE tubewall stresses and baseplate deflections, for the ¾", 1 ½", and 3" baseplate thickness test specimens. For each gage location of measured experimental stress, a gage number, whether the gage is measuring inner or outer stress, the radial location, the height above the baseplate, and the experimental and BASE finite element stress are given. Note, these charts only examine tubewall stresses from gage locations that were 0.75"/0.875", 2", and 5" above the baseplate.

In addition, at the bottom of each chart the mid baseplate deflection is given. This deflection is measured 1" from the edge of the baseplate on centerline on the compressive side of the pole. Baseplate deflection was under predicted by the BASE finite element models of both the ¾" and 1 ½" baseplate thickness specimens by 2.28 and 0.91 milli-inches (inch * 10^{-3}). The differences between the experimental and analytical deflections both represent approximately one quarter of each total experimental deflection. The 3" baseplate thickness specimen baseplate deflection was slightly over predicted by the finite element results compared to the experimental results. This slight disagreement is acceptable due to the measuring tolerance of the experimental test setup. The Linear Variable Distance Transducer, LVDT is able to measure very precisely, though the plunger due to the changing contact point with the baseplate may not be able to measure the exact deflection. In future discussions in Chapter 3, the concept that BASE finite element model was comparatively too stiff relative to the experimental results, will be explored. Though the baseplate deflection data does suggest that for some reason the test specimens with the more flexible baseplates do seem to have greater baseplate deflection compared to the BASE finite element results.

A quick inspection of the tubewall stress data of all three test specimens shown in Charts 3.3.1-3.3.3 indicates overall good data agreement. It also indicates the difficulty in examining and comparing the trends in agreement. A very clear trend is that the difference in experimental and analytical tubewall stresses is reasonably small in the 5" vertical gage location data. The hotspot location data, at the gage

location just above the upper fillet weld (0.75" above the baseplate for the ¾" and 1 ½" baseplate thickness specimens and 0.875" above the baseplate for the 3" baseplate thickness specimens) showed some considerable variations in experimental and analytical stresses. The gage data at the 2" location, in which stress was typically at an inversion point, as will be showed in Section 4.2.1, also in some instances showed considerable data agreement problems to a lesser degree than the hotspot stress data.

The hotspot stress data, given that the other data is in good agreement is the location of most concern and will be the focus of much of the following discussion. In order to briefly examine these trends in data agreement two approaches will be discussed. The first approach is to examine the data using a numerical or statistical approach. The second approach is to examine the data agreement as they relate to trends in stress and stress behavior over increasing baseplate thickness. Both approaches are helpful in understanding the data agreement.

The tubewall stress data of the three baseplate thickness specimens as previously discussed can be broken down into vertical gage location and specimen thickness to summarize the major trends in data agreement. Table 3.3.4 shows this effective summary presentation of the tubewall stress data. Note that the average absolute difference between the experimental and BASE finite element stresses for all of the 0.75", 2", and 5" data (including both inner and outer stress) is shown to decrease from 1.31 ksi for the ¾" baseplate thickness specimen to 0.32 ksi for the 1 ½" baseplate thickness specimen. The total average absolute difference between the experimental and BASE finite element stresses for all of the 0.75", 2", and 5" data

then slightly increases to 0.38 ksi for the 3" specimen. It is important to note that as seen in Tables 3.3.1-3.3.3 the values of hotspot stress considerably decrease with increasing baseplate thickness, thus the average absolute difference of 0.38 ksi for the 3" specimen makes up a considerably larger amount of the average experimental hotspot stress, than that of the 1 ½" baseplate thickness specimen.

Chart 3.3.4 also shows that the data agreement at the 2" and 5" gage locations is quite good. The average absolute difference between the experimental and BASE finite element stresses for all of the 2" and 5" tubewall stress data is consistently 0.15 ksi. By a simple visual inspection this difference represents less than 10% of the average experimental stress at the 2" and 5" gage locations. The final comparison of hotspot stress data is possibly the most significant, and provides a good summary of the issues of the next chart to be discussed. The trend in the average absolute difference between the experimental and BASE finite element stresses for the hotspot stress data, controls the trend in the total average absolute difference in stress data discussed above. Again there is a considerable decrease from the ¾" baseplate thickness specimen to the 1 ½" thickness specimen, as well as in increase in the average difference between the 1 ½" and 3" specimen, as indicated by the values in the table.

Table 3.3.5 displays the hotspot stress data results only from Tables 3.3.1-3.3.3, and allows for a better understanding of the results discussed in Table 3.3.4. The format of the table is identical to the first three tables discussed in this section. Two new columns of data are added. The first new column determines whether the

finite element data over or under predicts the experimental stress. Thus if the experimental stress is a compressive value of -2.49 ksi and the BASE finite element value is a greater compressive stress with a value of -5.64 ksi, the finite element result is defined to be an over prediction. The final column represents this over prediction by the absolute difference in the two stresses. In order to make the trends in the data more understandable, the highlights of the table are summarized below the table. As shown in the table the major trend in the ¾" specimen data is that the BASE finite element results consistently and considerably over predicted the experimental stresses at the direct tension and compression locations. This average over prediction of the hotspot stresses at the direct tensile and compressive radial location was 2.30 ksi. Conversely the BASE finite element results consistently and considerably under predicted the experimental stresses at the 45 degree tensile and compressive radial locations. This average under prediction of the hotspot stresses at the direct tensile and compressive radial location was 1.53 ksi.

The reason for this trend, as seen in the ¾" baseplate thickness specimen is clear. For example at the direct compression radial location the finite element results give a greater compressive outer stress value and a greater tensile inner stress value than the experimental data. This effectively increases the local bending stress, as was previously defined in Section 3.2. Thus the finite element model has more local bending stress in the direct tensile and compressive radial locations and less local bending stress in the 45 degree tensile and compressive radial locations as compared to the experimental data. Local bending stress and the radial distribution of local

bending stress according to finite element results will later be discussed in Section 4.2.1. One of the causes for the extra local bending stress is that the leveling nuts in the test setup were only wrench tightened by hand. Thus the connection permitted extra rigid body rotation of the baseplate at the leveling nuts, rather than bending occurring in the baseplate, which in turn induces the local bending stress. Section 4.3 will also address this issue with the test setup in regards to possible improvements that could have been made.

As previously seen in Table 3.3.4 the data agreement of the 1 ½" specimen was very good at the hotspot stress gage locations. Similarly in Table 3.3.5 it is seen that the data agreement is good, and that there are no observable trends in the data agreement. It is likely that the data agreement is predominantly affected by the human tolerances in gage application and variation in weld profile.

The 3" thick baseplate specimen shows an unexpected and unique trend in the data agreement. The outer stress at the hotspot stress location is shown to be in very good data agreement. The average absolute difference between experimental and BASE analytical stress data of the outer stress in the hotspot gage locations of the 3" specimens is 0.30 ksi. However the data agreement of the inner stress at the hotspot vertical gage locations is very poor as shown in Table 3.3.5. Note that at many locations the finite element stress is the opposite sign of the experimental inner stress, compressive instead of tensile, etc. This is very interesting as it is impossible that the tolerances in gage placement could be so severe as to cause such different stress behavior. As will be discussed as part of the calibration study, the influence of the

weld profile was studied. Limited study was made of the bottom fillet weld, though in one model studied a drastically different bottom fillet weld was evaluated. The results appeared to be quite similar to the typical model, thus suggesting that the geometry of the lower weld profile had little influence on the stress behavior in the tubewall. Again the problem with data agreement can be understood better by examining the data in a vertical stress profile plot as discussed in Section 4.2.1. Clearly it can be seen that the difference between the experimental data and the BASE finite element data can not be explained entirely by experimental error.

The best explanation that can be provided is that the difference in the lower weld geometry is slightly different than the lower weld geometry for a typical baseplate thickness. Another potential cause for the disagreement is that the local distortion of the tubewall may be introduced during the welding process. In the welding process either the upper or lower fillet weld is applied, in which great amounts of heat or expansion then contraction are applied to the socket connection. Thus the application of the second weld may induce some bending in the tubewall, which may be considerably greater than a connection with a standard thickness baseplate in which the distance between the upper and lower fillet welds is much smaller.

As previously discussed another approach to examining the data agreement between the experimental and analytical results is to look at the similarity of the trends in both sets of data. As there may be issues in the data agreement related to outlying data, which will affect one particular data point, the overall trends in both the BASE

finite element and experimental data should be compared. Figures 3.3.2 and 3.3.3 begin this approach examining the inner and outer hotspot stress data over increasing baseplate thickness. Note Figure 3.3.2 displays the experimental and BASE analytical hotspot stress data at the direct tension and compression radial locations over increasing baseplate thickness. Whereas Figure 3.3.3 displays the same comparison, only displaying results at the 45 degree tensile and compressive radial locations.

The most important comment to make about all of the plots is that overall, the data agreement of the finite element and experimental trends is very good. By examining the data trends rather than comparing single corresponding experimental and analytical values the accuracy of the finite element model can be assessed. For example, consider the case of comparing the experimental and BASE finite element inner hotspot stresses at the direct compression radial location (the upper plot in Figure 3.3.2) for a 3" baseplate thickness. Note that both the inner stresses for the 3" thick baseplate are very small, when compared to the same values for a 1 ½" or ¾"thick baseplate specimen. From this perspective the data agreement of the inner stress shows good agreement for thicker baseplates. However if one were to compare these two values numerically, the BASE finite element inner stress would be approximately half of the experimentally measured inner stress.

Another important issue regarding these four plots is the question of how to define outlying experimental and analytical data. As previously discussed, again it is shown that the data agreement for the ¾" thick specimen shows the greatest difference. This difference is by far the greatest at the direct compression radial

location as shown. It is very difficult to define exactly what is the outlying data. It is worth noting that the thinner the baseplate the more severe the strain gradient will be just above the weld toe. Thus the effects of gage placement tolerances have on data agreement also increases. Another related issue, involves comparing the results of the direct compression radial location plot to the results of the direct tension radial location plot. There is much better data agreement in the ¾" thick baseplate specimens for the direct tension radial location. The major difference between the two locations is that there is a hand access hole 13" above the baseplate at the direct tension location. Again it is impossible to know exactly why there is such a difference in the trends at the different location. It is possible that the difference in the two plots is indicating the presence of some type of local behavior due to leveling nut fixity in the ¾" thick specimen experimental data, which only occurred on the direct compressive radial location. This would be a significant conclusion, though due to the complexity of the behavior and the possibility that the experimental data could be inaccurate and only is given by a single gage no conclusions can be made.

Figure 3.3.4 displays similar plots, comparing and examining the trends in experimental and analytical mid-plane and local bending stress data over increasing baseplate thickness. Because both the mid-plane and local bending stresses rely on the inner and outer tubewall stress, it is arguable that if inaccurate inner and outer stress experimental data is given for one single gage location, that the mid-plane or local bending stress could be very inaccurate. The plots shown in the figures represent typical data agreement. Several other different locations and plots were examined and

evaluated during this comparison. Again the plots show that the trends are very similar, though not identical, as shown in the upper two plots. In addition it is very clearly seen that the comparison of single points of data can be slightly misleading with regards to the overall data agreement. The bottom plot in the figure, shows the local bending stress over increasing baseplate thickness. It is noted that for the ¾" baseplate thickness the BASE finite element results considerably over predict the actual experimentally measured local bending stress, as was previously discussed.

Section 3.4 Model Calibration

The three issues affecting modeling of sign structures discussed in Section 3.1, load path, contact and friction, and stress concentration are the common underlying theme in each of the six individual modeling studies. The six modeling studies examine the effect of tube wall thickness adjustments, leveling nut simplifications, weld profile alterations, standoff length adjustments, hand access hole reinforcing, and mesh refinement will be discussed. The objective of these studies and the model calibration study is primarily to better understand the modeled behavior of the specimens compared to the experimentally observed behavior of the structures. A major part of this better understanding involves determining the geometric variables which greatly influence tubewall stress behavior. Knowing which variables have the greatest influence on the behavior is important as to allow for extra attention to the critical variables. On a level of secondary importance, modeling geometry alterations that are found to improve the fit of the data may be incorporated in the final finite element series of models used in the final comparison to experimental data.

Having sufficient experimentally obtained data is critical in verifying which parameters influence finite element results, especially considering the occasional difficulty in data agreement. This difficulty was especially noted when dealing with the contact and friction modeling of the anchor rod/nut/baseplate connection. As previously mentioned, the issues and structural conditions of the specimens maybe so complicated and random it may not be possible to model the effects in a reasonable amount of time and effort. As previously discussed in the beginning of Section 3.3, complications in agreement between the finite element and experimental data are not limited to the modeling techniques and issues but include errors in the experimental data. At many locations the experimental strain data is measured in high stress gradients. At the gage location above the toe of the fillet weld the axial stress decrease at an approximate rate of 500 psi per 1/32" vertically up the pole. This extreme gradient unavoidably increases the potential for poor agreement between the measured and calculated data.

Many different finite element models were studied beginning several months prior to designing the test set-up and gage location plans. These preliminary models allowed for a very comprehensive understanding of the behavior of the structures, especially the local behavior at the baseplate. In these preliminary models several geometrical variations in the baseplate thickness, weld profile, and anchor rod to baseplate connection were considered. In addition to planning gage locations, these early series of models became invaluable in understanding many practical modeling problems, such as the level of refinement necessary to achieve consistent results, and

which factors had little effect on stresses and could be simplified to save analysis computational effort.

Prior to the experimental testing, a series of finite element models (for all three thicknesses) was studied. This series of models termed the BASE series represented the basic model that was determined through experience of the many earlier series of models. This series was primarily a direct geometric copy of structure geometry using a mesh refinement that was determined through experience. (Section 3.1 previously discusses the mesh sizes and simplifications used in great detail) The finite element strain and displacement data from the BASE series was compared to the experimental data for all three baseplate thicknesses in Section 3.3. Agreement between the finite element and experimental data was observed to be fairly good with larger deviation at the gage locations directly above the weld toe.

Several different parameters were varied to isolate the effects of various geometrical modifications. These modifications were of two types, ones that were justified as causing the finite element model to be more realistic, and others that were justified as adapting or calibrating the modeled geometry to behave more closely to the trends in the experimental data. Obviously careful observations of the trends in the data were made to select the modifications which improved agreement. The behavior of the baseplate to tubewall connection was deemed to be very complex, with stress fields possibly quite dependent on local effects, such as the exact conditions of the clamping force of the adjacent leveling nuts, erection imperfections such as the baseplate not being perfectly leveled, previous and undetectable out of plane

deformation to the tubewall, or variation in the fillet weld leg heights and widths, to name a few. These local effects could occur at random radial locations around the tubewall. Model calibration in the form of adjusting the geometry of the finite element models never considered these local variations, but rather applied one consistent geometry and set of boundary conditions.

Six main modeling alterations or calibrations were made: Tube wall thickness adjustments, weld profile alterations, standoff length adjustments, hand access hole reinforcing, mesh refinement, and leveling nut simplifications. The first four individual calibration studies will be discussed in Section 3.4.1. The calibration study and related work regarding the modeling simplifications used for the leveling nuts will be discussed in Section 3.4.2. Chapter 4 will begin with a brief summary of the results of the calibration study and any of the alterations discussed that were selected to be incorporated into the final finite element model.

Section 3.4.1: Calibration Study

Tube wall thickness

The finite element study examining the effect of tubewall thickness, stemmed from the uncertainty in accurately measuring specimen tubewall thickness local to the baseplate. The baseplate prevents measurement of the tubewall directly above the baseplate, using common, simple measuring devices. Using an ultrasonic depth meter the tubewall thickness was finally verified to be 0.23" inches just above the fillet weld. This value represents measurements at multiple locations, using the smallest dimension reading given by the depth meter. (When the depth meter is not held

perpendicularly to the curvature of a circular tube, it will measure extra thickness.) Initially this approximate value was measured at the top of the pole, using a digital micrometer, since it was the only location accessible to the measuring device. The depth meter thickness reading is in very good agreement with the micrometer readings of approximately 0.235". The "BASE" series model used a thinner tube wall thickness which was measured visually with a ruler. This thinner tubewall measurement was consistent with the specified values.

The influence tubewall thickness had on calculated stresses above the baseplate was studied by examining three different thicknesses. The finite element tubewall thicknesses were selected prior to using the depth meter to determine the actual tubewall thickness local to the baseplate. Models with tubewall thicknesses of 0.21875", 0.235", and 0.1875" were analyzed. The BASE series model had a tube wall thickness of 0.21875" (or 7/32"). Two additional models were chosen to be studied with either slightly larger or smaller tube wall thickness.

In general the purpose of each of the finite element studies is to determine how sensitive the structure is to the particular modeling variation. The degree of sensitivity determines the approach required to model the particular detail. If the finite element study shows the behavior of the structure is not sensitive to the detail, then severe attention to modeling the detail is not necessary. If the finite element results indicate that the structure is sensitive to a particular detail, the opposite approach must be taken. The actual detail must then be "quantified accurately" to obtain good agreement between experimental and finite element data. In the case of tube wall

thickness it is simple to utilize accurate measurement in the finite element model. However as will be later discussed particular details are difficult to quantify, and thus good judgment must be used in modeling and analyzing the detail. Obviously the exact measured dimension of the specimen tubewall thickness will be used in the model in this case.

The stress results of the various tubewall thickness finite element models are shown in Table 3.4.1.1. In terms of model calibration and possible alterations to the final model, the comparison of these values is somewhat unnecessary, as previously discussed the final model series will utilize the exact geometry of the structure. However it is critical though to understand how tolerances in measuring accuracy, as well as variability in the actual thickness of the structure can alter stress in the tubewall. It is also critical to understand the effects of small differences in tubewall thickness in terms of interpreting the data agreement between the finite element and experimental data. The overall purpose of this project is to examine the fatigue performance of the socket welded connection of the pole to the baseplate. The tubewall thickness will be shown to affect the fatigue performance. Hence tubewall thickness will be one of the design variables studied in the final parametric study to follow in Chapter 5. In this study a wider ranges of thickness will be examined, as the primary role of this current finite element study is to examine the role of small differences in tubewall thickness. However, the results of this study will provide base knowledge and be helpful in selecting tubewall thicknesses for the parametric study.

The stress results for the 100 pound cantilever end loading are shown, for gage location heights of 0.75", 2", and 5" above the ¾" thick baseplate. This particular finite element study was only conducted on the ¾" thick baseplate specimen. As the flexible ¾" thick baseplate specimen will accentuate the effects of tubewall thickness. Note the thick (t=0.235") and thin (t=0.1875") finite element models in tubewall thickness are respectively 0.01625" greater and 0.03125" less than the base model's tubewall thickness. Thus the increment of tubewall thickness is not constant. However, as shown in Figure 3.4.1.1 the relationship between hotspot stresses and baseplate deflection convincingly appears to be linear. Or at least appears to be linear under the small range of tubewall thicknesses. The plot shows selected outer hotspot stresses, though all of the gage locations exhibited a similar linear response.

As would be expected the stresses in the thick pole tubewall finite element model were reduced, and correspondingly the stresses in the thin pole tubewall finite element model were increased. Following the linear relationship shown in the plot, the average decrease as a percentage of the base finite element model was 94% for the thick tubewall model and 114% for the thin tubewall model, where the percentage of increase and decrease in stress is dependent on the amount of increase and decrease of the tubewall thickness, which is not at equal increments. The range in hotspot stress was quite large considering that the corresponding range in finite element tubewall thicknesses was only 0.0475". The range for inner and outer hotspot stresses at the direct compression and tension radial gage locations were 1.2 and 1.7 ksi respectively. And the average range in the hotspot stress data was 0.95 ksi. To a lesser, but still

considerable extent there was a large range in the stress data at gage locations 5" above the top of the baseplate, over the .05" variation in tubewall thickness. The average range in 5" stress data was 0.36 ksi. This is a very considerable range in the stress data, considering that it is only over difference in tubewall thickness that is less than $1/20^{th}$ of an inch, which would be difficult to measure with simple measuring tools. This range in stress is also quite large when considering its' percentage of the total stress, as the tubewall stresses 5" above the baseplate only range from approximately 1.0 to 2.0 ksi.

The value of the tubewall thickness to be used in the final model will be taken as the value measured by the ultrasonic depth meter, 0.23". The tubewall thickness finite element study has shown that differences in tubewall stresses are quite large over very small fluctuations in thickness. This sensitivity must be taken into consideration when examining data agreement, and will be further examined in the parametric study.

Mesh refinement

As discussed previously mesh refinement was well established through experience from the many series of models previously studied. However for the sake of completeness it was necessary to verify that the mesh refinement of the base model, was sufficient to provide consistent results. The process used in examining the role of mesh refinement essentially was a condensed convergence test. As the mesh refinement of the base model was deemed to be sufficient to provide accurate results by experience, only three refined finite element models were examined and compared

to the base model. If the base model was sufficiently refined for accuracy, then the new refined models would show nearly indistinguishable results. The three new refined models each refined a specific region of the base model, local to the pole to baseplate connection. By individually increasing the number of elements in specific locations, the base model could be checked for particular areas where mesh refinement was not sufficient to produce consistent results. The obvious benefit of examining the local mesh refinement of the base model was that the mesh would not be "over" refined, saving computation effort. Unfortunately due to time constraints the modeling refinement issue was only examined with the perspective of increasing mesh refinement. As will be seen the mesh refinement of the BASE model is sufficient to give adequate results. But it is quite possible that a lesser refined mesh could still give reasonable results, while reducing computational effort. Unfortunately though, the minimum level of mesh refinement required to give adequate results was not investigated.

A cross section of the ¾" thick baseplate specimen BASE model is shown in Figure 3.4.1.2. Note the typical vertical element height is 0.25", the other dimensions in the figure are proportional. In the figure only the portion of the cross section through the pole to baseplate connection is shown. As discussed in Section 3.1, the solid model geometry was created by revolving this plane around a central vertical axis. In this process it was possible to maintain all of the side lengths of the solid elements in this region to have a 0.25" side length. The other key features of the BASE model include: All of the solid elements local to the pole to baseplate

connection are all nearly 0.25". The cross section of the triangular upper fillet weld meshed with three 4-sided element cross sections, or 6-sided (20 node) brick elements. Also the element directly above the top of the fillet weld is subdivided in the global Y, vertical direction, into two elements with 0.125" element heights, as shown in the figure.

The first refined model analyzed is shown in Figure 3.4.1.3. The model was created by refining the BASE models region of solid tubewall elements, and is referred to as "DTW", shorthand for double tubewall thickness. As previously discussed the tubewall directly above the baseplate was modeled with solid elements, up to 11" above the baseplate. In the model DTW (double tubewall), these tubewall solid elements were subdivided radially through the tubewall cross section as shown. The tube wall element subdivision produced two element thicknesses through the thickness of the tubewall. This subdivision was extended all the way down to the bottom of the baseplate, as directed by the arrow in the figure. The justification for this refinement comes from the classic example of refinement convergence of bending in a beam. Solid elements, especially 1^{st} order, non parabolic elements, do have the tendency to be too stiff in bending, a result of parasitic shear. Thus with an increasing number of elements through the depth of the beam or thickness of the tubewall, the model improves its' ability to capture the bending.

The second refined model in the finite element mesh refinement study is shown in Figure 3.4.1.4. This model is referred to as REFIN, and is a logical extension of the mesh refinements made going from the BASE model to the DTW

model. In addition to providing two solid element thicknesses through the lower portion of the tubewall made of solid elements, additional solid elements were subdivided local to the baseplate to pole connection. As shown in the figure the elements making up the bottom section of tube wall were subdivided in the vertical, Global Y direction. These 0.125" vertical element height solid elements extended from the bottom of the baseplate to 1.25" above the top of the baseplate. In addition the upper fillet weld was also subdivided, creating elements with similarly sized cross sections. In addition to the solid elements directly below the upper fillet weld were subdivided into three elements across the horizontal leg of the fillet weld, as compared to two elements in the DTW model.

Note that in Figure 3.4.1.4, it appears that there are incompatible nodes, where adjacent element lengths are not the same such that nodes of one element do not share nodes of the adjacent element. Referring to the BASE model shown in Figure3.1.2.11, there is a gap between the continuation of the solid element tubewall and the baseplate, as indicated in the figure. This very small gap is somewhat difficult to see in Figures 3.4.1.2-3.4.1.4, but does exist between the elements. The gap shown in Figure 3.1.2.11 was exaggerated for illustration purposes.

The final model analyzed in the mesh refinement study examined the role of mesh refinement through the thickness of the baseplate. The typical vertical dimension of elements through the thickness of the baseplate was 0.25", with the other 2 dimensions kept as close to 0.25" as possible. This solid element cube size of 0.25" was attained through practical experience through studying many earlier series of

models. In order to verify the mesh refinement through the baseplate thickness of the base model additional element thicknesses were added. The model referred to as REFIN_BP utilized five 0.15" vertical element thicknesses through the baseplate thickness. In comparison to the BASE model which, utilized three elements through the base plate thickness, with vertical element thicknesses of 0.25". All other element dimensions in the horizontal plane remained the same as in the BASE model. A profile of the BASE and REFIN_BP finite element models are shown in Figures 3.4.1.5 and 3.4.1.6.

The results of the mesh refinement finite element study are shown in tabular format inTable 3.4.1.2. The particular stress results again relate to a 100 pound cantilever end load, and again only the results of ¾" baseplate thickness specimen are considered. As discussed, the refinement of the finite element mesh of the base model was selected based on a great deal of experience. The results are very indicative that this experience provided a level of mesh refinement able to provide consistent and accurate results. The average range in stress data for the hotspot and non hotspot stress data are 0.09 and 0.01 ksi respectively. This is a very acceptable range in stresses due to the different finite element mesh refinement schemes studied. According to the results of the mesh refinement study the future models used for final comparison to the experimental data will employ two solid elements through the tubewall thickness and a minimum of 4 element thicknesses through the baseplate thickness. The finite element models used in the parametric study will also utilize a similar mesh refinement.

Hand-Access-Hole

The finite element study of hand access hole geometry included the analysis and comparison of four models with different hand access hole geometry. The base model, which served as the primary model has been discussed in greater detail in section 3.1. As shown in Figure 3.4.1.7 the actual hand access hole has dimensions of approximately 11 ½" by 4 ½" and is located 13" above the top of the baseplate. Beginning at a height of 11" above the top of the baseplate, the tubewall is modeled using parabolic shell elements. Below which the structure was modeled entirely with parabolic solid elements. The hand access hole which is always on the direct tension side of the pole, is reinforced by a section of rounded rectangular tube of the same thickness as the pole (0.23"). The pole is cut out and the reinforcing tube is welded on the outside of the pole as shown in the photograph in Figure 3.4.1.7. Because the stress will be reasonably low in the reinforcement, the local behavior of the hand access hole is not a primary concern, and the impact the hand-access hole will have on the tubewall stress will be minimal a simple shell element to shell element connection was used to model the welded reinforcement. Even though this simple connection was used, it was still considerably difficult to create the model, as the pole shell elements are tapered. The BASE hand access hole geometry model, referred to again simply as BASE is shown in Figure 3.4.1.8.

There was reasonable confidence in the validity of this base model, especially considering its' lack of influence on critical stresses. Such that the finite element study of hand access hole geometry, was primarily interested in verifying this

modeling approach. Essentially there were two goals in this verification study: First to determine that for a wide range of modeled geometries there was little range in the results, such that it is not imperative to model the hand access hole exactly. Second was to verify that the base hand access hole geometry, was sufficiently stiff. This was a concern because the simple shell element to shell element connection would not account for the additional stiffness of the fillet weld used to connect the hand access hole reinforcement to the outside of the pole.

In addition to analyzing the base model with its simple shell element to shell element hand access hole geometry, three other hand access hole geometry models were studied. The other models included in the hand access hole finite element study were a doubly reinforced hand-access hole geometry, and two models with no hand access hole reinforcement at all. In order to examine a stiffer reinforcement geometry the doubly reinforced hand access hole model took the base hand access hole geometry and doubled the thickness of the shell elements in the reinforcement, and the pole shell elements surrounding the hand access hole as shown in the figure. This model is referred to as 2_HAH, and is shown in Figure 3.4.1.11. Note that in Figure 3.4.1.11 and 3.4.1.8 the relative thickness of the hand access hole shell elements are shown for illustrative purposes. The last two hand access hole geometry models differed in the shape of the non-reinforced hand access hole cutout. The finite element model referred to as 0_HAH utilized a hand access hole cutout identical to the BASE model geometry. The cutout as shown in the figure was a vertical rectangular shape with the corners clipped. The second hand access hole model utilized a cutout that

was plain vertical rectangle and was referred to as 0_HAH*. These two simple models attempted to determine whether the shape of the hand access hole had any influence on the tubewall stresses. The two hand access hole finite element models can be seen in Figures 3.4.1.9 and 3.4.1.10 respectively.

The comparison of the stress data of the four hand access hole geometry models is shown in tabular format in Table 3.4.1.3. Stress data for the 100 pound cantilever end load at the various radial locations around the tubewall, and at ¾", 2", and 5" above the top of the ¾" thick baseplate is displayed in this table. Overall the stresses and baseplate deflections were very similar between the four models, with fatigue critical stresses local to the fillet weld at the tubewall nearly identical. The modeling study proved to be very useful in ensuring that the hand access hole modeled geometry in the base model was sufficient as different modeled geometries would not influence the pertinent stress data.

The range in the stress and baseplate deflection data between the four different modeled hand access hole geometries is a good indicator of the limited influence the geometry has on tube wall stresses. Of the stress data examined in the study, only four locations show variation in stress to be greater than 200 psi, with many of the other locations with stress ranges less than 50 psi. As expected two of the four of these locations with modeled hand access geometry induced stress variations are located on the direct tension radial location below the hand access hole. The variation in finite element stress at the gage location 5" above the top of the baseplate, in the direct tension radial location was about 400 psi. And at the hotspot vertical location also in

the direct tension radial location the stress variation was roughly 250 psi. In addition there were two other hotspot gage locations where stress variations due to the different modeled hand access hole geometries, reached 200 psi, at the direct compression and 45 degree tension radial locations. In addition to these stress variations, there was also a noticeable variation in the baseplate deflection.

The data showed that the two non-reinforced hand access hole models 0_HAH and 0_HAH* behaved very similarly. This may indicate that the shape of the hand access hole doesn't affect the tubewall stresses drastically. This is significant in that due to the complexity of creating a mesh the smoothly curved hand access hole of the actual structure was simplified with straight segments and sharp corners. It was unavoidable that there is some difference in the shape of the modeled hand access hole geometry. However as a result of this study it would appear that the shape of the hand access hole does not drastically affect critical tubewall stresses.

The data also showed that the two models with reinforced hand access holes behaved similarly. The greatest difference in calculated stress between the double reinforced hand access hole geometry model and the base hand access hole model occurred at the direct tension radial location, 5" above the top of the baseplate. This gage location was the closest of all gage locations in the study to the hand access hole. The difference in outer stress was over 200 psi. However the stresses at the other gage locations especially hotspot gage locations were extremely similar for the two modeled geometries. Given this proximity in the stress data of the two reinforced hand access hole models, it was concluded that the base hand access hole geometry

was appropriate. This decision very much based on the close proximity of the finite element stress data of all of the modeled hand access geometries. And by default it can not be justified to double the thickness of the hand access hole reinforcement, nor remove it all together. In addition even if it was thought to be appropriate, it was shown that these changes would have little effect on the tubewall stresses anyway.

Stand off length

As previously discussed in the Section 3.1, regarding the basic geometric modeling techniques used, the modeled anchor rod to concrete constraint is highly simplified. Primarily the influence of vertical shear side friction on the anchor rods is neglected. Also the roller supports that restrain the modeled anchor rods from displacement in the horizontal plane are rigid. Where as in the actual structure, the concrete, which restrains the anchor rod is not rigid. Based on this difference in the restraints it would be logical that the modeled anchor rod stand-off length should be slightly greater than that of the actual structure. Considering that the tubewall stresses are not very sensitive to stand-off length, it is very reasonable that for practical purposes a finite element stand-off length of equal to actual is acceptable. And if not the modeled stand-off length would be assumed to not be considerably larger.

The finite element study of stand-off length considered four different stand-off lengths, S = 0.75", 1.625", 2.50", and 5.00". Surprisingly the stress and baseplate deflection data was linearly dependent on the stand-off length. Figure 3.4.1.12 shows many different separate trends in outer and inner stress at different gage locations over increasing stand-off length. For example at the compressive 45 degree location 5"

above the baseplate the outer and inner stress both gradually decrease, becoming more compressive. But at the direct compressive radial location at the hotspot vertical gage position, the inner stress gradually increases becoming more tensile while the outer stress gradually decreases becoming more compressive, thus increasing the local bending stress.

One significant trend in the finite element stand-off length study is that over reasonable stand-off lengths from 1 ½" to 2" according to the anchor rod constraint assumption made above there is realistically small range in the finite element tubewall stresses. An example of this realistically small range in hotspot stress is shown in Table 3.4.1.4. This typical range in stress is approximately 300 psi. Thus according to the finite element study, it may not be overly important to adjust modeled stand-off length to accommodate for the simplified modeled boundary conditions. Another significant trend in the stress data is that the influence of increased stand-off length increases the magnitude of all hotspot stresses thus increasing the local bending stress at all locations. The main deficiency in the finite element model is that it over predicts the local bending stress at the direct tension and compression locations (as it over predicts the magnitudes of the outer and inner stresses). Hence minimally increasing the bending equally at all locations due to the assumption of the boundary conditions can not be justified.

It is noted that stand-off length does slightly influence tubewall stresses, especially at unrealistically large stand-off lengths. However under realistic stand-off lengths little changes in tubewall stresses are created. In addition the minor increases

in tubewall stress don't improve the data agreement between the experimental and finite element data. Thus the actual stand-off length measured in the experimental test setup of 1 5/8" (and also used in the BASE model) will be used.

At this point it is worth briefly noting that a considerable amount of stress and deflection data were measured for the ¾" and 1 ½" baseplate thickness specimens, under different stand-off lengths. Over similar ranges in stand-off length, even smaller variation in tubewall stresses was observed. In fact many of the changes in tubewall stress due to changing stand-off length were found to be negligible due to the small fluctuation in the strain measuring instrumentation.

Weld profile

Another problem with the agreement between the calculated and experimental stress data is the inconsistency in hotspot stress data for the 3" thick baseplate specimen. As discussed data agreement improves greatly from the ¾" to 1 ½" thick baseplate specimens. However the trend does not continue with increasing baseplate thickness to the 3" thick specimen. In particular the inner hotspot finite element stresses from the BASE 3" model were in the poorest agreement to the experimental data. The previously mentioned explanation for this trend was that the tubewall stresses of the more flexible two baseplate specimens were dominated by the flexibility of the baseplate, rather than the stress concentration of the welded connection. But with the thicker baseplate this flexibility induced tube wall stress behavior diminishes and the tubewall stresses are then influenced predominantly by the stress concentration of the upper fillet weld. In this section of the calibration study

several different finite element weld profiles of both the ¾" and 3" thick specimen were examined. These finite element results were compared to the experimental results in hopes to improve the finite element modeling of the weld profile stress concentration, allowing for better data agreement.

Table 3.4.1.5 shows the results of slight alterations to the weld profile of the ¾" thick baseplate finite element model, primarily the concavity of the upper fillet weld. It was noted that the fillet weld of the test specimen is actually quite rounded off, as opposed to being a straight line from the vertical to horizontal leg. A photograph showing the profile of the upper fillet weld of the ¾" baseplate thickness specimen can is shown in Figure 3.4.1.1.3. Two different weld profile models were analyzed. They are referred to as WeldPRO and WeldPRO_2. As shown in Figure 3.4.1.14 WeldPRO_2 has a much more severe concavity or rounded upper fillet weld profile. For comparison the stress results for the base model termed "BASE" are also shown. Since making highly accurate measurements of the weld profile was not possible, as the dimensions of the profile did vary slightly at different locations, approximate concavities were used. As part of a separate and less important part of the weld profile study, another ¾" thick baseplate model with no bottom fillet weld was analyzed. The justification for analyzing this model was to see the extreme of the influence the bottom fillet weld and tubewall below the top of the baseplate have on tubewall stresses. The particular model, which is not shown is referred to as NoBW.

Table 3.4.1.5 shows the results of the weld profile finite element study on the ¾" baseplate thickness specimen. The results of the weld profile finite element study

showed an expected trend that smoothing out the jagged geometry of the weld profile would reduce the stress concentration. Altering the concavity of the weld profile had no effect on the tube wall stresses located 5" above the top of the baseplate. The stresses 0.75" and 2" did show variation due to the 3 different weld profile concavities. In a very consistent trend the outer and inner hotspot stresses for the first concavity model (WeldPRO) all decreased to approximately 90 percent of the BASE stress values, in which the upper fillet weld profile was simply modeled as a triangle. This 10 percent decrease in both inner and outer stress corresponds to a 10 percent decrease in bending stress. The results from the WeldPRO_2, or the most severely increased concavity model also showed decreased inner and outer hotspot stresses when compared to the first, lesser degree of concavity model. However this decrease was much less severe, showing the effect of continued increase in concavity diminishes. The 10 percent decrease in hotspot stresses may not seem like much, but was as much as a one ksi difference in stress at various locations in the ¾" thick baseplate specimen. Note the results of the finite element model without a bottom fillet weld (NoBW) surprisingly provide reasonable results when compared to the base ¾" model. This result is significant in that the lower fillet weld connection would seem not to be very important accurately modeling the tubewall stresses. For this reason the no further work was conducted studying the effect of the lower fillet weld

In addition to examining the role that modeled weld profile concavity had on tube wall stresses in the ¾" thick baseplate specimen, a similar finite element study was conducted on the 3" specimen. In this study two different concavities were

examined. However these weld concavity models both had increased vertical fillet weld lengths of 0.5625", instead of the 0.50" vertical fillet weld leg length used in the BASE models. These models are referred to as WeldPRO_VL and WeldPRO_2_VL. Again the second concavity model has more severely increased concavity as shown in Figure3.4.1.15. For comparison an upper weld geometry identical to WeldPRO_VL was studied only with the standard 0.50" vertical fillet weld height. This model is referred to as WeldPRO. In addition two other weld profile variations to the original base model were analyzed. These two models termed BASE A and BASE B, examined the influence of the length of the gap between the tube wall and baseplate tubewall cutout. The BASE A model shortened this gap slightly, and the BASE B model eliminated this gap, making the entire weld profile into one solid fixture. The differences between the BASE model and these two gap length models are illustrated in Figure 3.4.1.16.

The results of the concavity and weld profile finite element study of the 3" thick baseplate specimen showed a consistent trend in hotspot stress, as compared to the results for the ¾" thick baseplate. Table 3.4.1.6 presents this calibration study data for 3" thick baseplate specimen. The 3" specimen study showed that finite element tube wall stresses are not as sensitive to slight variations in the weld profile, as in the ¾" thick baseplate specimen. The results of the study show that while the weld profile of the 3" specimen does dictate the hotspot tubewall stresses, inaccuracies in modeling the weld profile do not account for the large differences in data agreement between the finite element and experimental data. Previously it was thought that the as the

baseplate stiffness was increased that the tubewall stresses were more sensitive to weld profile, explaining the poor data agreement. However the results of this particular study show that this is very unlikely.

The most positive result of the 3" baseplate thickness finite element weld profile study was that altering the weld profile, and hence the stress concentration, has little to no effect on the stresses 5" above the baseplate. This trend was also seen in the ¾" thick baseplate weld profile study, and with a stiffer baseplate it would be expected even more. Similar to the ¾" study, it was also found that with increasing concavity, or increasing the smoothness of the weld profile the bending stress at the direct tension and compression locations was reduced. The reduction in bending stress from the base model to the first and second concavity models showed considerably lesser decrease in stress. In both the direct compression and tension hotspot gage location the decrease in outer stress was only 0.13 ksi, or 94% of the outer finite element stress of the base model. The absolute value of decrease in bending stress at the hotspot gage locations, at the direct compression and tension locations, between the BASE model and the first concavity model is 0.18 ksi.

In addition to examining the role of concavity in the weld profile, in both the ¾" and 3" thick baseplate specimens, the weld profile study also took a brief, though incomplete look at vertical fillet weld leg height. The study examined the effect of the proximity of the hotspot gage location to the top of the vertical fillet weld. Comparing the stress results of the two pairs of concavity models, with a vertical fillet weld height of 0.50" and 0.5625" shows significant results. Again the data shows that there is

practically no difference in stress at the non hotspot gage locations, with varying vertical fillet leg heights. The difference in the hotspot stress is reasonably small, though noticeable. The largest difference in stress between the two different vertical fillet legs is seen at the direct tension and compression hotspot locations. The range in hotspot stress for both the outer and inner stresses is approximately 0.25 ksi for each stress. Thus the inner, outer, and local bending hotspot stresses increase by 0.25 ksi at the direct tension and compression locations when the vertical fillet leg is increased to 0.5625" from 0.50", a difference of $1/16^{th}$ of an inch.

These results certainly have many implications for the interpretation and study of data agreement. Through natural variation in the weld profile of the actual specimens and small human error in gage locations there are many opportunities for error of $1/16^{th}$ of an inch. Thus as previously discussed in multiple sections it would be expected that there would be a certain amount of scatter in the hotspot stress data agreement.

Finally the three inch weld profile study also included two models with different gap lengths as discussed above. The results showed that eliminating the gap between the tubewall and the baseplate pole cutout hole does alter the hotspot stress data, in the range of one tenth of a ksi. This variation in the stress data is not significant as to select either modeling option as correct, nor deem either modeling approach unacceptable. Thus the gap as discussed in Section 3.1 will remain in the final modeling technique.

Ultimately the results of the weld profile studies of both the ¾" and 3" thick baseplate specimens corrects the preconceived theory of the behavior, that fine changes to the weld profile alter the stresses in the tubewall. What the combined study on the ¾" and 3" specimen shows is that the supposed influence that concavity and various weld profiles had on the tube wall stresses in the ¾" specimen may not be entirely the results of the stress concentration effect, but may be caused by the change in flexibility as well. Note that because of the very thin and flexible baseplate, the weld profile, particularly the amount of solid material in the fillet weld makes a significant contribution the stiffness of the baseplate. Where as in the case of the 3" thick baseplate specimen, slight changes to the weld profile make only small changes to the overall stiffness of the baseplate, and thus there is very little difference in the tubewall stress data between the 3" specimen weld profile models. This conclusion is evident in examining the finite element baseplate deflections. For the ¾" specimen slight changes in the weld profile do create small differences in baseplate deflection. However in the 3" thick baseplate specimen models there is no difference in the baseplate deflections. Another key result of the study is the influence of the upper fillet weld leg lengths. The influence must be examined further in additional studies as due to time constraints the behavior is not fully understood. The stress concentration effect of the weld profile does however have a slight effect on tubewall stress. In the final modeling of the specimens more accurate upper weld profile dimensions will be considered, including the vertical and horizontal fillet weld leg lengths, and the concavity of the weld profile.

Section 3.4.2: Calibration Study (Leveling Nut Connection)

Leveling Nut Connection

The connection between the leveling nuts and baseplate became one of the most difficult aspects of the structure to model. For this reason it was decided to discuss this, the most significant finite element modeling study last. As previously shown in several different figures, the leveling nuts are the only component to transfer load from the baseplate to the anchor rods. Nearly 20 different variations and simplifications of this connection were studied in order to determine the most effective modeling technique and to achieve analysis results with the best possible agreement with the experimental data. Finite element analysis showed that the manner that the complicated connection was modeled could greatly alter the stress directly above the weld toe and moderately alter stresses at locations much higher up the tube wall. As discussed earlier in Section 3.1, contact elements were not incorporated into the finite element model, for several reasons. Primarily, that contact elements would be difficult to include in such a finely meshed model, and the distribution of the initial gaps and preload forces applied were essentially unknown.

Several factors complicate this connection. The major complication is because the connection is made entirely by contact and friction between the baseplate and leveling nut surfaces. Friction to a lesser extent affected the modeling and experimental issues related to the connection. As for the most part the baseplate is restrained from sliding against the leveling nuts. Though it was noted that during static load tests, especially for the thinner baseplates, (primarily the ¾" and

occasionally the 1 ½" thick baseplate) that upon completion of the test, the load having been removed, residual stresses still remained, and were at times as a large as several ksi directly above the weld toe. These stresses were likely the result of the baseplate sliding against the leveling nuts during the application of the load, and then upon the removal of the load failing to slide back. It was noted that by repeating the static tests these residual stresses diminished until they were negligible. This was most likely due to "shake-down" in the specimen and fixture.

With respect to modeling the friction between the leveling nuts and base plate surfaces, the infinitesimal amount of slip that might occur in the field was neglected. Friction was neglected primarily because in the structures natural setting corrosion and oxidation would occur to the surfaces increasing the friction and making it impossible for the baseplate to slip. Additionally an infinitesimal change in the position of the leveling nuts as the baseplate slipped would not drastically increase stress on the structure, the only additional stress would be due to the P-delta effect.

Modeling the complicated contact interaction between the leveling nuts and baseplate surfaces was more critical than friction, as it drastically affected the baseplate flexibility and stresses in the pole tubewall. The main difficulty in modeling the contact condition, is that the stresses applied throughout the interfaces of the two surfaces is not necessarily constant. To describe the leveling nut and baseplate surfaces to be in contact is actually quite vague, as the term contact only implies that they two surfaces exert pressure onto one another. Contact can range from complete preload contact, which occurs when the anchor rod has achieved its maximum preload

tension, to initial contact, which occurs as the leveling nut first makes contact with the baseplate as the nut is hand tightened. Initial contact will be discussed in greater detail shortly, as the condition was used to closely examine exactly how the ¾" baseplate actually makes contact with the leveling nuts. In initial contact, visual gaps can be seen between the leveling nuts and baseplate. In a perfect structure there would be no gaps, and the two surfaces would be exactly parallel. These gaps and contact points can be the result of many factors, primarily the out of straightness of the leveling nut surfaces due to out of straight anchor rods or the connection between the anchor rod threading and the leveling nut, height differences of the vertical position of the leveling nuts, and the deflected shape of the baseplate. Upon further tightening, the leveling nut visual contact occurs in which there are no longer any visible gaps between the leveling nuts and the baseplate. This mostly likely is misleading as the contact is still likely to be superficial, as the outer edges of the nuts and washers may be raised, but there still may be gaps between the two surfaces. After more tightening of the leveling nuts a condition of partial and full load bearing is reached. In this condition the pressure exerted on the baseplate by the leveling nuts is not equal. And finally if the leveling nuts are tightened to the maximum tensile capacity of the anchor rod, the contact between the two surfaces will approach a constant distribution of pressure.

As more complex elements were not used, the contact connection between the leveling nuts and baseplate was modified using two simple methods to alter the stiffness of the connection. The first method was to simply alter the stiffness property

of the material of the leveling nuts. This first method will be referred to as "leveling nut softening". The Young's modulus of the steel sign structures, was assumed to be 29,000 ksi. Without material testing this value was chosen, though it may be an under or over prediction. This first method simply altered the Young's modulus of the leveling nuts, to simulate a more flexible connection. The Young's modulus of the leveling nuts ranged from slightly greater than to much less than the assumed value.

The second method which was found to be more relevant to the experimental data, involved assuming the load bearing contact surface was less than the actual visual contact surface and adjusting the base model such that only the contact connection was a solid piece. Thus at locations of the contact interface where contact was superficial, and not transferring load, there was a physical gap in the model. This second method will be referred to as "partial leveling nuts". The benefit of the second approach is that the fixity of the baseplate can be altered to affect the flexibility of the baseplate at certain locations, where the soft leveling nut method is more limited. To verify these assumptions for this partial leveling nut method, the leveling nuts of the ¾" baseplate thickness specimen was closely examined. The results of this physical investigation, and the results of a pin supported finite element model, in addition to the ample amount of experimental data justify these simple modeling solutions and will be discussed further. The two modeling alteration methods and their results will be discussed.

Leveling Nut Softening

Adjusting the Young's modulus or the stiffness of the material of the leveling nuts proved insufficient in modeling the contact conditions between the leveling nuts and the baseplate. This conclusion became apparent by comparing the influence of a wide range of leveling nut material stiffness to the experimental data. As discussed previously the trend in the data fit was that the finite element data greatly over predicted the local bending stresses at the direct tension and compression gage locations, especially the ones directly above the weld toe. Essentially the model was allowing more local deformation at the baseplate to tubewall connection at these two locations. It was determined that it would be possible that the fixity the leveling nuts applied to the baseplate could be the cause of this difference between the model and the test specimens.

As expected the baseplate down lift deflection (on the compression side of the pole), measured one-half inch from the edge of the baseplate centerline, parallel with the mast-arm axis, increased with decreasing leveling nut stiffness. This baseplate down-lift deflection and similarly the corresponding up-lift deflection on the opposite side of the baseplate are good indicators of baseplate flexibility. The local bending stress behavior at the critical weld toe location is highly dependent on the relative rotation of the baseplate with respect to the tubewall. In order to achieve this small relative rotation the baseplate must deflect considerably at the point of the measured baseplate deflection. Figure 3.4.2.1 shows the relationship between baseplate deflection and leveling nut stiffness, E. The plot shows the resulting finite element baseplate deflection due to the standard 100 pound cantilever end load, over

decreasing leveling nut elasticity, E. As would be expected baseplate deflection at mid-baseplate drastically increases as the stiffness of the leveling nuts are reduced. The experimentally measured baseplate deflection for the ¾" specimen is also indicated in the plot. Considering the leveling nut Young's modulus to be the only factor influencing the baseplate deflection, a Young's modulus value of approximately 20,000 ksi corresponds to the experimental deflection.

Table 3.4.2.1 presents similar results in a tabular format. The BASE series finite element model was altered, simply by changing the Young's modulus, E of the leveling nut element material properties. The Young's modulus of the entire steel sign structure was assumed to be 29,000 ksi. Eight different values of E were used for the leveling nuts, ranging from 5,000 ksi to 33,000 ksi. The modeling study was performed and compared to experimental results to only the ¾" thick baseplate specimen, as it was assumed to be the most sensitive to baseplate flexibility, and thus most sensitive to the fixity of the leveling nuts. The experimental data was compared at the direct tension and direct compression radial locations in line with the mast-arm axis, as well as the 45 degree tension and compression radial locations in line with the anchor rods. The inner and outer stresses were compared at the gage locations 0.75", 2", and 5" above the top of the baseplate.

Table 3.4.2.1 visually shows this concept of matching the experimentally determined value of stress to a corresponding Young's modulus value of the leveling nut. This approach is certainly opposite to the actual model calibration process. In no way does the model calibration process involve random selection of variables, but is

helpful in further understanding the influence the leveling nut connection has on the pole stress behavior. For purposes of illustrating the structural behavior it is helpful to examine the improvements in data agreement, with respects to certain gage locations and different leveling nut stiffness. The table displays experimental stress values for static load testing of 100 pound cantilever loading. The stresses are given for all four radial gage locations, Comp180, Tens00, Comp45, and Tens45, and at heights above the baseplate of 0.75", 2" and 5". Shown to the right of the experimental stresses are the finite element results for the same static loading. The different columns represent the BASE series base model, with different values of leveling nut modulus of elasticity. The shaded finite element values represent the approximate value of modulus of elasticity which corresponds to the experimental stress value. When the experimental stress is such that the obvious trend in stress over elasticity implies that the value of elasticity required to yield the experimental stress is greater than 33000 then it was noted in the column marked "E greater than 33000".

The highlights shown in Table 3.4.2.1 very clearly suggests that the fixity and hence stiffness the leveling nuts impart on the baseplate may not be consistently applied in all directions. But rather the leveling nuts, which are not tightened to the capacity of the anchor rod, distribute stiffness to the tubewall to baseplate connection based on the contact between the leveling nuts and the baseplate. The definite trend of the data is that the experimental data at the direct tension and compression locations is better fit by finite element data with stiffer leveling nuts. But the experimental data at

the 45 degree radial locations in line with the anchor rods is better fit by finite element data with more flexible leveling nuts.

The same relationship between leveling nut stiffness and compression hotspot stress directly in line with the mast-arm and compressive stress in line with the anchor rods is visually shown in Figure 3.4.2.2. The figure presents the same behavior as previously discussed in the tabular format. The plot shows the trends of two random stresses due to decreasing leveling nut stiffness. These random stresses were taken from the finite element results in Table 3.4.2.1, but are unnamed to avoid confusion. Also shown are the experimentally observed stresses. Again it is clearly shown that the trend in stress behavior due to decreasing the material stiffness of the leveling nuts does not adequately account for data agreement of the stress data as a whole. As shown in the figure, the experimental value of Stress 1 could be obtained if the leveling nuts were modeled with much less stiff material properties. Though at the same time the trend clearly shows that Stress 2 would only be obtained if the leveling nuts were modeled with much stiffer material properties.

Physical Contact Study

In an effort to better understand the actual contact behavior of the leveling nut to baseplate connection a physical examination was conducted on the contact surface. In this simple study, feeler gages were used to determine if gaps between the two contact surfaces formed when leveling nuts were loosened. The need for the examination became apparent after the completion of the experimental testing and during the finite element calibration process. Finite element data showed that the

modeling simplification and assumptions used in recreating the leveling nut to baseplate connection could considerably alter pole tube wall stresses. In addition it was found that the several different approaches to the connection provided a range of different results. The main physical justification of these different modeling approaches, including leveling nut softening and the use of partial leveling nuts, is the complex contact behavior. Thus the physical examination would provide proof for this assumption.

The examination of all four anchor rods was performed on the ¾" thick baseplate specimen with the mast-arm attached. A stand-off length of approximately 1 5/8" was used, and the specimen was sanded at the approximate locations of contact, to remove excess corrosion, which had occurred since the specimen was tested. The general procedure was simply to loosen the "non contact leveling nut" (under the mast-arm dead load). Then retighten it by hand until the nut first encountered resistance from contacting the baseplate. Obviously in the experimental load testing, the leveling nuts were applying a much greater fixity to the baseplate. This loosely tightened condition was chosen to allow for the baseplate to displace as it would naturally. In the experimental condition in which the anchor rods were not likely to reach a full preload force, it might have been possible on a microscopic scale for the baseplate to flex as it would in this loosely tightened condition. The assumption made prior to examining the structure was that under this loosely tightened support condition, the contact between the leveling nuts and baseplate would represent the locations of maximum contact force under the full hand tightened condition. Thus by

using a feeler gage, which is nothing more than a very thin, and accurately measured strip of metal, to physically detect where contact and gaps occur at the baseplate to leveling nut contact interfaces.

In theory the physical examination was a very good practical solution to obtain actual structural measurements to support unique modeling solutions. One issue, which has been previously discussed as a possible source of poor data agreement, again hindered the conclusiveness of the physical examination of the leveling nut connection. This problem is the leveling and straightness (or out-of-straightness) of the baseplate and leveling nuts. This issue that became apparent in the experimental testing is not unrealistic to a structure in the field and pertains to the geometric perfection that the structure is erected with. Two major sources of erecting imperfection exist, how well the four pairs of leveling nuts and the baseplate are leveled, and the straightness of the baseplate, the leveling nuts, washers, and anchor rods. The purpose of the physical examination was to determine the areas of true contact between the leveling nuts and the baseplate, but the influence of either baseplate misalignment or baseplate/leveling nut/anchor rod out of straightness could really dominate the contact conditions of leveling nut connection.

To put the influence of erection imperfections into perspective imagine the following highly simplified hypothetical case illustrated in Figure 3.4.2.3 Consider a baseplate out of level by just 1/16" over the centerline-to-centerline anchor rod spacing of 14", and assume a deflected shape due to this imperfection as a rigid rotation, as the leveling nuts are in a loosely tightened condition, as they were in the

physical feeler gage examination. Thus for leveling nuts of approximately a diameter of two inches, the relative deflection between the two contact points would be (2"/12")*1/16" which is approximately 10 milli-inches. Experimentally it was shown that under fully hand tightened leveling nut connection conditions maximum baseplate deflection under static loading of the 100 pound cantilever loading of the ¾" thick baseplate was in the magnitude of only 9 milli-inches at the location of maximum baseplate deflection, at the baseplate centerline. Obviously this example highly simplifies the bending of the baseplate, and the degree of fixity or clamping force which was applied to the baseplate by the wrench tightened leveling nuts are very much unknown. Though as this example shows it is very possible that a very slight leveling imperfection could alter the contact conditions of the baseplate to leveling nut connection.

If the baseplate was perfectly level, and fixed by partially tight, wrench tightened leveling nuts the behavior of the contact would be much simpler and dominated by the deflected shape of the baseplate. The mechanism that would determine the contact between the baseplate and leveling nuts may be referred to as prying. Figure 3.4.2.4 illustrates this behavior. Note the figure shows a profile of the tension side of the baseplate. The tensile uplift action acts to deform the baseplate such that contact occurs as shown in the figure. Note that because the leveling nuts are not completely tightened there is room for very small deformations, indicated by the exaggerated spacing between the leveling nuts and the baseplate. Referring back to Figure 3.4.2.3, which showed the baseplate leveling imperfection influence on the

contact conditions of the baseplate, it is evident that the two contact behaviors act against each other.

Pinned Finite Element Model

It would appear that the contact conditions between the leveling nut pairs and the baseplate would be primarily dictated by baseplate leveling imperfections and prying. However the description of these two mechanisms influencing the contact conditions has only been explained in two dimensions. In order to examine the leveling nut contact behavior with a different approach a "pinned" restrained finite element model was studied. This "pinned" model eliminated the solid element leveling nuts and anchor rods. The anchor rod hole was filled in with solid elements with the same baseplate thickness, and a restraint in the global X,Y, and Z directions, pinned was added at all four of the anchor rod locations. Figure 3.4.2.5 shows the deflected shape of this model. Note the left tension anchor rod position is blocked off, as it will be the focus of the deflected shape study.

Figure 3.4.2.6 shows the plan view of the boxed off anchor rod location. Note the deflections are measured at the indicated points, with theta being measured as shown. The deflections are plotted below. Note that the maximum locations of deflection are shown for the baseplate in a fixity condition where it is free to rotate. Thus the pinned model shows that as expected the baseplates maximum deflection local to the leveling nuts will be in the direction of the maximum uplift or tension side of the baseplate. It is slightly angled in towards the center of the pole. The

corresponding location of maximum downward deflection occurs directly opposite of it.

The results of the physical feeler gage examination were not completely inconclusive. The results offer a direct account of the complexity of the actual connection, which can not be obtained in a finite element model. Using a finite element model with "pinned" support conditions as a guide assumptions about the contact surface were made, and will be discussed after the results of the feeler gage inspection. Actually the results of the inspection showed that contact surfaces were often located at locations as expected, based on the pinned finite element model, and contact assumptions of baseplate leveling imperfection and prying. Considering the effects of imperfections in the erection process, the results support these assumption reasonably well.

Figure 3.4.2.7 shows half of the results of the feeler gage leveling nut contact inspection. The results of the testing on the right and left compression anchor rods are presented. Note for both the left and right anchor rod, the gap locations are shown for both the top and bottom leveling nut. The complexity of the contact conditions between the leveling nuts and baseplate are evident. The two dashed line boxed in locations indicate that the gap locations would indicate prying contact conditions. The right compression bottom leveling nut gap locations is very indicative of the prying behavior discussed in Figure 3.4.2.4. In this particular compression location the opposite deflected shape would be expected and a gap should develop between the

bottom leveling nut to baseplate interface towards the outside left and right edge of the baseplate, which was observed in the feeler gage examination.

Partial Leveling Nuts

It was decided that a very simple, yet unconventional approach was the best alternative available to model the leveling nut to baseplate connection. By simply removing material from the leveling nuts from the non-load bearing locations, the contact pressure exerted on the baseplate was reasonably simulated. And the reduced stiffness of the hand tightened leveling nut to anchor rod connection was also simulated by less solid material in the model. More than 17 different modeled geometries were investigated in the process to better understand the connection. Several of these as modeled connections are shown in Figure 3.4.2.8. The calibration study for partial leveling nuts was primarily conducted by comparing finite element data with the ¾" thick baseplate experimental data. As the leveling nut connection will influence the stresses in fatigue critical tubewall locations the most when the baseplate is able to assume a more severe deflected shape, governed by the leveling nut connection fixity. By this logic the 3" thick baseplate model will be fairly insensitive to different modeled leveling nut connections. Thus the difference in hotspot tubewall stresses between the finite element modeled structures with and without partial leveling nuts will be greater in the ¾" baseplate models, when compared to the 3" thick baseplate models. Table 3.4.2.2 shows this trend displaying the comparison of the results of the BASE and a partial leveling nut model for the 3"

thick baseplate specimen. Comparing the difference in stress data between the BASE finite element models and the finite element models using partial wedge nuts, of the3" thick baseplate it can be clearly seen that the difference is not too severe. In many gage locations the difference is negligible. Thus it is quite obvious that in studying the effect of the leveling nut to baseplate connection, the trends in connection fixity will be more apparent if studied on the more flexible ¾" thick baseplate specimen. In addition as will be discussed this partial leveling nut solution will not be used in the parametric study. Because the effects of the partial leveling nut modeling technique are not significant in thicker baseplate specimens they will not be considered. Thus the partial leveling nut solution will only be utilized for the purpose of attempting to obtain the best possible data agreement in the final finite element comparison as discussed in the beginning of Chapter 4.

Table 3.4.2.3 displays the results of the partial leveling nut modeling option termed WN7. It is noted that the same partial leveling nut geometry was used in the previous table for the 3" baseplate thickness specimen. Figure 3.4.2.9 shows a close up of this partial leveling nut geometry. The geometry is such that it considerably decreases the rotational resistance of the full solid element leveling nut connection and uses 90 degree "wedges" placed in line with the anchor rod and the center of the pole, in locations consistent with prying as discussed above. The method used to select this partial leveling nut modeling option, simply involved examining the various modeling results with the experimentally obtained results. Several different modeling options proved to be effective in minimizing the differences in data agreement.

In summary of this task, two simple observations were made in this very large comparison of different data and partial leveling. The first observation showed that given the 17 different partial leveling nut modeling options, there were very large ranges in stress data. These large differences between different leveling nut modeling options, existed not only at the hotspot stress locations but in the gage locations 5" above the baseplate. The second observation seemed to suggest that any partial leveling nut modeling option was only minimizing the error in data agreement. Whether the difference in data agreement is due to local fixity effects of the leveling nuts or the experimental error is too great at certain locations it appears that there may be no simple modeling solution to the data agreement problem.

By examining the different connection types it becomes clear that the modeled connection type can be effective in minimizing the poor data agreement. Considering this numerical comparison of accuracy and the discussion of the simplified leveling nut behavior the model referred to as WN7 was selected as the most accurate method to model the leveling nut connection. However due to the problem discussed above and the fact that the different leveling nut connections do give similar results, this selection of a final leveling nut modeling simplification will be made cautiously.

Section 3.5: Finite Element Summary

Section 3.5.1: Summary of Data Agreement

Given the rather lengthy discussion of various finite element geometry studies, and comparison to the experiential data in Chapter 3, the difficulty in gaining perfect data agreement between finite element and experimental data is evident. Considering

the significant stress gradient, the degree of variability in the leveling nut to baseplate fixity conditions, the thin tubewall geometry itself, and many other factors, agreement between finite element and experimental data is difficult to attain. However as discussed in Section 3.2 overall data agreement is quite good. The data agreement suggests that local effects may play a role in stress behavior in the tubewall, adjacent to the socket connection. The primary goal of the finite element calibration study was to verify the modeling procedures and techniques as to allow for the parametric study to be discussed later in Chapter 5. The results of the lengthy calibration study of Chapter 3 and the future final finite element data comparison to experimental data will satisfactorily show that the results of the parametric study will be indicative of the static behavior of the structure over a wide range of baseplate flexibilities.

There were two major trends in data agreement observed that were not able to be resolved by the finite element calibration study. These trends may be the result of the leveling nut baseplate fixity conditions. Section 4.3 discusses a few different improvements to the test setup and instrumentation plan that may resolve these trends in data agreement.

- At direct tension and compression radial locations, outer, inner, and local bending tubewall stresses are drastically over predicted by finite element analysis, as discussed in Section 3.2. This over prediction is greatest in ¾" thick baseplate, and hotspot stresses at the direct radial locations are in reasonable agreement for 1 ½" specimen. Experimental stress data from the other vertical gage locations at the direct radial locations was shown to be in

good agreement. As well as the data from 45 degree radial locations, in line with the anchor rods, including hotspot gage location data, which was generally in good agreement with finite element stress data.

- Poor hotspot stress agreement becomes more evident in the 3" specimen data. The 3" specimen data is particularly confusing since the ¾" specimen data agreement is clearly the result of flexibility and local fixity conditions at the direct tension and compression locations. A good improvement in the hot spot stress agreement is achieved from the ¾" specimen to the 1 ½" specimen. Yet the improvement to data agreement diverges as the thickness increases to 3". The hotspot outer tubewall stress data appears to be in reasonable agreement. However the inner tubewall stresses are consistently in poor agreement. Though the magnitudes of both the experimental and analytical inner stresses are small compared to the corresponding ¾" specimen data, the experimental and analytical data disagree in the sense of stress (a tensile experimental inner hotspot stress corresponding to compressive analytical inner hotspot stress).

Section 3.5.2: Summary of Calibration Study

Tubewall thickness: Prior to beginning the calibration finite element study the most accurate tubewall measurement gave a thickness of 0.22". There was some uncertainty to whether this was an accurate measurement. The primary intent of the tubewall thickness calibration study was to investigate the influence of small changes in tubewall thickness. It was found that small changes in tubewall stress due to the

modified tubewall thicknesses were the result of the change of pole area and inertia, and not the stiffness of the pole. Using more advanced measurement tools a tubewall thickness of 0.23" inches was measured.

RESULT: The result of the study showed that tubewall thickness does not drastically influence tubewall stress beyond that would be expected due to the change in the cross section properties. The most accurate tubewall thickness measurement of 0.23" will be used in the final finite element geometry.

Mesh Refinement: Finite element data showed little to no change due to increasing refinement.

RESULT: Slight increases to the mesh refinement were made in the final series of finite element models, compared to the previous models of the calibration study. Particularly utilizing two elements through tubewall thickness and providing at least five elements through all baseplate thicknesses. The mesh size initially selected is adequate.

Hand Access Hole: Finite element data shows that various different as-modeled hand access hole geometries have little effect on hotspot stresses and some minor effect on stress data at gage locations closer to the hand access hole. The minor effects show little variation with different as-modeled hand access hole geometries.

RESULT: Use the simple shell to shell connection with measured dimensions of hand access hole reinforcement thickness, depth, height, and width.

Stand-off Length: FE data showed that a wide range of stand-off lengths will result in very small changes in tubewall stresses and baseplate deflections. Altering stand-off length to unreasonable dimensions didn't seem to improve the overall trend data agreement. Thus stand-off length as shown experimentally plays very little role in altering tubewall stresses.

RESULT: Use 1 5/8" stand off length as in BASE models, which represents the average measured stand-off length of the primary test setup.

Weld Profile: Increasing Concavity of weld profile, as is case in specimens shows limited effect in 3" specimens, and more noticeable effect in ¾" specimen. Reduction in local bending stresses in the ¾" specimen is fairly constant, approximately 750 psi. Reduction bending stress in 3" specimen seems to be more localized to direct tension and compression radial locations approximately 200 psi.

RESULT: Include weld profile concavity, and horizontal and vertical weld dimensions as much as possible due to measuring tolerances and variation in the weld profile.

Leveling Nut Connection: The leveling nut to baseplate connection is likely not completely fixed, as assumed in the BASE model. Through studying many different finite element connection modeling simplifications, one model referred to as WN7, seemed to improve data agreement, and fit into the discussed understanding of the connection behavior in Section 3.2.

RESULT: In final data comparison the final finite element model shall utilize this particular as-modeled connection, utilizing the WN7 partial leveling nut geometry. However the same model without the partial leveling nut connection was examined and provided nearly identical results.

Section 3.5.3: Summary of Final Finite Element Geometry

The following changes were made to the BASE finite element model for the final finite element comparison presented in the beginning of Chapter 4:

- Final modeled baseplate geometry will be the same for all 3 specimens as very small differences in measurements were rarely present, and differences were small enough to be result of limitations of measuring equipment.
- Square baseplate sides of 17", isosceles triangle cut-out of 1" by 1", anchor rod spacing of 14 3/16" will be used.
- All baseplate thickness measurements indicated that nominal thicknesses ¾", 1 ½", and 3" are appropriate.

- Tubewall thickness for all three pole specimens and hand access hole reinforcement will be taken as 0.23" as measured by the ultrasonic depth meter. A tubewall thickness of 0.18" will be used for the mast-arm specimen.
- Pole base diameters and tapers will be based on the individual specimen measurements, and not taken as one common pole geometry as in the BASE model analysis, even though differences are small. Base diameter and taper measurements will be converted into linear form;

  D [in] = base diam. - taper [in/ft] * Y

  Where the both the taper and base diameter are given accurate to the three significant figures. Thus modeled geometries will represent the measured geometries exactly. (See Section 2.1 for specimen diameters and tapers)
- For the final model to experimental data comparison, weld profile measurements will be made for all three specimens. One profile will be made representative of the average weld profile, as accurately as possible. (See section 2.1 for specimen weld profile geometry)
- The same finite element mesh baseplate horizontal plot only template will be used on all three models, with the outer nodes along the center pole cut-out, radially enlarged, or decreased to accommodate the given specimen.

3/4" Thick Baseplate Specimen

Gage #	Outside or Inside	Radial Location	Height above baseplate [in]	Exp. Stress [ksi]	Average if Necessary	FE Stress "BASE"
5	O	C.; 180 ;	5	-1.32		-1.46
6	I		5	-1.18		-1.30
11	O	C.; 180 ;	0.75	-2.49		-5.04
12	I		0.75	5.07		8.33
9	O	C.; 180 ;	2	2.34		1.91
10	I		2	-2.39		-2.43
15	O	T.; 0 ;	5	0.95		1.27
16	I		5	0.90		1.14
21	O	T.; 0 ;	0.75	3.88		4.84
22	I		0.75	-8.51		-8.08
19	O	T.; 0 ;	2	-2.52		-1.91
20	I		2	2.38		2.33
27	O	C.; 45 ; L	5	-1.82		-1.71
28	I		5	-1.61		-1.53
33	O	C.; 45 ; L	0.75	-11.76	-11.11	-8.30
34	I		0.75	9.08	8.85	6.64
45	O	C.; 45 ; R	0.75	-10.45		
46	I		0.75	8.62		
31	O	C.; 45 ; L	2	-0.38	-0.38	-0.53
32	I		2	-2.87	-2.87	-2.71
37	O	T.; 45 ; L	5	1.99		1.77
38	I		5	1.74		1.56
43	O	T.; 45 ; L	0.75	9.96	9.76	8.09
44	I		0.75	-7.84	-7.86	-6.47
23	O	T.; 45 ; R	0.75	9.56		
24	I		0.75	-7.87		
41	O	T.; 45 ; L	2	0.60	0.60	0.53
42	I		2	2.86	2.86	2.67
Baseplate Deflection [milli-inch]			LVDT	-9.17		-6.89

Table 3.3.1: Experimental and Analytical Data Comparison;
BASE Model, 3/4" Baseplate Thickness

1 1/2 " Thick Baseplate Specimen

Gage #	Outside or Inside	Radial Location	Height above baseplate [in]	Exp. Stress [ksi]	Average if Necessary	FE Stress "BASE"
8	O	C.; 180 ;	5	-1.35		-1.54
9	I		5	-1.34		-1.46
14	O	C.; 180 ;	0.75	-3.03		-3.74
15	I		0.75	4.14		4.23
12	O	C.; 180 ;	2	0.64		0.29
13	I		2	-2.04		-2.16
18	O	T.; 0 ;	5	1.17		1.30
19	I		5	1.16		1.25
24	O	T.; 0 ;	0.75	3.00		3.50
25	I		0.75	-3.14		-4.04
22	O	T.; 0 ;	2	-0.56		-0.35
23	I		2	2.02		2.00
38	O	C.; 45 ; L	5	-1.86		-1.57
39	I		5	-1.63		-1.43
44	O	C.; 45 ; L	0.75	-5.01		-4.52
45	I		0.75	1.90		2.41
42	O	C.; 45 ; L	2	-1.17		-0.93
43	I		2	-2.38		-2.02
28	O	T.; 45 ; R	5	1.74	1.85	1.63
29	I		5	1.50	1.60	1.46
46	O	T.; 45 ; L	5	1.96		
47	I		5	1.70		
34	O	T.; 45 ; R	0.75	4.88	5.06	4.35
35	I		0.75	-2.60	-2.65	-2.30
50	O	T.; 45 ; L	0.75	5.23		
51	I		0.75	-2.69		
48	O	T.; 45 ; L	2	1.11	0.95	0.92
49	I		2	2.34	2.21	1.98
32	O	T.; 45 ; R	2	0.80		
33	I		2	2.09		
Baseplate Deflection [milli-inch]			LVDT	-3.85		-2.94

Table 3.3.2: Experimental and Analytical Data Comparison;
BASE Model, 1 1/2" Baseplate Thickness

3 " Thick Baseplate Specimen

Gage #	Outside or Inside	Radial Location	Height above baseplate [in]	Exp. Stress [ksi]	Average if Necessary	FE Stress "BASE"
2	O	C.; 180 ;	5	-1.66		-1.75
3	I		5	-1.61		-1.67
6	O	C.; 180 ;	0.875	-2.44		-2.54
7	I		0.875	-1.17		0.75
4	O	C.; 180 ;	2	-0.58		-0.82
5	I		2	-2.12		-2.11
8	O	T.; 0 ;	5	1.23		1.44
9	I		5	1.24		1.40
12	O	T.; 0 ;	0.875	2.17		2.28
13	I		0.875	0.75		-0.73
10	O	T.; 0 ;	2	0.44		0.67
11	I		2	1.91		1.87
14	O	C.; 45 ; L	5	-1.53		-1.41
15	I		5	-1.39		-1.32
18	O	C.; 45 ; L	0.875	-2.97	-2.81	-2.38
19	I		0.875	-1.03	-0.99	0.21
20	O	C.; 45 ; R	0.875	-2.65		
21	I		0.875	-0.96		
16	O	C.; 45 ; L	2	-1.20	-1.20	-1.04
17	I		2	-1.78	-1.78	-1.60
22	O	T.; 45 ; L	5	1.71		1.47
23	I		5	1.48		1.35
26	O	T.; 45 ; L	0.875	2.65	2.66	2.26
27	I		0.875	0.98	0.96	-0.17
28	O	T.; 45 ;R	0.875	2.67		
29	I		0.875	0.95		
24	O	T.; 45 ; L	2	1.17	1.17	1.02
25	I		2	1.83	1.83	1.56
Baseplate Deflection [milli-inch]			LVDT	-1.42		-1.60

Table 3.3.3: Experimental and Analytical Data Comparison;
BASE Model, 3" Baseplate Thickness

	Total Avgerage Difference (ksi)	Y=2"&5" Avg. Diference (ksi)	Y=0.75 or 0.875" ** Avg. Diference (ksi)
3/4"	1.31	0.16	1.92
1 1/2"	0.32	0.15	0.49
3"	0.38	0.15	0.85

Table 3.3.4: Numeric Data Agreement Summary; Absolute Average Difference between Experimental and BASE FE Data, by Specimen and Vertical Gage Location

** Note due to different weld sizes of test specimens gage location nearest to vertical fillet weld is 0.75" above baseplate for 3/4" and 1 1/2" thick baseplate specimens, and 0.875" for 3" thick baseplate specimen.

	Gage #	Outside Inside	Radial Loc.	Height Above Baseplate [in]	Exp. Stress [ksi]	FE BASE Stress [ksi]	Over/ Under Prediction	Difference [ksi]
3/4" Thick Baseplate	11	O	C.; 180 ;	0.75	-2.49	-5.64	Over	3.15
	12	I		0.75	5.07	9.18	Over	4.11
	21	O	T.; 0 ;	0.75	3.88	5.43	Over	1.54
	22	I		0.75	-8.51	-8.90	Over	0.39
	33	O	C;45 ;Avg.	0.75	-11.76	-9.09	Under	2.67
	34	I		0.75	9.08	7.37	Under	1.70
	43	O	T.;45 ;Avg.	0.75	9.96	8.85	Under	1.10
	44	I		0.75	-7.84	-7.18	Under	0.66
1 1/2" Thick Baseplate	14	O	C.; 180 ;	0.75	-3.03	-3.58	Over	0.55
	15	I		0.75	4.14	3.98	Under	0.16
	24	O	T.; 0 ;	0.75	3.00	3.36	Over	0.36
	25	I		0.75	-3.14	-3.81	Over	0.66
	44	O	C;45 ;Avg.	0.75	-5.01	-4.42	Under	0.58
	45	I		0.75	1.90	2.15	Over	0.25
	34	O	T.;45 ;Avg.	0.75	4.88	4.26	Under	0.63
	35	I		0.75	-2.60	-2.05	Under	0.55
3" Thick Baseplate	6	O	C.; 180 ;	0.875	-2.44	-2.54	Over	0.10
	7	I		0.875	-1.17	0.75	Under	1.91
	12	O	T.; 0 ;	0.875	2.17	2.28	Over	0.11
	13	I		0.875	0.75	-0.73	Under	1.48
	18	O	C;45 ;Avg.	0.875	-2.97	-2.38	Under	0.59
	19	I		0.875	-1.03	0.21	Under	1.24
	26	O	T.;45 ;Avg.	0.875	2.65	2.26	Under	0.39
	27	I		0.875	0.98	-0.17	Under	1.15

Table 3.3.5: Hotspot (gage location closest to vertical weld toe) Stress Data Agreement Comparison

Table Summary

Average Over Prediction (By FE Over Exp. Value) at Direct Tension and Compression Radial Locations (3/4" Spec.) **2.30**

Average Under Prediction (By FE under Exp. Value) at Tension and Compression 45 degree Radial Locations (3/4" Spec.) **1.53**

Data Agreement for 1 1/2" Specimen Good. There is no drastic observable pattern in the data agreement

In the 3" specimen note the very poor agreement with the inside gages which are shown highlighted

3/4" Baseplate Thickness Specimen

					t =	0.21875" BASE	0.1875 (Thin)	0.235 (Thick)
Gage #	Out / Inside	Radial Loc.	Height Above Baseplate [in]	Exp. Stress [ksi]	Avg. if Nec.	FE BASE Stress [ksi]	FE ThTW Stress [ksi]	FE ThkTW Stress [ksi]
5	O	C.; 180;	5	-1.32		-1.50	-1.74	-1.40
6	I		5	-1.18		-1.33	-1.58	-1.25
11	O	C.; 180;	0.75	-2.49		-5.64	-6.40	-5.18
12	I		0.75	5.07		9.18	10.34	8.63
9	O	C.; 180;	2	2.34		2.01	2.17	1.87
10	I		2	-2.39		-2.54	-3.27	-2.24
15	O	T.; 0 ;	5	0.95		1.29	1.51	1.21
16	I		5	0.90		1.16	1.39	1.09
21	O	T.; 0 ;	0.75	3.88		5.43	6.19	4.95
22	I		0.75	-8.51		-8.90	-10.07	-8.36
19	O	T.; 0 ;	2	-2.52		-2.01	-2.17	-1.88
20	I		2	2.38		2.43	3.15	2.15
27	O	C; 45; L	5	-1.82		-1.80	-2.11	-1.68
28	I		5	-1.61		-1.60	-1.85	-1.51
33	O	C; 45; L	0.75	-11.76	-11.11	-9.09	-9.39	-8.75
34	I		0.75	9.08	8.85	7.37	7.51	7.29
45	O	C; 45; L	0.75	-10.45				
46	I		0.75	8.62				
31	O	C; 45; L	2	-0.38	-0.38	-0.58	-0.60	-0.60
32	I		2	-2.87	-2.87	-2.86	-3.52	-2.56
37	O	T; 45; L	5	1.99		1.87	2.17	1.74
38	I		5	1.74		1.64	1.90	1.54
43	O	T; 45; L	0.75	9.96	9.76	8.85	9.17	8.52
44	I		0.75	-7.84	-7.86	-7.18	-7.33	-7.10
23	O	T; 45; L	0.75	9.56				
24	I		0.75	-7.87				
41	O	T; 45; L	2	0.60	0.60	0.58	0.60	0.60
42	I		2	2.86	2.86	2.81	3.46	2.51
			LVDT	-9.17		-7.14	-7.42	-7.05

Table 3.4.1.1: Tubewal Thickness Calibration Study Results

FE ThTW	Thin tubewall thickness=0.1875"
FE ThkTW	Thick Tubewall thickness=0.235"
BASE	Standard Tubewall thickness=0.21875"

Average Range of Stress Values at Y=0.75"	0.95 ksi
Average Range of Stress Values at Y=5"	0.36 ksi
Average Increase in Stress of ThkTW ***	114%
Average Increase in Stress of ThTW ***	94%

*** Compared to BASE

3/4" Baseplate

Gage #	Out / Inside	Radial Loc.	Height Above Base-plate [in]	Exp. Stress [ksi]	Avg. if Nec.	FE BASE Stress [ksi]	FE REFIN Stress [ksi]	FE DTW Stress [ksi]	FE REFIN BP Stress [ksi]	Range [ksi]
5	O	C;180;	5	-1.32		-1.50	-1.49	-1.49	-1.50	0.01
6	I		5	-1.18		-1.33	-1.33	-1.33	-1.33	0.00
11	O	C;180;	0.75	-2.49		-5.64	-5.59	-5.51	-5.54	0.13
12	I		0.75	5.07		9.18	9.19	9.15	9.02	0.16
9	O	C;180;	2	2.34		2.01	2.00	2.00	1.99	0.02
10	I		2	-2.39		-2.54	-2.55	-2.54	-2.53	0.02
15	O	T;0;	5	0.95		1.29	1.29	1.29	1.30	0.00
16	I		5	0.90		1.16	1.16	1.16	1.16	0.00
21	O	T;0;	0.75	3.88		5.43	5.37	5.29	5.33	0.14
22	I		0.75	-8.51		-8.90	-8.91	-8.88	-8.76	0.16
19	O	T;0;	2	-2.52		-2.01	-2.01	-2.01	-1.99	0.02
20	I		2	2.38		2.43	2.45	2.44	2.42	0.03
27	O	C;45;L	5	-1.82		-1.80	-1.80	-1.80	-1.80	0.00
28	I		5	-1.61		-1.60	-1.60	-1.60	-1.60	0.00
33	O	C;45;L	0.75	-11.76	-11.11	-9.09	-9.04	-8.98	-9.06	0.00
34	I		0.75	9.08	8.85	7.37	7.40	7.40	7.34	0.00
45	O	C;45;L	0.75	-10.45						
46	I		0.75	8.62						
31	O	C;45;L	2	-0.38	-0.38	-0.58	-0.58	-0.58	-0.58	0.01
32	I		2	-2.87	-2.87	-2.86	-2.87	-2.87	-2.86	0.01
37	O	T;45;L	5	1.99		1.87	1.87	1.87	1.87	0.01
38	I		5	1.74		1.64	1.64	1.64	1.64	0.00
43	O	T;45;L	0.75	9.96	9.76	8.85	8.80	8.74	8.82	0.11
44	I		0.75	-7.84	-7.86	-7.18	-7.21	-7.20	-7.15	0.06
23	O	T;45;L	0.75	9.56						
24	I		0.75	-7.87						
41	O	T;45;L	2	0.60	0.60	0.58	0.58	0.58	0.58	0.01
42	I		2	2.86	2.86	2.81	2.82	2.81	2.81	0.01
	LVDT [milli-inch] (Baseplate Deflection)			-9.17		-7.14	-7.17	-7.17	-7.24	0.10

Table 3.4.1.2: Mesh Refinement Calibration Study Results
(Note See descriptions of mesh refinement in Section 3.4.1)

3/4" Baseplate

Gage #	Out / Inside	Radial Loc.	Height Above Base-plate [in]	FE BASE Stress [ksi]	FE 2_HAH Stress [ksi]	FE 0_HAH Stress [ksi]	FE 0_HAH* Stress [ksi]	Range [ksi]
5	O	C;180;	5	-1.50	-1.49	-1.50	-1.50	0.01
6	I		5	-1.33	-1.33	-1.34	-1.34	0.01
11	O	C;180;	0.75	-5.64	-5.58	-5.75	-5.77	0.19
12	I		0.75	9.18	9.11	9.32	9.35	0.25
9	O	C;180;	2	2.01	2.00	2.03	2.03	0.03
10	I		2	-2.54	-2.53	-2.56	-2.56	0.04
15	O	T;0;	5	1.29	1.39	1.06	0.98	0.40
16	I		5	1.16	1.24	0.99	0.93	0.31
21	O	T;0;	0.75	5.43	5.48	5.23	5.18	0.30
22	I		0.75	-8.90	-8.94	-8.73	-8.71	0.23
19	O	T;0;	2	-2.01	-2.00	-2.08	-2.10	0.10
20	I		2	2.43	2.46	2.34	2.31	0.15
27	O	C;45;L	5	-1.80	-1.79	-1.83	-1.84	0.05
28	I		5	-1.60	-1.59	-1.63	-1.63	0.04
33	O	C;45;L	0.75	-9.09	-9.08	-9.15	-9.16	0.08
34	I		0.75	7.37	7.37	7.41	7.42	0.04
45	O	C;45;L	0.75					
46	I		0.75					
31	O	C;45;L	2	-0.58	-0.56	-0.60	-0.60	0.03
32	I		2	-2.86	-2.85	-2.88	-2.88	0.03
37	O	T;45;L	5	1.87	1.82	2.00	2.05	0.23
38	I		5	1.64	1.60	1.74	1.77	0.16
43	O	T;45;L	0.75	8.85	8.87	8.88	8.89	0.04
44	I		0.75	-7.18	-7.21	-7.16	-7.16	0.05
23	O	T;45;L	0.75					
24	I		0.75					
41	O	T;45;L	2	0.58	0.56	0.63	0.65	0.08
42	I		2	2.81	2.80	2.84	2.85	0.05
	LVDT [milli-inch] (Baseplate Deflection)			-7.14	-7.10	-7.24	-7.26	0.16

Table 3.4.1.3: Hand Access Hole Geometry Calibration Study Results
(Note See descriptions of hand access hole geometries in Section 3.4.1)

3/4" Baseplate

			Stand-off Length *** (S):			S=0.75"	S=1 5/8"	S=2.5"	S=5"
Gage #	Out / Inside	Radial Loc.	Height Above Base-plate [in]	Exp. Stress [ksi]	Avg. if Nec.	FE Stress [ksi]	FE BASE Stress [ksi]	FE Stress [ksi]	FE Stress [ksi]
5	O	C;180;	5	-1.32		-1.54	-1.50	-1.43	-1.25
6	I		5	-1.18		-1.37	-1.33	-1.28	-1.13
11	O	C;180;	0.75	-2.49		-5.43	-5.64	-5.77	-5.99
12	I		0.75	5.07		8.76	9.18	9.55	10.38
9	O	C;180;	2	2.34		1.88	2.01	2.16	2.55
10	I		2	-2.39		-2.59	-2.54	-2.48	-2.36
15	O	T;0;	5	0.95		1.33	1.29	1.23	1.06
16	I		5	0.90		1.20	1.16	1.11	0.98
21	O	T;0;	0.75	3.88		5.22	5.43	5.57	5.78
22	I		0.75	-8.51		-8.49	-8.90	-9.27	-10.08
19	O	T;0;	2	-2.52		-1.89	-2.01	-2.15	-2.53
20	I		2	2.38		2.48	2.43	2.38	2.27
27	O	C;45;L	5	-1.82		-1.77	-1.80	-1.86	-1.99
28	I		5	-1.61		-1.58	-1.60	-1.64	-1.73
33	O	C;45;L	0.75	-11.76	-11.11	-8.70	-9.09	-9.54	-10.64
34	I		0.75	9.08	8.85	6.88	7.37	7.91	9.20
45	O	C;45;L	0.75	-10.45					
46	I		0.75	8.62					
31	O	C;45;L	2	-0.38	-0.38	-0.62	-0.58	-0.55	-0.49
32	I		2	-2.87	-2.87	-2.78	-2.86	-2.96	-3.20
37	O	T;45;L	5	1.99		1.84	1.87	1.92	2.06
38	I		5	1.74		1.62	1.64	1.68	1.77
43	O	T;45;L	0.75	9.96	9.76	8.48	8.85	9.29	10.36
44	I		0.75	-7.84	-7.86	-6.69	-7.18	-7.70	-8.95
23	O	T;45;L	0.75	9.56					
24	I		0.75	-7.87					
41	O	T;45;L	2	0.60	0.60	0.62	0.58	0.55	0.50
42	I		2	2.86	2.86	2.73	2.81	2.90	3.14
	LVDT [milli-inch] (Baseplate Deflection)			-9.17		-6.47	-7.14	-7.91	-9.90

Table 3.4.1.4: Stand-off Length Calibration Study Results

*** Stand-off length refers to the length of anchor rod between the top of the concrete foundation and the bottom of the bottom leveling nut.

3/4" Baseplate

Gage #	Out / Inside	Radial Loc.	Height Above Base-plate [in]	Exp. Stress [ksi]	Avg. if Nec.	FE BASE (3/4") Stress [ksi]	FE Weld _PRO (3/4") Stress [ksi]	FE Weld _PRO 2 (3/4") Stress [ksi]	FE NoBW (3/4") Stress [ksi]
5	O	C;180;	5	-1.32		-1.50	-1.49	-1.49	-1.61
6	I		5	-1.18		-1.33	-1.33	-1.33	-1.40
11	O	C;180;	0.75	-2.49		-5.64	-4.99	-4.87	-4.78
12	I		0.75	5.07		9.18	8.44	8.30	8.07
9	O	C;180;	2	2.34		2.01	2.00	2.00	1.88
10	I		2	-2.39		-2.54	-2.60	-2.60	-2.82
15	O	T;0;	5	0.95		1.29	1.29	1.29	1.41
16	I		5	0.90		1.16	1.16	1.16	1.23
21	O	T;0;	0.75	3.88		5.43	4.78	4.67	4.57
22	I		0.75	-8.51		-8.90	-8.20	-8.06	-7.82
19	O	T;0;	2	-2.52		-2.01	-2.01	-2.00	-1.89
20	I		2	2.38		2.43	2.50	2.50	2.73
27	O	C;45;L	5	-1.82		-1.80	-1.80	-1.80	-1.72
28	I		5	-1.61		-1.60	-1.60	-1.60	-1.55
33	O	C;45;L	0.75	-11.76	-11.11	-9.09	-8.45	-8.36	-9.00
34	I		0.75	9.08	8.85	7.37	6.71	6.61	7.63
45	O	C;45;L	0.75	-10.45					
46	I		0.75	8.62					
31	O	C;45;L	2	-0.38	-0.38	-0.58	-0.55	-0.56	-0.49
32	I		2	-2.87	-2.87	-2.86	-2.97	-2.99	-2.72
37	O	T;45;L	5	1.99		1.87	1.87	1.87	1.79
38	I		5	1.74		1.64	1.64	1.64	1.60
43	O	T;45;L	0.75	9.96	9.76	8.85	8.22	8.15	8.76
44	I		0.75	-7.84	-7.86	-7.18	-6.53	-6.44	-7.43
23	O	T;45;L	0.75	9.56					
24	I		0.75	-7.87					
41	O	T;45;L	2	0.60	0.60	0.58	0.55	0.56	0.50
42	I		2	2.86	2.86	2.81	3.08	2.93	2.68
	LVDT [milli-inch] (Baseplate Deflection)			-9.17		-7.14	-7.32	-7.37	-7.57

Table 3.4.1.5: Weld Profile Calibration Study Results for the 3/4" Baseplate Thickness Specimen

3 " Baseplate

Gage #	Out / Inside	Radial Loc.	Height Above Base-plate [in]	Exp. Stress [ksi]	Avg. if Nec.	FE BASE (3") Stress [ksi]	FE BASE A (3") Stress [ksi]	FE BASE B (3") Stress [ksi]	FE WELD PRO (3") Stress [ksi]	FE WELD _PRO _VL (3") Stress [ksi]	FE WELD _PRO_2 _VL (3") Stress [ksi]
2	O	C;180;	5	-1.66		-1.85	-1.85	-1.85	-1.85	-1.85	-1.85
3	I		5	-1.61		-1.76	-1.76	-1.76	-1.76	-1.76	-1.76
6	O	C;180;	0.875	-2.44		-2.39	-2.38	-2.29	-2.26	-2.52	-2.37
7	I		0.875	-1.17		0.36	0.34	0.21	0.12	0.41	0.24
4	O	C;180;	2	-0.58		-0.90	-0.90	-0.92	-0.91	-0.90	-0.91
5	I		2	-2.12		-2.28	-2.28	-2.27	-2.28	-2.27	-2.27
8	O	T;0;	5	1.23		1.52	1.52	1.52	1.52	1.52	1.52
9	I		5	1.24		1.48	1.48	1.48	1.48	1.48	1.48
12	O	T;0;	0.875	2.17		2.15	2.13	2.05	2.02	2.26	2.12
13	I		0.875	0.75		-0.39	-0.37	-0.25	-0.16	-0.43	-0.26
10	O	T;0;	2	0.44		0.74	0.74	0.77	0.75	0.74	0.75
11	I		2	1.91		2.03	2.03	2.02	2.03	2.02	2.02
14	O	C;45;L	5	-1.53		-1.49	-1.49	-1.49	-1.49	-1.49	-1.50
15	I		5	-1.39		-1.40	-1.40	-1.40	-1.40	-1.40	-1.40
18	O	C;45;L	0.875	-2.97	-2.81	-2.30	-2.29	-2.23	-2.23	-2.41	-2.31
19	I		0.875	-1.03	-0.99	-0.07	-0.09	-0.20	-0.21	-0.02	-0.13
20	O	C;45;L	0.875	-2.65							
21	I		0.875	-0.96							
16	O	C;45;L	2	-1.20	-1.20	-1.11	-1.11	-1.13	-1.11	-1.11	-1.11
17	I		2	-1.78	-1.78	-1.73	-1.73	-1.72	-1.74	-1.73	-1.73
22	O	T;45;L	5	1.71		1.56	1.56	1.56	1.56	1.56	1.56
23	I		5	1.48		1.43	1.43	1.43	1.44	1.43	1.44
26	O	T;45;L	0.875	2.65	2.66	2.19	2.17	2.11	2.12	2.28	2.20
27	I		0.875	0.98	0.96	0.10	0.13	0.23	0.24	0.06	0.16
28	O	T;45;L	0.875	2.67							
29	I		0.875	0.95							
24	O	T;45;L	2	1.17	1.17	1.09	1.09	1.11	1.09	1.09	1.09
25	I		2	1.83	1.83	1.69	1.69	1.68	1.70	1.69	1.69
LVDT [milli-inch] (Baseplate Deflection)				-1.42		-1.66	-1.65	-1.65	-1.66	-1.66	-1.66

Table 3.4.1.6: Weld Profile Calibration Study Results for the 3" Baseplate Thickness Specimen

3/4" Baseplate (Stresses Calc. from Solid Y normal Strains)

(E = 29,000 ksi)

Gage #	Out / Inside	Radial Loc.	Height Above Base-plate [in]	Exp. Stress [ksi]	Avg. if Nec.	E Greater than 33000	SLN E=31,000 ksi	SLN E=33,000 ksi	FE BASE Stress [ksi]	SLN E=26,667 ksi	SLN E=26,667 ksi	SLN E=26,667 ksi	SLN E=26,667 ksi	SLN E=26,667 ksi
5	O	C180	5	-1.32			-1.3	-1.4	-1.5	-1.6	-1.8	-1.9	-3.1	-8.7
6	I		5	-1.18			-1.2	-1.2	-1.3	-1.4	-1.6	-1.7	-2.7	-7.8
11	O	C181	0.75	-2.49		> than	-4.9	-5.2	-5.6	-6.1	-6.6	-7.3	-11.4	-31.5
12	I		0.75	5.07		> than	8.0	8.5	9.2	9.9	10.8	11.9	18.6	51.7
9	O	C182	2	2.34			1.7	1.9	2.0	2.2	2.4	2.6	4.1	11.4
10	I		2	-2.39			-1.9	-2.4	-2.5	-2.7	-3.0	-3.3	-5.2	-14.4
15	O	T 00	5	0.95		> than	1.1	1.2	1.2	1.4	1.5	1.7	2.8	8.2
16	I		5	0.90		> than	1.0	1.1	1.3	1.3	1.4	1.5	2.5	7.3
21	O	T 01	0.75	3.88		> than	4.7	5.0	5.4	5.9	6.4	7.1	11.2	31.3
22	I		0.75	-8.51			-7.7	-8.2	-8.9	-9.6	-10.5	-11.6	-18.3	-51.1
19	O	T 02	2	-2.52			-1.7	-1.9	-2.0	-2.2	-2.4	-2.6	-4.1	-11.3
20	I		2	2.38			2.1	2.3	2.4	2.6	2.9	3.2	5.0	14.2
27	O	C45L	5	-1.82			-1.6	-1.7	-1.8	-1.9	-2.1	-2.4	-3.7	-10.2
28	I		5	-1.61			-1.4	-1.5	-1.6	-1.7	-1.9	-2.1	-3.3	-9.0
33	O	C45L	0.75	-11.76	-11.11		-7.9	-8.4	-9.1	-9.8	-10.7	-14.3	-18.7	-52.5
34	I		0.75	9.08	8.85		6.4	6.8	7.4	7.9	8.7	9.6	15.2	42.7
45	O	C45R	0.75	-10.45										
46	I		0.75	8.62										
31	O	C45L	2	-0.38	-0.38	> than	-0.5	-0.5	-0.6	-0.6	-0.7	-0.8	-1.2	-3.2
32	I		2	-2.87	-2.87		-2.5	-2.6	-2.9	-3.1	-3.4	-3.7	-5.9	-16.5
37	O	T45L	5	1.99			1.6	1.7	1.9	2.0	2.2	2.4	3.8	10.2
38	I		5	1.74			1.4	1.5	1.6	1.8	1.9	2.1	3.3	9.1
43	O	T45L	0.75	9.96	9.76		7.7	8.2	8.9	9.5	10.5	11.6	18.2	51.2
44	I		0.75	-7.84	-7.86		-6.2	-6.6	-7.2	-7.7	-8.5	-9.4	-14.8	-41.7
23	O	T45R	0.75	9.56										
24	I		0.75	-7.87										
41	O	T45L	2	0.60	0.60		0.5	0.5	0.6	0.6	0.7	0.8	1.2	3.2
42	I		2	2.86	2.86		2.4	2.6	2.8	3.0	3.3	3.7	5.8	16.1
LVDT [milli-inch] (Baseplate Deflection)				-9.17			-6.2	-6.6	-7.1	-7.7	-8.4	-9.3	-14.5	-40.5

Table 3.4.2.1: Leveling Nut Material Property "Softening" Calibration Study Results for the 3" Baseplate Thickness Specimen

3 " Baseplate

Gage #	Out / Inside	Radial Loc.	Height Above Base-plate [in]	Exp. Stress [ksi]	Avg. if Nec.	FE BASE (3") Stress [ksi]	FE WN7 (3") Stress [ksi]	Difference [ksi]
2	O	C.; 180 ;	5	-1.66		-1.85	-1.83	0.03
3	I		5	-1.61		-1.76	-1.75	0.02
6	O	C.; 180 ;	0.875	-2.44		-2.39	-2.34	0.05
7	I		0.875	-1.17		0.36	0.31	0.05
4	O	C.; 180 ;	2	-0.58		-0.90	-0.90	0.01
5	I		2	-2.12		-2.28	-2.24	0.04
8	O	T.; 0 ;	5	1.23		1.52	1.49	0.03
9	I		5	1.24		1.48	1.45	0.03
12	O	T.; 0 ;	0.875	2.17		2.15	2.13	0.02
13	I		0.875	0.75		-0.39	-0.65	0.26
10	O	T.; 0 ;	2	0.44		0.74	0.57	0.17
11	I		2	1.91		2.03	2.07	0.04
14	O	C.; 45 ; L	5	-1.53		-1.49	-1.51	0.01
15	I		5	-1.39		-1.40	-1.41	0.01
18	O	C.; 45 ; L	0.875	-2.97	-2.81	-2.30	-2.29	0.02
19	I		0.875	-1.03	-0.99	-0.07	-0.18	0.11
20	O	C.; 45 ; R	0.875	-2.65				
21	I		0.875	-0.96				
16	O	C.; 45 ; L	2	-1.20	-1.20	-1.11	-1.17	0.06
17	I		2	-1.78	-1.78	-1.73	-1.71	0.02
22	O	T.; 45 ; L	5	1.71		1.56	1.59	0.03
23	I		5	1.48		1.43	1.45	0.02
26	O	T.; 45 ; L	0.875	2.65	2.66	2.19	2.33	0.15
27	I		0.875	0.98	0.96	0.10	-0.07	0.17
28	O	T.; 45 ;R	0.875	2.67				
29	I		0.875	0.95				
24	O	T.; 45 ; L	2	1.17	1.17	1.09	1.05	0.03
25	I		2	1.83	1.83	1.69	1.78	0.09
	LVDT [milli-inch] (Baseplate Deflection)			-1.42		-1.66	-1.85	0.19

Table 3.4.2.2: Leveling Nut Calibration Study Results; 3" Baseplate thickness specimen comparision BASE and WN7

3/4" Baseplate

Gage #	Out / Inside	Radial Loc.	Height Above Base-plate [in]	Exp. Stress [ksi]	Avg. if Nec.	FE BASE (3/4") Stress [ksi]	FE WN7 (3/4") Stress [ksi]	Difference [ksi]
5	O	C.; 180 ;	5	-1.32		-1.50	-1.29	0.20
6	I		5	-1.18		-1.33	-1.17	0.16
11	O	C.; 180 ;	0.75	-2.49		-5.64	-5.46	0.18
12	I		0.75	5.07		9.18	9.55	0.38
9	O	C.; 180 ;	2	2.34		2.01	2.38	0.37
10	I		2	-2.39		-2.54	-2.39	0.15
15	O	T.; 0 ;	5	0.95		1.16	1.10	0.06
16	I		5	0.90		1.29	1.01	0.28
21	O	T.; 0 ;	0.75	3.88		5.43	5.27	0.16
22	I		0.75	-8.51		-8.90	-9.28	0.38
19	O	T.; 0 ;	2	-2.52		-2.01	-2.37	0.36
20	I		2	2.38		2.43	2.30	0.14
27	O	C.; 45 ; L	5	-1.82		-1.80	-1.95	0.14
28	I		5	-1.61		-1.60	-1.71	0.11
33	O	C.; 45 ; L	0.75	-11.76	-11.11	-9.09	-10.14	1.05
34	I		0.75	9.08	8.85	7.37	8.29	0.92
45	O	C.; 45 ; R	0.75	-10.45				0.00
46	I		0.75	8.62				0.00
31	O	C.; 45 ; L	2	-0.38	-0.38	-0.58	-0.64	0.06
32	I		2	-2.87	-2.87	-2.86	-3.09	0.22
37	O	T.; 45 ; L	5	1.99		1.87	2.01	0.14
38	I		5	1.74		1.64	1.75	0.11
43	O	T.; 45 ; L	0.75	9.96	9.76	8.85	9.88	1.03
44	I		0.75	-7.84	-7.86	-7.18	-8.07	0.89
23	O	T.; 45 ; R	0.75	9.56				0.00
24	I		0.75	-7.87				0.00
41	O	T.; 45 ; L	2	0.60	0.60	0.58	0.65	0.07
42	I		2	2.86	2.86	2.81	3.03	0.22
	LVDT [milli-inch] (Baseplate Deflection)			-9.17		-7.14	-8.66	1.52

Table 3.4.2.3: Leveling Nut Calibration Study Results; 3/4" Baseplate thickness specimen comparision BASE and WN7

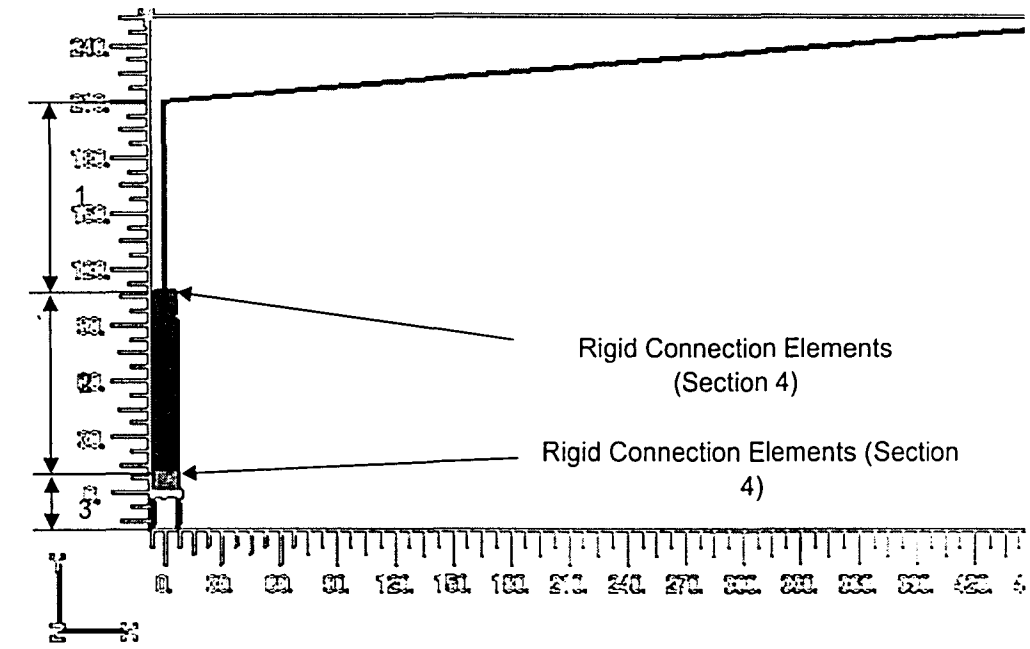

Figure 3.1.2.1: Basic Geometry of BASE Finite Element Model

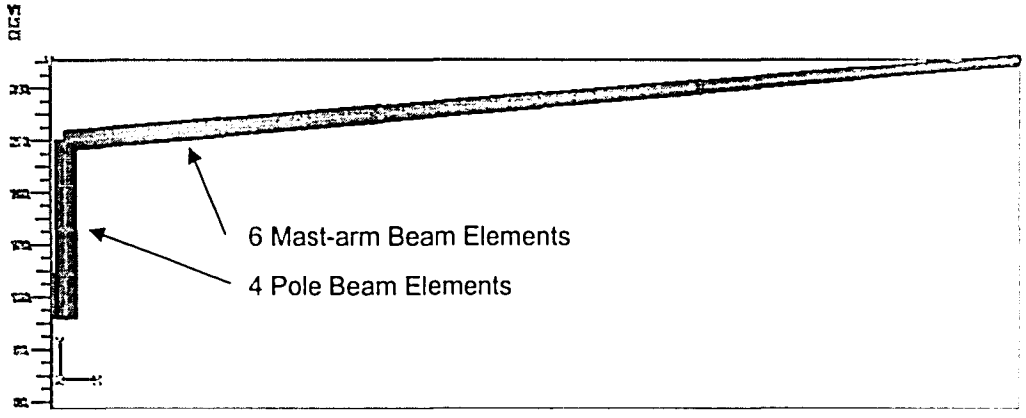

Figure 3.1.2.2: Basic Finite Element Geometry, Mast-arm and Upper Pole Beam Elements

Mast-arm Beam Element Worksheet

MA Measurements Assume t=.21875

X [ft]	Circ [in]	R out [in]	R in [in]
0	34.625	5.51074	5.29199
14	28.5	4.535916	4.317166
28	22.25	3.541197	3.322447
44	15.25	2.427113	2.208363

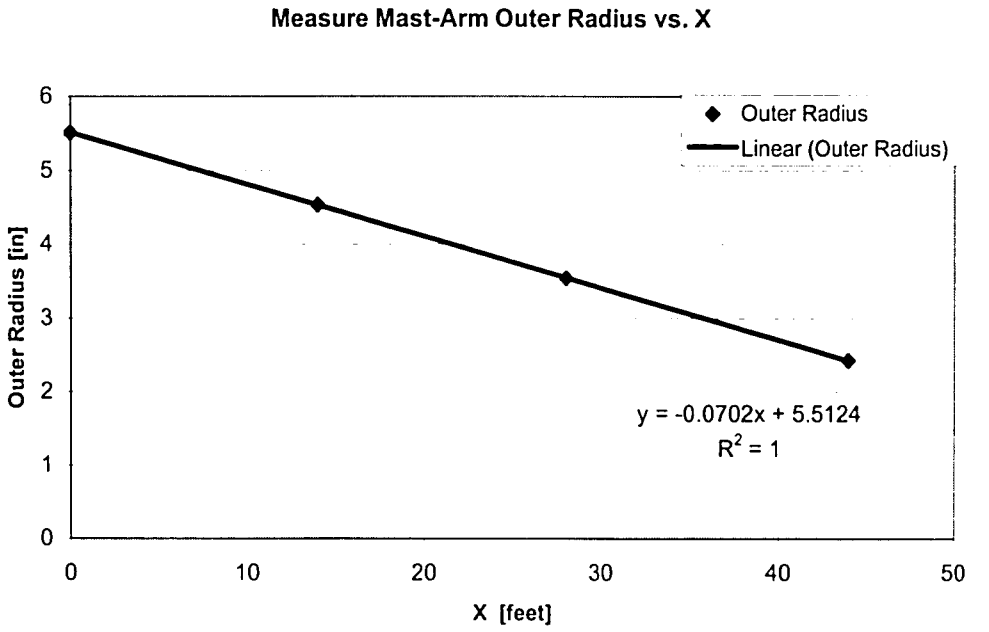

Mast arm length 44 feet 528 in

Use (6) 88 inch beam elements

X [in]		X Mid [in]	[ft]	R out [in]	
0	88	44	3.666667	5.255	Bm5
88	0	44	3.666667	5.255	Bm6
0	0	0	0	5.5124	Bm7
0	0	0	0	5.5124	Bm8
0	0	0	0	5.5124	Bm9
0	0	0	0	5.5124	Bm10

Assume Angle of 5 degrees with horizontal

Y =46.02" and X is 526.0"

Figure 3.1.2.3: Figure showing Mast-arm Beam Element Worksheet Used to Determine Element Properties in Mast-arm

Figure 3.1.2.4: Beam Element Excel Worksheet Used to Determine Upper Pole Beam Element Properties (Page 1 of 2)

Pole Beam Element Worksheet (Page 1 of 2)

Pole Circumfrence Measurements

ft	in		Circ. [in]	Outer Diam. [in]	Height above Bp. (Y) [ft]
3	5	0.125	41.13	13.09049	0
3	2	0.25	38.25	12.17535	6
3	0	0.5	36.50	11.61831	10
2	9	0.875	33.88	10.78275	16

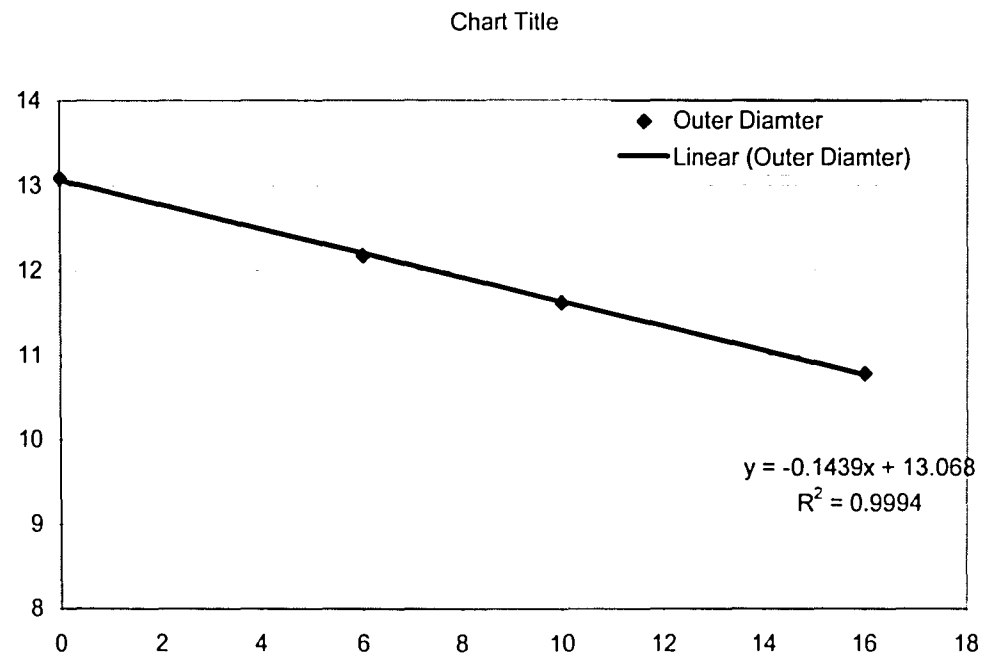

Figure 3.2.1.2.4: Pole Beam Element Selection Worksheet

USE THESE VALUES:

Base Diameter 13.1 inches
Taper per foot -.144 inches diameter per foot

Diameter is D=13.1-.144* Y; Where Y is height above t.o. Bp. in feet

Y=11 in (End Solid; Begin Shell Elements)

t=.21875

Y	D out	r out	r in	r mid
0.916667	12.968	6.484	6.26525	6.374625

Figure 3.1.2.4 Continued: Beam Element Excel Worksheet Used to Determine Upper Pole Beam Element Properties (Page 1 of 2)

Pole Beam Element Worksheet (Page 2 of 2)

Y=108 in (Begin Beam Element)

Y	D out	r out	r in	r mid
9	11.804	5.902	5.68325	5.792625

Y=210 in Top of Column

Y	D out	r out	r in	r mid
17.5	10.58	5.29	5.07125	5.180625

Beam elements from y =108 to y = 210

Use 4 25.5 inch elements

Bm1 **Y=120.75 in** (Y=108 to 133.5)

t=.21875

Y	D out	r out	r in	r mid
10.0625	11.651	5.8255	5.60675	5.72

Bm2 **Y=146.25 in** (Y= 133.5 to 159)

Y	D out	r out	r in	r mid
12.1875	11.345	5.6725	5.45375	5.563

Bm3 **Y=171.75 in** (Y= 159 to 184.5)

Y	D out	r out	r in	r mid
14.3125	11.039	5.5195	5.30075	5.41

Bm4 **Y=197.25 in** (Y= 184.5 to 210)

Y	D out	r out	r in	r mid
16.4375	10.733	5.3665	5.14775	5.257

Figure 3.2.1.2.4: Pole Beam Element Selection Worksheet Continued

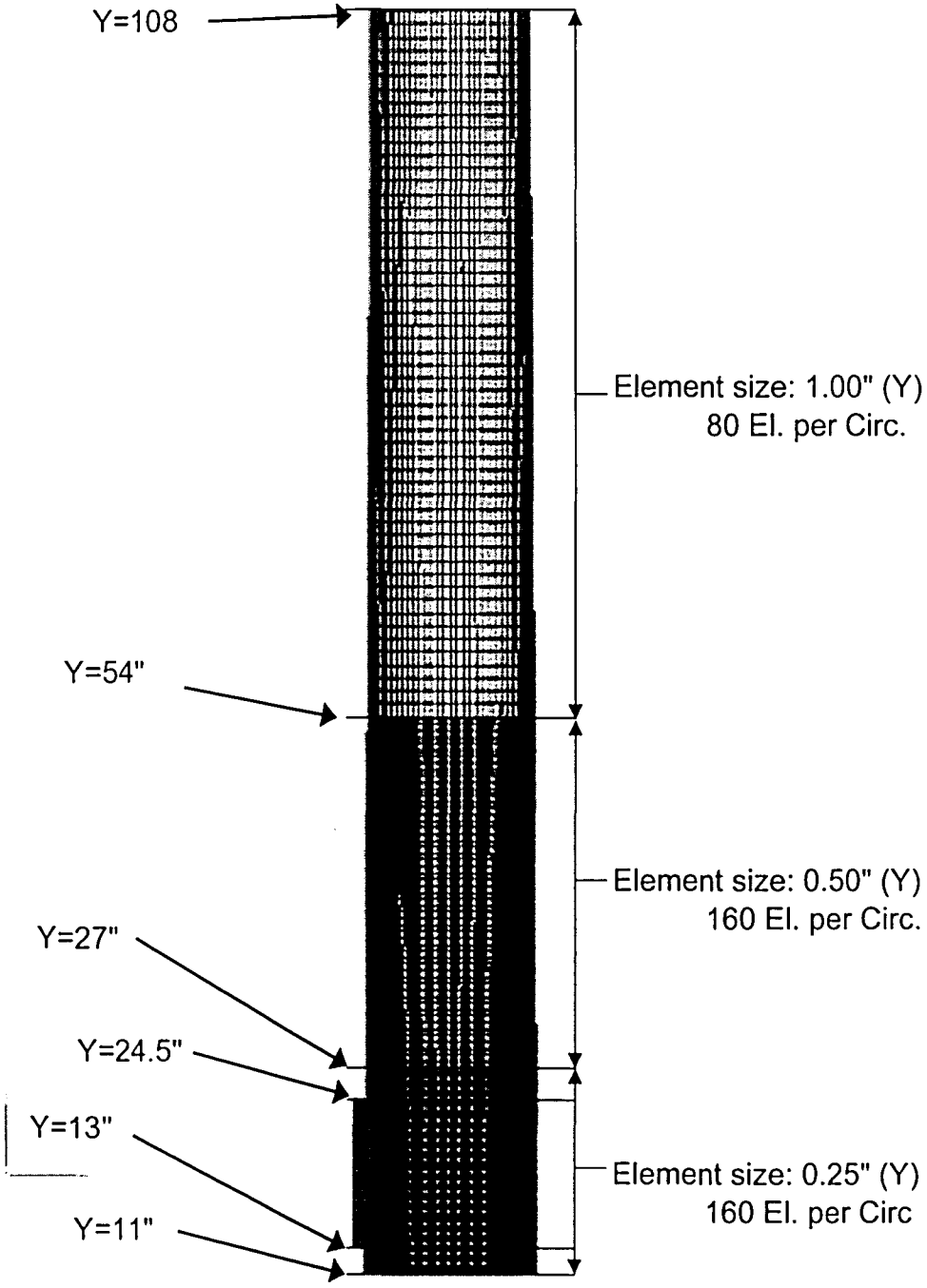

Figure 3.1.2.5: Diagram of Shell Elements used in Pole

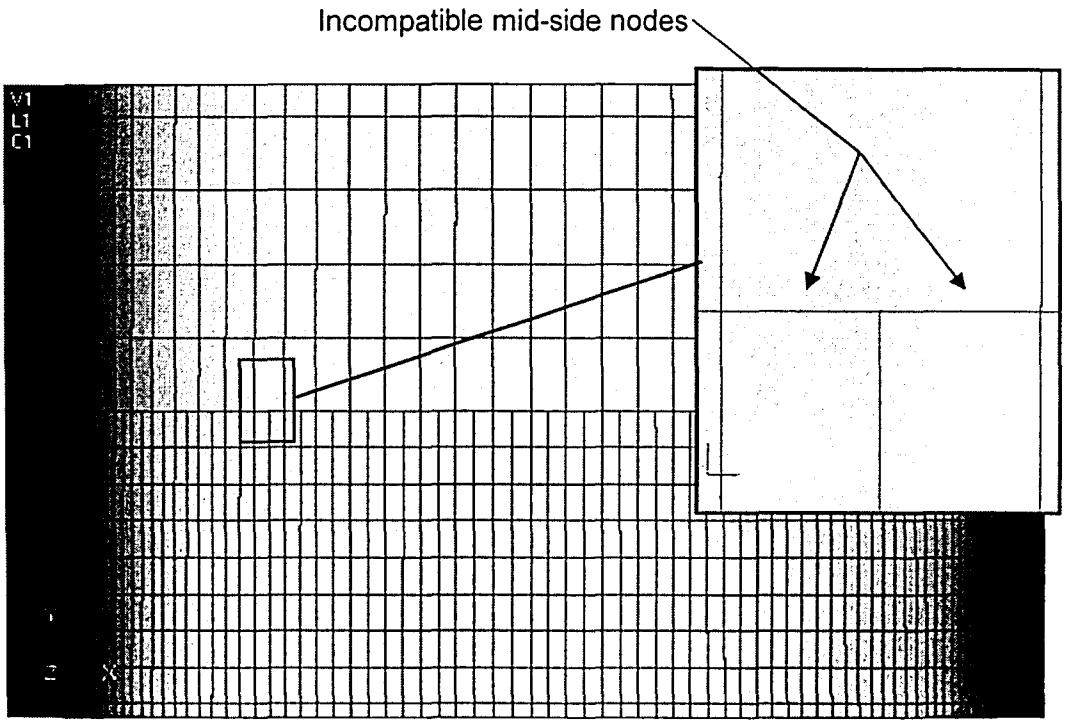

Figure 3.1.2.6: Diagram Showning Incompatible nodes at Pole Shell Element Transition

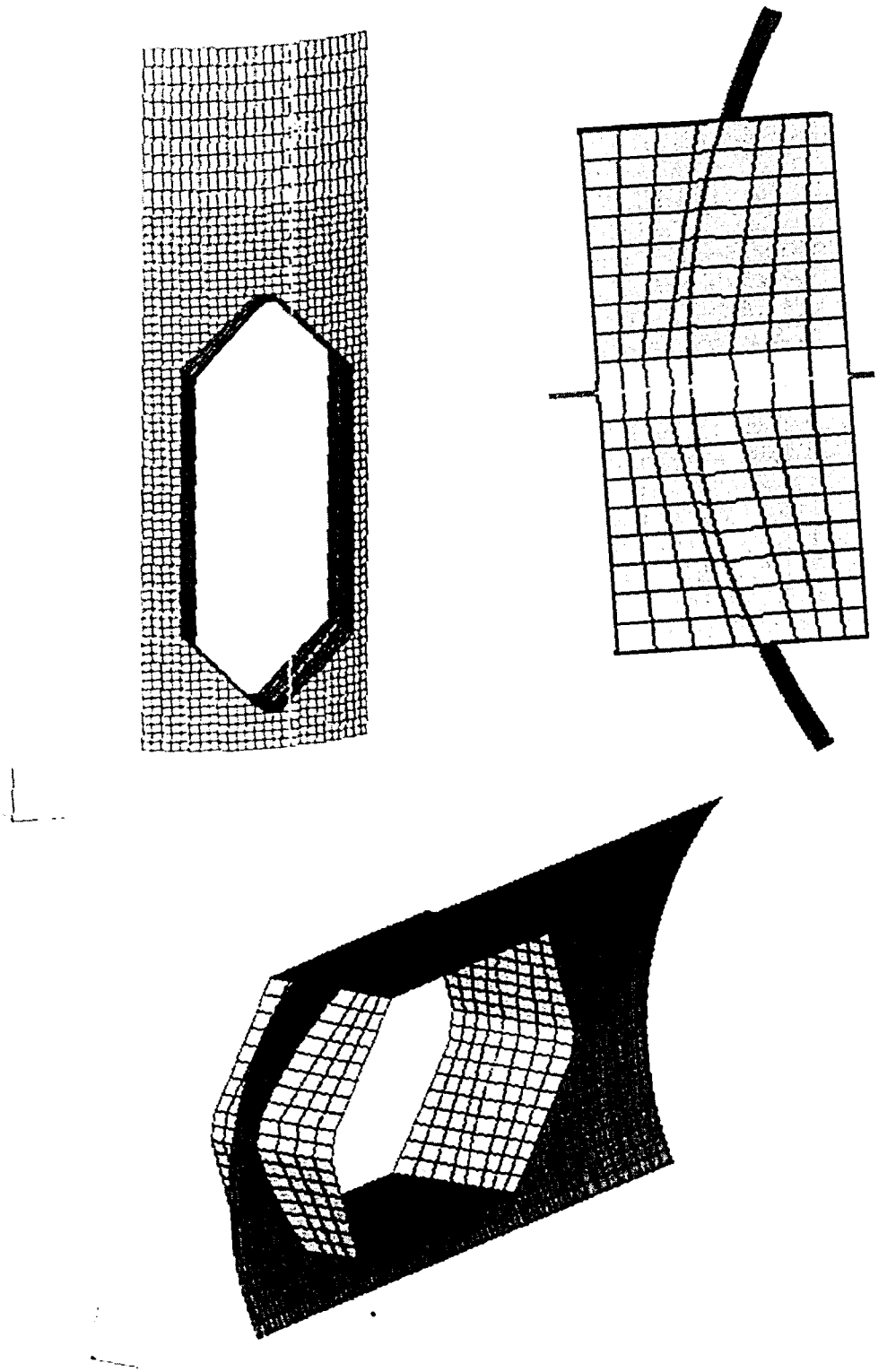

Figure 3.1.2.7: Multiple Views of As-Modeled Hand Access Hole Detail

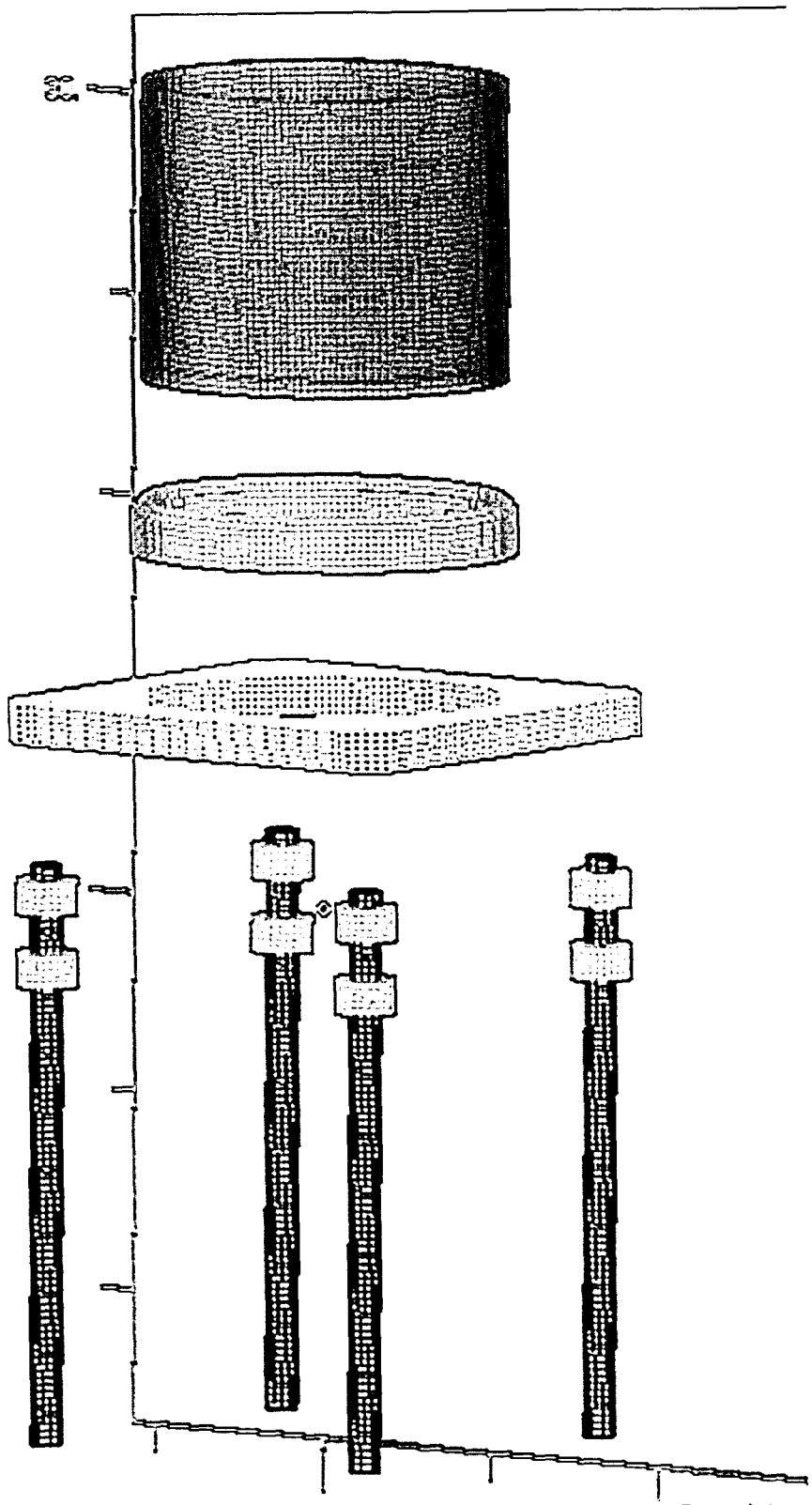

Figure 3.1.2.8: Solid Element Finite Element Model, Lower Pole, Weld, Baseplate, Leveling Nuts, and Anchor Rods

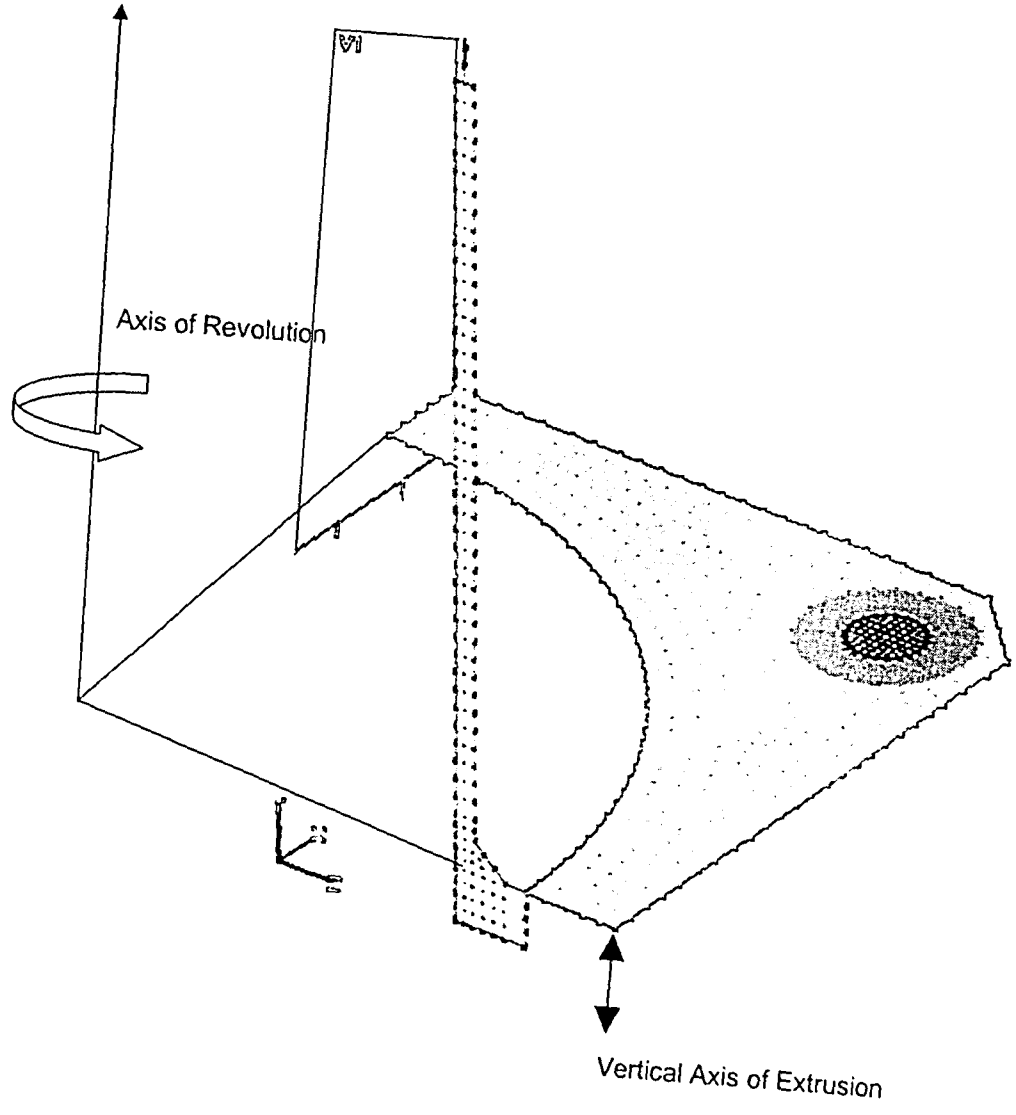

Figure 3.1.2.9: Diagram of Extrusion and Revolution Planes used to Create Solid Element Mesh

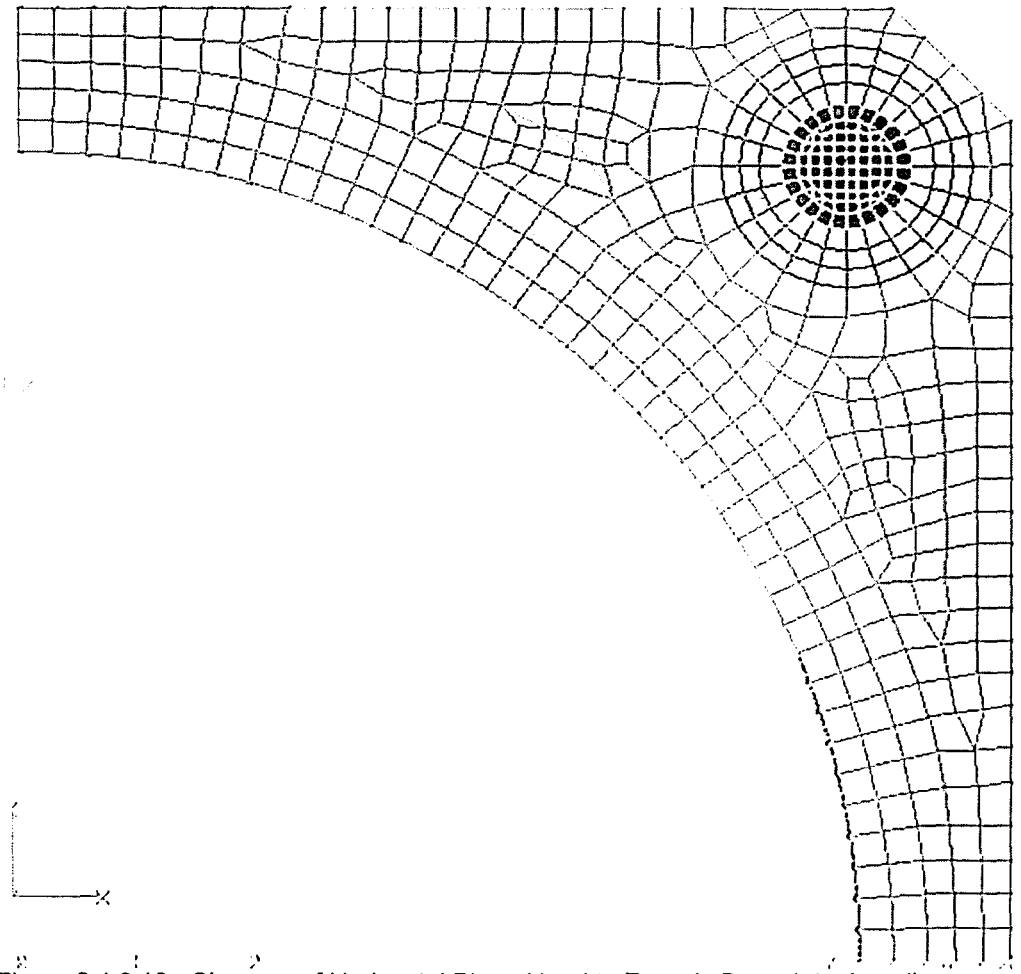

Figure 3.1.2.10: Close up of Horizontal Plane Used to Extrude Baseplate, Leveling Nuts and Anchor Rods

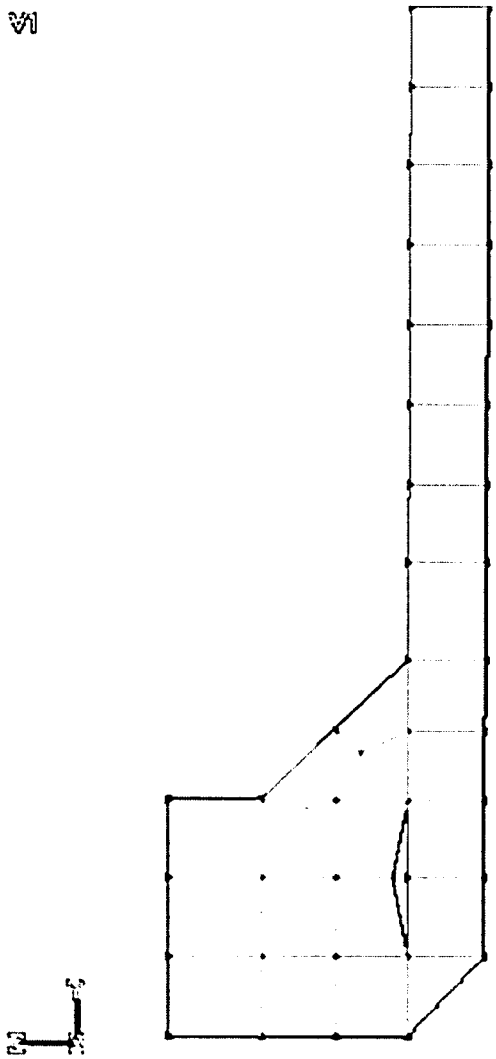

Figure 3.1.2.11: Close up of Typical Radial Plane of Elements used to Revolve Pole and Weld Solid Elements

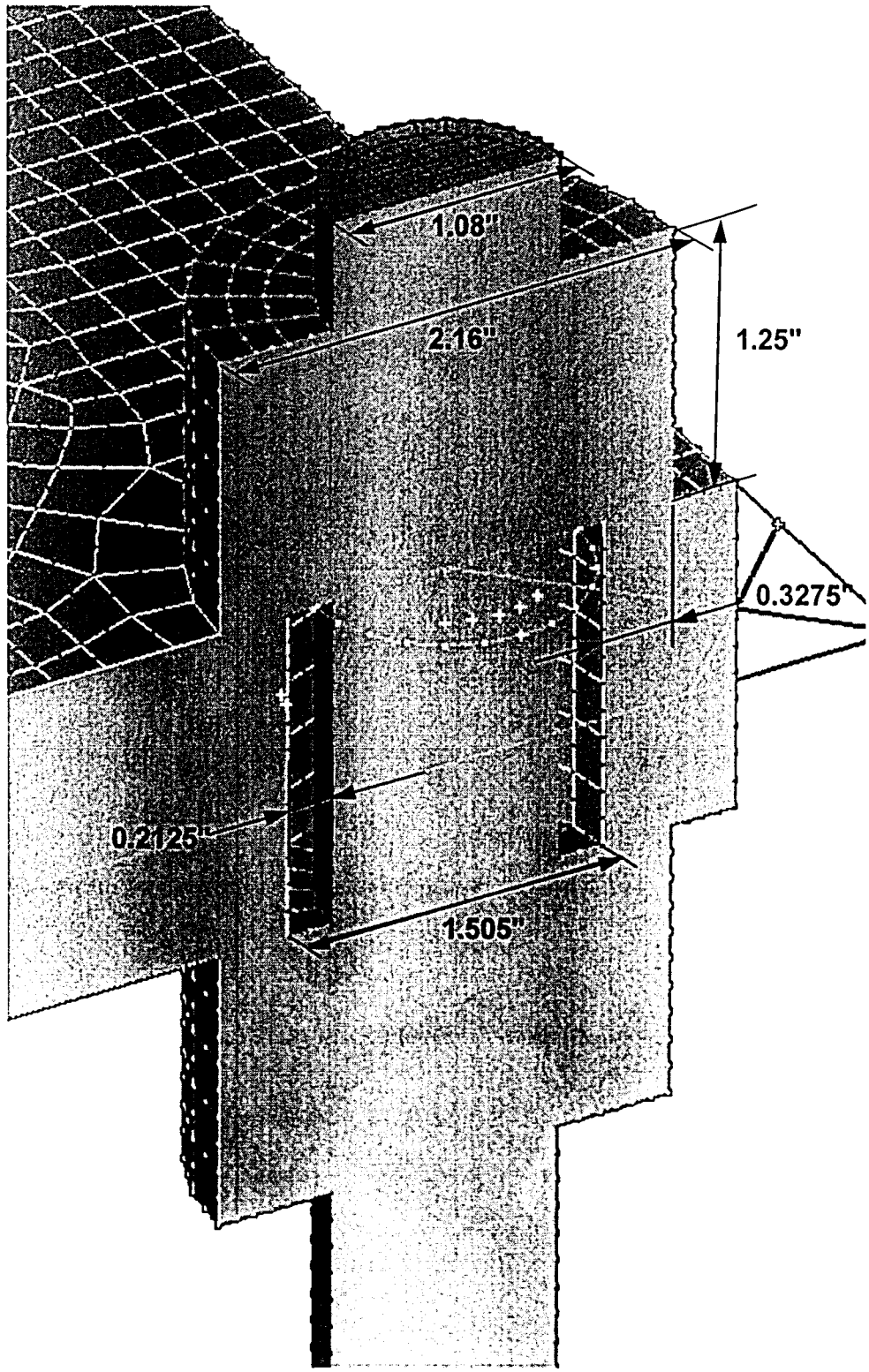

Figure 3.1.2.12: Cross Section Through Finite Element Modeled Leveling Nut to Baseplate Connection

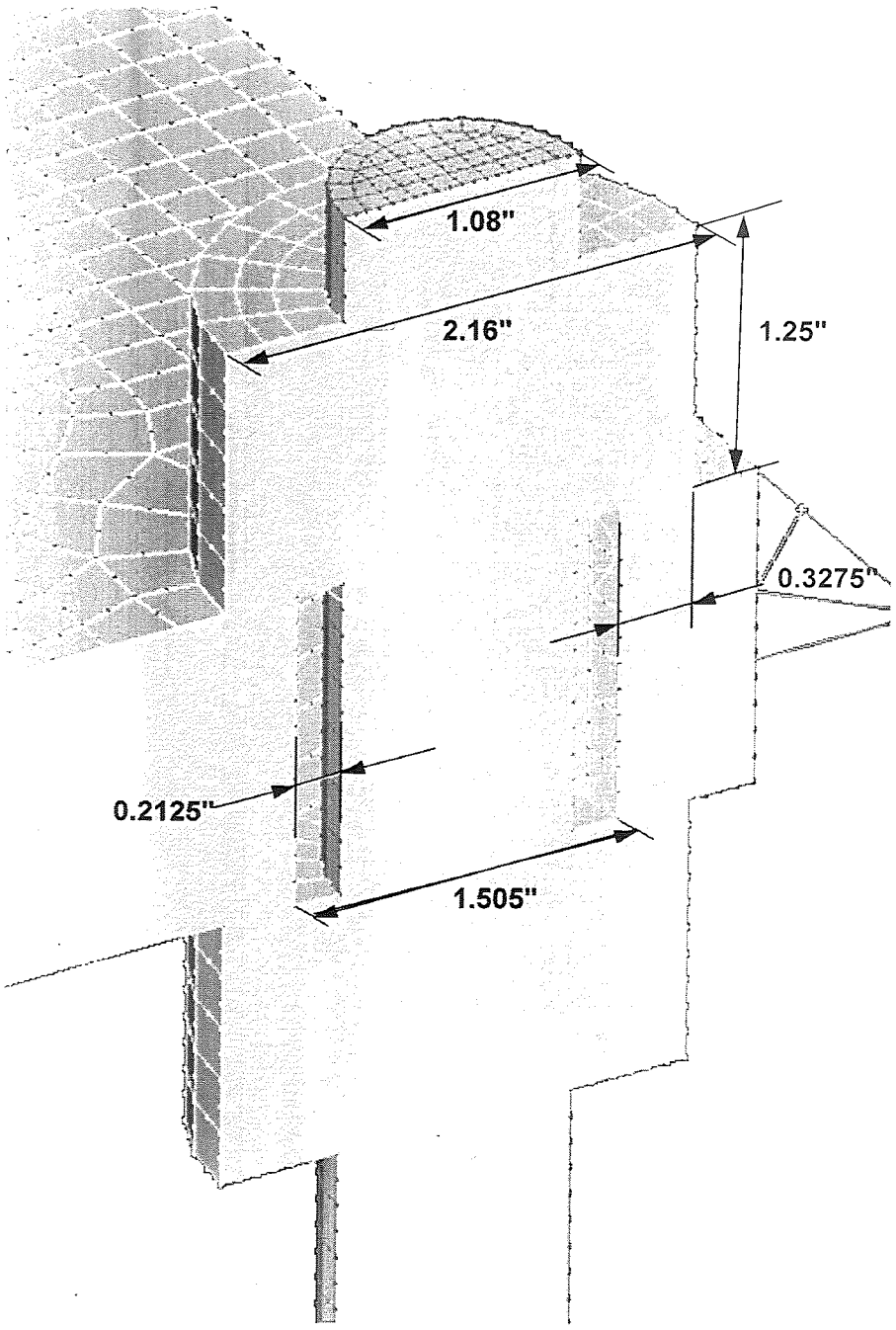

Figure 3.1.2.12: Cross Section Through Finite Element Modeled Leveling Nut to Baseplate Connection

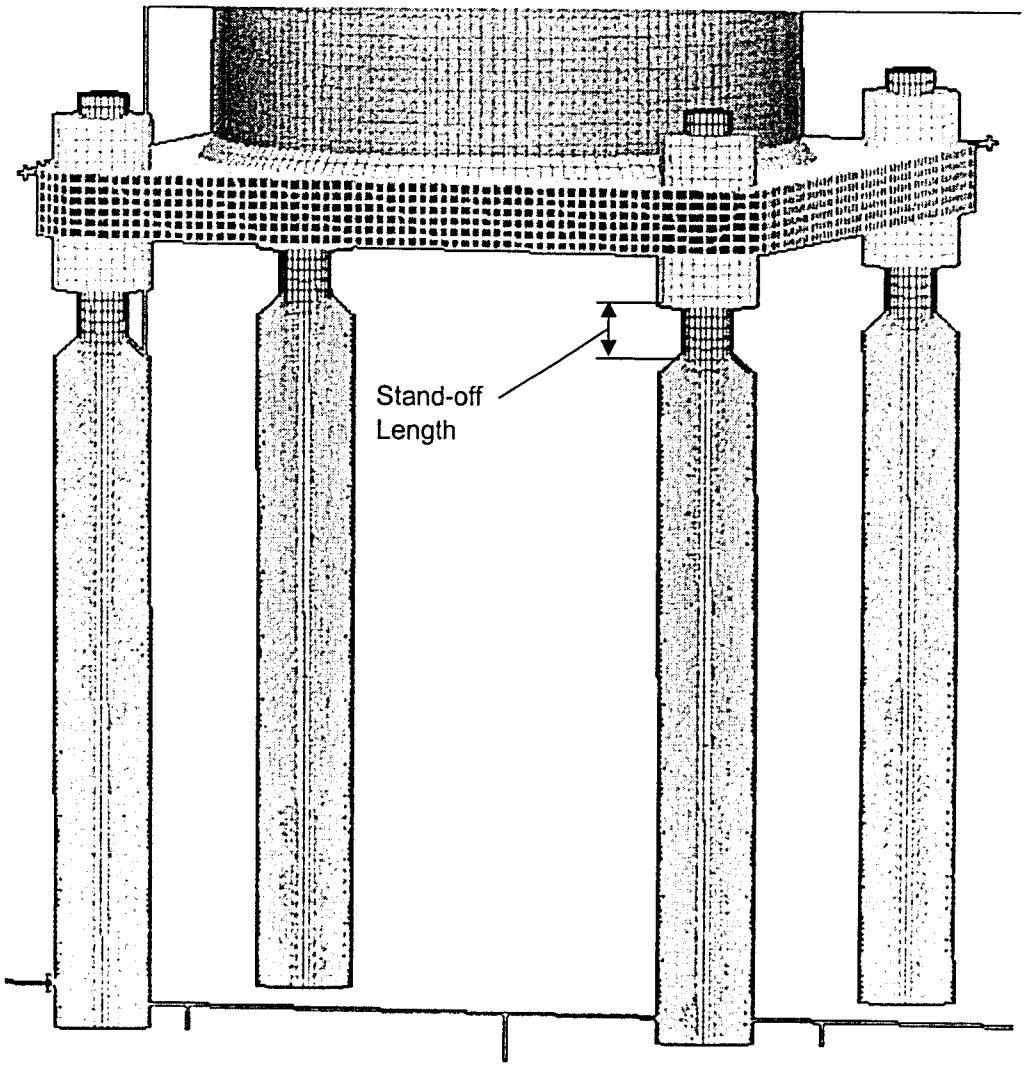

Figure 3.1.2.13: Anchor Rod Surface Constraints, Representative of Concrete Foundataion

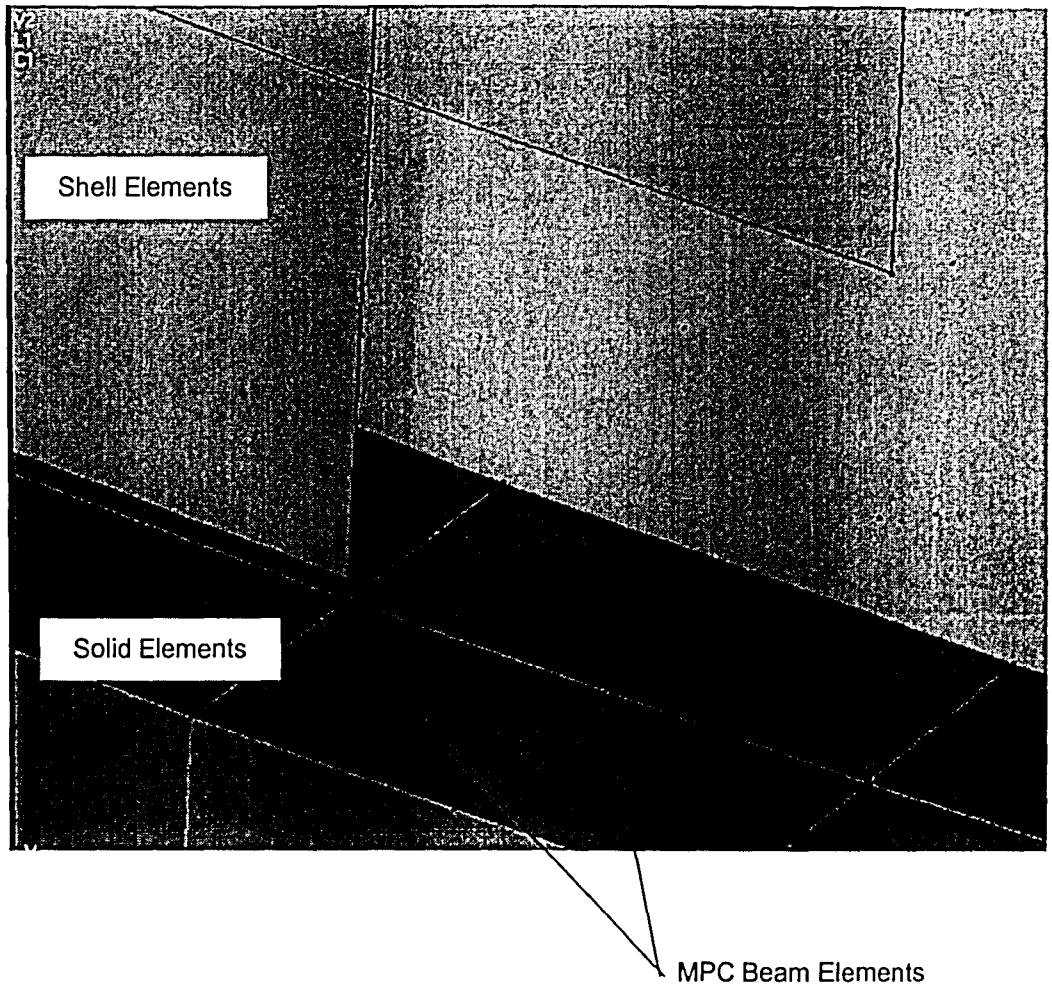

Figure 3.1.2.14: Rigid Beam Elements in Shell to Solid Element Interface

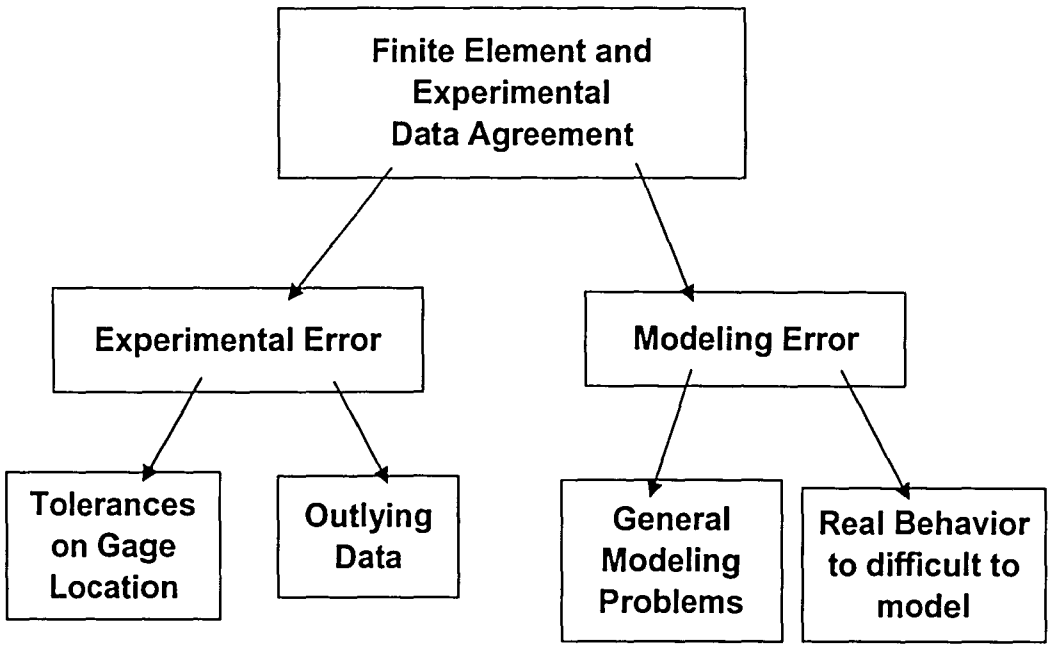

Figure 3.3.1: Flowchart representing some of the issues considered in comparison of experimental and finite element data agreement comparison.

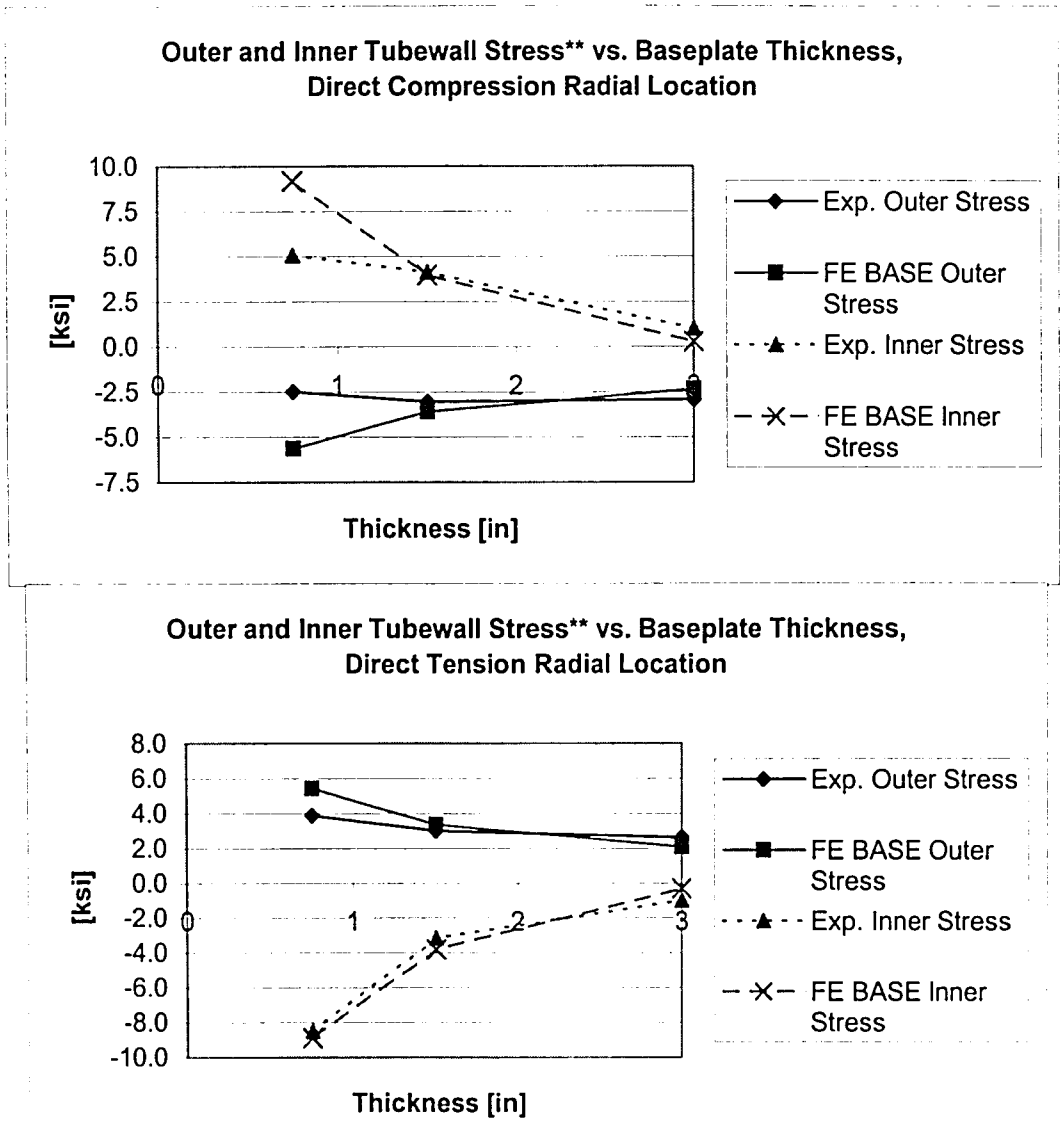

Figure 3.3.2: Comparison of BASE FE and Experimental Outer and Inner Tubewall Stress over Increasing Baseplate Thickness at the Direct Tensile and Compressive Radial Locations (In Line with Mast-arm Axis)

** Stress refers to "hotspot" stress with gage location just above weld toe For the 3/4" and 1 1/2" Baseplate Thickness Specimens 0.75" above the Baseplate; for the 3" Baseplate Thickness Specimen 0.875" above the baseplate.

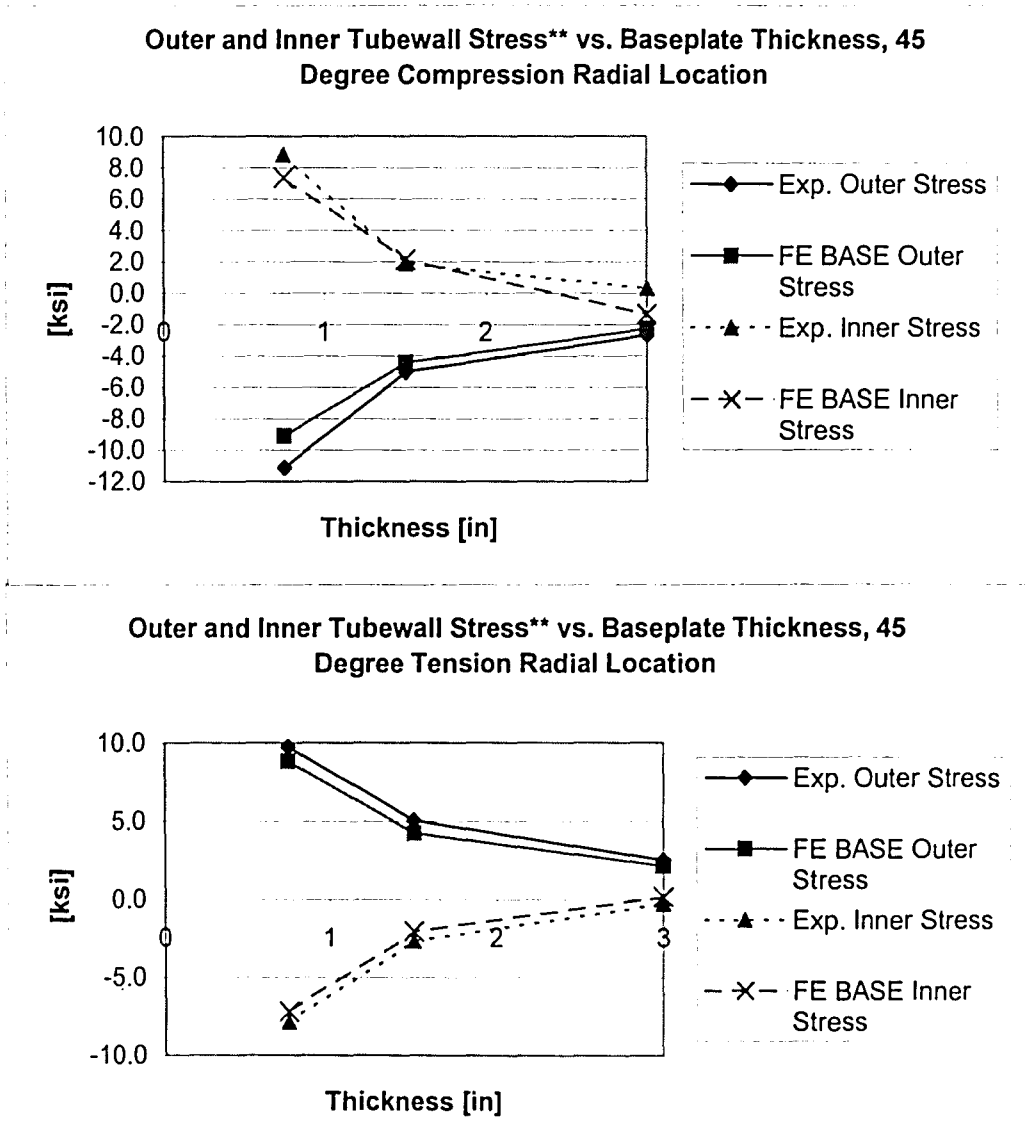

Figure 3.3.3: Comparison of BASE FE and Experimental Outer and Inner Tubewall Stress over Increasing Baseplate Thickness at the 45 Degree Tensile and Compressive Radial Locations (In Line with Anchor Rods)

** Stress refers to "hotspot" stress with gage location just above weld toe
For the 3/4" and 1 1/2" Baseplate Thickness Specimens 0.75" above the Baseplate; for the 3" Baseplate Thickness Specimen 0.875" above the baseplate.

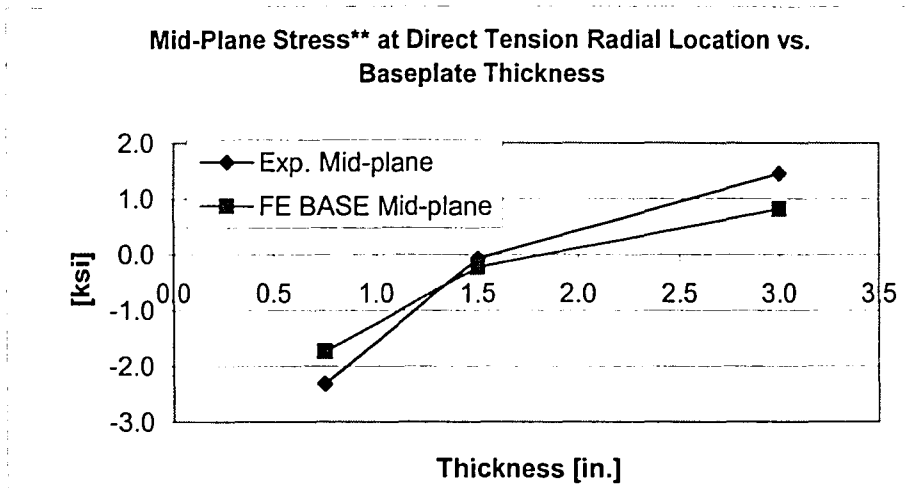

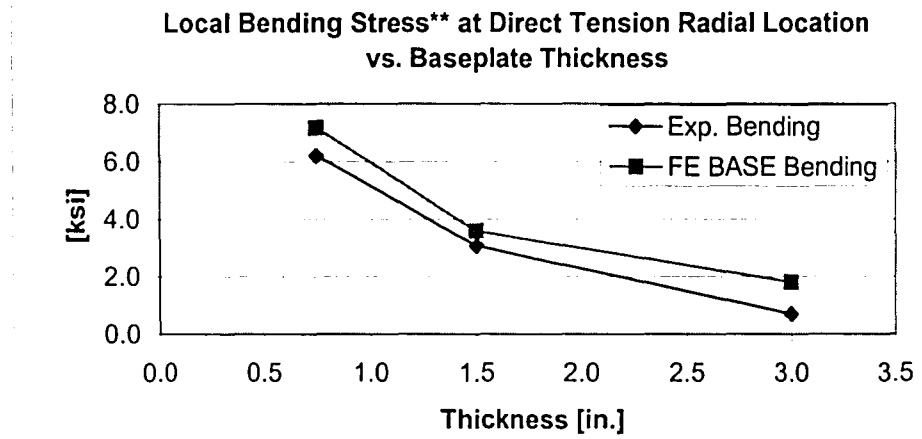

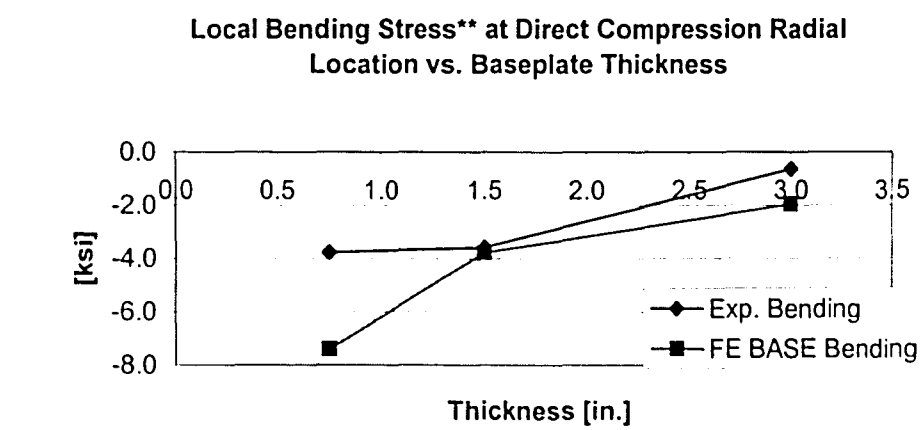

Figure 3.3.4: Comparison of BASE FE and Experimental Mid-Plane and Local Bending Stress Over Increasing Baseplate Thickness

** Stress refers to "hotspot" stress with gage location just above weld toe

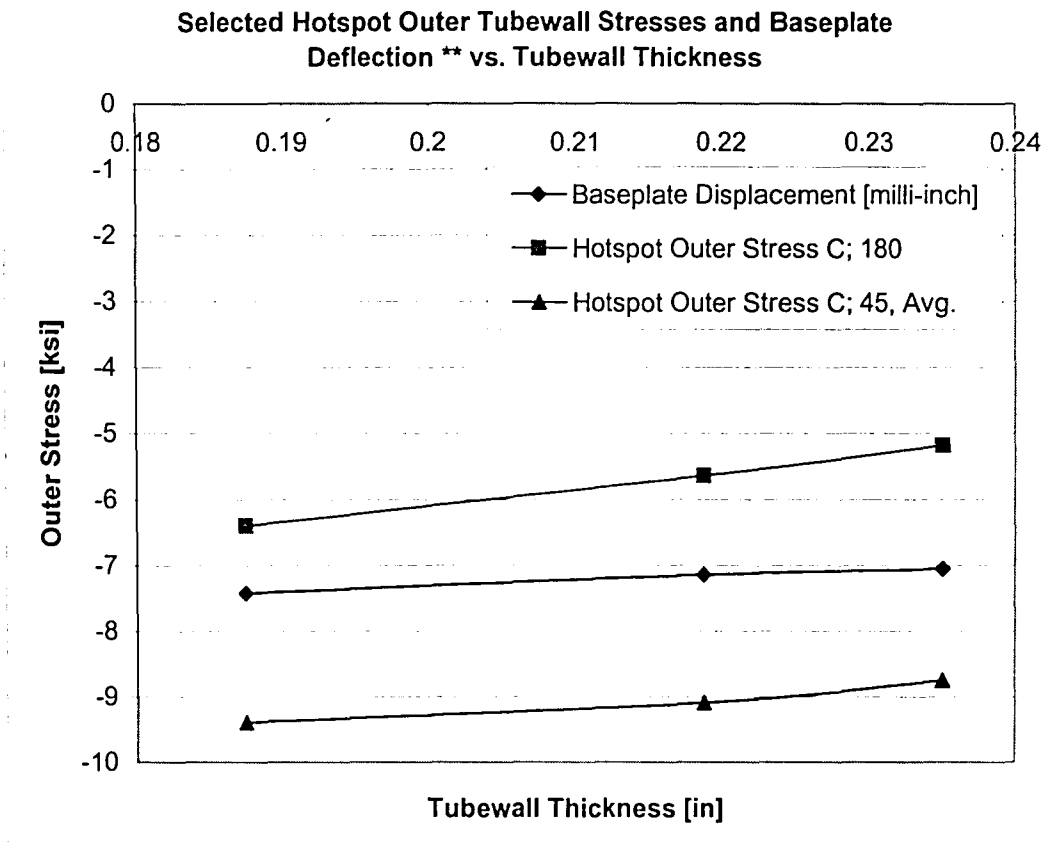

Figure 3.4.1.1: Tubewall Thickness Calibration Study Results

** Selected hotspot outer tubewall stresses from 3/4" baseplate thickness specimen at gage location 0.75" above the baseplate.

** Baseplate deflection measured on the ocmpressive side of the baseplate, on the mast-arm axis, 1" away from edge of baseplate. (Given in milli-inches or 10^-3*inch)

Figure 3.4.1.2: Cross Section of BASE Finite Element Model with Standard Mesh Refiniement

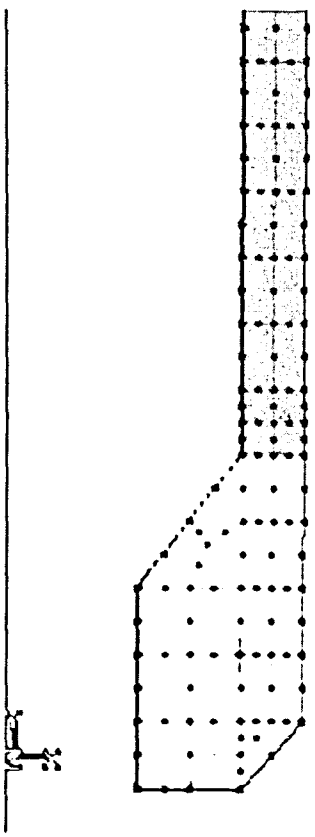

Figure 3.4.1.3: Cross Section of DTW Finite Element Model with two elements through the pole tubewall thickness

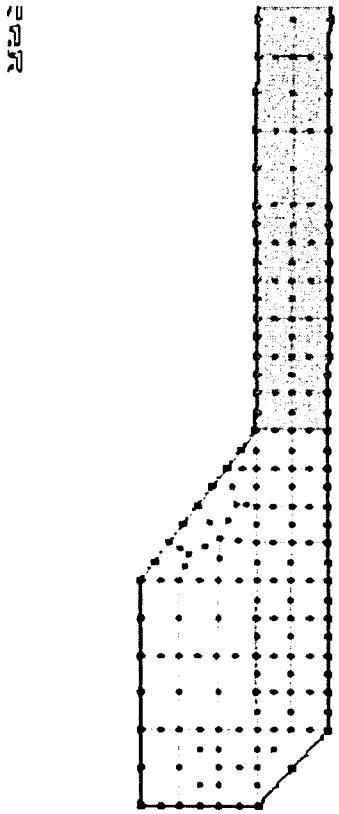

Figure 3.4.1.4: Cross Section of REFIN Finite Element Model with additional mesh refinement as compared to DTW

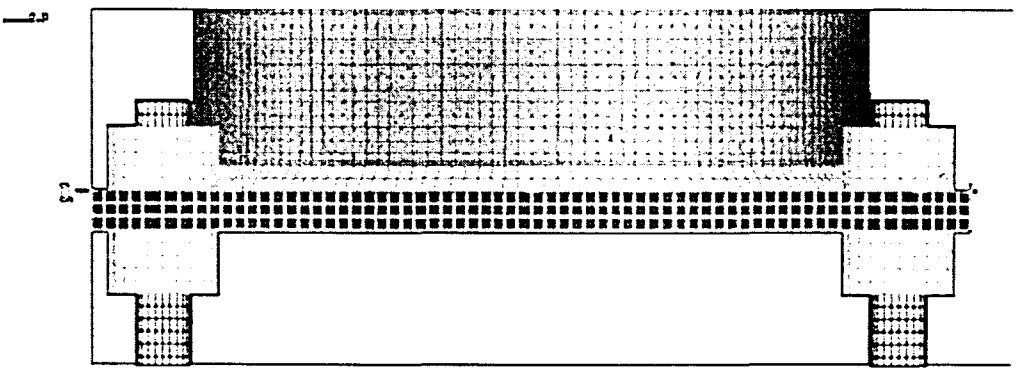

Figure 3.4.1.5: Profile of BASE Finite Element Model (Note 3 elements through 3/4" thick baseplate or one element thickness per 0.25" of baseplate thickness)

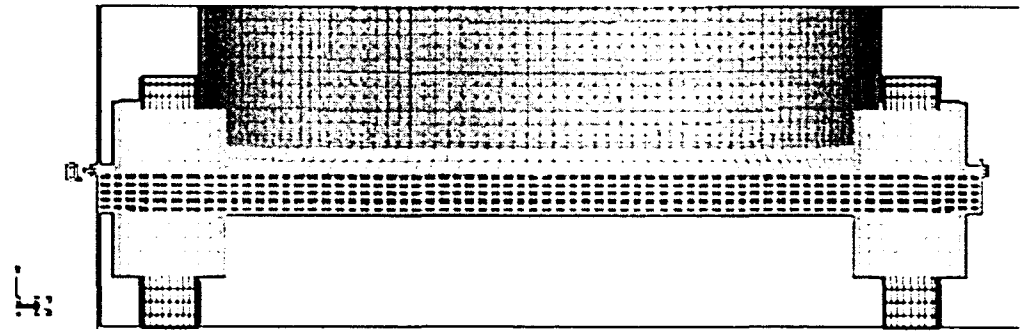

Figure 3.4.1.6: Profile of REFIN_BP Finite Element Model with Increased Refinement Through Baseplate Thickness (Note 5 elements through the 3/4" baseplate shown here or similar increase in mesh refinement for other 2 specimens)

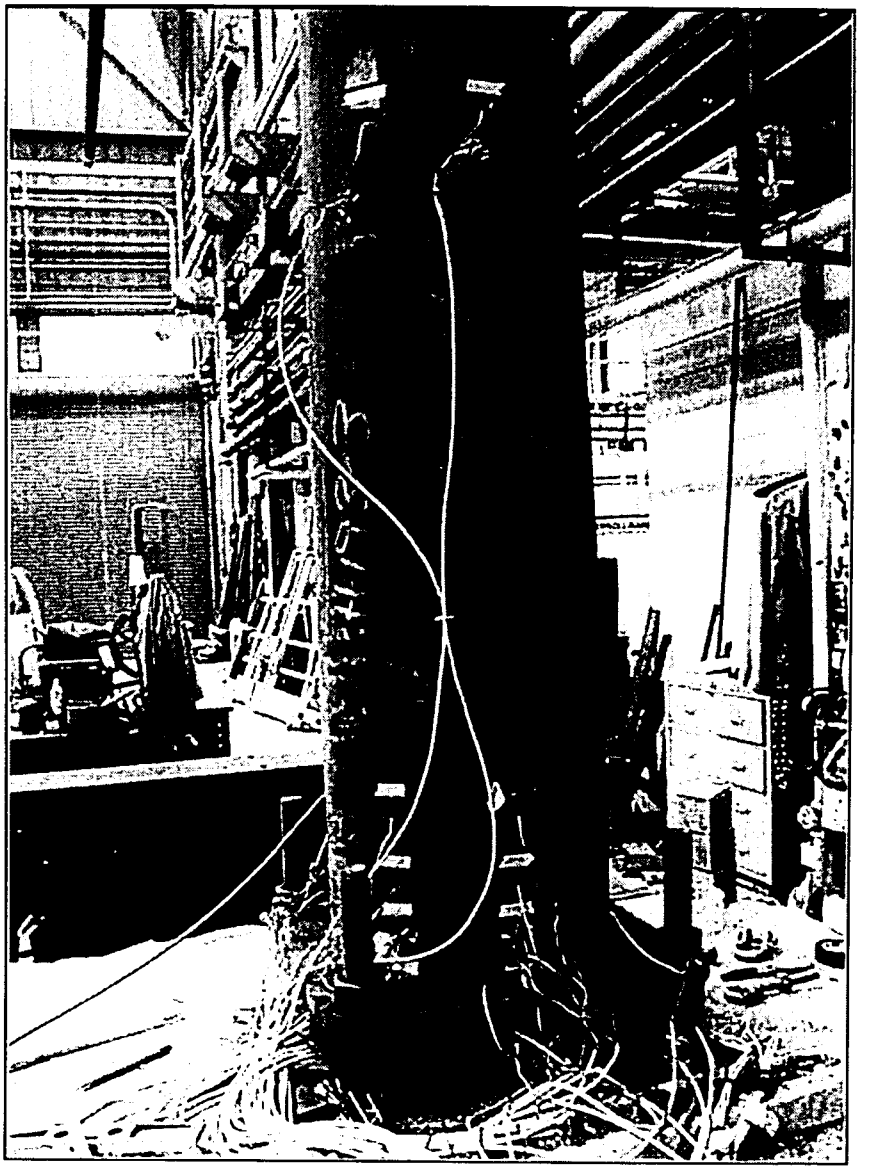

Figure 3.4.1.7: Photograph of Hand Access Hole

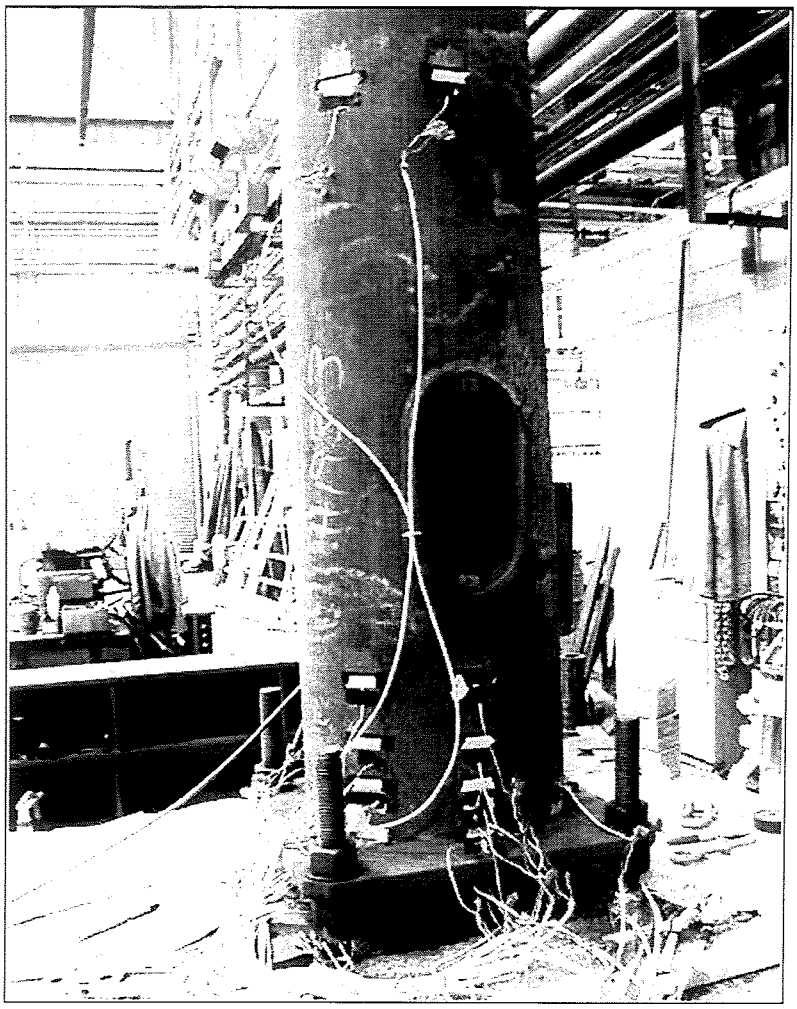

Figure 3.4.1.7: Photograph of Hand Access Hole

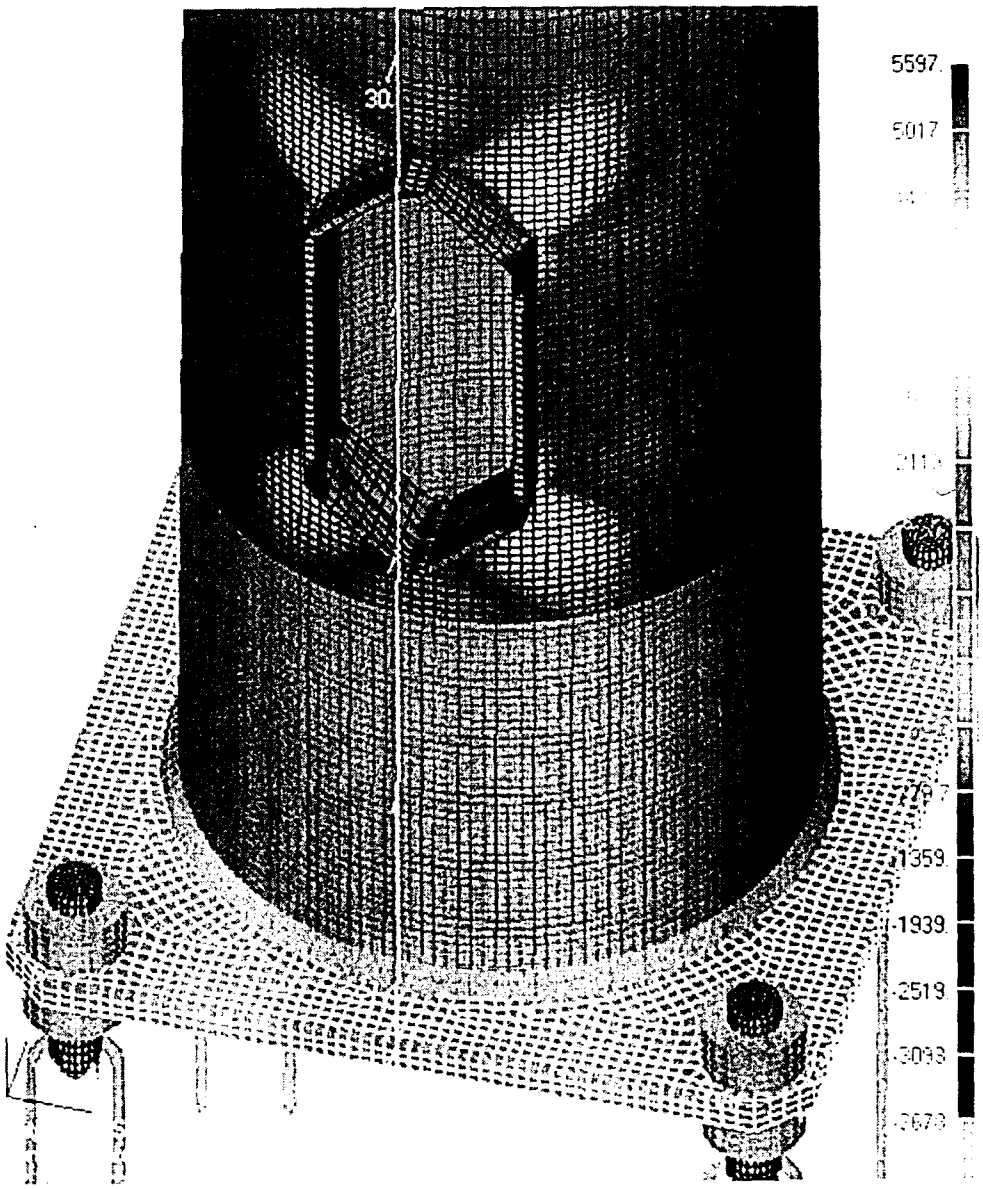

Figure 3.4.1.8: Hand Access Hole Calibration Study Finite Element Model: BASE
(Standard hand access hole geometry)

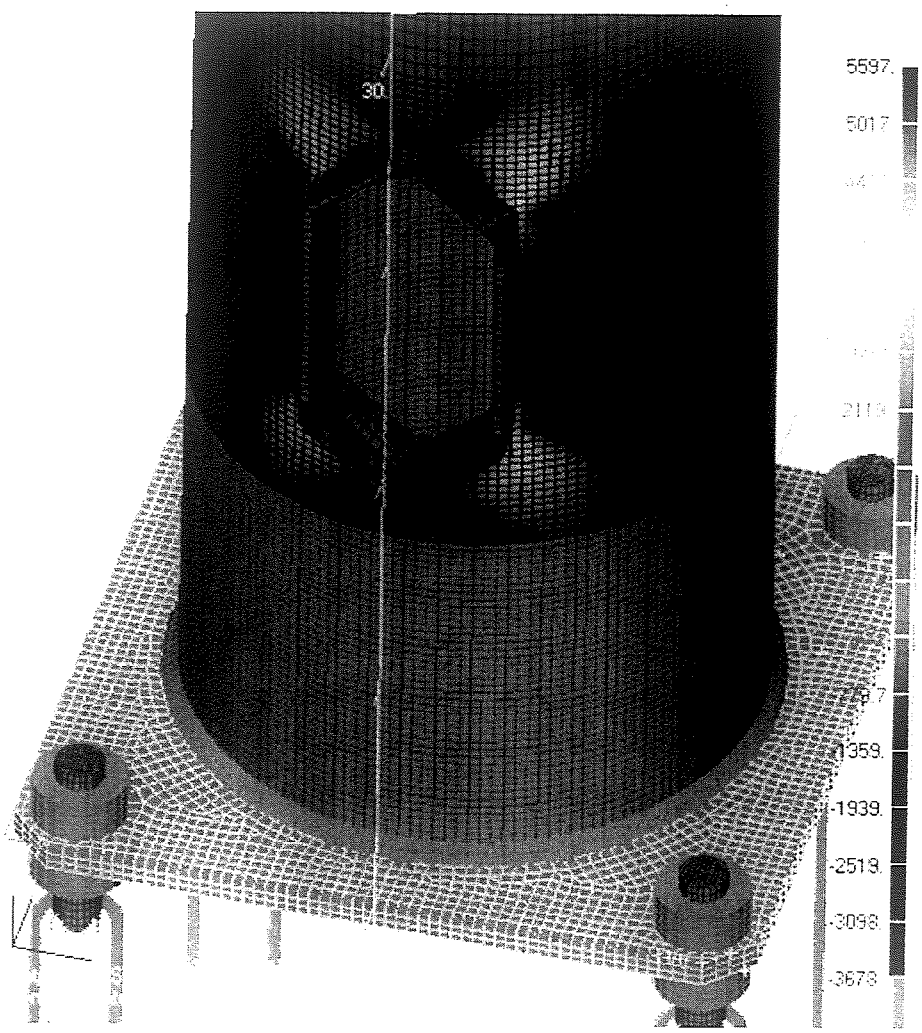

Figure 3.4.1.8: Hand Access Hole Calibration Study Finite Element Model: BASE
(Standard hand access hole geometry)

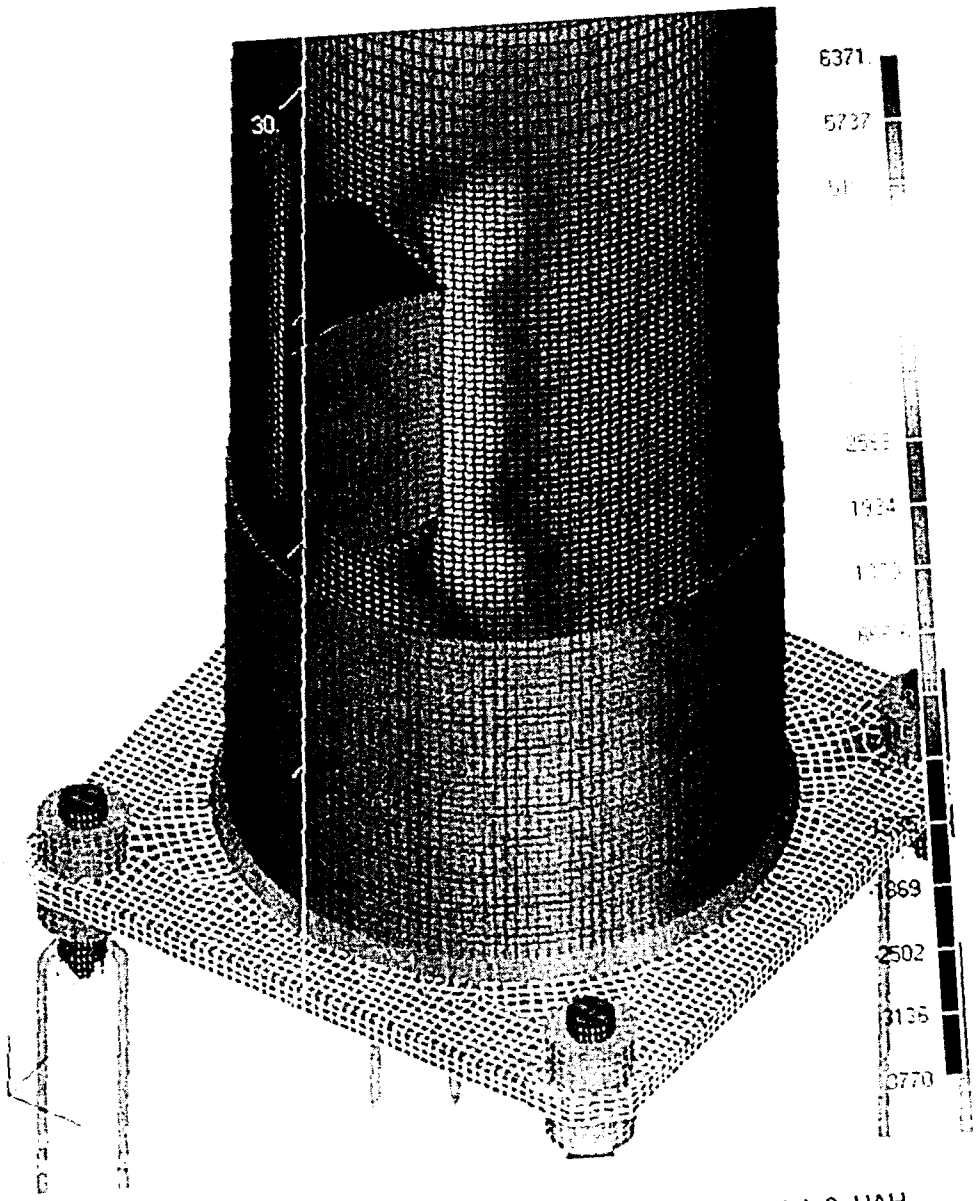

Figure 3.4.1.9: Hand Access Hole Calibration Study Finite Element Model: 0_HAH
(No hand access hole reinforcement, with standard approximate shape)

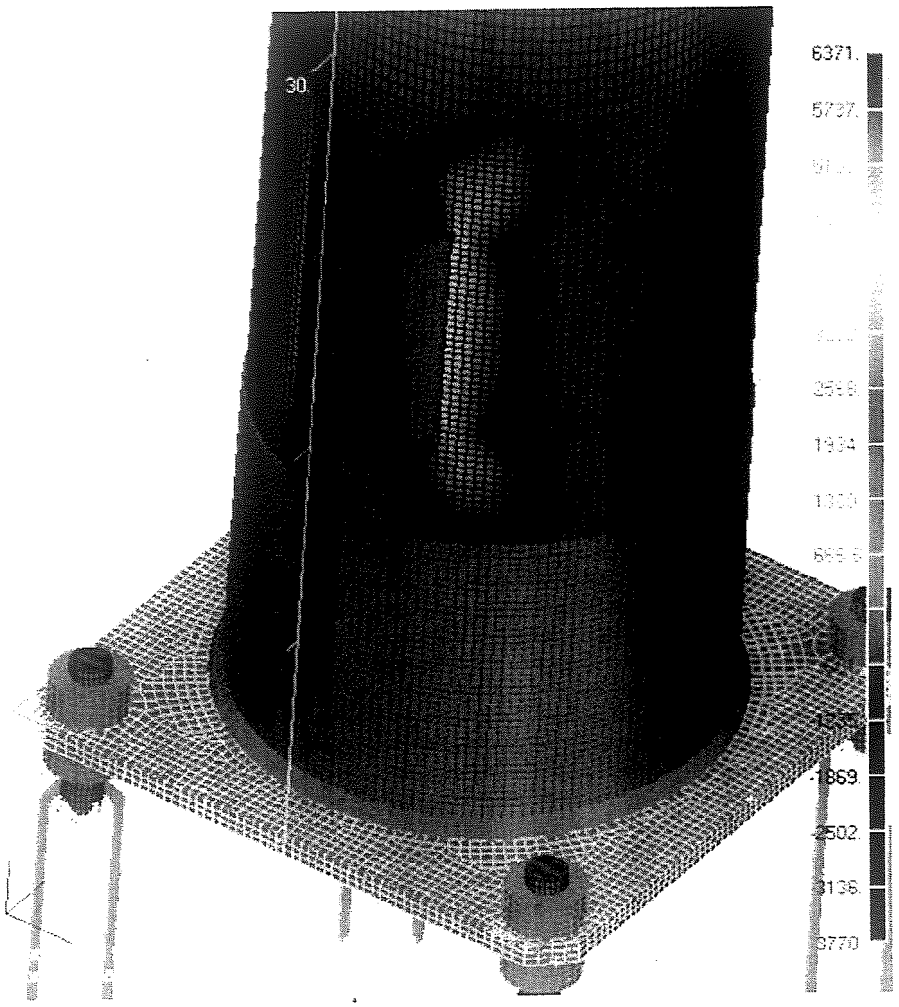

Figure 3.4.1.9: Hand Access Hole Calibration Study Finite Element Model: 0_HAH
(No hand access hole reinforcement, with standard approximate shape)

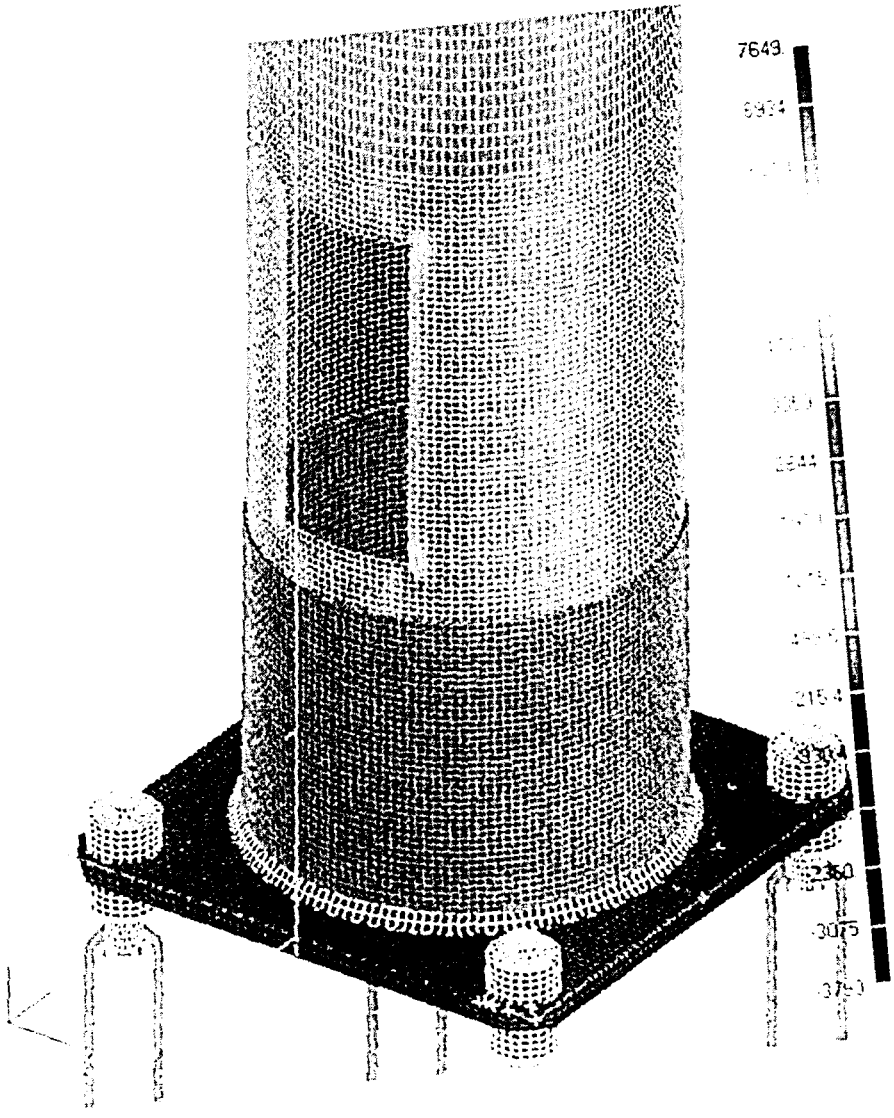

Figure 3.4.1.10: Hand Access Hole Calibration Study Finite Element Model: 0_HAH*
(No hand access hole reinforcement, with rectangular shaped hole)

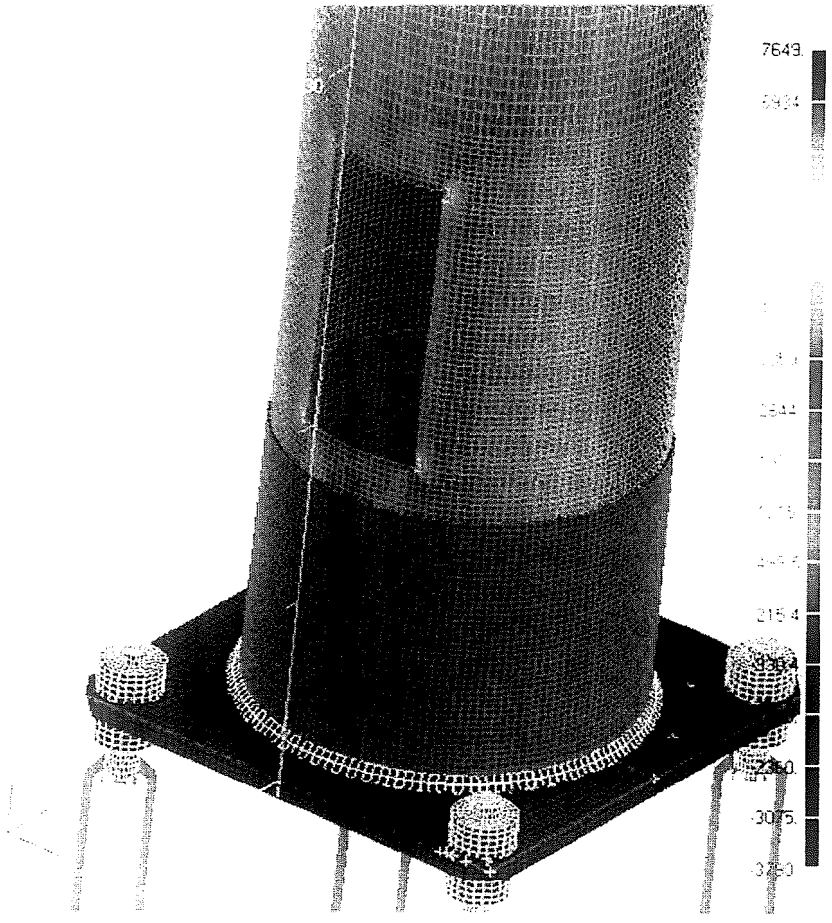

Figure 3.4.1.10: Hand Access Hole Calibration Study Finite Element Model: 0_HAH*
(No hand access hole reinforcement, with rectangular shaped hole)

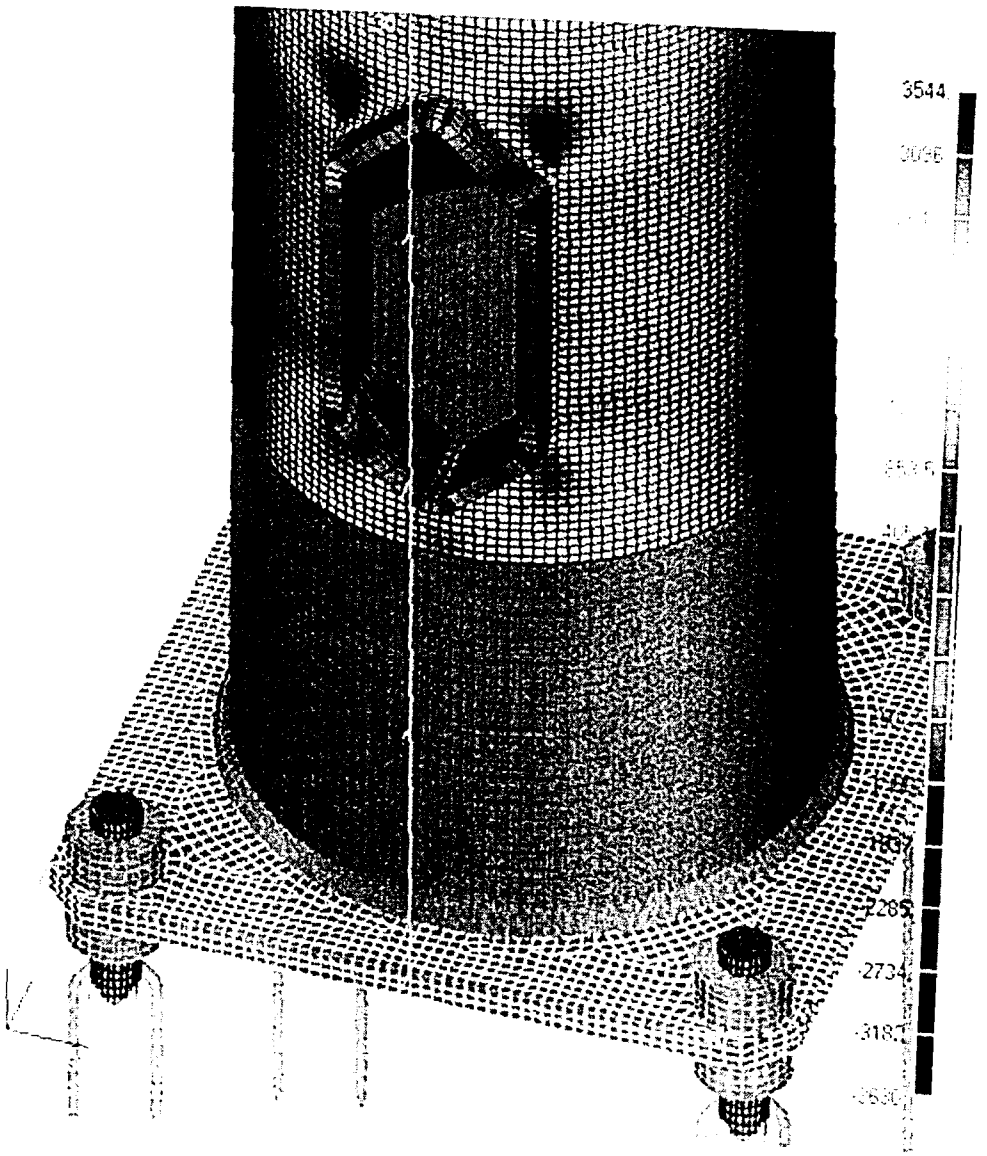

Figure 3.4.1.11: Hand Access Hole Calibration Study Finite Element Model: 2_HAH
(Hand access hole reiforcement plate thickness is doubled)

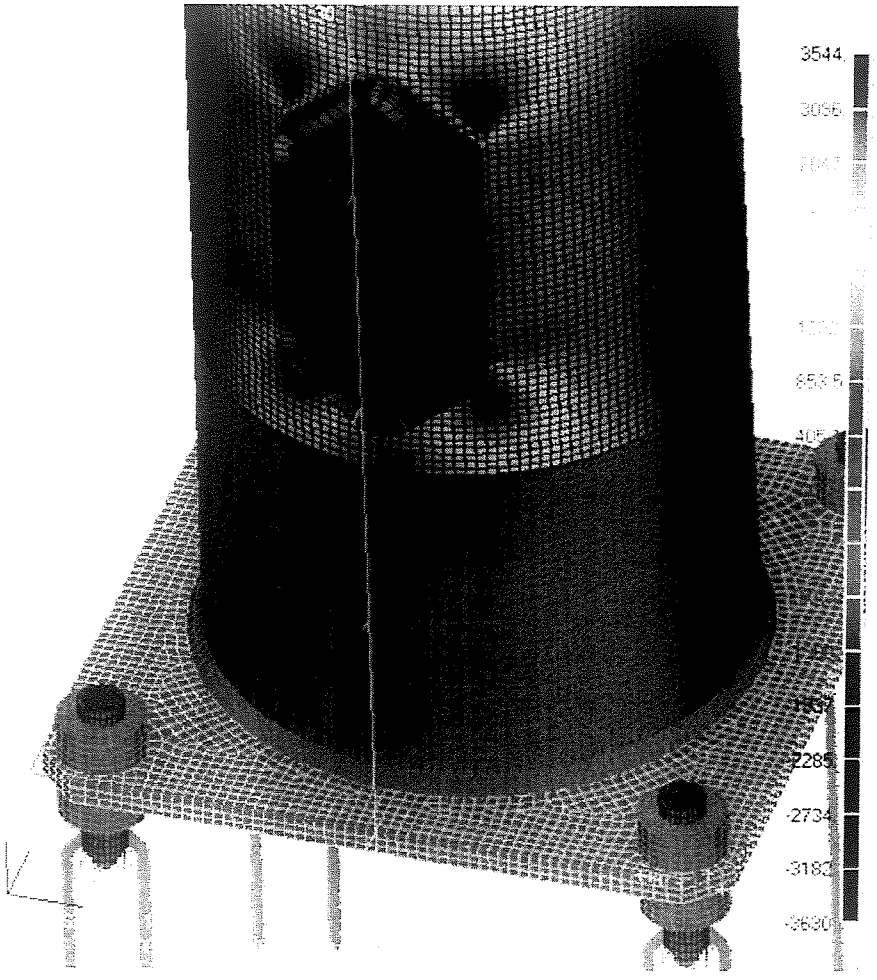

Figure 3.4.1.11: Hand Access Hole Calibration Study Finite Element Model: 2_HAH
(Hand access hole reiforcement plate thickness is doubled)

Various Tubewall Stresses and Baseplate Deflections vs. Stand-off Length

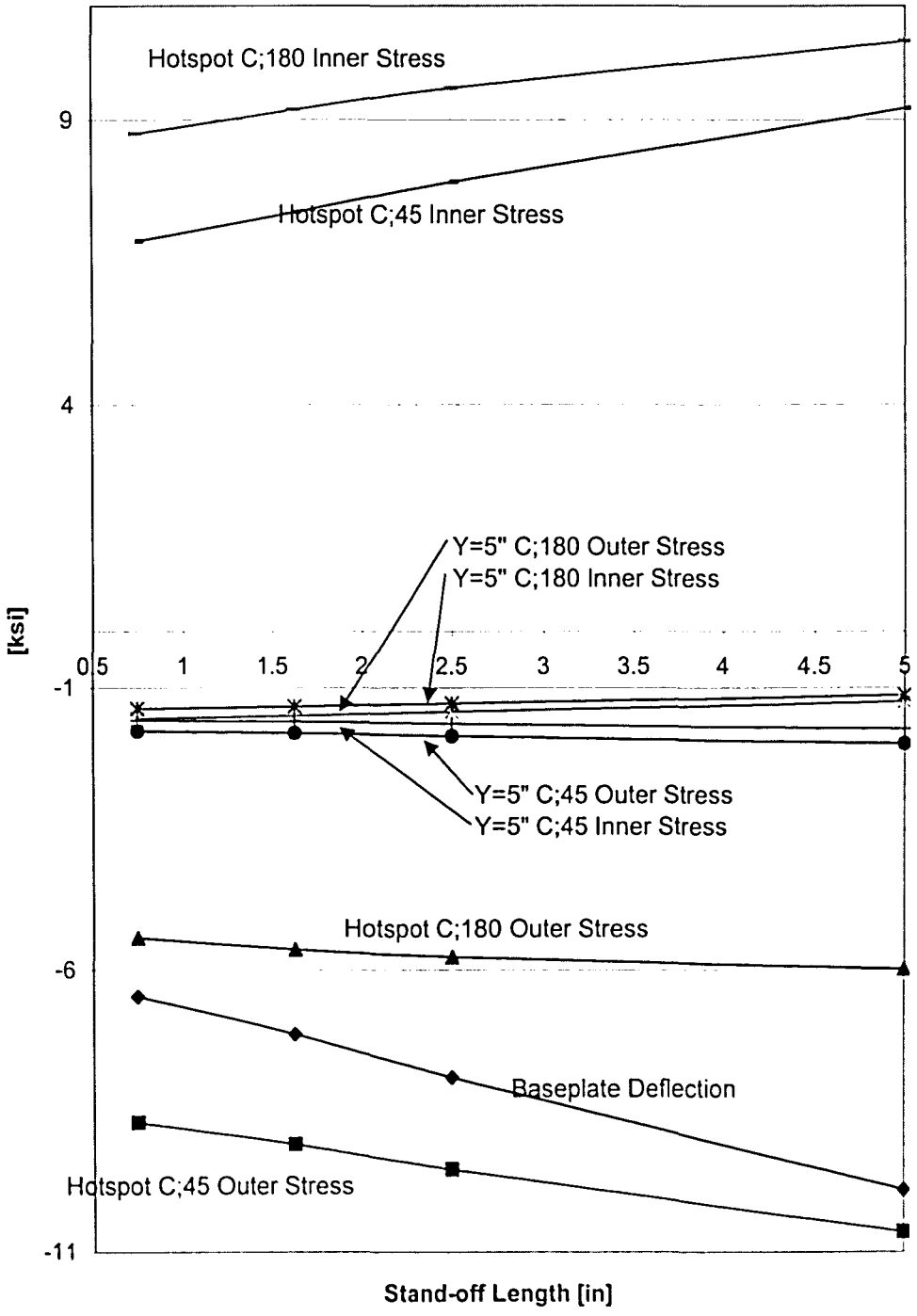

Figure 3.4.1.12: Stand-off Length Calibration Study Results

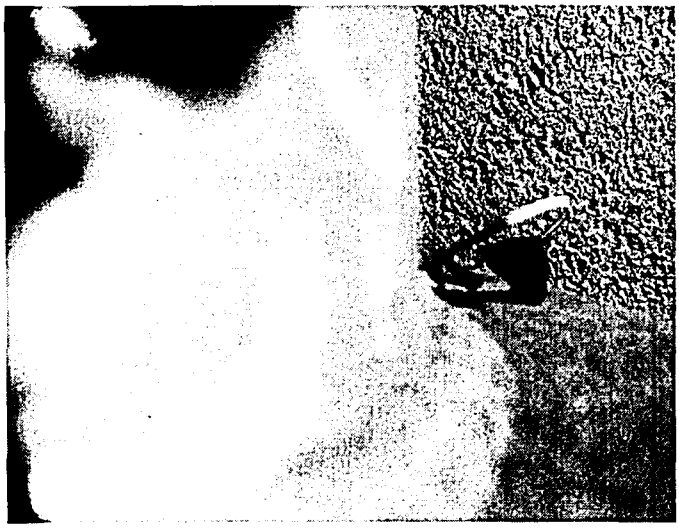

Figure 3.4.1.13: Photograph of Upper Fillet Weld Profile of 3/4" Baseplate Thickness Specimen

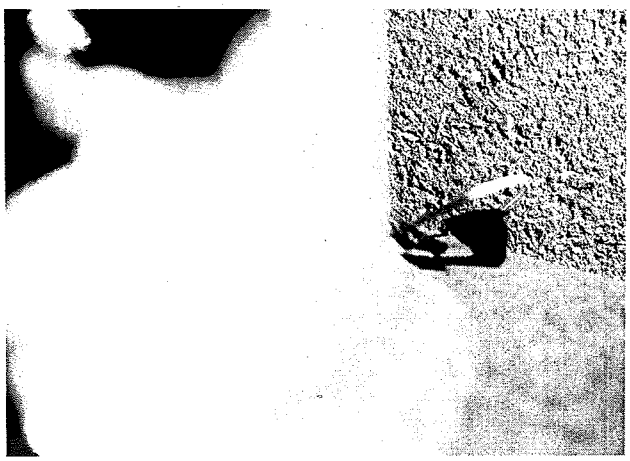

Figure 3.4.1.13: Photograph of Upper Fillet Weld Profile of 3/4" Baseplate Thickness Specimen

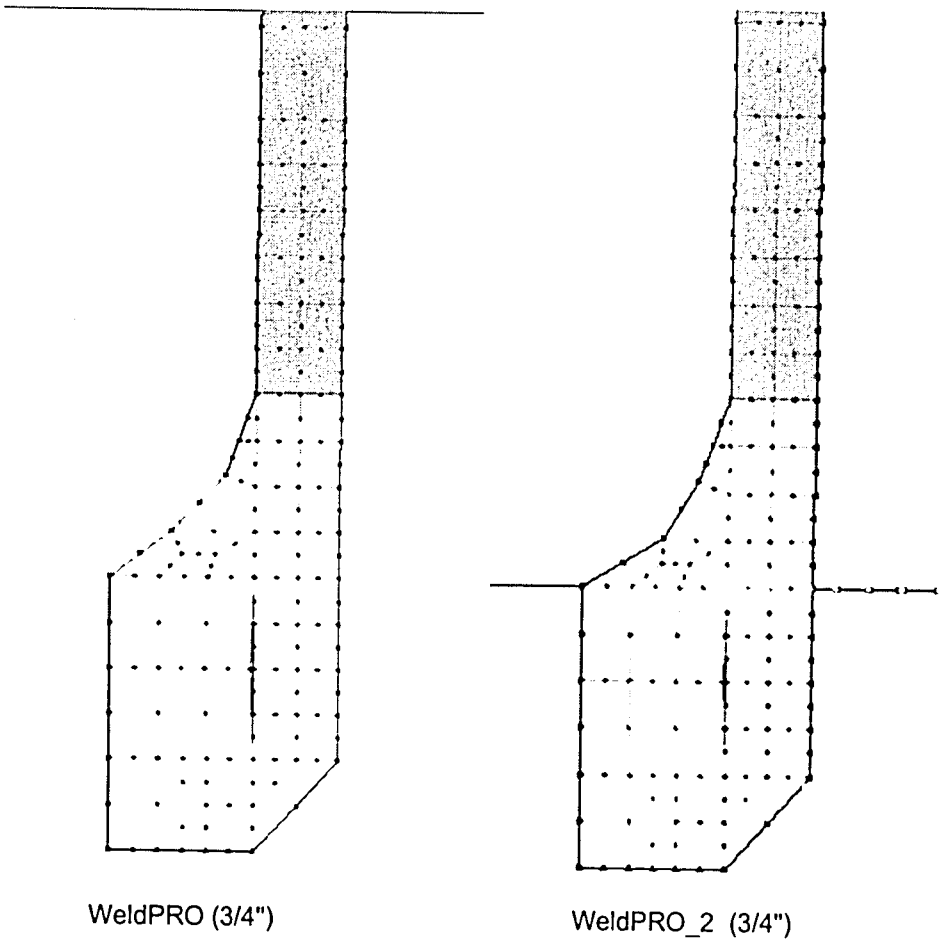

Figure 3.4.1.14: Cross Sections Through Weld Profile Finite Element Models for the 3/4" Baseplate Thickenss Specimen

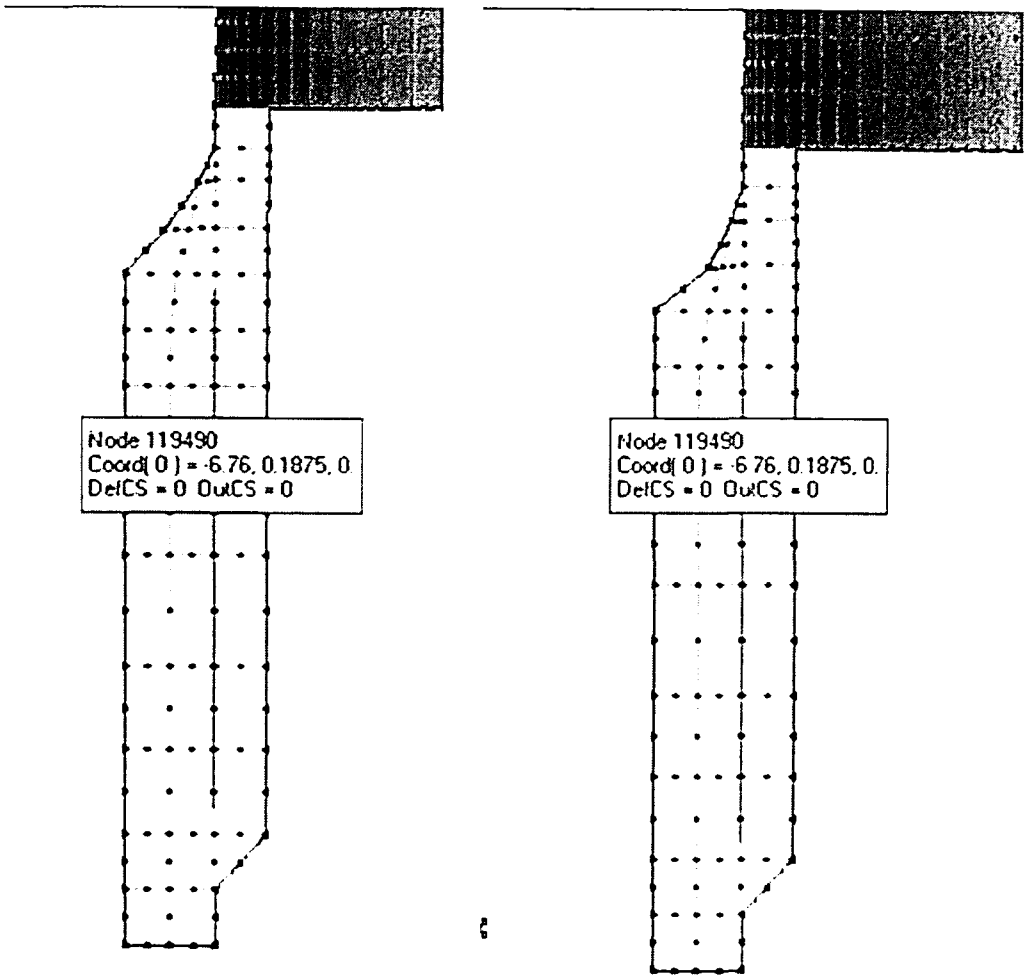

WeldPRO_VL (3")

WeldPRO_2_VL (3")

Figure 3.4.1.15: Cross Sections Through Weld Profile Finite Element Models for the 3" Baseplate Thickenss Specimen

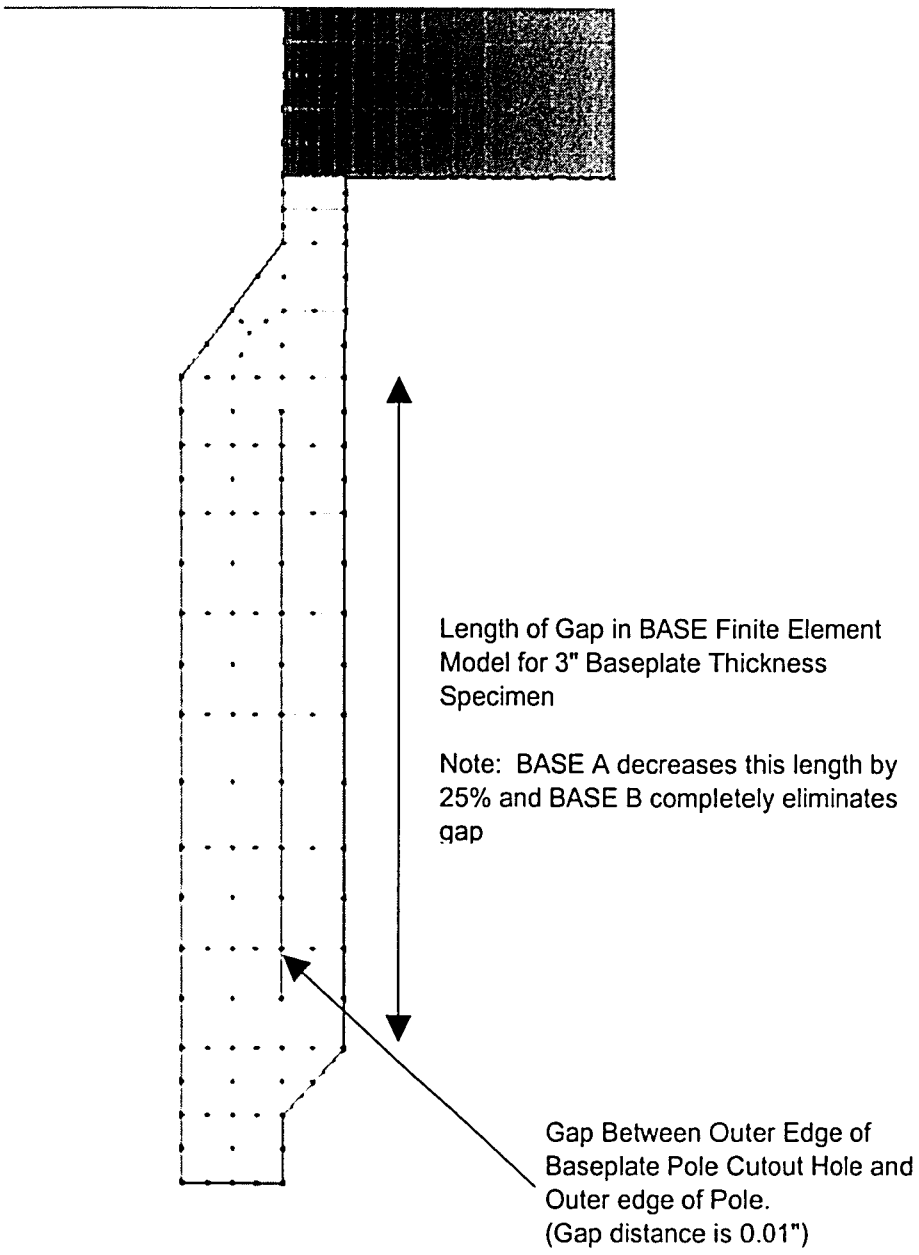

Figure 3.4.1.16: Cross Sections Through Weld Profile Finite Element Models Illustrating Different Gap Length Models for the 3" Baseplate Thickenss Specimen

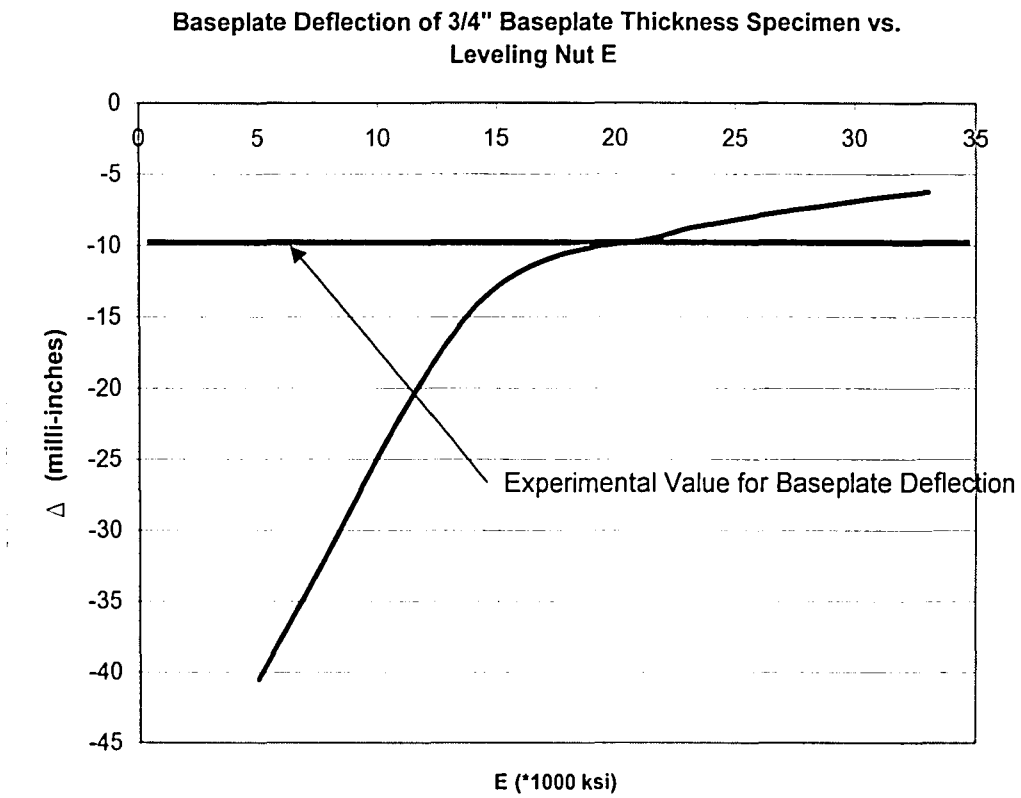

Figure 3.4.2.1: Leveling Nut "Softening" Approach to Leveling Nut Calibration Results

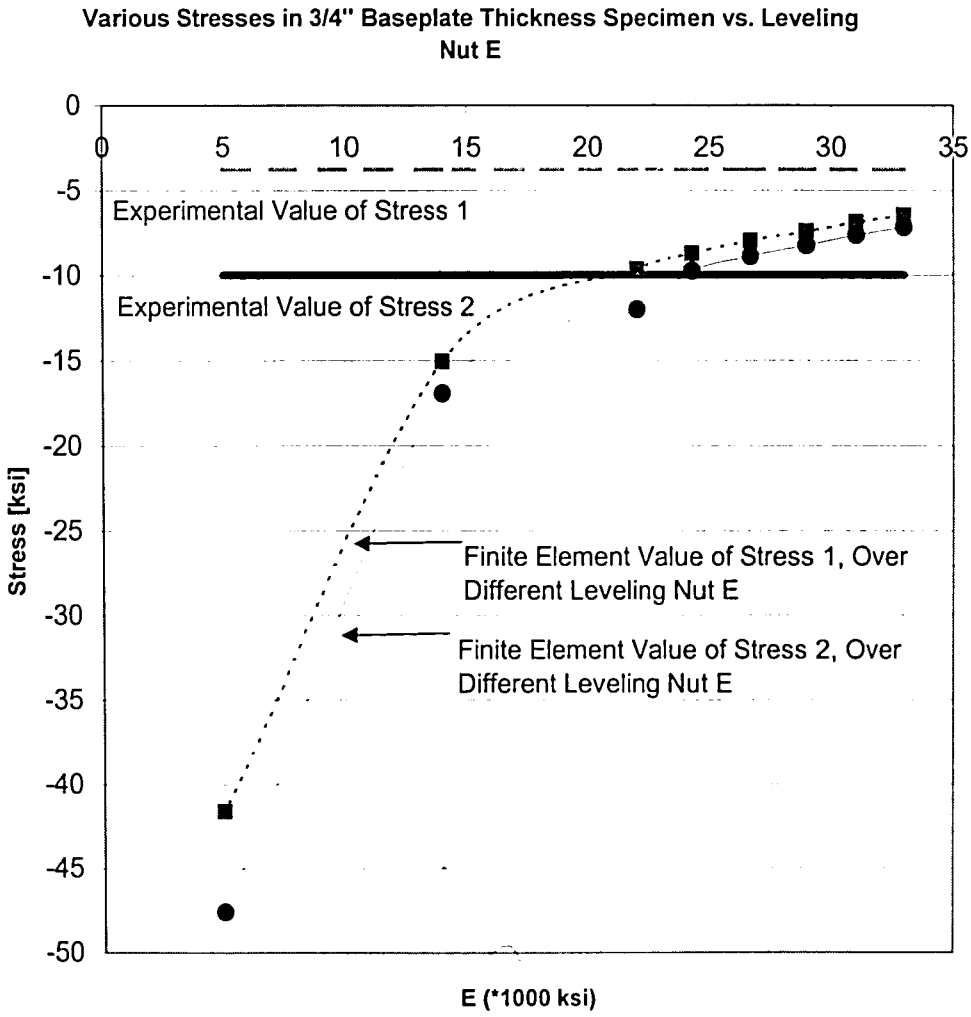

Figure 3.4.2.2: Leveling Nut "Softening" Approach to Leveling Nut Calibration Results

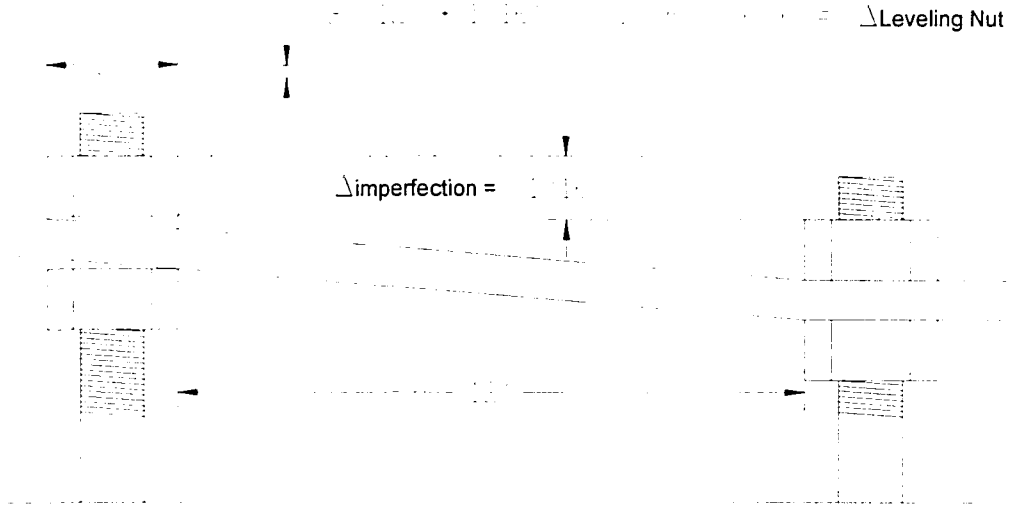

Figure 3.4.2.3: Leveling Nut Calibration Study Results; Diagram showing influence of baseplate out of level imperfections on the contact between the wrench tightened leveling nuts and the baseplate

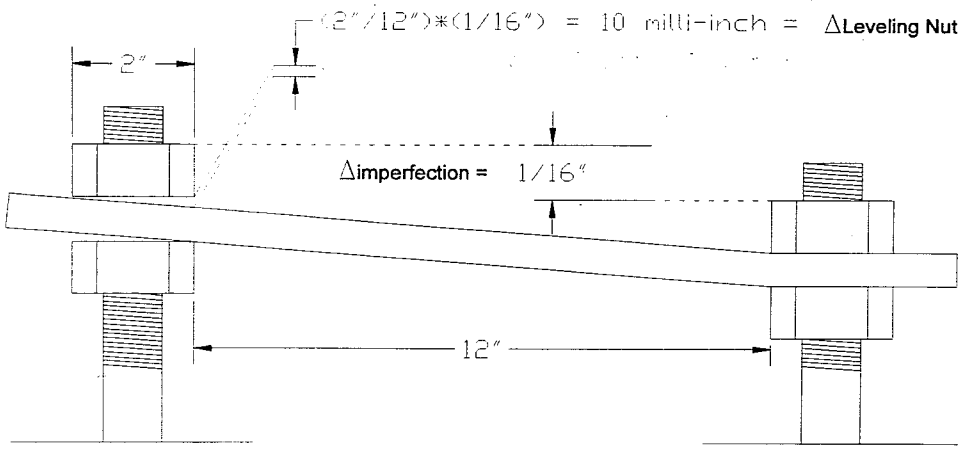

Figure 3.4.2.3: Leveling Nut Calibration Study Results; Diagram showing influence of baseplate out of level imperfections on the contact between the wrench tightened leveling nuts and the baseplate

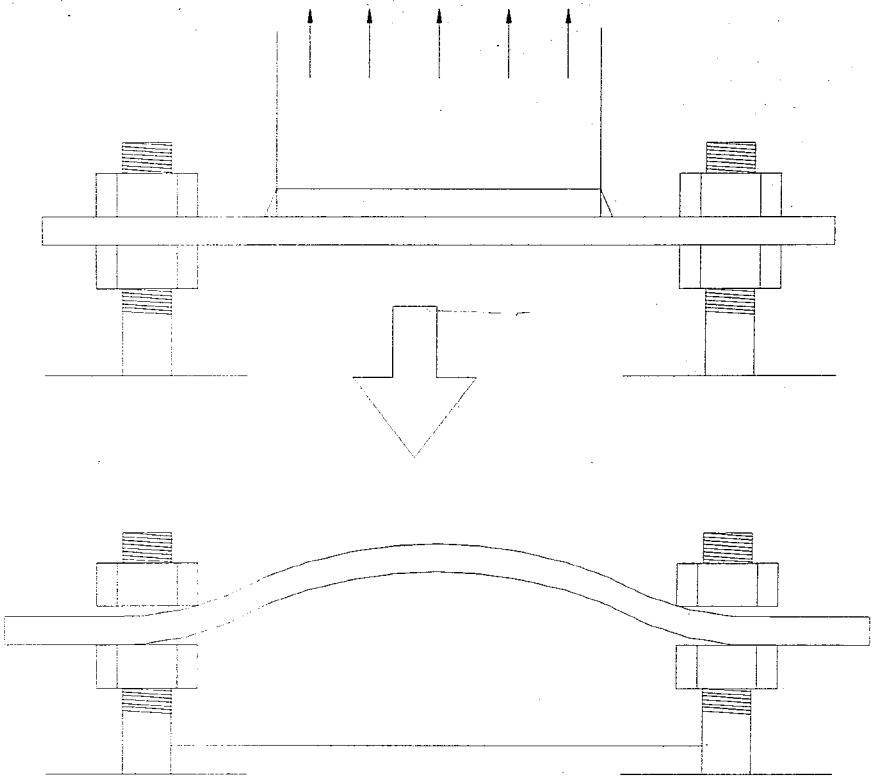

Figure 3.4.2.4: Leveling Nut Calibration Study Results; Diagram showing prying behavior due to partially tightened leveling nuts.

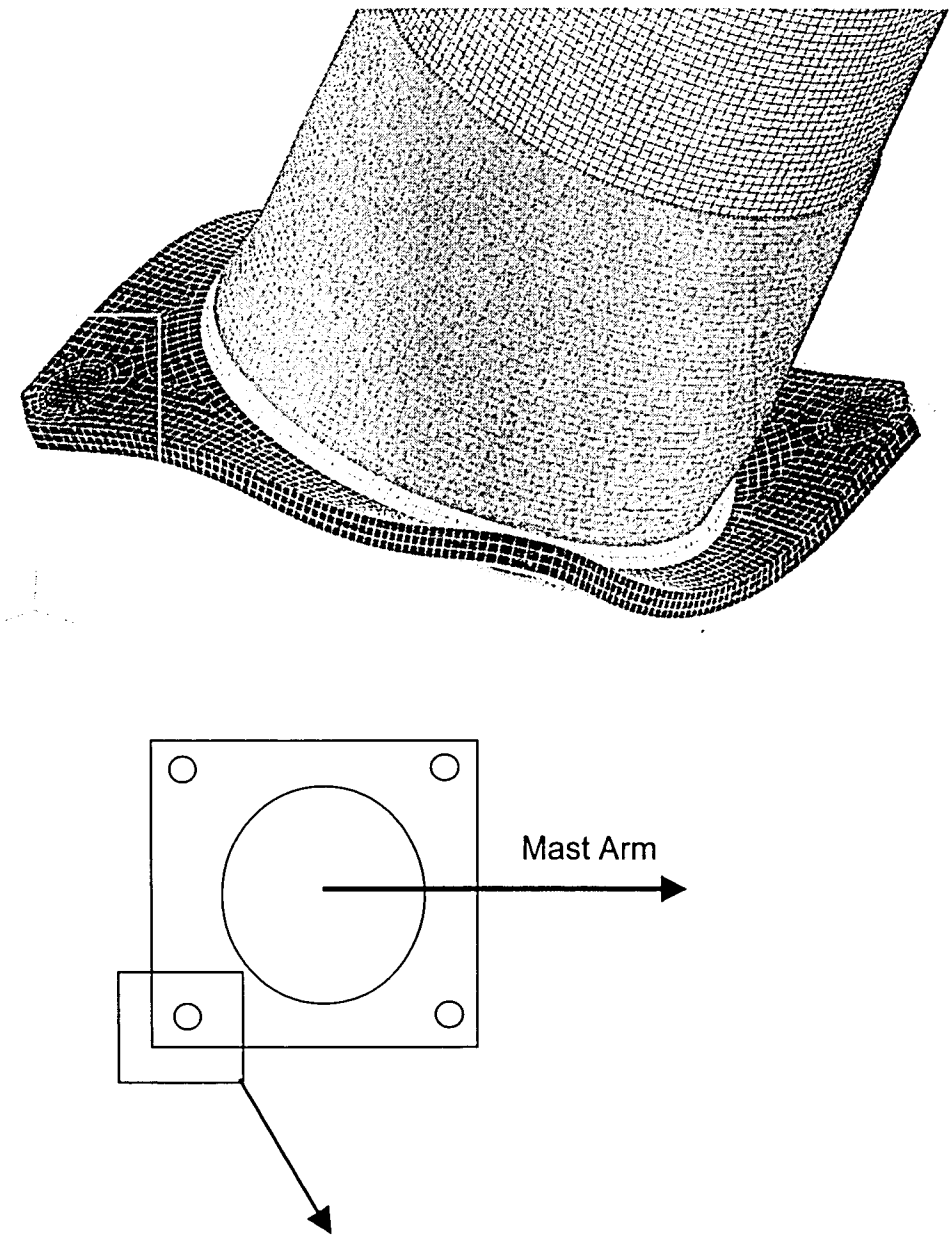

Figure 3.4.2.5: Leveling Nut Calibration Study Results; Pinned finite element model (above) and location of pinned baseplate deflection study (below)

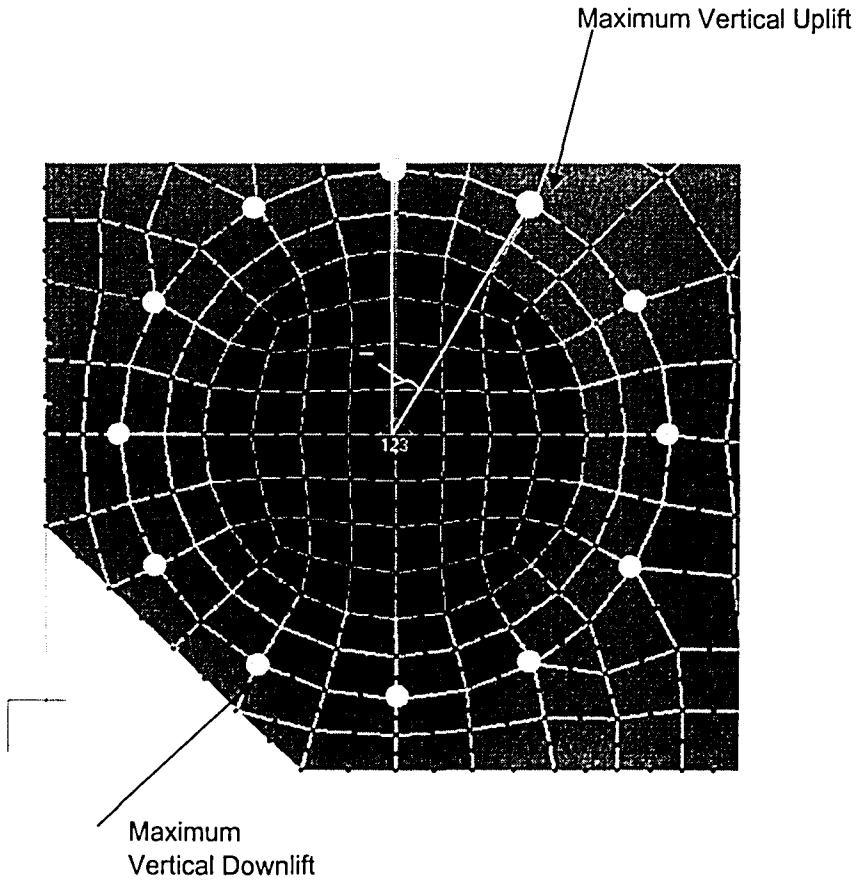

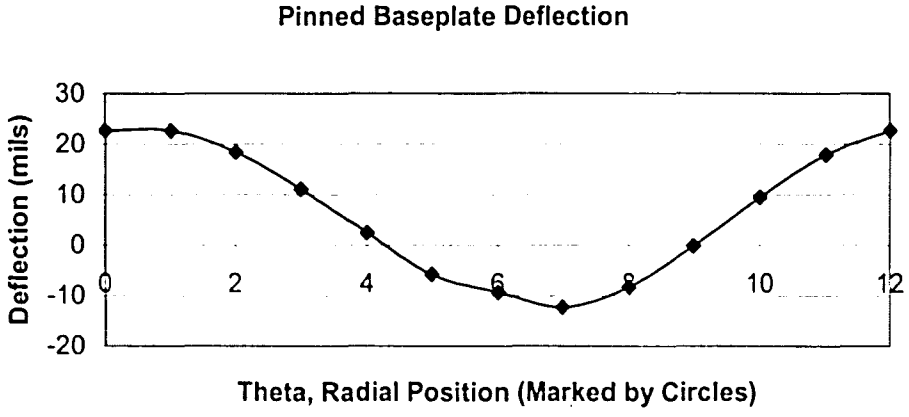

Figure 3.4.2.6: Leveling Nut Calibration Study Results; Pinned baseplate deflection

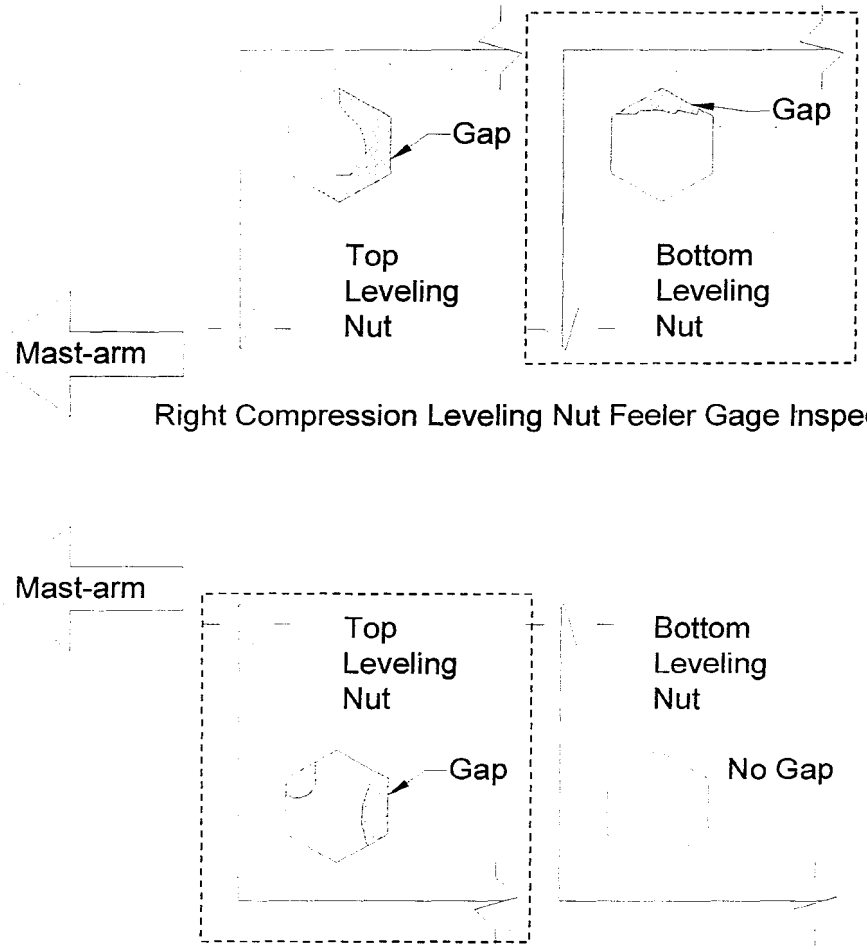

Figure 3.4.2.7: Leveling Nut Calibration Study Results; Diagram of gap locations found in feeler gage leveling nut contact inspection

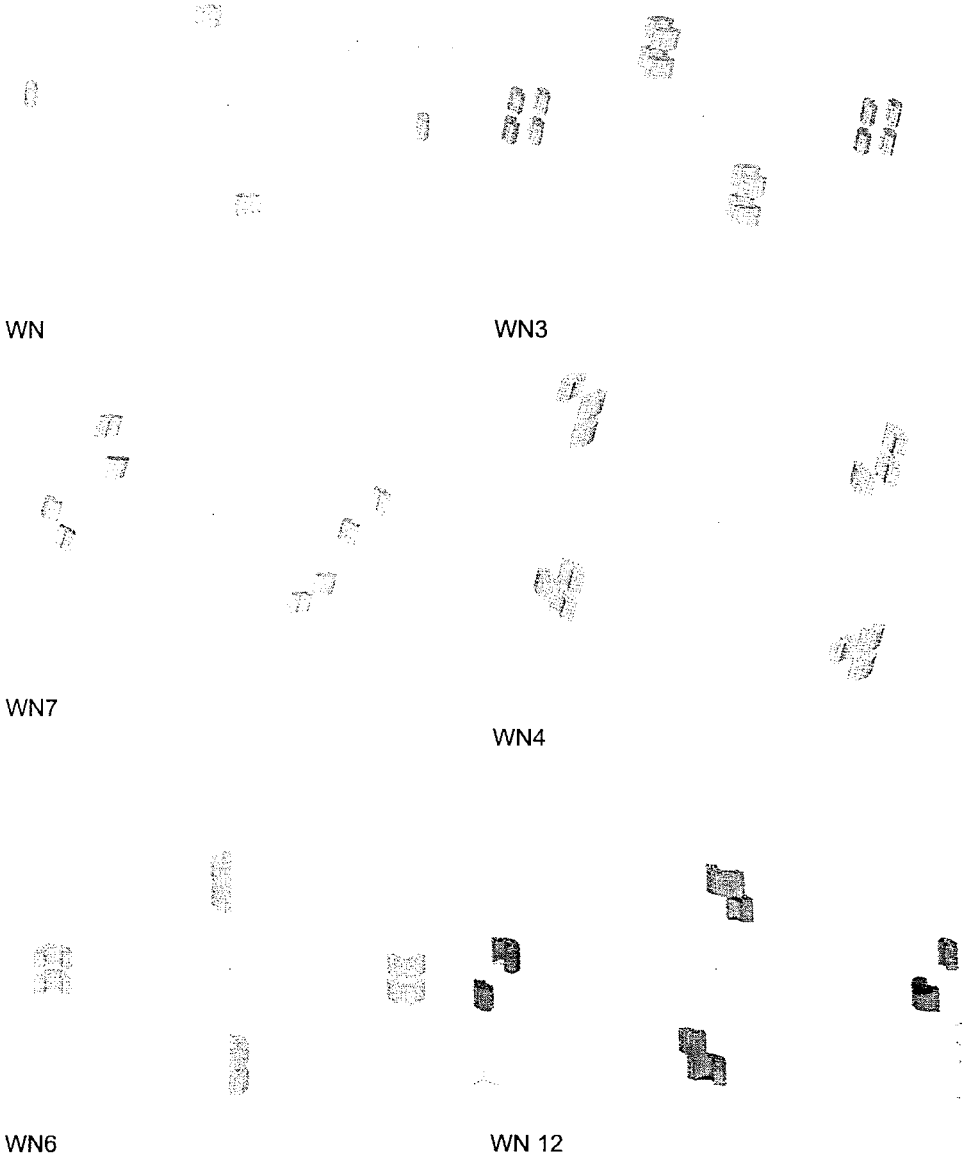

Figure 3.4.2.8: Leveling Nut Calibration Study; Several different partial levelin nut modeling options out of the 17 that were studied.

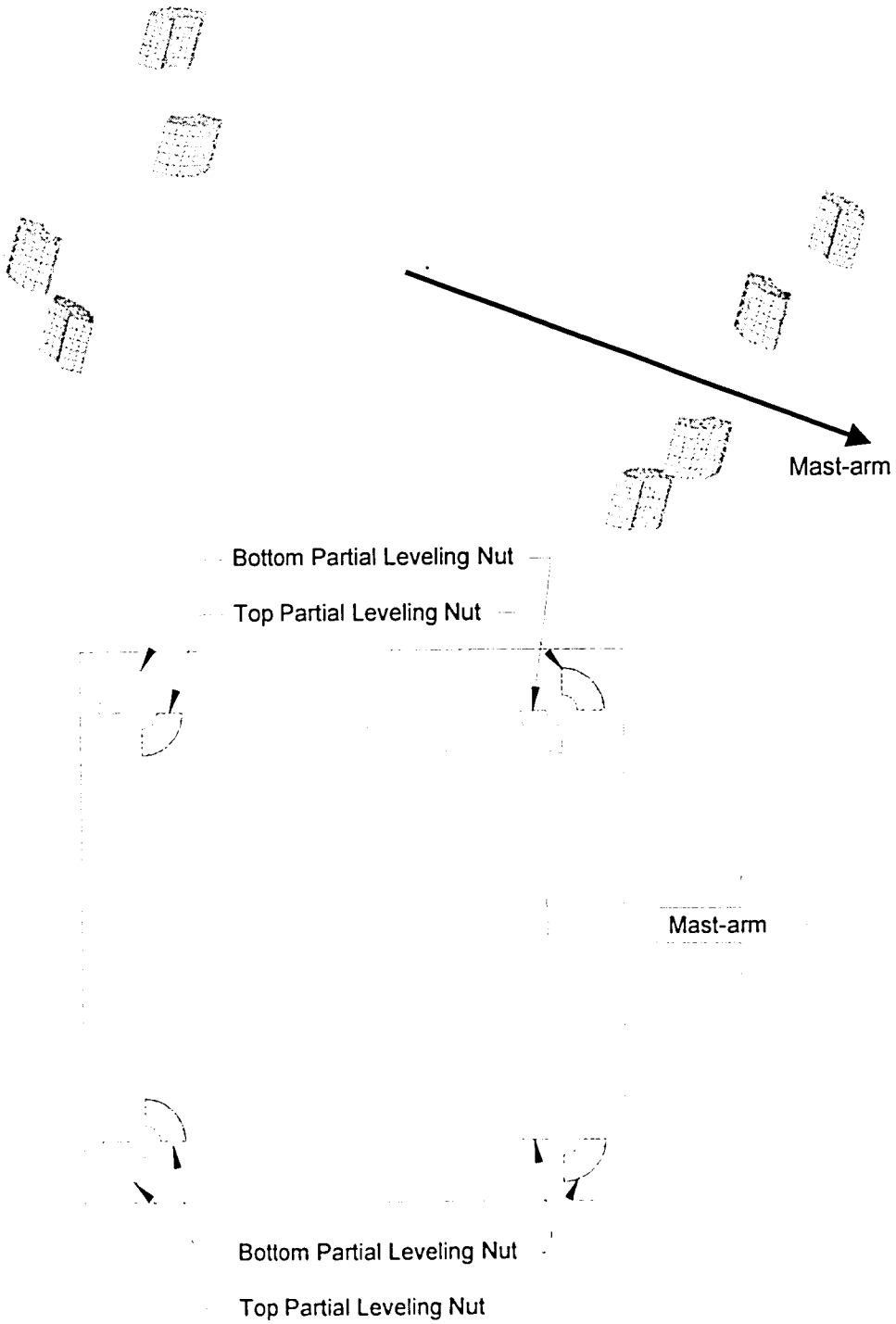

Figure 3.4.2.9: Leveling Nut Calibration Study; Close up of WN7 partial leveling nut modeling option (above), plan view of WN7 (below)

Chapter 4

Chapter 4 will focus on the behavior of welded socket connections. Both the results of finite element analysis and experimental testing will be discussed. Both the pole to baseplate and the mast-arm to endplate welded socket connections will be discussed. The results of chapter four provides the basis for the parametric study of Chapter 5, which will focus on fatigue performance. Chapter 4 begins by verifying finite element results correspond to experimental static testing data, thus validating the modeling techniques used in the parametric study. This discussion of data agreement is brief, merely presenting the two sets of data, with an emphasis on how the stress behavior influences data agreement. Chapter 4 then discusses the stress behavior and distribution in the tubewall, adjacent to the vertical weld toe of the socket connection. As mentioned before this is the location that sign structure fatigue research indicates fatigue cracking occurs. Chapter 4 also documents the results of two different unique experimental tests which may have a strong influence on fatigue performance. These tests involve stresses developed by baseplate leveling imperfections and different mast-arm bolting and fixity conditions. Chapter 4 concludes with a brief discussion regarding some possible improvements to the experimental test setup and instrumentation plan, that may have improved the understanding of the behavior and data agreement.

Section 4.1: Final Modeling and Experimental Results

The following section discusses the results of the final finite element model discussed above as well as the comparison of those results to experimental data of the

tubewall (Section 4.2.1), the experimental results of the baseplate leveling tests (Section 4.2.2), and the experimental results of the mast-arm testing (Section 4.2.3). Considering the difficulty involved, overall the finite element and experimental data agree very well. Through combined finite element and experimental study, the understanding of the behavior of mast-arm and pole socket welded connections has been greatly improved. Though no finite element studies were conducted specifically on the mast-arm, the experimental data collected shows very similar trends as those observed in the pole specimens. Also included in this section will be a discussion of some rather unusual behavioral issues of socket welded connections. The behavior observed in the baseplate leveling tests and the mast-arm washer spacer test, though overlooked in industry and research, could have serious implications on future design improvements and testing of socket welded sign structures.

Section 4.2.1: Final Finite Element and Experimental Tubewall Data

This subsection has two major objectives. The first is to briefly discuss the final comparison of experimental and finite element data. The second and primary objective is to discuss the behavior of pole to baseplate welded socket connections, particularly the stress distribution patterns in the tubewall adjacent to the upper fillet weld toe. The previous Section (4.1) summarized the outcome of the finite element calibration study, and the improvements and adjustments made to the final series of finite element models. One of the major result of the lengthy calibration study was that due to the complex structural properties and fixity conditions of the structure, the finite element agreement to experimental data may be limited. Improvement made to

the final finite element models, do show some improvement in data agreement between finite element and experimental data. Though similar problems exist in the data agreement as discussed previously, overall agreement with the final models is good. The main focus of the subsection, discussing the behavior of stress distribution, will also indicate the difficulty of obtaining agreement between finite element and experimental data. Chapter four will conclude with a discussion of possible sources of error in and improvements that could be made to both the finite element and experimental studies in an effort to improve data agreement (Section 4.3). These errors and improvements are very inter-related and may influence data agreement.

Final Discussion of Data Agreement

Tables 4.2.1.1 - 4.2.1.3 show the comparison of both tubewall experimental and finite element stresses, for the three baseplate thickness pole specimens. The finite element stress data shown is from the final series of finite element models with the improvements and adjustments discussed in Chapter 3. Overall there is a considerable improvement between the data agreement of this final series and the BASE finite element models discussed in the calibration study. The data in the first three Tables is presented in tabular format without statistical manipulation. Inspection of hotspot stress data (the stress measured closest to the weld toe), shows that the percent difference with respect to the mean stress value (the average of the finite element and experimental stress) rarely exceeds 15%. The percent difference at the other gage locations drastically improves as well. In general data agreement was especially good for the ¾" and 1 ½" baseplate thickness specimens. The finite

element results for the 3" baseplate thickness specimen again showed a concerning trend in poor data agreement between hotspot inner stresses. The 3" baseplate specimen data showed good agreement with hotspot outer stresses, and at the gage locations 2" and 5" above the baseplate. Additionally Figures 4.2.1.16 and 4.2.1.18, display the 3" specimen experimental and analytical stress data, in a vertical stress profile plot.

This problem with data agreement in the 3" baseplate specimen inner stress and the other minor data agreement issues are best examined through visual inspection of the vertical tubewall stress profile. In this manner the influence of the steep stress gradient can readily be seen, particularly with respect to naturally occurring experimental variation in stress and data agreement. The influence of the large stress gradient is illustrated in Figure 4.2.1.4. The resulting experimental and finite element stress profiles at the direct compression radial location due to the 100 pound cantilever end load is shown. The difference between the finite element and the experimental stress values is shown with the horizontal arrow. The corresponding difference in height above the baseplate is shown with a vertical arrow. The approximately linear stress gradient in region shown is typically 16 ksi per one inch of height above the baseplate, or 250 psi per 1/64". In regions of high strain gradients, agreement can be poor, for the reasons already discussed.

Vertical Stress Distribution Behavior Adjacent to Tubewall Weld Toe

As discussed one of the primary objectives of the study is to determine how baseplate flexibility effects fatigue performance. As discussed in the related research

section (1.6), two major cantilevered sign structure fatigue research studies on welded socket connections have shown that fatigue cracking and failure occurs at in the tubewall adjacent to the welded connection. This subsection will discuss the stress and local bending behavior in the pole tubewall adjacent to the critical fatigue location, the upper weld toe of the socket connection. In discussing the stress behavior and distribution in the tubewall it is very convenient to draw comparisons to the nominal or simple beam theory predicted stress behavior, used in the nominal stress fatigue design approach. As discussed in Section 1.5, the nominal stress fatigue design approach makes use of fatigue testing data results for different categories of fatigue connections. This fatigue testing data is used to assign nominally calculated, limiting stress ranges due to fatigue loading. Designers then adjust the pole geometry, primarily diameter and thickness, for these stress range limits. The major problem with this approach, as it relates to this study, is that tubewall stresses are drastically influenced by baseplate flexibility. Baseplate flexibility is a design parameter that under the nominal stress fatigue design approach, is not accounted for, and is not sufficiently accounted for nor fully understood in fatigue testing results. The final chapter (5), will discuss the parametric finite element study, which will attempt to determine the relationship baseplate flexibility has on tubewall stresses and to quantify baseplate flexibility. The following subsection will discuss the vertical stress distribution in the tubewall and explain how and why the stresses change with increasing height above the baseplate. The section will also discuss the distribution of stress around the circumference of the pole tubewall. In addition to the local bending

behavior, which will be most evident in vertical tubewall stress plots, a mid-plane stress, load path effect is also present in the tubewall behavior. This mid-plane stress is best shown in the radial stress distribution plots.

As strain data was typically measured at 4 different radial locations and up to 8" up the tubewall, for the three pole specimens, a considerable amount of data has been accumulated. What complicates this abundance of data, is that the behavior at the different radial locations is typically different. This difference in stress behavior is primarily concerning the stresses at the direct compression and tension compared to the 45 degree compression and tension locations. Aside from the minor stress effects of the hand access hole, tension and compressive stress data of corresponding radial locations experimentally and especially analytically showed a consistent equal and opposite relationship. Due to this abundance of data, as well as other reasons, several different vertical tubewall stress profiles are presented. Figures 4.2.1.4-18, show vertical tubewall stress distributions, including finite element and experimental data comparison and local bending and mid-plane stress distribution plots for all three specimens. These plots are all taken from the standard 100 pound cantilever end loading and the vertical axis is height about the baseplate. Note that finite element data is plotted beginning at the upper weld toe of the upper fillet weld of the socket connection. These stress profiles are important as visual inspection of the stress data clearly shows the full extent of the tubewall stress behavior and data agreement in a manner that tabular data cannot. Additionally these vertical and radial stress plots will also be the basis for the data collected and plotted in the parametric study in Chapter 5.

Having just discussed the abundance of data and the differences between different radial locations, there is a very clear, consistent, and definable flexibility effect common in the stress profiles adjacent to the socket connection at all radial locations (with the possible exception of those near the traditional neutral axis location). The simple and general description of the stress distribution will follow. After this description several additional points will be made regarding the more complex aspects of vertical stress profile and explaining the structural mechanism producing the stress distribution.

Prior to beginning the discussion of the vertical stress distribution results it is convenient to introduce two different types of stresses, mid-plane and local bending tubewall stress. Mid-plane stress, as the name would suggest is the stress in the center of the tubewall. Considering that stress within the tubewall varies linearly, the mid-plane stress is simply the average of the inner and outer tubewall stresses. Local bending tubewall stress to be discussed in greater detail later, is simply the difference between the mid-plane stress and the inner and outer tubewall stresses. The sign convention used in the study results in positive or tensile local bending stresses, if tension is being applied to the outer tubewall surface and compression is being applied to the inner tubewall surface.

The simplified approach to describing the typical vertical stress profile involves three typical vertical locations, shown in Figure 4.2.1.4. These locations and the general description apply to all locations and baseplate thicknesses. For illustrative purposes the stress profile in Figure 4.2.1.4 will be discussed to illustrate

the general behavior. At the first point marked as 1 in the plot, just above the weld toe, the outer and inner stresses are drastically different when compared to each other. Of course in simple beam theory the inner and outer stresses for a thin walled section are nearly the same. From this location to the point marked as 2 in the plot there is a very steep gradient in both inner and outer stress until they reach a peak value. As discussed in Section 1.5, Koenigs refers to this point as a valley, thus in future references this point will be termed the valley stress point (Koenigs 2003). The location of this valley stress point is consistently appears to be at approximately 2" above the baseplate, or approximately 1 ½" above the weld toe, with a slight variation of no more than 1/8". At this valley stress point the outer and inner stresses reach a minimum or maximum in the stress sense of the radial location. As shown in Figure 4.2.1.4, the outer stress reaches its' most non-compressive value of stress, while the inner stress reaches its most compressive value of stress. From this location to the location marked as point 3, both inner and outer stresses begin a gradual convergence to the simple beam theory predicted nominal stress. Complete convergence to this value of stress, would appear to occur 8" away from the baseplate in the compression regions. However as shown in the both the tension and tension 45 degree plots convergence to the nominal stress does not occur as the hand access hole produces local bending and prevents simple beam theory behavior, in which strain would be proportional to the distance from the neutral axis.

Three major points need to be discussed to complete the description of the behavior of the vertical stress distribution observed in the three baseplate thickness

pole specimens. These three points also provide an explanation as to how the structural behavior, baseplate flexibility, and deformations relate to the resulting stress profiles. The first major point discusses the stress profile difference and how it relates to local bending stress. The second point discusses how mid-plane stress and load path issues influence the vertical stress profiles at different radial locations. The third and final point to be made regarding the structural and vertical stress profile behavior, discusses how local bending, baseplate flexibility and deformation relate to the vertical stress distribution in the tubewall. The following paragraph will discuss these points, attempting to generalize the behavior at all radial locations, and explain the influence baseplate flexibility has on the particular issue.

Stress Profile Difference: The behavior in the vertical positions noted as 1 and 2, is marked by an extreme stress gradient as previously discussed. The unique profile in this region is defined by the flexibility effect on tubewall stresses. The stress profile between points 1 and 2 is defined by the peak stress in the tubewall just above the weld toe and the valley, or minimum stress value, which was found to typically occur approximately 2" above the baseplate. This difference between the two extreme values of stress, termed the stress profile difference provides a reasonable indicator of the flexibility effect in tubewall stress distribution. The concept of a stress profile difference can be applied to both experimental and finite element stress data, as well as to outer, inner, and local bending stresses in the tubewall. Given reliable data, local bending stress seems to be the logical choice to apply the stress profile difference

concept to, as it provides a measure of both the inner and outer stresses together. The difference in bending stress at the hotspot vertical location and the valley location thus would provide a flexibility parameter that includes the total flexibility effect of both the baseplate and tubewall. It is particularly useful to compare baseplate (or endplate) flexibility effects in structures either at different radial locations or with different tube geometries. The stress profile difference provides a good indicator of the flexibility effect as can be seen in the given Pole specimen Figures (4.2.1.4-4.2.1.19), and will be discussed in future discussion of endplate flexibility.

Mid-plane Stress and Load Path Effects: Mid-plane stress and load path effects are more conveniently displayed in a radial stress distribution plot, but do influence vertical stress profile data. Radial plots will be shown and discussed shortly. Mid-plane stress, the stress in the center of the tubewall is a good indicator of the load path with the tubewall. To explain the concept of load path, as it relates to baseplate flexibility it is convenient to consider the case of a sign structure with a typical downward vertical load. In satisfying equilibrium the two pairs of back and front anchor rods must respectively develop a tension and compressive axial reaction. In addition a bending stress distribution in which axial stress is proportional to the distance away from the horizontal neutral axis develops in the mast-arm, and a combined axial stress distribution with the additional resultant shear force divided by the pole area, develops in the pole tube. The baseplate then must transfer this distribution of stress from the pole to the anchor rod reactions. Because the anchor

rods are located at the corners of the baseplate, the pole radial locations that have the highest nominal stresses (absent from the flexibility effect) are located at the most flexible locations of the baseplate. In a manner similar to the classic elastic axial stress distribution problem shown in Figure 4.2.1.1A, due to the flexibility of the baseplate at the direct tensile and compressive locations, the compressive and tensile stresses cannot be effectively transferred into the baseplate. This behavior is very apparent in the radial diagrams, to be discussed shortly but can also be seen in the comparison of stress profiles at the direct compression or tension locations and the stress profiles at the 45 degree tension or compression locations. Comparing the direct compression and compression 45 vertical stress distribution profiles, as shown in Figure 4.2.15, this behavior is evident. In the direct compression radial location, the mid-plane stress is actually in tension from directly above the weld toe to up 2" above the baseplate. The profile at the compression 45 degree is different in that mid-plane stress is always compressive, as this is the load of the compressive anchor rod. A unique behavior of the vertical stress profile behavior is the manner that outer and inner stresses converge to the nominal simple beam theory stresses. In particular the stresses always follow the convergence of the mid-plane stress. Thus stresses at direct radial locations always converge from their opposite sense and stresses at 45 degree radial location converge from the same sense. As shown in Figure 4.2.1.5, the mid-plane stress adjacent to the fillet weld is opposite of its expected sense, and thus the inner and outer stresses converge from this opposite sense, becoming more compressive further away from the baseplate. This behavior is not trivial, but rather

very significant, because this direct location is the typical location that one would measure strain. Thus at this location, direct compression or tension, the outer stress will be less than the simple beam theory nominal stress, until convergence is reached.

Bending Deformation Relation to Stresses in Tubewall:

Baseplate flexibility primarily influences tubewall stresses local to the socket connection in two ways. As discussed above, baseplate flexibility influences tubewall stresses by the mid-plane load path effect. The second way baseplate flexibility influences tubewall stresses local to the baseplate is through local bending behavior. Comparing the two effects of baseplate flexibility, local bending behavior has a much greater influence on tubewall stress, especially in flexible baseplates. Local bending behavior influences tubewall stress, through the local deformations of the tubewall to baseplate fillet welded connection. The translational and rotational deformations of the baseplate and tubewall, as well as the relative rotational deformations between the tubewall and baseplate influence the tubewall stresses. The main idea of local bending behavior is that the baseplate local to the tubewall has different flexibilities at different locations along the tubewall to baseplate interface. The baseplate is typically the most flexible at mid baseplate along the mast-arm axis at the direct tension and compression radial locations. This flexibility allows for out-of-plane deformations near the baseplate, thus the primary prerequisite of simple beam theory is not met, as plane sections do not remain plane. The flexibility of the baseplate and tubewall both contribute to the overall stiffness of the connection, and determine the local deformations. The flexibility hence is determined by several structure geometric

aspects such as baseplate thickness, anchor rod spacing, leveling nut fixity, fillet weld geometry, pole stiffness, and tubewall thickness. The local bending effect of baseplate flexibility on tubewall stress though should not be confused with the p-d effect. Secondary effects, or the amplification of stresses due to the bending created by deformation, were considered and found not to be significant for the small deformations and elastic loads.

The most convenient way to explain the flexibility induced local bending influence on tubewall stresses is to show sections through the deformed structure. Beginning with the behavior of the tubewall at the direct compression and tension radial locations, Figure 4.2.1.3A shows a cross section of the deformed baseplate and tubewall through the mast-arm axis. As the behavior at the compressive side and the tensile side, is the same, only the behavior at the tensile side will be discussed. Note it may be convenient to refer back to the vertical stress profile diagrams at the direct tension radial locations, including Figures 4.2.1.9 (3/4" specimen), 4.2.1.13 (1 ½" specimen), and 4.2.1.17 (3" specimen). Defining positive local bending stress as that which will create tension on the outer tubewall surface and compression on the inner tubewall surface, the local bending stress in the tubewall is positive from the top of the vertical fillet weld toe until a height of approximately 1.25" above the baseplate, or approximately 0.75" inches above the vertical fillet weld toe. According to the definition of bending stress, in this region the tubewall deformation is such that tension is being applied to the outer surface, and compression is being applied to the inner surface. Figure 4.2.1.4A shows a close up of the direct tension location, note

that the curvature of this region matches the local bending stress. As shown in Figure 4.2.1.4, above this region, an inflection point occurs and the curvature of the tubewall changes. As shown in the vertical stress profiles, this same location corresponds to the change of sign of the local bending stress. Thus a compressive stress is applied to the outer tubewall surface, due to the deformation of the tubewall. As discussed previously the mid-plane stress at the direct tension (and compression) radial location for more flexible baseplates is compressive. Thus the positive value of the magnitude of bending stress added to the negative (compressive) value of mid-plane stress gives the outer tubewall stress. Thus at both the direct compressive and tensile radial locations the two major effects of baseplate flexibility, the mid-plane load path effect and the local bending stress deformation effect act in opposite magnitude. This offsetting relationship between to the two different baseplate flexibility influences can also be seen numerically in the vertical stress profiles. The behavior can also be seen clearly in radial stress distribution diagrams, especially in comparison with 45 degree radial locations which, will be discussed next.

The local bending stress and deformation behavior is shown in Figure 4.2.1.2A, a deformed model cross-section through the diagonal axis. Again the discussion will focus on the tension side, as the behavior on the compression side is the same. The local deformation of the baseplate to tubewall connection at the tension 45 degree radial location is considerably different than that of the direct tension radial location, above. Note that due to the closer proximity to the leveling nut, the baseplates translation is impeded, and replaced by a rotation. Also note that the

relative rotation between the tubewall and the baseplate is much larger than in the deformed structure at the direct tension radial location. As will be shown in the future discussion of radial stress distribution diagrams, local bending stress is typically greater at the 45 degree radial locations, than at the direct tension radial locations further away from the anchor rod and leveling nut connection which provides fixity to the baseplate. Though no close up is shown, the same behavior as discussed above exists in the tubewall at the tension 45 degree location. From the top of the vertical weld toe up to a height of approximately 1.5" above the baseplate, the tubewall deforms such that positive local bending stress is applied. As shown in the figure the curvature shows tension on the outer tubewall surface, and compression on the inner tubewall surface. The difference in the 45 degree radial location behavior is that the mid-plane stress is in tension. Thus an additive relationship develops and the tensile local bending stress is additive with the tensile mid-plane stress.

Weld Profile Effects on Local Outer Stress Gradient: An interesting point regarding the vertical distribution of outer tubewall stress was unexpectedly uncovered in developing the parametric study. This unexpected observation regarded the bottom portion of the finite element data displayed in the vertical stress distribution plots. Particularly the behavior of outer tubewall stress less than 1/8" directly above the upper fillet weld toe. As shown in Figures 4.2.1.4-4.2.1.19, outer stress of the 1 ½" and 3" thick baseplate specimens has a small "kink" at the 45 degree tensile radial locations. Such that the outer stress directly located at the edge of the weld toe (which

correspond to the lowest data point or the beginning of the plotted stress) decreases, and is less than the stresses located vertically above it. This behavior is not seen in the 1 ½" or 3" specimen data at the direct tensile radial location. This behavior, marked by the kink at the weld toe, at the 45 degree radial location, is also not seen in both the ¾" specimen direct or 45 degree tensile radial location data.

This trend in this behavior of outer stress at the weld toe for the three specimens, was overlooked for the most part, given the small magnitudes of the difference in stress. The behavior was then recognized in the development of the parametric study, in which the exact values of these outer stresses near the weld toe were more important. The weld toe profile of the parametric study was the same weld profile of the 1 ½" thick baseplate specimen, which is considerably larger than the small weld profile of the 3/4" specimen. Thus it strongly appears that the behavior involves the size and inertial properties of the weld profile. The inertial properties of the larger weld profiles act to reduce local deformations directly at the edge of the weld toe, as would be expected. Unfortunately due to time constraints, the effects of different weld profiles have not been covered in any significant depth. This unexpected observation is really an indication of the enormity of the factors that influence flexibility effects in socket connections. It indicates that more finite element work studying the effects of weld profile geometry could be performed. Additionally it indicates that though the study has attempted to cover the typical geometry of the structure, the study does not cover the wide range of possible geometries, which do influence flexibility and behavior.

Radial Stress Distribution Behavior Adjacent to Tubewall Weld Toe

The main objective of the study is to determine the influence of baseplate flexibility on fatigue performance and design of sign structures utilizing welded socket connections. Thus it is critical to determine how baseplate flexibility behavior influences tubewall stresses local to the vertical fillet weld of the socket connection, particularly how these local tubewall stresses differ from nominal design values, derived from simple beam theory analysis, and the trends in flexibility influenced behavior under decreasing baseplate flexibility. The following discussion focused on this complex three dimensional behavior, discussing the stress behavior and profile in the vertical plane. Several key aspects of the baseplate flexibility induced tubewall behavior have been discussed. The following discussion will review the behavior as it relates to the radial distribution of stress. In addition comments will be made regarding the trend in tubewall stress behavior under increasing baseplate flexibility.

Prior to discussing the radial stress distribution, a couple of quick notes must be made to aid in the understanding of the radial distribution charts used to illustrate the behavior. Figure 4.2.1.20 is the first of 5 radial distribution figures to be discussed. Additional illustrations have been added so that this plot can serve as an example of the method the stress distribution data is presented. The following discussion focuses on the results of static end cantilever loading of 100 pounds. This section only serves to discuss the radial distribution of behavior, thus no experimental data will be used or compared to the finite element results. The finite element results

presented are the same results as have been previously discussed and conform to the exact structural geometries of the test specimens. As discussed previously, the critical fatigue location is at the tubewall adjacent to the veridical fillet weld toe, thus finite element stress data from this region has been used in the creation of the plots. All stress data is taken from the inner and outer tubewall, at the hotspot or experimental gage location closest to the weld toe. Specific to radial distribution plots, data points are plotted on a radial plot. These data points represent various finite element stresses recorded at 11.25° intervals, or 8 intervals per 90°. The orientation of the baseplate and mast-arm are indicated with the mast-arm pointing up the page, and tension being at the bottom of the page. For every interval around the tubewall the values of stress are plotted. Note that some of the plots are more clear, when stress values are presented as absolute values, thus negative values appear in the same position as positive values. The description of these plots will indicate the behavior, though vertical stress distributions can be referred to as well to provide this information.

Figure 4.2.1.20 shows the radial axial stress distribution plot for the ¾" thick baseplate specimen. This particular thickness represents an extreme in baseplate flexibility, and hence the radial distribution of stress also represents the extreme in stress behavior and radial distribution. First note that the symmetry in the stress distribution, about the mast-arm axis, as well as the neutral axis. Symmetry about the mast-arm axis is expected, as the structure geometry, restraints, and loading are symmetric. The symmetry about the neutral axis, is much less exact, though still in very good agreement. This would also be expected as aside from the relatively small

value of axial stress transferred by the pole, the bending and baseplate flexibility conditions are the same on the tension and compression sides of the baseplate.

The outer tubewall stress distribution, beginning at the direct compression location, reads a value of 5 ksi. As discussed previously this value is actually a compressive or thought of as a negative 5 ksi. Following the outer tubewall stress around the pole towards the right compressive anchor rod, the outer stress becomes more compressive reaching a value close to -10 ksi. Continuing along the tubewall in a clockwise radial direction, the outer stress decreases to a stress of approximately zero. Likewise on the tension side of the neutral axis, the outer stress is always tensile or positive. Again the maximum outer stress is recorded at a radial location approximately in line with the anchor rod. In future discussion, this location and flexibility trend of this location of this maximum outer stress will be discussed. Additionally the tensile outer stress also is considerably less at the direct location, than at the 45 degree radial location of maximum stress.

The inner tubewall stress follows a more regular radial distribution pattern. However two important aspects of the stress distribution must be made clear. First, the inner stress behaves opposite to the expected sense of the stress, such that the values shown on the traditional compressive side of the tubewall (above the traditional neutral axis) are tensile, and on the traditional tension side of the baseplate the inner stresses are compressive. The simple explanation of this behavior especially for very flexible baseplates, follows that at the direct tensile and compressive regions, due to the baseplate flexibility effect, the mid-plane stress is small and the bending stress is

still reasonably high. Thus the inner and outer stresses are roughly equal and apposite. The second point regarding the inner stress distribution is important to the observer that is not overly familiar with the radial plotting scheme used. It would appear that at the direct compression (or tension locations), the inner stress reaches a maximum, then slowly decreases toward the 45 degree radial position. However the stress shown is actually constant for the first three intervals. This is a fairly interesting point, that the inner stresses on the compressive and tensile sides of the pole are constant over a good portion of the inner tubewall.

As discussed previously the local bending stress in the tubewall does slightly increase at 45 degree radial locations, especially in flexible baseplates. As shown the maximum bending stress occurs in line with the anchor rod (at 45 degree radial locations) on the tensile side of the baseplate. Though on the compressive side of the pole, the maximum bending stress occurs closer to the direct location, though approximately in line with the anchor rod. The local bending stress as discussed regarding the vertical profiles provides a compressive or negative value on the entire compressive side of the pole and tensile or positive value of local bending stress on the traditional tension side of the pole. As discussed previously, this translates to a compressive force being applied on the outer tubewall due to deformation on the compressive side of the pole and likewise a tensile stress on the traditional tensile side of the pole.

The strange shaped stress plot in the center of Figure 4.2.1.20 is the mid-plane stress. The behavior of the mid-plane stress has already been discussed, in the vertical

stress profile section, and will be further discussed shortly. At the present time, note that first the magnitude of the mid-plane stress, and thus load path effects is much smaller compared to the magnitude of the local bending stress and thus deformation effects. Also the shape of the plot, as previously discussed is representative of mid-plane stresses being opposite of the traditional sense (e.g. compressive on the traditional tensile side of the pole) at the direct tension and compression radial locations. And at the 45 degree radial locations, in line with the anchor rods, the mid-plane stress is of the expected sense. Thus the shape reflects, the mid-plane stress changing signs. Finally it is important to illustrate the relationship between the inner, outer, local bending and mid-plane tubewall stresses, as discussed previously in the vertical stress distribution discussion. According to the sign convention adopted, the outer tubewall stress is the local bending stress added to the mid-plane stress, and the inner stress is the negative local bending stress added to the mid-plane stress. Examining the traditional tension side of the pole, and at the direct tensile radial location, note that the positive local bending stress added to the negative mid-plane stress reduces the outer stress at the direct radial location. At the 45 degree radial locations, in line with the tension anchor rods, note that the mid-plane stress is also tensile, thus the outer stress in increased as it is the product of both the positive and tensile local bending and mid-stress.

Figure 4.2.1.21 shows the radial diagram of the 3" specimen, representing the opposite extreme in baseplate flexibility. The same additive relationships exist between the various tubewall stresses, though the distribution and relative magnitudes

are considerably different from the ¾" thick specimen. The outer, inner and local bending tubewall stresses are all very much less than those of the more flexible ¾" baseplate specimen. Note that the flexibility effect, both due to mid-plane, load path effects and the local bending effect, is not as apparent as in the ¾" specimen, as can be seen in the outer stress profile. Note that the outer stress profile does not have the distinguishable decrease in outer stress at the direct tension and compression locations. There is some small decrease in outer stress at the direct tensile and compressive radial locations, but not nearly as much as in the ¾" baseplate. Note that similar to the ¾" specimen, the outer stress and the local bending stress behave in the expected sense, with compressive (negative) stresses in the traditional compressive side of the neutral axis. The inner stress is opposite of the traditional state of stress, such that inner stresses on the traditional compressive side of the pole, are all tensile. Another major difference between the radial stress profiles of the ¾" and 3" baseplate specimens is that the 3" inner stress magnitudes are very much smaller when compared to the outer stress magnitudes. In the ¾" thick baseplate specimen, the inner and outer stresses though different in shape are approximately of the same magnitude.

Figures 4.2.1.22-24 plot (in order) the mid-plane stress, local bending stress, and finally outer tubewall stress of the three different baseplate thickness specimens, showing the trend of baseplate flexibility on radial stress distribution. As discussed previously the ¾" thick specimen mid-plane stress plot produced a rather unique shape. This shape is shown, as well as the mid-plane stress radial plots of the 3" and 1

½" thick baseplate specimens, in Figure 4.2.1.22. Note for this figure only, the actual values of stress not the absolute values are plotted. As illustrated in the plot, the ¾" mid-plane stress is positive or tensile in the direct compression region, and negative or compressive in the direct tension radial location. Again the mid-plane stresses at the 45 degree radial locations, in line with the anchor rods follow the traditional sense, with compression and tension at their traditional locations relative to the neutral axis. The most important trend to note in the figure is that the mid-plane stress distribution changes with increasing baseplate thickness or increasing baseplate stiffness. First note that mid-plane stresses of the three different baseplate thickness specimens is very consistent at the 45 degree radial locations. It may even appear that with increasing thickness, a constant value of mid-plane stress is reached at these 45 degree radial locations. This is indicated by the fact that there is very little difference between the 1 ½" and 3" data, when compared to the difference between the 1 ½" and ¾" data at these locations. In addition with increasing baseplate thickness the mid-plane stress at the direct compression and tension locations, decreases, so that the sense of the stress conforms to the traditional state of stress.

Figure 4.2.1.23 presents similar data, illustrating the trend in local bending tubewall stress over increasing baseplate thickness. Note first that the magnitudes of local bending stress decrease considerably, possibly in a non-linear or exponentially with increasing baseplate thickness. The other key point to make regarding the radial distribution of the local bending stress, is that due to increasing baseplate thickness, the shape of the local bending stress profile also changes. In the ¾" thick baseplate

specimen data, there is a noticeable decrease in the local bending stress at the direct tension or compression radial locations. However this dip in local bending stresses is not considerable in the 1 ½" and 3" baseplate thickness data.

Given the trends of mid-plane and local bending tubewall stresses with increasing baseplate thickness, the radial distribution of outer tubewall stresses will also decrease in magnitude and become more regular. Figure 4.2.1.24 shows the radial distribution of outer tubewall stress for all three baseplate thickness specimens, and the nominal simple beam theory predicted outer stress distribution. Again note that with increasing baseplate thickness and hence increasing baseplate stiffness, outer tubewall stress located in line with anchor rods, decrease, producing a radial stress distribution profile similar in shape to that of simple beam theory.

Section 4.2.2: Baseplate Leveling Test Results

The procedure used in the baseplate leveling tests and the justification for studying the influence of out-of-level erection imperfection loading was previously discussed in Sections 2.4. In summary the baseplate leveling tests were performed by recording tubewall strain and baseplate displacement data through a series of enforced baseplate positions. The testing sequence began with the baseplate of the pole specimen in a level position, as indicated by simple leveling measuring equipment. The baseplate was then raised up 1/16" of an inch, measured in line with the anchor rod. The leveling nuts were raised in order to achieve the enforced baseplate displacement. As this process typically resulted in some fairly sizable mast-arm oscillations, the specimen was allowed to come to rest, and the baseplate was raised an

additional 1/32". Again the specimen was allowed to come to rest, after which it was enforced back to its' original position. The major justification for this testing was to see the influence of a reasonably small erection imperfection on tubewall stress. These small imperfections are likely common in the erection process, as well are the stresses produced by the imperfections. The test results may also have some implications considering the use of UIT weld treatment to sign structure pole socketed connections. Particularly that if in the design process a UIT treated specimen may be considered to be in an initial state of compression at the tube wall side weld toe. However if construction imperfections are present, especially baseplate leveling error this assumption of compression at the weld toe may be incorrect.

Baseplate leveling tests were performed on all three pole specimens. The first specimen tested, the 1 ½" thick baseplate pole specimen received the most attention in the testing program, and thus has the most data available for analysis. Due to the abundance of data on the 1 ½" baseplate pole specimen, it will be the primary focus of this section. As expected due to the unique fixity conditions between the leveling nut pairs and the baseplate there is some scatter in the data. In addition another source of scatter in the data related to the measuring tolerance, as it was difficult to accurately measure the small enforced baseplate displacement, without complex measuring equipment. The scatter in the baseplate leveling data however is minor, and is only significant in showing that the influence of fixity in the leveling nuts is a complex behavior. The objective of the baseplate leveling testing, never intended to determine an exact response due to the behavior, but examined the problem through a case study

type approach. Several data records were taken of each specific test to provide a range of data, which in turn provides a very reasonable value for the strains induced in the tubewall.

A typical data record is shown in Figure 4.2.2.1A. Note that after the baseplate is returned to its original position where under a simple linear elastic analysis approach would correspond to zero stresses, one particular gage has a considerable non-zero stress. This data result was fairly common, and could be minimized by repeating the same baseplate leveling test, to reseat the baseplate. The result was indicative of a change in the fixity and hence deflected shape of the baseplate, such that when the baseplate was returned to its' original position a different state of stress was induced in the tubewall due to baseplate bending. The influence of this 'unseating' was ultimately not able to be controlled by the test-set up. The influence on the data was minimized as much as possible.

Prior to beginning the discussion of the experimental results, it is helpful to make use of the symmetrical characteristics of the behavior observed in finite element and experimental study. The highly symmetric geometry of the pole specimens and baseplate leveling imperfection loading, including symmetry about the mast-arm axis, neutral axis, and the diagonal axis (between opposite anchor rods), results in a highly symmetric stress distribution. Through finite element analysis trends in symmetry were verified. The effects of the hand access hole, which is the only non-symmetric aspect of the pole geometry, were shown to be negligible adjacent to the tubewall weld toe. Typically the resulting percent differences due to the hand access hole were

smaller than eight percent. Experimental strain data also confirms these symmetries, though due to scatter in the testing data, finite element study was required to ensure that the symmetry trends existed. The finite element and experimental baseplate leveling imperfection test results showed a total of five different symmetries. These symmetries included symmetry with the loading location, loading direction and the resulting stress profile itself. The simplified method used in simulating the finite element baseplate leveling imperfection loading, and other details of the finite element analysis will later be discussed, prior to the discussion of the results.

These five symmetries are illustrated Figure 4.2.2.2 and Figure 4.2.2.3. Because the reasoning for all of the symmetries is fairly intuitive a quick review of the figures will be presented. The first symmetry, shown as Symmetry 1, indicates that the stress profile is symmetric about the diagonal axis of the anchor rod causing the baseplate to be out of level. This is fairly simple to see as the structure geometry (neglecting the hand access hole), loading, and reactions are all symmetric about the diagonal axis. The second symmetry is also fairly straight forward. As shown an upward enforced baseplate deflection results in an equal-and-opposite stress compared to that resulting from a downward enforced baseplate deflection. The final three symmetries follow the same pattern. The general symmetry involves two different loadings applied, that are symmetric, and then corresponding stresses, at points symmetric about the same axis, will be the same. The third symmetry shows that if two enforced baseplate loadings are symmetric about the mast-arm, then resulting stresses due to the two loadings at points symmetric about the mast-arm will be the

same. The fourth symmetry follows the same exact explanation, except the symmetry is about the pole neutral axis. The fifth symmetry is a logical extension of the third and fourth symmetry behaviors. Through geometric principles and verified in finite element study, the same symmetry behavior is true about the two diagonal axis.

A very simple approach to the baseplate leveling test finite element models was taken. The objective of the modeling was primarily to verify the rough symmetry relationships seen in the experimental data. The finite element modeling made use of the same models used in the comparison with the static cantilever end loading, except instead of applying an end load, an enforced displacement loading was applied. The baseplate leveling test models were the same, except for the as modeled leveling nuts. The leveling nuts were not modeled using the partial leveling nuts as used in the final finite element models. Because the simplified approach to modeling the displacement loading, local modeled deformations were too great, thus complete leveling nuts were used. The enforced nodal displacement was applied to anchor rod nodes, at the mid-height of the baseplate. This plane of nodes at the mid height of the baseplate, was allowed to translate in the horizontal plane, though because all of the nodes of the plane were enforced to displace to the same displacement, local rotation of the anchor rod was prevented. Figure 4.2.2.3 shows a model section through the anchor rod, showing the horizontal plane of vertical nodal displacement loading. It is noted that this as modeled loading method is a simplified approach, and not intended to provide exact results, but results that can be used to aid the understanding of the experimental results.

Due to the highly symmetric stress results of the enforced baseplate leveling imperfection tests, the number of different tests performed involving raising and lowering different baseplate locations, could have been considerably reduced. The strain results from the multiple configurations of baseplate leveling tests enforcing upward and downward baseplate displacements at the different leveling nut locations however can easily be compared given the symmetric behavior. Considering the scatter in the experimental data and the objective to gain insight into the magnitude of stress induced in the tubewall adjacent to the weld toe it is only appropriate to consider the maximum stress magnitude. The local effects of leveling nuts and the slight non-symmetric behavior of the hand access hole may slightly influence the obtained stress results. However the symmetry comparisons of the experimental data and comparison of experimental and finite element analysis data was very good.

Figure 4.2.2.4 shows the deflected modeled structure under baseplate leveling imperfection loading, for the 1 ½" thick baseplate pole specimen. Note as indicated the specific enforced displacement is an upward 3/32" at the left tension anchor rod location. The right tension and right compression anchor rods are indicated, with the view of the left compression anchor rod partially obstructed. Note the considerable amount of local deformation to the loading anchor rod, and that most of the deformation occurs in the anchor rods. As indicated by the lack of curvature in the displaced shape, the deformation of the baseplate is primarily due to a rotation of the baseplate. The bending in the baseplate is minimal when compared to that of the anchor rods. Through the diagonal axis between the left tension and right

compression anchor rod the baseplate is combined in clamping the pole tube and driving a compressive force up the diagonal section of the tubewall. On the opposite diagonal axis through the right tension and left compression anchor rod, the baseplate is being pulled upward by the resultant tensile force. The behavior through this axis is similar to the application of a large upward tensile load, concentric with the vertical pole axis.

Table 4.2.2.1 shows the finite element results of the baseplate leveling imperfection loading discussed above. The model shows the finite element results of the 1 ½" thick baseplate specimen, with an enforced upward baseplate deflection of 3/32" at the left tension anchor rod location. The finite element outer tubewall stresses are plotted on 45 degree intervals. Selected experimental values are shown in boxes, at the gage locations available. Overall the finite element and experimentally measured outer stresses are in good agreement considering the approximate nature of the modeled loading, the local effects of the leveling nut fixity, and the general scatter of the data. As discussed previously, the maximum tensile stresses are observed at the diagonal opposite to the enforced displacement location. The experimental results for this particular test show a tensile stress of 18 ksi at both diagonal locations, as shown. The finite element tensile stresses of 20 ksi are in good agreement with the experimental data. As discussed, compressive stresses are located on the diagonal axis in line with the enforced baseplate displacement. The two finite element outer stresses on the axis are -20 and -14 ksi. As would be expected due to the large equivalent upward force applied to the corner of the baseplate (equivalent to the upward

displacement), a large compressive force and compressive stress is generated in the adjacent tubewall as the stiffness of the pole tube acts to restrain the enforced displacement. The experimental stress measured at the right 45 degree tension radial location is in the similar range of the finite element stress data. The remaining radial locations, including the direct tension and compression and the left and right neutral axis radial locations, are locations of low outer tubewall stress, as shown. Finite element stress data agreement is in good agreement considering that both values are low, though on occasion the difference relative the magnitude of the values may be high. Again this agreement at these locations of low stress is acceptable, due to the localized fixity effects and scatter of the experimental baseplate leveling test data.

Figures 4.2.2.2 and 4.2.2.3 are provided to illustrate the symmetry of the resulting baseplate leveling experimental stresses. Figure 4.2.2.2 illustrates the symmetry of the stress profile about the diagonal axis of the baseplate leveling imperfection loading (discussed previously as Symmetry #1). Again the average stress results for the 1 ½" thick baseplate specimen under a 3/32" upward enforced baseplate deflection at the left tension is shown. According to the symmetry about the diagonal loading axis, there should be three symmetry relationships, considering if strains were measured on a 45 degree radial interval at hotspot vertical locations (0.75" above the baseplate). Because strain was not measured at the right neutral axis location, only two symmetry relationships exist between the hotspot experimental stresses. These similar stresses are marked in the table by the different shades of grey. Note that the symmetry between the corresponding finite element stresses is quite

good, though not perfect due to the non-symmetric effect of the hand access hole. The experimental data shows the symmetry of the stress distribution to be not so well defined. This may be caused by local leveling nut fixities and scatter in the experimental data. The symmetry of the stress profile can also be seen in the plots previously discussed in Table 4.2.2.1. Note the axis of symmetry is indicated.

Table 4.2.2.3 demonstrates a different type of symmetry condition of the baseplate leveling tests. The experimental hotspot stress results of two different baseplate leveling imperfections on the 1 ½" thick baseplate specimen are shown in tabular form. The results in the first column are for the imperfection loading case with an upward deflection of 3/32" at the left compression anchor rod. The second column of stress data shows the results of the same loading only at the left tension anchor rod location. Note that these two different loadings are symmetric about the pole neutral axis, and thus would apply to the symmetry relationships discussed Symmetry #4. Thus the stress results of the two different loadings should be equal, when located symmetrically about the neutral axis. The symmetry relationships of the hotspot or gage locations 0.75" above the baseplate that should exist according to the finite element symmetry are shown below the table and indicated with arrows. These symmetry relationships are simply based on the symmetry of a circular pole, and neglect the influence of the non-symmetric hand access hole. The experimental data of the two different loadings shows a rough symmetric behavior, as paired symmetric stresses match the magnitude of stress, reasonably well. It is also important to notice that the for some reason it appears that the magnitude of experimental stresses

measured in the left compression anchor rod location test seem to be consistently greater than that of the left tension anchor rod test. The data obtained for both of the tests represents an average of several tests, thus minimizing the possible influence of experimental and measuring error. The difference in magnitudes that according to symmetry and finite element study should exist, may be accounted for by local leveling nut fixity issues.

This comparison of the two symmetric baseplate imperfection loading is typical of baseplate testing. This scatter in data, likely due to the local and unpredictable nature of the leveling nut connections, makes it difficult to determine the average maximum tensile stress due to baseplate leveling imperfection loading. Examining all of the different leveling tests performed, removing outlying data, and averaging the maximum stress magnitudes of the response was performed on the experimental results for all three baseplate specimens. Table 4.2.2.4 displays the average experimental stress representing the maximum tensile stress due to a baseplate leveling imperfection of 3/32". Also shown in the plot are the corresponding maximum baseplate leveling imperfection stresses as determined by finite element analysis. Note the finite element and experimental results both show that baseplate flexibility does influence the hotspot stress induced in imperfection loading. A rough linear relationship appears to exist, as shown in the plot in Table 4.2.2.4. As shown in the plot the finite element predicted baseplate leveling imperfection stresses are a slight under-prediction of the experimental stress values.

Section 4.2.3: Mast-Arm Test Results

The mast-arm specimen experimental testing program consisted of three components: The first component was a static load testing of the mast-arm specimen, similar to the static tests performed on the three pole specimens. The second component of the mast-arm testing was a series of tests termed "spacer tests". These tests used a similar static load testing, but examined the behavior of the mast-arm specimen with a washer "spacer" preventing contact between the mast-arm endplate and the flange plate of the pole specimen. The final component of the mast-arm testing involved examining the resulting stress behavior in the mast-arm tubewall when a tension bolt was removed.

Static Cantilever End Load Testing

As the pole to baseplate welded socket connection was the primary concern of the study, the welded socket connection between the mast-arm and endplate was a secondary concern. The socket connection of the mast-arm and endplate was only studied by experimental testing, as no finite element analysis was performed. However, as discussed previously a considerable number of strain gages were used to capture the behavior of the welded connection as well as possible. The difficulty of this objective was increased by the fact that no gages could be applied to the inside of the mast-arm tubewall. (See the discussion of the mast-arm strain gage plan for more details in Section 2.3. Prior to the experimental testing of the mast-arm socket connection it was believed that the behavior of the mast-arm socket connection would be similar to the behavior observed experimentally and through finite element study of the pole socket connection to the baseplate. Because the mast-arm endplate has

different fixity conditions than the pole baseplate, the flexibility induced behavior in the pole tubewall as discussed earlier, might not be observed to the same degree in the mast-arm connection. The endplate is less flexible than the baseplate for two primary reasons: First on the compression side of the mast-arm, the endplate bears against the flange plate of the built-up box, which is less flexible than the conditions of the baseplate, in which the baseplate can deflect freely. Also, the four mast-arm bolts provide a clamping force, holding the endplate fixed to the flangeplate, which is much more stiff than the baseplate fixity. At the leveling nut to baseplate connection, due to the flexibility of the stand-off length of the anchor rods, the baseplate is much more free to rotate, than the endplate.

That is not to say that the behavior of the mast-arm to endplate welded socket connection can be influenced by endplate flexibility. Though the fixity of the endplate decreases the flexibility effect the geometry of the endplate and mast-arm when compared to that of the baseplate and pole can actually increase the flexibility effect. Two aspects of the endplate and mast-arm geometry primarily contribute to the flexibility effect. First, due to the general design of the built-up box detail, the flange plate must be wider than the diameter of the pole to allow for the mast-arm bolts to be tightened. Essentially the nature of this design spreads out the spacing between the mast-arm bolts, to a distance comparable the baseplate anchor rod spacing. In addition the diameter of the mast-arm at the endplate is decreased. Thus referring back to the simply supported beam analogy, the increase in span length produces a more flexible endplate, which allows increased endplate deflection and rotation causing an increase

in local bending stresses. The second aspect of the endplate and mast-arm geometry that contributes to the flexibility effect is the tubewall thickness. Because mast-arm spans can be quite long, it is often essential to use a thinner tubewall thickness, than in a pole section. This thinner tubewall is much more flexible, and does not prevent endplate deformation as well as a stiffer, thicker tubewall. Because of these two particular aspects of endplate geometry, the effect endplate flexibility plays in mast-arm welded socket connection behavior must be considered.

To begin the discussion of the experimental results of the mast-arm testing it is first helpful to compare the endplate geometry with the pole specimen baseplate geometry of the 1 ½" thick baseplate specimen. As discussed in the paragraph above the endplate bolt spacing and thinner tubewall thickness both contribute to the flexibility effect. The geometry comparison is shown in Table 4.2.3.1. Note the difference in baseplate and endplate geometry. While the mast-arm endplate is slightly thicker than the pole baseplate (1.75" compared to 1.5"), the bolt/anchor rod spacing is slightly greater in the mast-arm specimen (14.75" compared to 14.19"). The flexibility of the mast-arm endplate is also increased because the tube diameter and tubewall thickness is only 11.0" and 0.18" compared to the 13" diameter and 0.23" thickness for the pole specimen. This tube geometry is countered by the fact that the mast-arm endplate has a greater width of endplate to bend. Since the mast-arm endplate side lengths are slightly bigger than the pole baseplate and the mast-arm tube diameter is slightly smaller, there is more endplate material to bend. Referring back to the analogy of a simply supported beam at the sides of the endplate between

the tube circle cutout and the sides, the width of the beam is larger, and thus less flexible. There is one final aspect of the structure geometry influencing the comparison of the flexibility of the endplate and baseplate. In comparing the experimental results, the fixity of the two nutted connections may also influence the comparison. The mast-arm bolts were mechanically tightened to their full capacity, while the baseplate anchor rods were hand tightened only. Thus the tightening method used would likely influence the mast-arm endplate to be stiffer, comparatively with the baseplate connection.

Because no finite element analysis was performed on the mast-arm connection the mast-arm experimental data and behavior must be compared to the corresponding pole data and behavior. The comparison of mast-arm and pole experimental stress profile is shown in Figures 4.2.3.2 and 4.2.3.3 respectively. Note that in both the mast-arm and pole profile experimental outer tubewall stresses are given in distance away from the top of the baseplate or endplate. Both figures plot the outer stress in the tension radial locations under a static 100 pound cantilever end load. Figure 4.2.3.3 additionally plots the outer stress distribution at the 45 degree tension radial location for comparison. The tube wall stresses of the 1 ½" thick baseplate pole specimen and the mast-arm specimen compare very well in both magnitude and shape of the stress profile. The outer stress at the tension radial location of the mast-arm connection, shown in Figure 4.2.3.2 follows the flexibility induced pattern as discussed previously in Section 4.2.1. Note that directly above the weld toe of the mast-arm socket connection, the outer stresses are considerably elevated from the

nominal stress. With increasing distance away from the endplate the outer tubewall stress decreases until it reaches a minimum at a distance approximately 2" away from the endplate. From this minimum it slowly begins to approach nominal value for tubewall stress. This stress profile behavior is exactly the same as was observed in the pole socket welded connections. The one primary difference in the profiles is that as shown in Figure 4.2.3.3 the outer stresses measured 8" above the baseplate are beginning to diverge as the hand access hole reinforcing is influencing the stress profile.

The magnitudes of the outer tubewall stress profile are also very similar to those of the pole socket connection. The magnitudes of the experimental outer tubewall stress profiles of the two connections can be compared by two stress parameters, the value of the hotspot stress and the stress profile difference, the difference between the hotspot outer tubewall stress and the minimum outer tubewall stress at the "valley" location. Note that as discussed above it is difficult to quantify the baseplate flexibility effects in the tubewall stress profile as other effects, primarily the stress concentration of the weld toe influence the stress profile. Note the hotspot stress locations, or the gage locations closest to the weld toe, are not necessarily consistent between different pole and mast-arm specimens due to differences in weld geometry. The valley location of stress determined by experimental testing, though close, is not necessarily at the exact 2" gage location also. However the difference in the somewhat arbitrarily located hotspot stress and the valley outer stress as discussed in Section 4.2.1, does reasonably well in indicating the degree baseplate flexibility

influences tubewall stresses. The tension hotspot outer stress of the mast-arm is approximately 4.5 ksi, compared to the tension hotspot outer stress of the pole of approximately 3.0 ksi. As would be expected the comparatively more flexible pole socket connection, shows the greatest outer tubewall stress difference of approximately 3.5 ksi, compared to the stress difference of approximately 2.0 ksi of the mast-arm connection. In Figure 4.2.3.3 the pole outer tubewall stress profile at the tension 45 degree radial location is also shown. Note the magnitude of the hotspot stress is much greater than the tension radial location, as well the magnitude of hotspot stress of the mast-arm hotspot tension outer stress. As seen in Figure 4.2.3.5, the similarity in the pole 1 ½" baseplate specimen tension 45 degree radial location stress magnitudes at the hotspot and valley locations are very similar to those of the mast-arm specimen at the tension radial location. This is significant in that for theses two particular stress profiles, one represents the maximum experimentally measured tensile stresses on the pole specimen and the other the maximum tensile stresses on the mast-arm specimen. Thus from the perspective of elastic stresses adjacent to the weld toe, the experimental data shows that: Both welded socket connections, at the mast-arm and at the baseplate, develop similar magnitudes of outer stresses, though at different locations. Additionally the stress profiles in the tubewall adjacent to the mast-arm to endplate socket connection follows the same pattern of the pole to baseplate welded socket connection discussed in Section 4.2.1.

Washer "Spacer" Static Load Tests

In order to examine the influence that the contact between the endplate and flangeplate has on the mast-arms tubewall stresses, static load tests were repeated with common washers preventing contact between the endplate and the flangeplate surfaces. This same method, placing a "spacer" between to prevent the stiffening effect when endplate's compressive side is allowed to contact the flangeplate was also used in the University of Texas mast-arm fatigue testing program, as discussed in Section 1.5. The static load tests were performed identically in procedure as the static load testing discussed previously, except with spacer washers. Additional information regarding the testing procedure is discussed in Section 2.4.

Given the previous discussion of the mast-arm specimen experimental outer tubewall stress profiles, the discussion of "spacer" test results will begin by examining the difference in the stress profiles of the two different endplate fixity conditions. Outer tubewall stress profiles are shown in Figures 4.2.3.4-7. Note each stress profile shows the experimental stress results of the 99 pound cantilever end load test. And each plot represents the stress profile local to the endplate to mast-arm socket connection, at each of the four radial locations gaged, including the direct compression and direct tension radial locations, and the tension 45 and compression 45 radial locations both located in line with the mast-arm bolts, oriented 45 degrees from the direct tension or compression locations. In each plot the stress profiles of the two different endplate fixity conditions are compared. The results clearly show that the more flexible endplate fixity condition (with the washer spacers preventing endplate

contact), consistently produces greater hotspot stresses, and also has considerably larger stress profile differences. Note that in Figure 4.2.3.7 the 2" stress data (gage #53) for the spacer fixity condition is shown as zero due to a instrumentation problem. Also note that as seen in Table 4.2.3.8, at gage locations symmetric about the mast-arm axis 48/49 and 54/55 duplicate stress data was recorded. In addition, a very reasonable, opposite symmetry condition between corresponding tension and compression gage locations is also shown in Figure 4.2.3.7. Given this symmetry it is reasonable to believe that if gage #53 was working properly it would have measured a strain equivalent to approximately 1.5 ksi, as indicated by the asterisk in the plot in Figure 4.2.3.7. The comparison of the "with spacer" stress profile results with the simple beam theory nominal outer stresses should also be noted. In all the stress profiles the experimental "with spacer" values of outer stress are less than the values determined by simple beam theory analysis. This trend is supported by the strain measurements 3" from the weld toe (Which would correspond to a distance of approximately 3 ¾" away from the endplate) made in the University of Texas fatigue research, discussed in Section 1.5.

Tables 4.2.3.8 and 4.2.3.9 show the resulting stress data comparison discussed above in a tabular form. Table 4.2.3.9 provides a summary of the stress profile data for the static mast-arm testing with and without spacers. Beginning with the without spacer results, the radial distribution of experimental hotspot outer stress roughly followed simple beam theory. The largest stresses were located at the direct gage locations (tension and compression), or the locations the furthest away from the

neutral axis. The average ratio between the stresses measured at the direct and 45 degree locations was 0.71, which equates well to the ratio of calculated simple beam theory stresses, the cosine of 45 degrees or approximately 0.707. In addition the without spacer experimental outer tubewall stress profile data also showed an expected trend regarding stress profile difference. Stress profile difference was a minimum at the 45 degree radial locations, as would be expected due to their proximity to the bolts. In addition the direct tension radial location stress profile difference is slightly larger than that of the direct compression radial location. As expected the compression location would likely be a stiffer local endplate fixity due to the contact between the endplate and the flangeplate. This stiffer connection would slightly limit the local bending behavior on the compression side, as indicated by the smaller stress profile difference.

The outer stress experimental results of the mast-arm connection with spacers also follow the same trends in flexibility. As the spacer connection detail increases the endplate flexibility, all of the experimental hotspot stresses increase compared to the standard bolted endplate connection. The increase in experimental hotspot stresses was measured to be approximately 0.5 ksi and 0.9 ksi for the direct compression/tension and 45 degree tension/45 degree compression radial locations, respectively. This increase represents a greater than 10% increase in experimental hotspot stress. The uneven increase in stress at the two different regions skewed the ratio of 45 degree to direct radial locations to approximately 0.82. Thus the stresses measured were not following the simple beam theory distribution, similar the behavior

discussed previously in the pole specimens. The increased flexibility caused by the endplate fixity had a drastic effect in changing the hotspot stress magnitudes and distribution. In addition to altering the hotspot stress data, the increase in endplate flexibility was also evident in the dramatic increase of the stress profile differences, which increased more than 60% of their non-spacer original values.

One other significant experimental result, obtained in the mast-arm spacer test was the recording of bending stress in the uplift and down lift portions of the endplate. As discussed in the instrumentation and gage plans in Section 2.3, two strain gages were placed on center, with gage length parallel and directly in line with the centerline of the anchor rods; one gage on the tension (uplift) side and the other on the compressive (downlift) side. These gages are numbered 56 (uplift) and 57 (downlift). Strains at similar locations on baseplate specimens were also measured, however the discussion of those results have been omitted due to the lack of clarity in the data, possibly due to local fixity conditions of the hand-tightened leveling nuts. The strains measured at these locations on the mast-arm endplate show very good results. The stresses measured with the endplate in a contact type fixity are relatively small, as seen in the bottom of Table 4.2.3.8. In addition under the non spacer fixity condition the magnitude of the stress in the compressive location is smaller than the similar stress in the tension region. This is also as expected due to the fact that the flexibility and local bending behavior of the compressive region is limited by contact. In the more flexible endplate fixity condition with the washers present, the stresses measured drastically increased, to nearly four times the stresses measured in the typical endplate bolted

fixity. The uplift and downlift stresses also show a very good equal and opposite relationship as would be expected.

Mast-Arm Bolt Removal Testing

Another practical problem involving the mast-arm to endplate welded socket connection detail that was studied was the loss or loosening of a mast-arm bolt. The condition arises when over time or due to improper tightening during erection, a mast-arm bolt loosens, altering the stresses in the mast-arm tubewall. Surprisingly this condition is not that uncommon in field inspection. To determine the stresses generated by this type of loading, and how the mast-arm distributes stress upon loosing tension in a mast-arm bolt, two simple static tests were performed using the same instrumentation and loading. These tests were only concerned with the two bolts in tension. The first test simply involved recording the strain history generated when a tension anchor rod was loosened. All mast-arm bolts, as previously discussed in Section 2.2, were tightened with sufficiently to preload the bolts. This release test was performed twice once on the left tension bolt and then again on the right tension bolt. Additionally a static load test using the standard 100 pound cantilever end loading was performed twice once on the structure with left and right mast-arm bolts absent.

The results of the bolt removal mast-arm testing are fairly straight forward and do not directly pertain to the baseplate flexibility relationship. Thus the data will be discussed fairly quickly. Figures 4.2.3.1 and 4.2.3.2 are related to the mast-arm bolt removal test. Figure 4.2.3.1 show the data record of the release of a tension bolt. Note that fairly large stresses are induced, however the largest stresses induced in the

tubewall are compressive. Figure 4.2.3.2 shows a photograph of the gap developed by the release of the left tension bolt. Note that the gap was measured to be 4/64", and the gap developed when the right tension bolt was released was measured to be 2 to 3/64".

Table 4.2.3.10 shows the result of mast-arm bolt removal test and Table 4.2.3.11 shows the results of the static load testing of the mast-arm with an absent tension bolt (for both the left and right bolts). As mentioned earlier upon the release of a tension mast-arm bolt, strain measurements show that at a majority of the gage locations, compressive stresses are induced. An interesting change in stress is shown at the uplift gage (#56) previously discussed. When the mast-arm is erected, the stress distribution in the endplate is bearing its' own self weight, hence tension stresses are locked into the uplift location at erection. Upon release of both the left and right tension mast-arm bolts, that stress is released as indicated by the fairly equal and sizable stress induced in both cases. The same response is also shown at the 45 degree tension location (gage #54), in which the locked in tensile stress of approximately 17 ksi is released when the left tension bolt is released. The most import trend in the new stress distribution pattern in the mast-arm under an absent tension bolt condition is shown in Table 4.2.3.11, in the far right column. It shows that the outer tubewall tensile stresses due to absent tension bolts at both the left and right tension 45 degree radial locations increases on average by 60% of the stress under normal fixity conditions. Thus, as common sense would suggest, a missing mast-arm bolt is a serious condition raising tubewall stresses. The test shows that a missing tension

mast-arm bolt would increase the stress by approximately 60% of its' typical value at that location. This maximum tensile stress experimentally measured in an absent tension bolt endplate fixity of 5.4 ksi is nearly 1 ksi larger than the maximum experimentally measured tensile stress in a typical endplate fixity condition, of 4.5 ksi.

Section 4.3: Improvements to Finite Element and Experimental Setup

In the course of the study, both in the finite element analysis and analysis of experimental data it was realized that certain improvements could have been made. As part of the natural experimental process, unfortunately these improvements could not have been foreseen, prior to examining the results of the various components of the study. Observations and conclusions were made that indicated that such steps may have improved the data agreement between analytical and experimental results.

In hindsight, two adjustments to the experimental test setup, would be made given the analysis of the finite element and experimental data. Initially it was thought that local leveling nut to baseplate fixity conditions would have little or no effect on structural behavior and tubewall stresses. The test setup, the procedure used to erect and level the baseplate structure on the leveling nuts mimicked the simple procedure used in the field.

Given some of the problems with data agreement, two alterations to the test setup would be added to the experimental testing program. These alterations would not be intended to better represent real in service conditions, but to aid in producing structural fixity conditions that would more closely represent the simplified approach used to model the leveling nut connections.

The first would be to eliminate any possible influence of baseplate out of straightness or baseplate leveling imperfection loading. Using some type of laser leveling equipment, the baseplate and leveling nuts could be leveled much more effectively, than the simple levels used to adjust the nuts and baseplate. The second step would be to perform static load testing with leveling nuts that were hydraulically tightened, to the capacity of the anchor rod. This would nearly eliminate any questions as to the fixity of the leveling nut connections, and much better represent the solid modeling technique used to model the leveling nut to baseplate interface.

In addition to altering the fixity of the leveling nut connection a few simple improvements to the instrumentation plan would also be helpful in measuring these local effects. Maximum baseplate deflection was only measured at the maximum down-lift location, because there was a strain gage applied on the opposite tensile location. This deflection is very significant in comparison to the finite element model, as it clearly suggests the model's baseplate flexibility relative to the experimental baseplate flexibility. It is also a very small deflection to experimentally measure, thus it would be recommended that several Linear Variable Displacement Transducers be included in the instrumentation plan. Another shortcoming of the gage plan involves the assumption that stresses would be symmetric about the mast-arm axis. Local fixity effects that may influence tubewall stresses were not considered, thus there is very little room for verification of tubewall stress symmetry. Thus it would also be recommended that additional duplicate stress data be supplied by the instrumentation

plan. Matching gages at symmetric locations not just at gage locations just off the weld toe, but a couple inches above the weld toe as well.

Given the discussion of possible improvements, it is worth noting that instead of altering the fixity conditions of the test setup, improvement to the finite element model could also be made. The use of contact elements may improve data agreement. However the preload force and initial gap between the leveling nut elements and the baseplate would have to be defined. This complicated, and likely somewhat arbitrary definition of these parameters may not improve data agreement, and thus was not considered. However the use of these elements are likely necessary for accurate analysis of the mast-arm welded socket connection.

FINAL DATA COMPARISON: 3/4" Thick Baseplate

Height above Bp. [in]	Rad. Location	Gage #	Exp. Outer Stress [ksi]	FE FIN* Outer Stress [ksi]	Gage #	Exp. Inner Stress [ksi]	FE FIN* Inner Stress [ksi]
8	C.; 180 ;	3	-1.58	-1.68	4	-1.55	-1.62
5	C.; 180 ;	5	-1.32	-1.44	6	-1.18	-1.28
3	C.; 180 ;	7	0.50	0.03	8	-2.17	-2.26
2	C.; 180 ;	9	2.34	2.13	10	-2.39	-2.49
0.75	C.; 180 ;	11	-2.49	-5.10	12	5.07	8.70

Height above Bp. [in]	Rad. Location	Gage #	Exp. Outer Stress [ksi]	FE FIN* Outer Stress [ksi]	Gage #	Exp. Inner Stress [ksi]	FE FIN* Inner Stress [ksi]
36	T.; 0 ;	1	1.91	1.62			
8	T.; 0 ;	13	0.96	1.04	14	1.13	1.13
5	T.; 0 ;	15	0.95	0.96	16	0.90	0.88
3	T.; 0 ;	17	-0.69	-0.67	18	1.90	1.86
2	T.; 0 ;	19	-2.52	-2.45	20	2.38	2.13
0.75	T.; 0 ;	21	3.88	4.60	22	-8.51	-8.62

Height above Bp. [in]	Rad. Location	Gage #	Exp. Outer Stress [ksi]	FE FIN* Outer Stress [ksi]	Gage #	Exp. Inner Stress [ksi]	FE FIN* Inner Stress [ksi]
8	C.; 45 ; L	25	-1.50	-1.51	26	-1.44	-1.45
5	C.; 45 ; L	27	-1.82	-1.83	28	-1.61	-1.61
3	C.; 45 ; L	29	-0.94	-1.19	30	-2.93	-2.78
2	C.; 45 ; L	31	-0.38	-0.55	32	-2.87	-2.91
0.75	C.; 45 ; Avg.	33/45	-11.11	-8.76	34/46	8.85	7.04

Height above Bp. [in]	Rad. Location	Gage #	Exp. Outer Stress [ksi]	FE FIN* Outer Stress [ksi]	Gage #	Exp. Inner Stress [ksi]	FE FIN* Inner Stress [ksi]
36	T.; 45 ; L	2	1.35	1.37			
8	T.; 45 ; L	35	1.81	1.71	36	1.67	1.57
5	T.; 45 ; L	37	1.99	1.91	38	1.74	1.66
3	T.; 45 ; L	39	1.25	1.16	40	2.84	2.90
2	T.; 45 ; L	41	0.60	0.46	42	2.86	2.99
0.75	T.; 45 ; Avg.	43/23	9.76	9.24	44/24	-7.86	-7.69

Table 4.2.1.1: Final Data Comparison: 3/4" Thick Baseplate

* "FIN" refers to final finite elment model series, with alterations sumarized in Section 4.1 including weld concavity, "partial" leveling nuts, and individually measured pole and weld profile geometry

FINAL DATA COMPARISON: 1 1/2" Thick Baseplate

Height above Bp. [in]	Rad. Location	Gage #	Exp. Outer Stress [ksi]	FE FIN* Outer Stress [ksi]	Gage #	Exp. Inner Stress [ksi]	FE FIN* Inner Stress [ksi]
42	C.; 180 ;	1	-1.99	-1.75			
8	C.; 180 ;	6	-1.54	-1.68	7	-1.59	-1.65
5	C.; 180 ;	8	-1.35	-1.55	9	-1.34	-1.46
3	C.; 180 ;	10	-0.43	-0.64	11	-1.93	-2.03
2	C.; 180 ;	12	0.64	0.37	13	-2.04	-2.20
0.75	C.; 180 ;	14	-3.03	-3.68	15	4.14	4.26

Height above Bp. [in]	Rad. Location	Gage #	Exp. Outer Stress [ksi]	FE FIN* Outer Stress [ksi]	Gage #	Exp. Inner Stress [ksi]	FE FIN* Inner Stress [ksi]
42	T; 00 ;	2	-1.99	1.64			
36	T; 00 ;	3	-1.54	1.57			
8	T; 00 ;	16	0.89	1.09	17	1.21	1.17
5	T; 00 ;	18	1.17	1.10	19	1.16	1.09
3	T; 00 ;	20	0.40	0.25	21	1.81	1.69
2	T; 00 ;	22	-0.56	-0.73	23	2.02	1.88
0.75	T; 00 ;	24	3.00	3.33	25	-3.14	-4.50

Height above Bp. [in]	Rad. Location	Gage #	Exp. Outer Stress [ksi]	FE FIN* Outer Stress [ksi]	Gage #	Exp. Inner Stress [ksi]	FE FIN* Inner Stress [ksi]
8	C; 45 ;	36	-1.61	-1.46	37	-1.46	-1.39
5	C; 45 ;	38	-1.86	-1.64	39	-1.63	-1.47
3	C; 45 ;	40	-1.55	-1.33	41	-2.36	-2.04
2	C; 45 ;	42	-1.17	-0.99	43	-2.38	-2.12
0.75	C; 45 ;	44	-5.01	-4.61	45	1.90	2.37

Height above Bp. [in]	Rad. Location	Gage #	Exp. Outer Stress [ksi]	FE FIN* Outer Stress [ksi]	Gage #	Exp. Inner Stress [ksi]	FE FIN* Inner Stress [ksi]
42	T; 45; R	4	1.40	1.35			
36	T; 45; R	5	1.48	1.36			
8	T; 45; R	26	1.76	1.66	27	1.51	1.51
5	T; 45; Avg.	28/46	1.96	1.71	29/47	1.60	1.51
3	T; 45; R	30	1.23	0.00	31	2.05	0.00
2	T; 45; Avg.	32/48	1.11	0.92	33/49	2.21	2.15
0.75	T; 45; Avg.	34/50	5.06	4.76	35/51	-2.65	-2.65

Table 4.2.1.2: Final Data Comparison: 1 1/2" Thick Baseplate

FINAL DATA COMPARISON: 3" Thick Baseplate

Height above Bp. [in]	Rad. Location	Gage #	Exp. Outer Stress [ksi]	FE FIN* Outer Stress [ksi]	Gage #	Exp. Inner Stress [ksi]	FE FIN* Inner Stress [ksi]
5	C.; 180 ;	2	-1.66	-1.79	3	-1.61	-1.70
2	C.; 180 ;	4	-0.58	-0.87	5	-2.12	-2.14
0.875	C.; 180 ;	6	-2.44	-2.48	7	-1.17	0.57

Height above Bp. [in]	Rad. Location	Gage #	Exp. Outer Stress [ksi]	FE FIN* Outer Stress [ksi]	Gage #	Exp. Inner Stress [ksi]	FE FIN* Inner Stress [ksi]
36	T.; 0;	1	1.83	1.55			
5	T.; 0;	8	1.23	1.37	9	1.24	1.34
2	T.; 0;	10	0.42	0.53	11	1.89	1.84
0.875	T.; 0;	12	2.17	2.11	13	0.75	-0.79

Height above Bp. [in]	Rad. Location	Gage #	Exp. Outer Stress [ksi]	FE FIN* Outer Stress [ksi]	Gage #	Exp. Inner Stress [ksi]	FE FIN* Inner Stress [ksi]
5	C.; 45 ; L	14	-1.53	-1.42	15	-1.39	-1.33
2	C.; 45 ; L	16	-1.20	-1.07	17	-1.78	-1.60
0.875	C.; 45 ; Avg.	18/20	-2.81	-2.33	19/21	-0.99	0.08

Height above Bp. [in]	Rad. Location	Gage #	Exp. Outer Stress [ksi]	FE FIN* Outer Stress [ksi]	Gage #	Exp. Inner Stress [ksi]	FE FIN* Inner Stress [ksi]
5	T.; 45 ; L	22	1.71	1.49	23	1.48	1.36
2	T.; 45 ; L	24	1.17	1.02	25	1.83	1.61
0.875	T.; 45 ; Avg.	26/28	2.66	2.29	27/29	0.96	-0.16

Table 4.2.1.3: Final Data Comparison: 3" Thick Baseplate

Gage Location Data			Test:	Left Tension Anchor Rod Up 3/32"		
Inside / Outside	Radial Location	Height Above Baseplate	Gage Number	Average Induced Stress [ksi]	Finite Element Stress [ksi]	
O	C.; 180 ;	0.75	CH_14	-1.16	-1.17	
I		0.75	CH_15	0.86		
O	T.; 0 ;	0.75	CH_24	-0.71	2.8	**
I		0.75	CH_25	1.81		
O	T.; 45 ; R	0.75	CH_34	18.33	19.98	***
I		0.75	CH_35	0.55		
O	C.; 45 ; L	0.75	CH_44	17.66	20.36	***
I		0.75	CH_45	1.85		
O	T.; 45 ; L	0.75	CH_50	-21.84	-14.23	
I		0.75	CH_51	3.73		
O	T.; 22.5 ; R	0.75	CH_56	11.22		
I		0.75	CH_57	1.11		
O	NA.; 90 ; L	0.75	CH_62	1.07	2.54	**
I		0.75	CH_63	2.16		

By Symetry #1, For Left Tension Anchor Rod Imperfection:

** NA Left should equal Tension 00

*** Compression 45 Left should equal Tension 45 Right
Compression 180 should equal Neutral Axis Right

Table 4.2.2.2: Baseplate Leveling Imperfection Testing Symetry Comparison: Part 1; 1 1/2" Thick Baseplate

Gage Location Data			Test:	Left Compression Anchor Rod Up 3/32"		Left Tension Anchor Rod Up 3/32"
Inside / Outside	Radial Location	Height Above Baseplate	Gage Number	Average Induced Stress [ksi]		Average Induced Stress [ksi]
O	C.; 180 ;	0.75	CH_14	-0.09	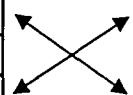	-1.16
I		0.75	CH_15	2.87		0.86
O	T.; 0 ;	0.75	CH_24	-1.13		-0.71
I		0.75	CH_25	0.57		1.81
O	T.; 45 ; R	0.75	CH_34	-23.17		18.33
I		0.75	CH_35	2.86		0.55
O	C.; 45 ; L	0.75	CH_44	-28.05	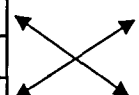	17.66
I		0.75	CH_45	0.94		1.85
O	T.; 45 ; L	0.75	CH_50	21.26		-21.84
I		0.75	CH_51	0.74		3.73
O	T.; 22.5 ; R	0.75	CH_56	-13.62		11.22
I		0.75	CH_57	2.35		1.11
O	NA.; 90 ; L	0.75	CH_62	-0.92		1.07
I		0.75	CH_63	2.27		2.16

By Symetry #4, given the available experimental gage locations

Data from Left Compression Up		Data from Left Tension Up
Compression 180	Should Equal	Tension 00
Tension 00	Should Equal	Compression 180
Compression 45 Left	Should Equal	Tension 45 Left
Tension 45 Left	Should Equal	Compression 45 Left

Tabel 4.2.2.3: Baseplate Leveling Imperfection Testing Symetry Comparison: Part 2; 1 1/2" Thick Baseplate

Baseplate Specimen Thickness	Averaged Experimental Hotspot Stress ** [ksi]	Finite Element Hotspot Stress * [ksi]	
3/4"	28	26	(Y=0.75")
1 1/2"	23	20	(Y=0.75")
3"	18	15	(Y=0.875")

Note:

** Maximum experimental stresses taken only at hotspot gage locations that are 0.75"/.875" above the top of the baseplate. Maximum stress values averaged for all different baseplate imperfection tests, disregarding outlying test data records.

* Maximum finite element stresses taken at corresponding gage locations, which typciacally closely represent the maximum outer tubewall stress for the given hotspot vertical gage height.

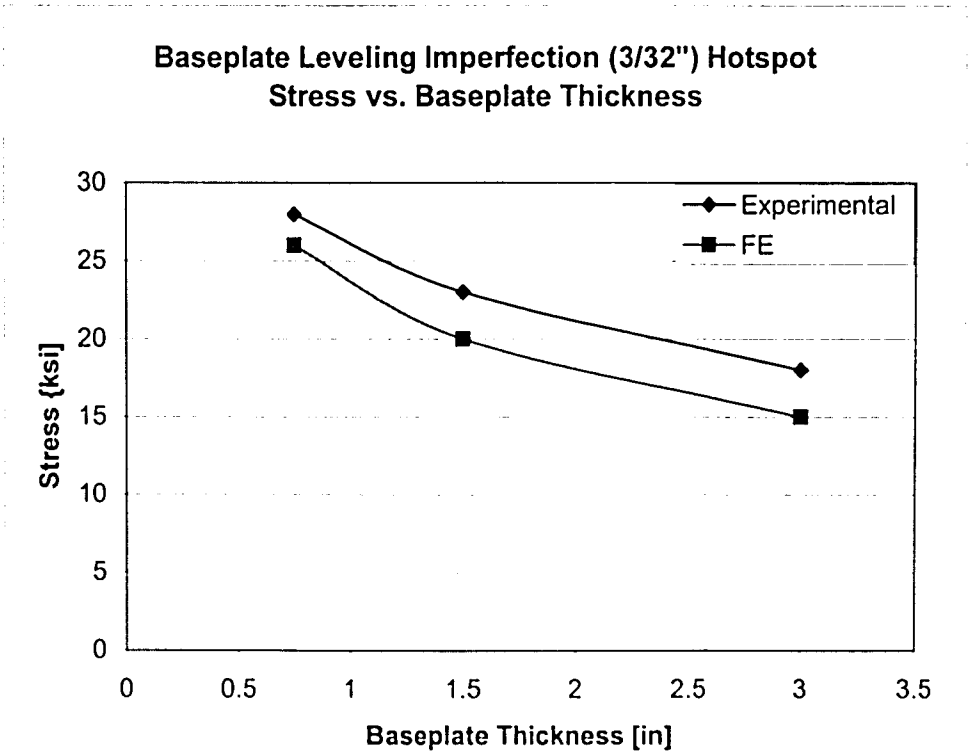

Table 4.2.2.4: Baseplate Leveling Imperfection Testing Summary
Finite Element vs. Average Experimental Maximum Stress

Endplate and 1 1/2" Thick Baseplate Specimen

	Mast-Arm Dimensions [in]	Pole Dimensions [in]
Endplate/Baseplate Square Side Length	17.25	17.0
Endplate/Baseplate Thickness	1.75	1.50
M.A. Bolt/Anchor Rod Spacing	14.75	14.19
M.A./Pole Outer Diameter at Base	11.0	13.0
M.A./Pole Tubewall Thickness	0.18	0.23

Table 4.2.3.1: Endplate and 1 1/2" Thick Baseplate Specimen Comparison

Mast-Arm "Spacer" Testing Results

Gage #	Location	Radial Loc	Height above Baseplate [in]	w/spacers P=100# Tubewall Stress [ksi]		P=100# Tubewall Stress [ksi]		Absolute Stress Increase [ksi]
34	M.A.	C; 180	8	-3.17		-3.28		
35	M.A.		5	-3.11		-3.26		
36	M.A.		3	-2.67		-3.01		
37	M.A.		2	-1.56		-2.54		-0.98
38	M.A.		7/8	-4.92		-4.36		0.56
39	M.A.	T; 00	8	3.23		3.26		
40	M.A.		5	3.14		3.23		
41	M.A.		3	2.77		3.02		
42	M.A.		2	1.69		2.51		-0.81
43	M.A.		7/8	4.91		4.46		0.45
44	M.A.	C;45;L	8	-2.40		-2.39		
45	M.A.		5	-2.51		-2.47		
46	M.A.		3	-2.29		-2.27		
47	M.A.		2	-1.61		-1.92		-0.31
48	M.A.		7/8	-4.05		-3.19		0.87
49	M.A.	C;45;R	7/8	-3.99		-3.20		0.79
50	M.A.	T;45;L	8	2.36		2.35		
51	M.A.		5	2.47		2.40		
52	M.A.		3	2.28		2.17		
53	M.A.		2	-0.01	**	1.85		-1.85
54	M.A.		7/8	4.08		3.04		1.05
55	M.A.	T;45;R	7/8	4.01		3.22		0.79
56	Endplate Top	Uplift	T; 00	1.96		0.57		1.39
57	Endplate Bottom	Downlift	C; 180	-1.97		-0.36		1.61
	LVDT	[mils]		-1.28		-1.41		
	Spot	[in]		-5.06		-5.06		

** Instrumentation Problem - Bad Gage

Table 4.2.3.8: Mast-Arm "Spacer" Test Results

Experimental "Hotspot" Stress and Stress Profile Difference Summary of "Spacer" Test Comparison

Radial Location	"Hotspot" Outer Stress [ksi]	"Hotspot" Outer Stress w/Spacer [ksi]	Stress Profile Difference [ksi]	Stress Profile Difference w/Spacer [ksi]
Compr.; 180	-4.4	-4.9	1.8	3.4
Tens.; 00	4.5	4.9	2	3.2
Compr. ; 45	-3.2	-4	1.3	2.4
Tens. ; 45	3.1	4	1.3	NA

NA - Not available due to instrumentation problem.

Table 4.2.3.9: Experimental "Hotspot" Stress and Stress Profile Difference Summary of "Spacer" Test Comparison

Mast-Arm Experimental Testing Results: M.A. Bolt Removal Test

M.A. Outer Tubewall Stress Induced Upon Removal of Bolt

Gage #	Location	Radial Location	Height above Baseplate	Induced Stress [ksi] Left Top M.A. Bolt Released	Induced Stress [ksi] Right Top M.A. Bolt Released
34	M.A.	C; 180	8	-1.04	-0.56
35	M.A.		5	-1.70	-0.91
36	M.A.		3	-1.89	-1.13
37	M.A.		2	-1.53	-0.94
38	M.A.		7/8	-4.50	-2.41
39	M.A.	T; 180	8	0.15	0.45
40	M.A.		5	0.72	0.84
41	M.A.		3	1.62	1.87
42	M.A.		2	4.79	4.32
43	M.A.		7/8	-2.06	-0.39
44	M.A.	C;45;L	8	4.76	-2.25
45	M.A.		5	5.62	-2.34
46	M.A.		3	6.56	-2.20
47	M.A.		2	9.94	-2.24
48	M.A.		7/8	5.63	-3.05
49	M.A.	C;45;R	7/8	-6.03	3.66
50	M.A.	T;45;L	8	-5.28	2.82
51	M.A.		5	-7.04	3.29
52	M.A.		3	-7.67	3.47
53	M.A.		2	0.00	0.00
54	M.A.		7/8	-16.99	2.62
55	M.A.	T;45;R	7/8	5.31	-11.68
56	Endplate Top	Uplift	T; 00	-7.85	-7.39
57	Endplate Bottom	Downlift	C; 180	-0.09	0.31
		LVDT	mils	-0.87	0.01
		StringPot	In.	-0.78	-0.39

Table 4.2.3.10: Mast-arm Experimental Testing Results: M.A. Bolt Removal Test

Mast-Arm Experimental Testing Results: M.A. Bolt Removal Test

M.A. Outer Tubewall Stress Due to Static Load

Gage #	Location	Radial Location	Height above Baseplate	99# Cantilever End Load Test: No Left Top M.A. Bolt- Outer Stress [ksi]	99# Cantilever End Load Test: No Right Top M.A. Bolt- Outer Stress [ksi]		99# Cantilever End Load Test- Outer Stress [ksi]	Percent Increase
34	M.A.	C; 180	8	-3.83	-3.57		-3.28	
35	M.A.		5	-4.00	-3.63		-3.26	
36	M.A.		3	-3.72	-3.39		-3.01	
37	M.A.		2	-2.98	-2.73		-2.54	
38	M.A.		7/8	-6.42	-5.58		-4.36	
39	M.A.	T; 180	8	2.73	2.85		3.26	
40	M.A.		5	2.65	2.76		3.23	
41	M.A.		3	2.26	2.48		3.02	
42	M.A.		2	1.23	1.64		2.51	
43	M.A.		7/8	4.23	4.33		4.46	
44	M.A.	C;45;L	8	-1.38	-3.32		-2.39	
45	M.A.		5	-1.21	-3.53		-2.47	
46	M.A.		3	-0.77	-3.31		-2.27	
47	M.A.		2	0.32	-2.92		-1.92	
48	M.A.		7/8	-2.05	-4.83		-3.19	
49	M.A.	C;45;R	7/8	-5.32	-1.87		-3.20	
50	M.A.	T;45;L	8	1.32	3.20		2.35	
51	M.A.		5	1.17	3.44		2.40	
52	M.A.		3	0.90	3.37		2.17	
53	M.A.		2	0.00	0.00	*	1.85	
54	M.A.		7/8	1.70	4.84		3.04	59%
55	M.A.	T;45;R	7/8	5.38	1.92		3.22	67%
56	Endplate Top	Uplift	T; 00	2.07	1.35		0.57	
57	Endplate Bottom	Downlift	C; 180	-0.62	-0.45		-0.36	
		LVDT	mils	-1.39	-1.37		-1.41	
		StringPot	In.	-5.35	-5.16		-5.06	

* Bad Gage!

Table 4.2.3.11: Mast-Arm Experimental Testing Results: MA Bolt Removal Test

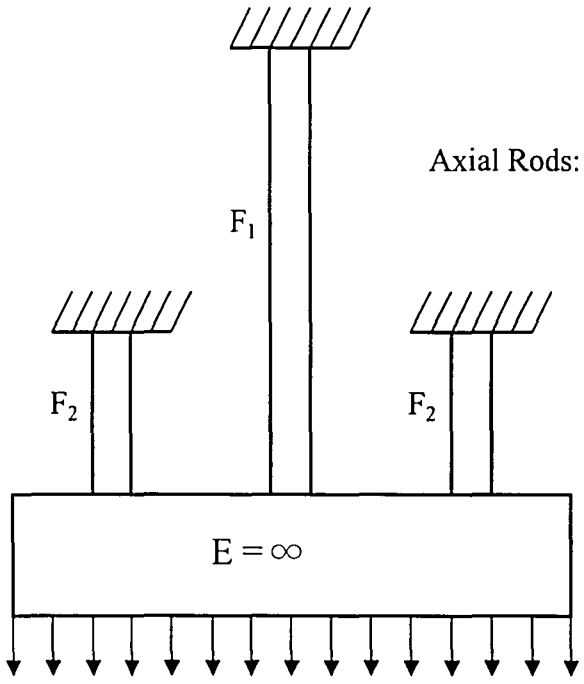

Tensi
Radi

Figure 4.2.1.1A: Static example problem conceptually illustrating flexibility and load path affect. Due to flexibility of center axial rod $F_1 < F_2$, similar to the mid-plane stress in the tubewall adjacent to the direct tension and compression radial locations.

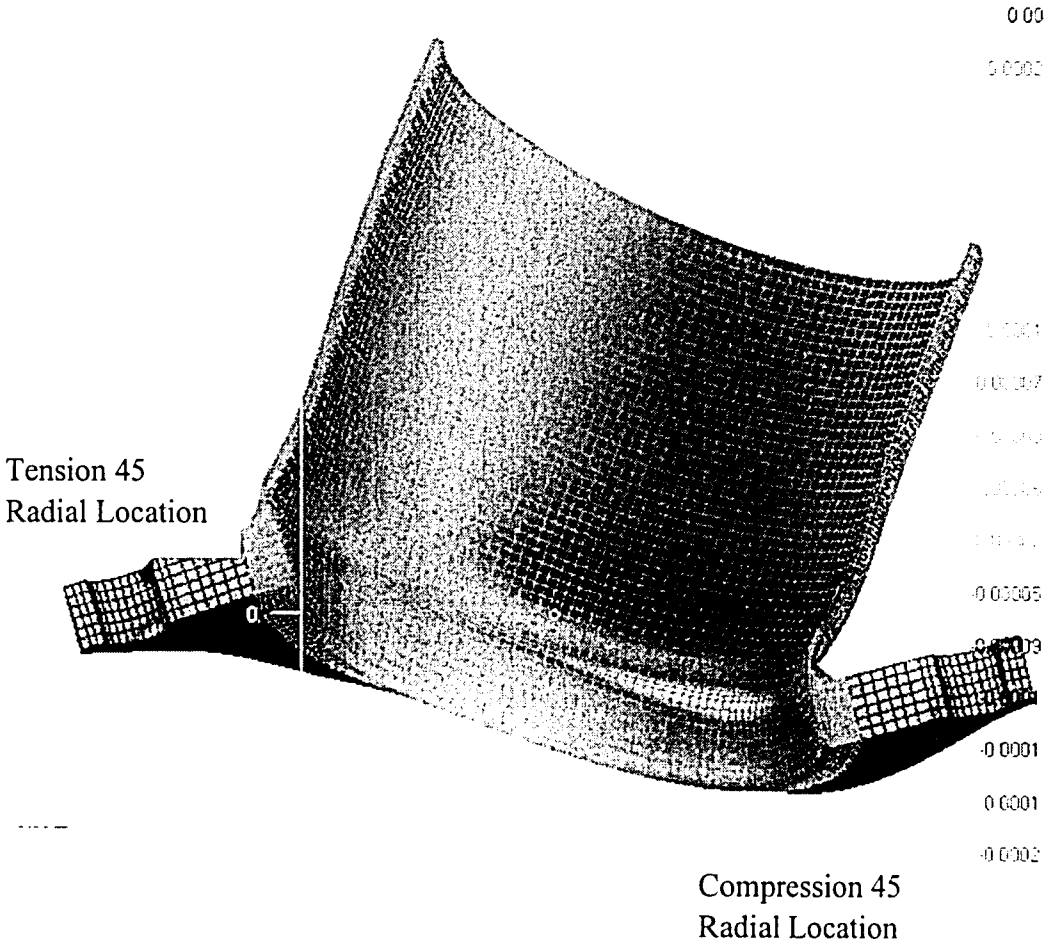

Figure 4.2.1.2A: Model Cross-Section through Diagonal Axis

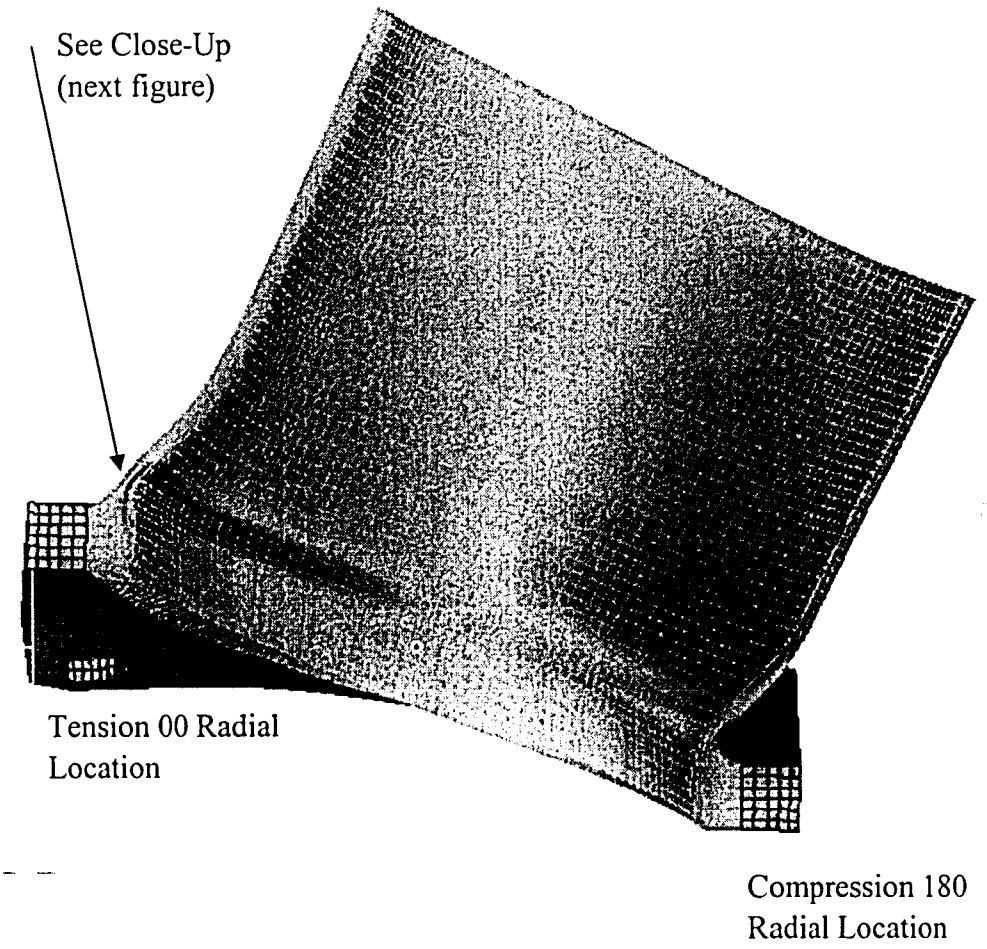

Figure 4.2.1.3A: Model Cross-Section through Mast-Arm Axis

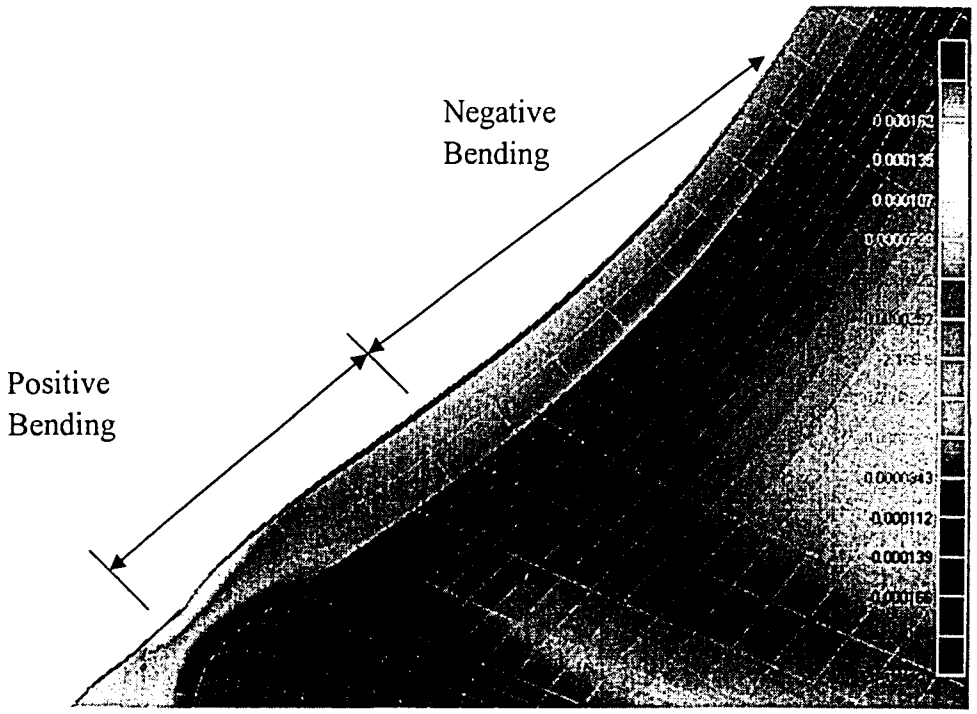

Figure 4.2.1.4A: Close-Up View of Tension Side Tubewall Adjacent to Weld Toe
(shown in previous figure)

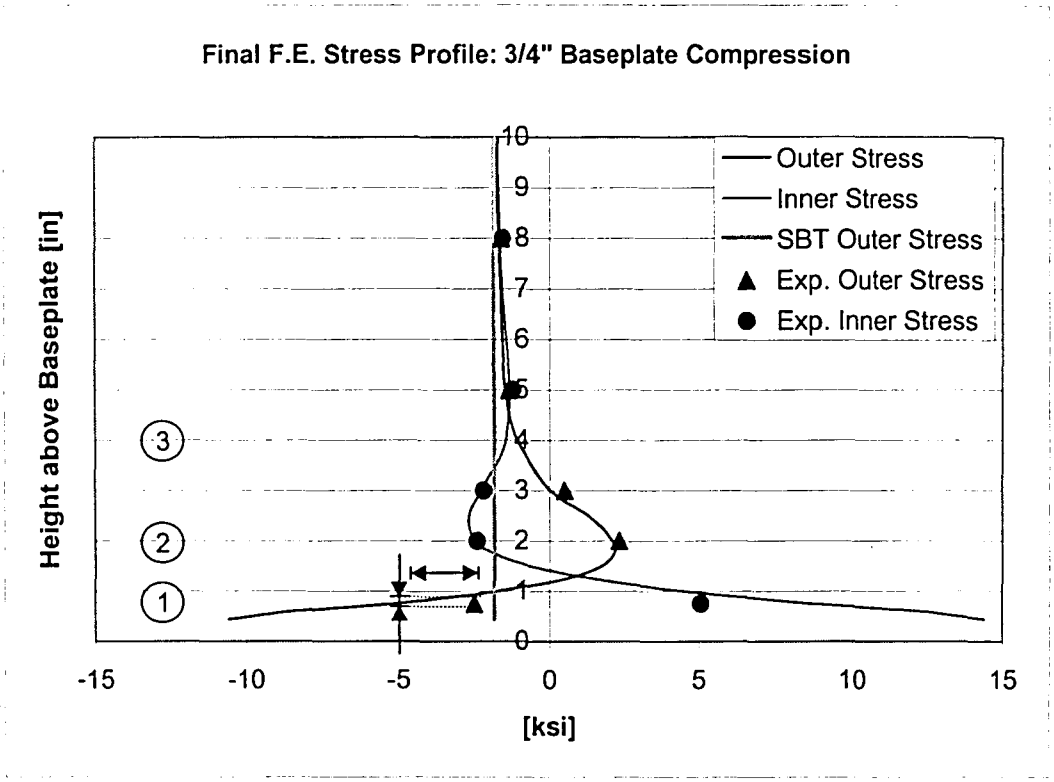

Figure 4.2.1.4: Final F.E. Stress Profile: 3/4" Baseplate Specimen

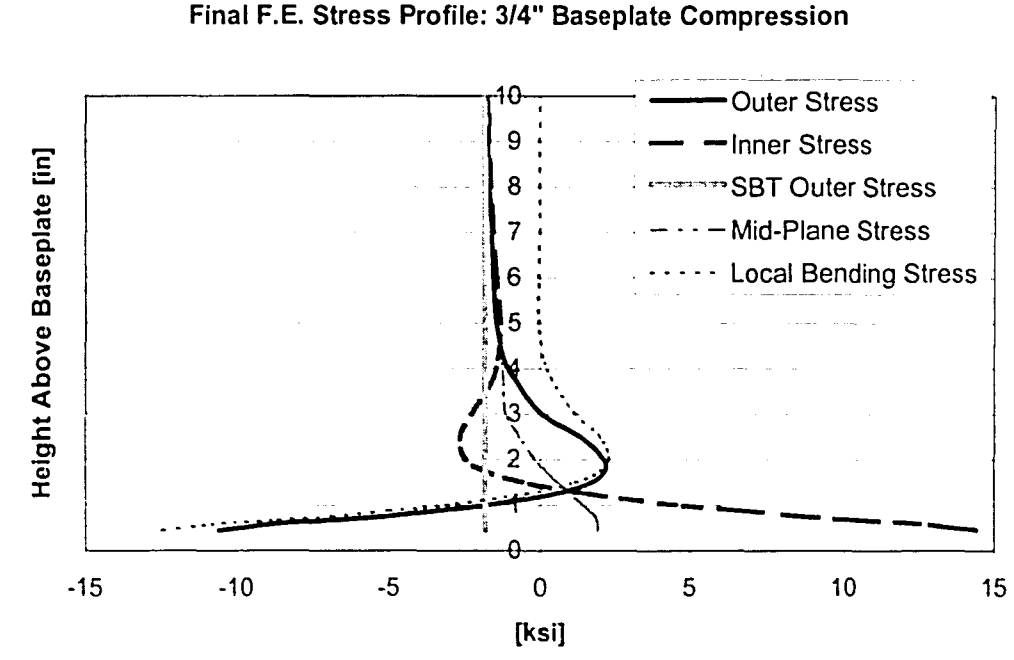

Figure 4.2.1.5: Final F.E. Stress Profile: 3/4" Baseplate Specimen

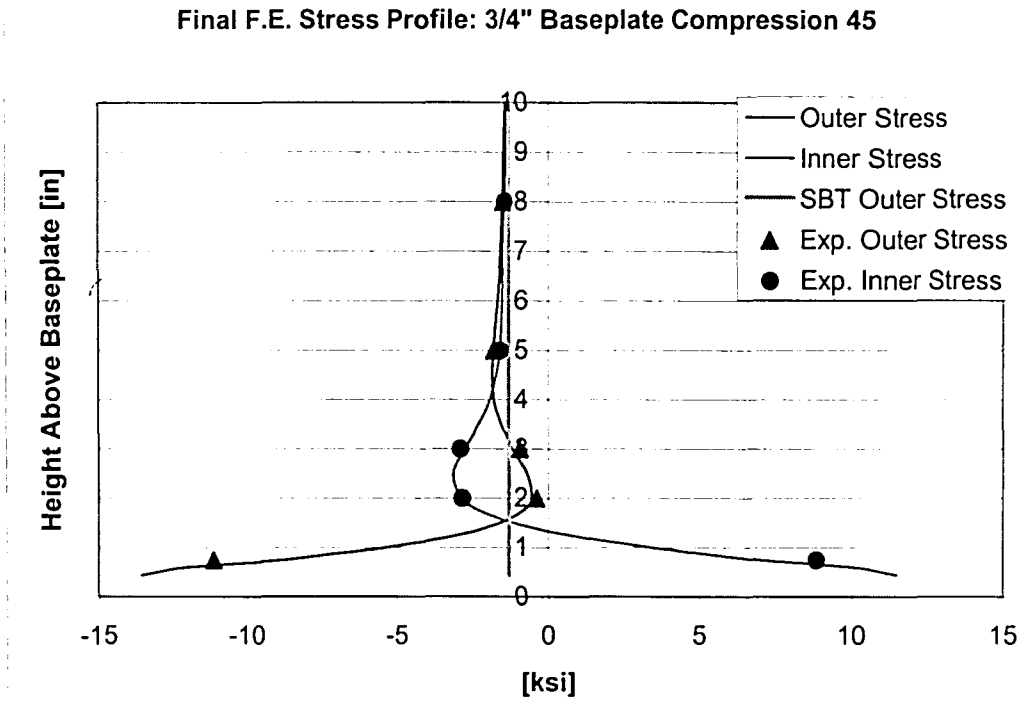

Figure 4.2.1.6: Final F.E. Stress Profile: 3/4" Baseplate, Compression 45

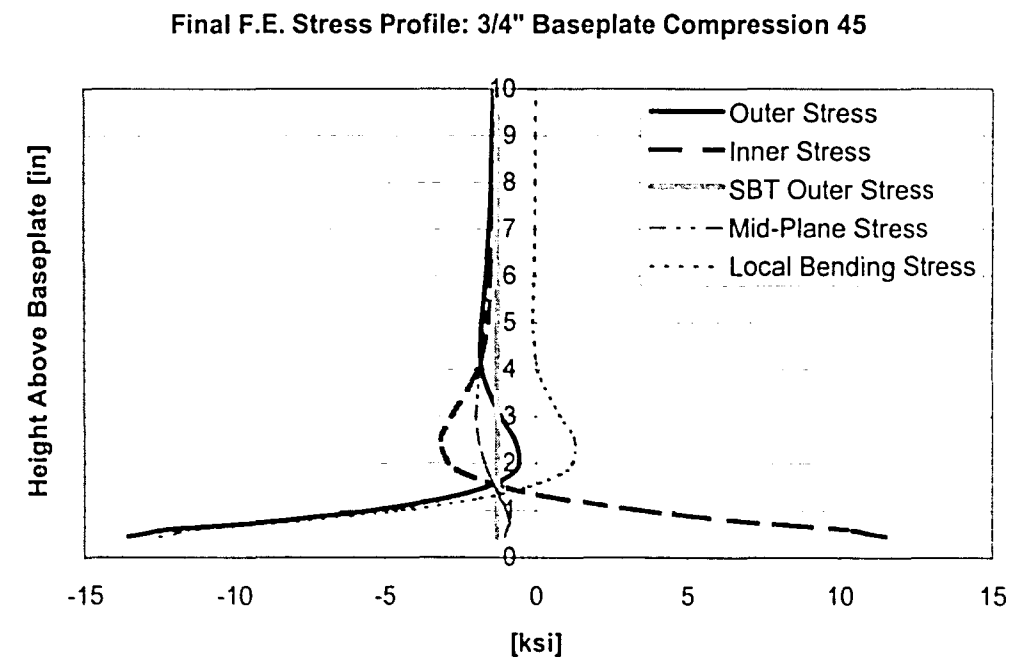

Figure 4.2.1.7: Final F.E. Stress Profile: 3/4" Baseplate, Compression 45

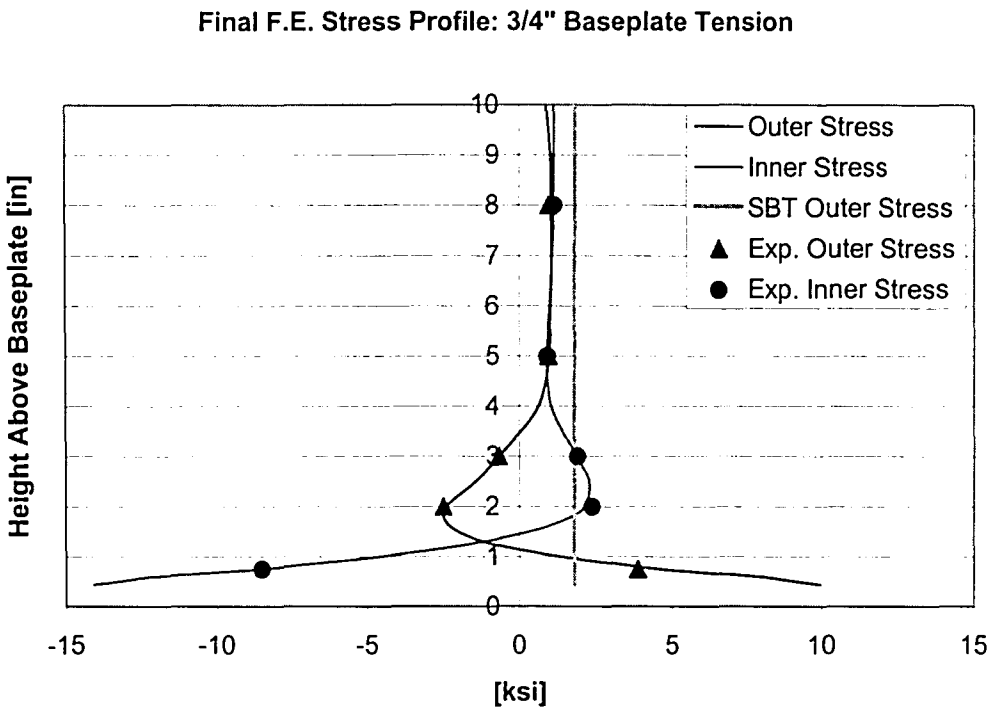

Figure 4.2.1.8: Final F.E. Stress Profile: 3/4" Baseplate, Tension

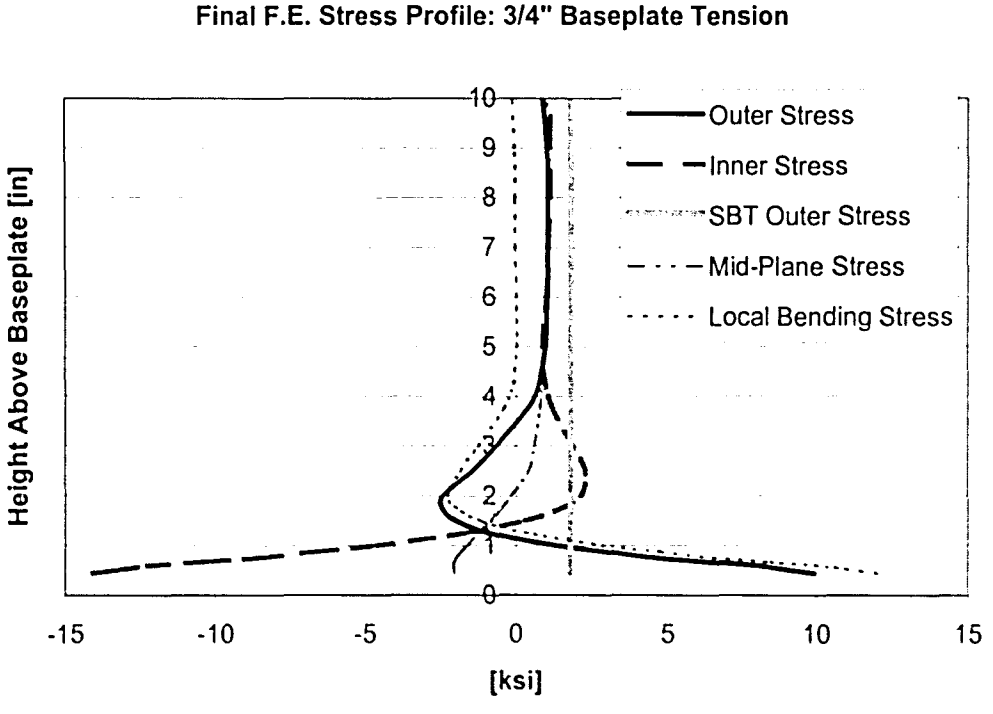

Figure 4.2.1.9: Final F.E. Stress Profile: 3/4" Baseplate, Tension

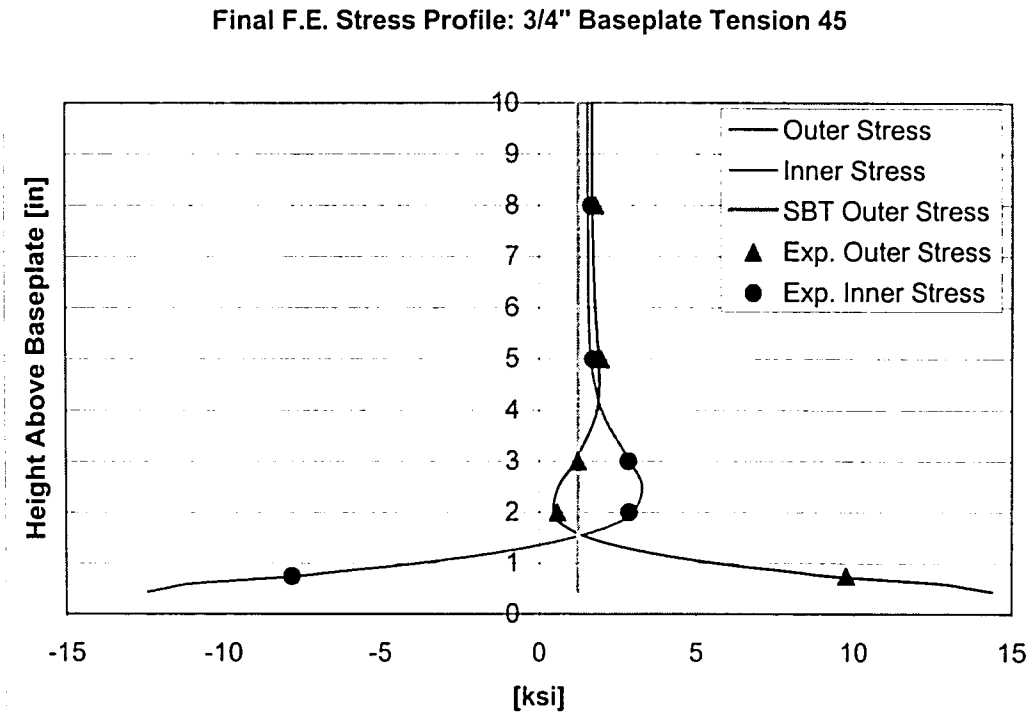

Figure 4.2.1.10: Final FE Stress Profile: 3/4" Baseplate Tension 45

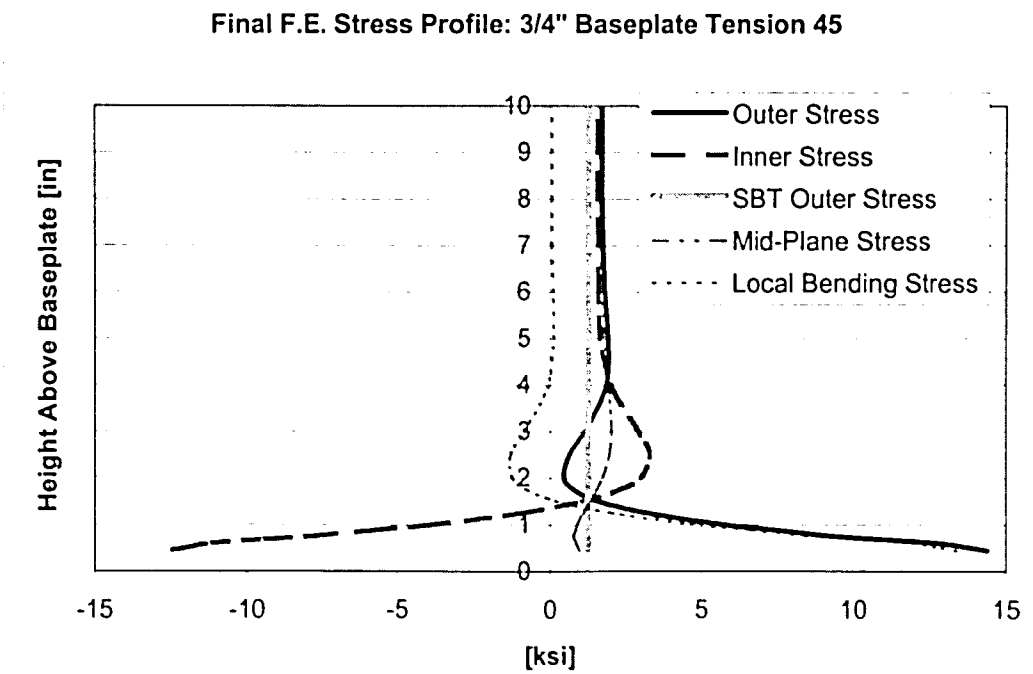

Figure 4.2.1.11: Final FE Stress Profile: 3/4" Baseplate Tension 45

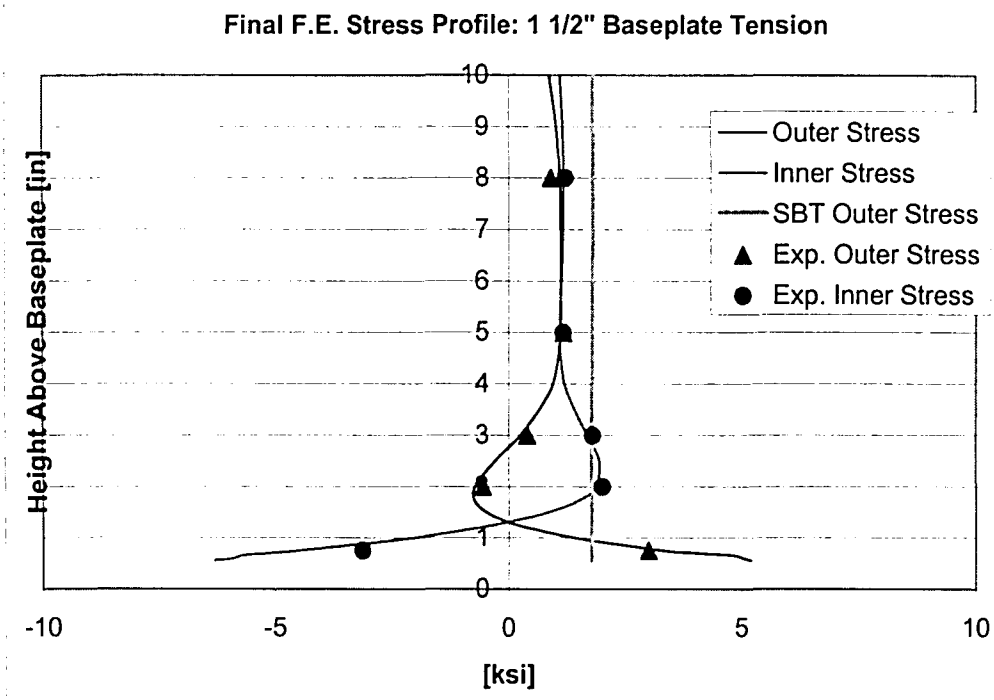

Figure 4.2.1.12: Final FE Stress Profile: 1 1/2" Baseplate Tension

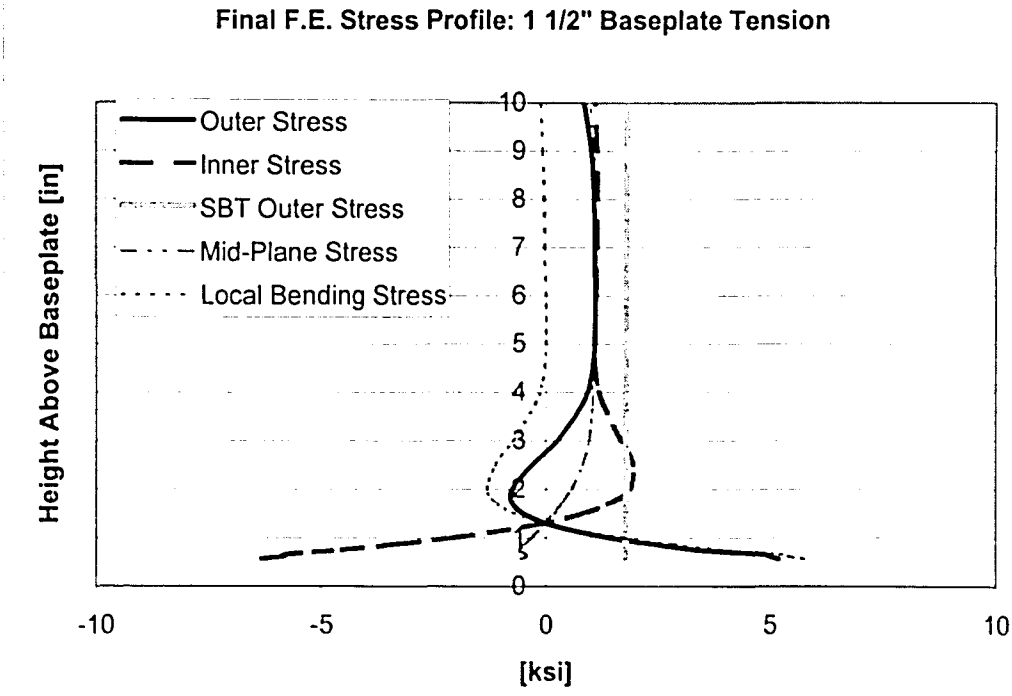

Figure 4.2.1.13: Final FE Stress Profile: 1 1/2" Baseplate Tension

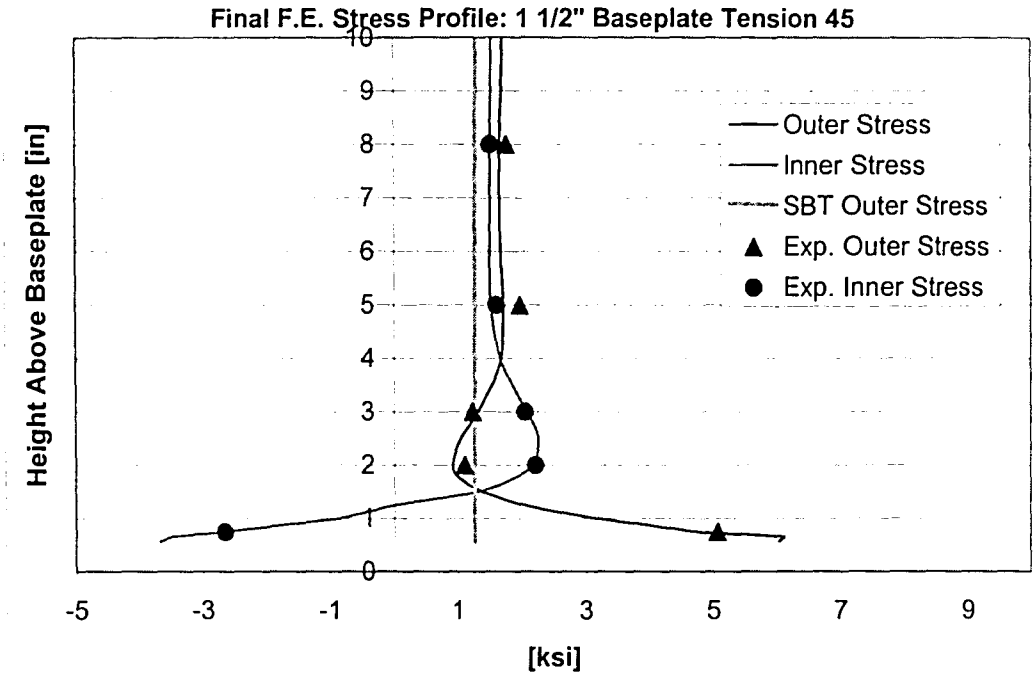

Figure 4.2.1.14: Final FE Stress Profile: 1 1/2" Baseplate, Tension 45

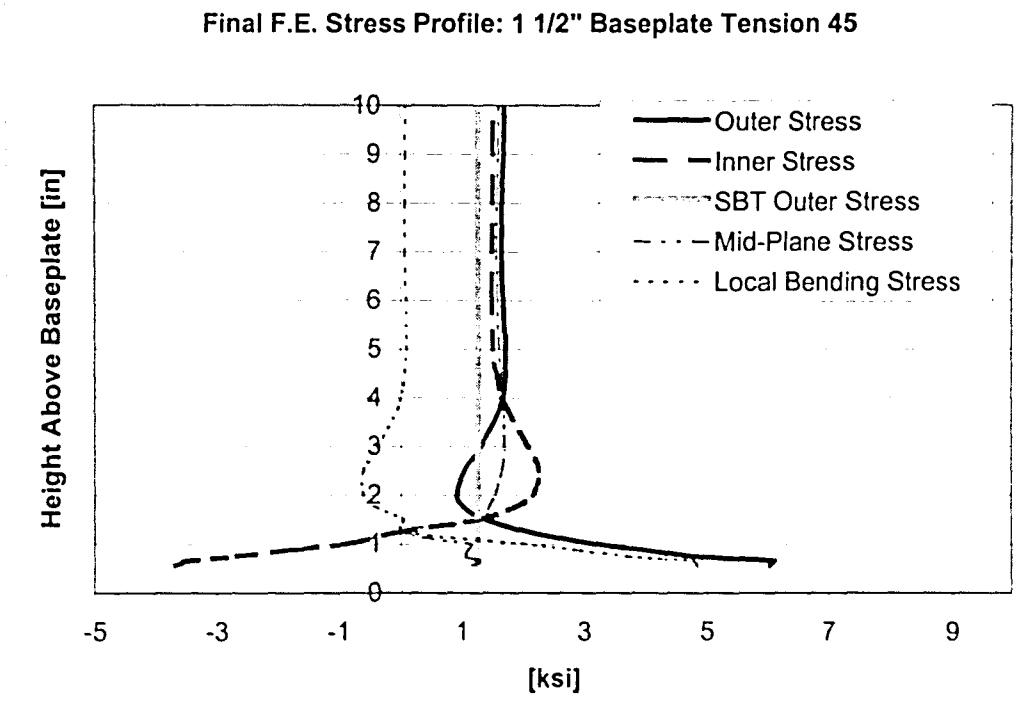

Figure 4.2.1.15: Final FE Stress Profile: 1 1/2" Baseplate, Tension 45

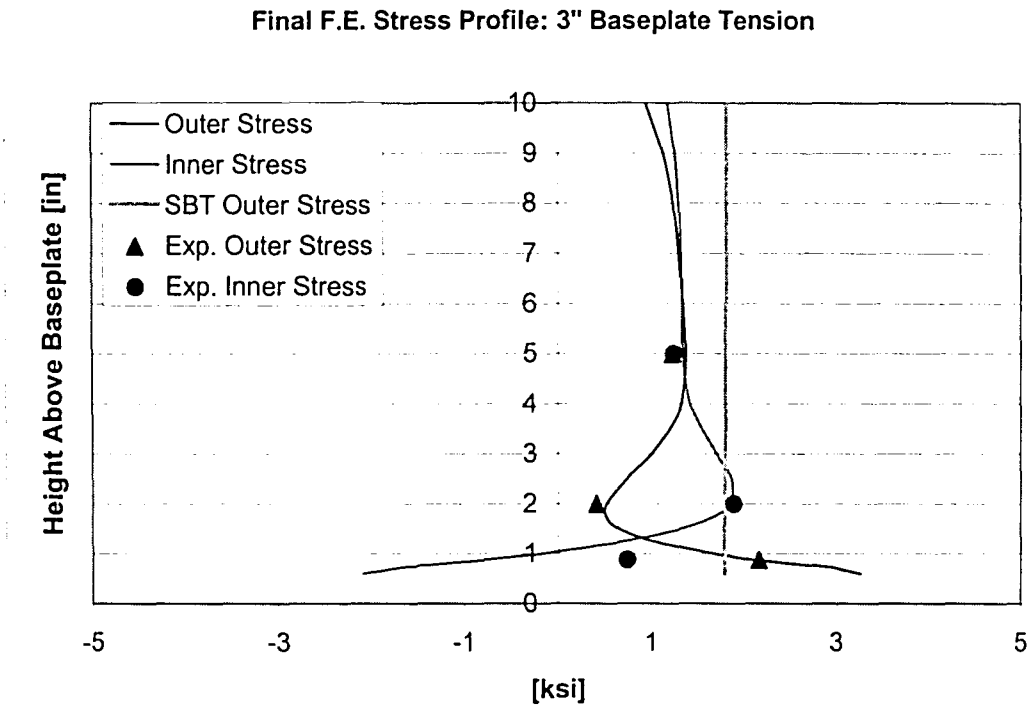

Figure 4.2.1.16: Final FE Stress Profile: 3" Baseplate, Tension

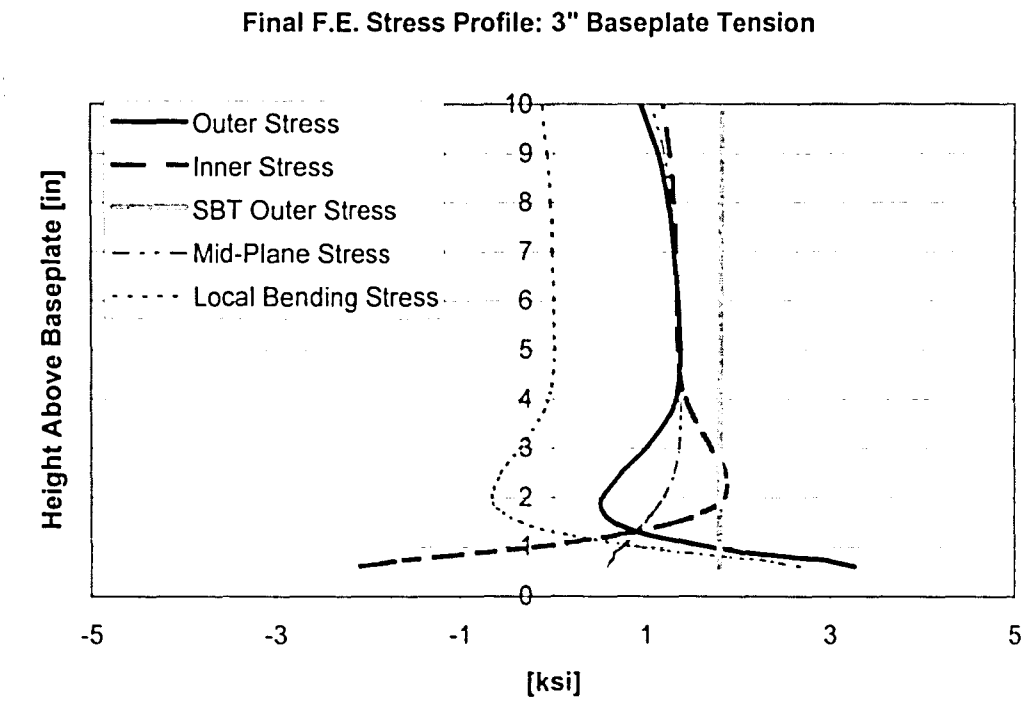

Figure 4.2.1.17: Final FE Stress Profile: 3" Baseplate, Tension

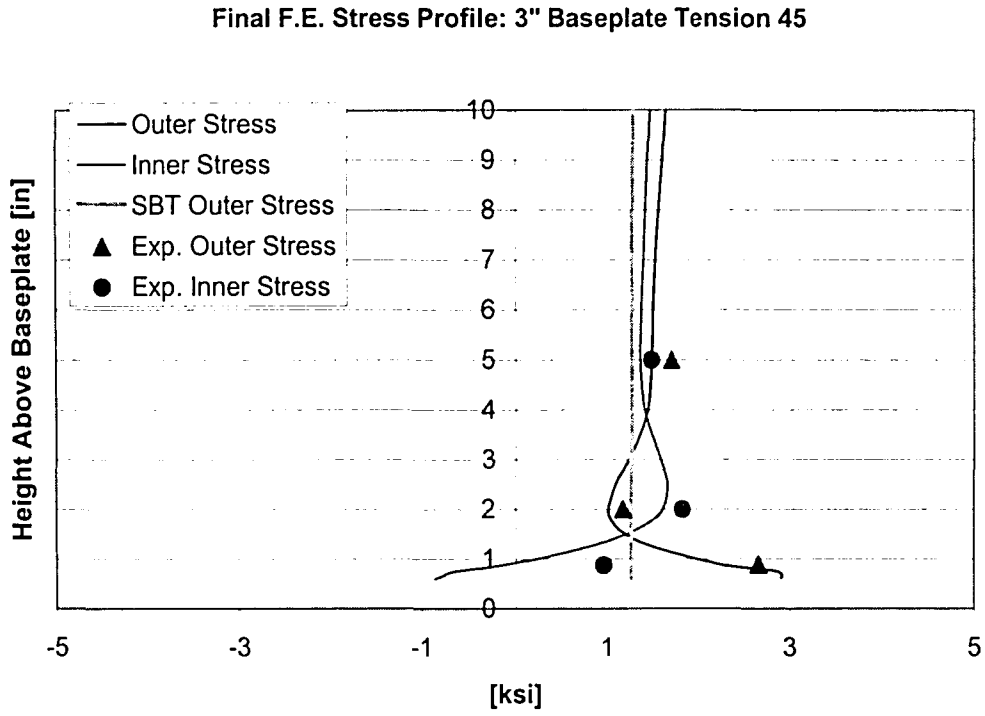

Figure 4.2.1.18: Final FE Stress Profile: 3" Baseplate Tension 45

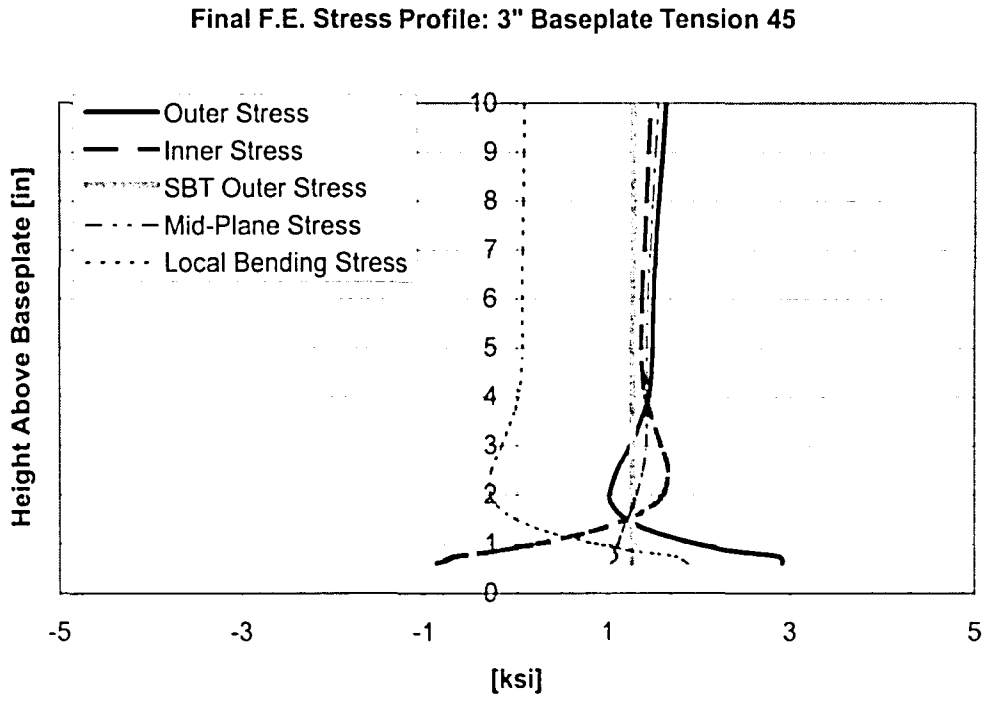

Figure 4.2.1.19: Final FE Stress Profile: 3" Baseplate Tension 45

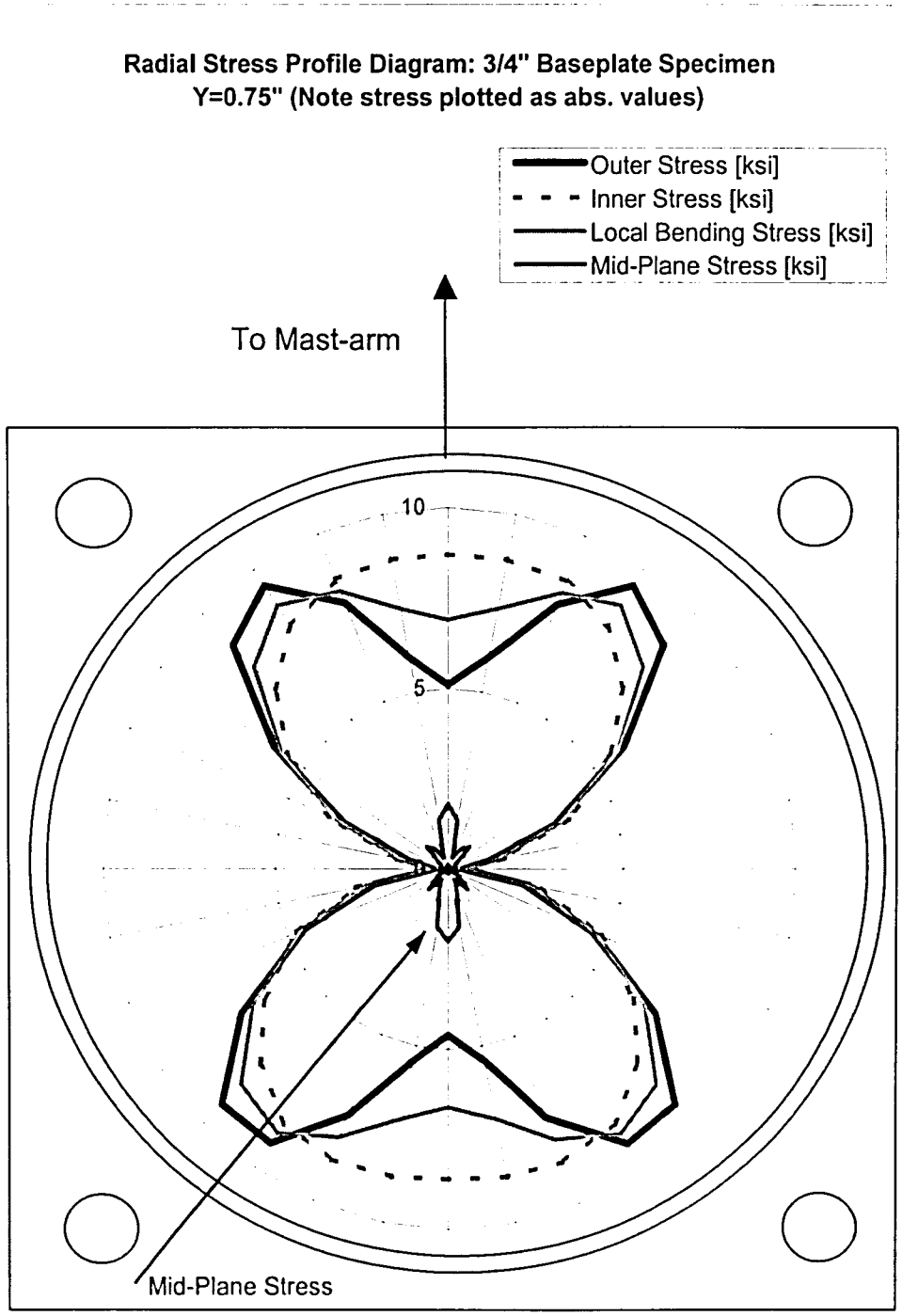

Figure 4.2.1.20: Radial Stress Profile Diagram: 3/4" Baseplate

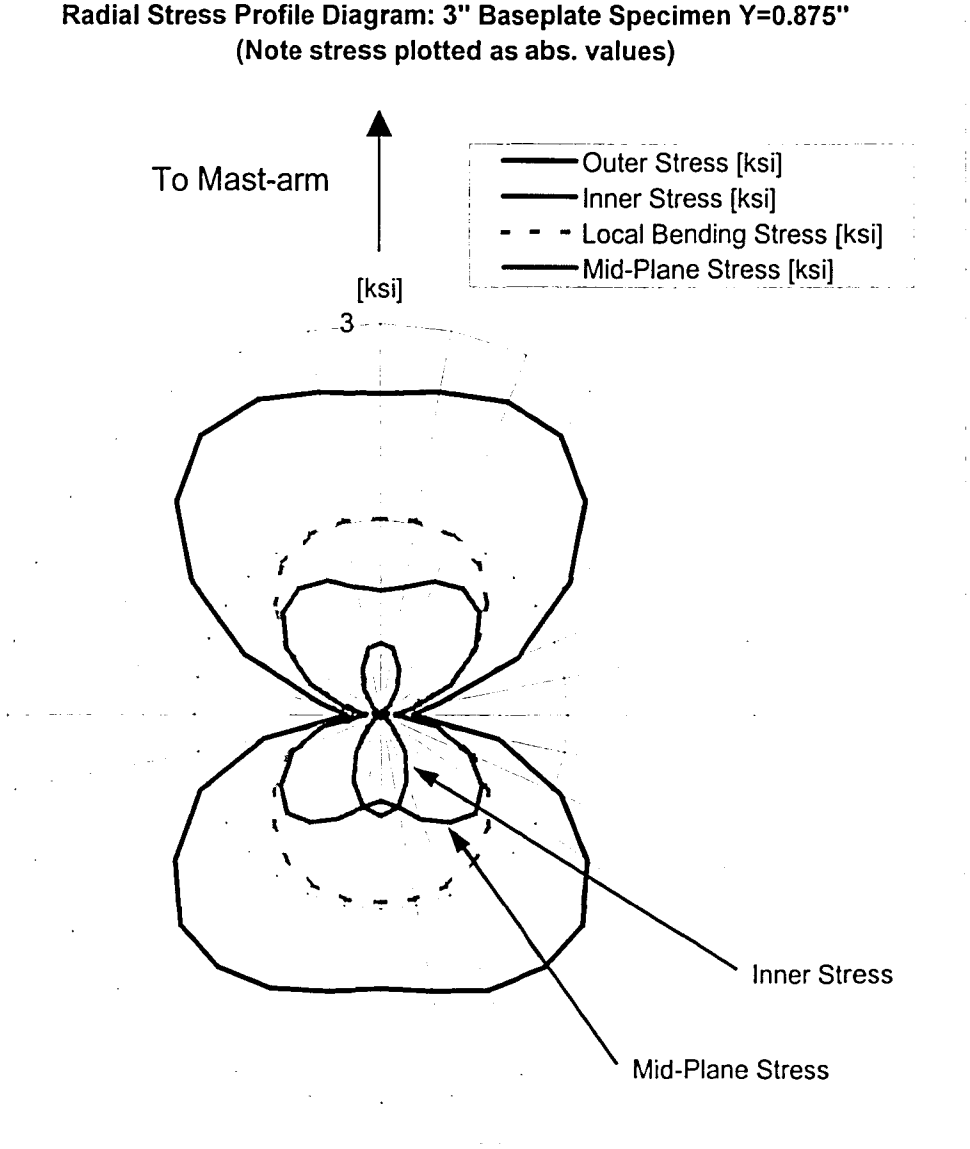

Figure 4.2.1.21: Radial Stress Profile Diagram: 3" Baseplate

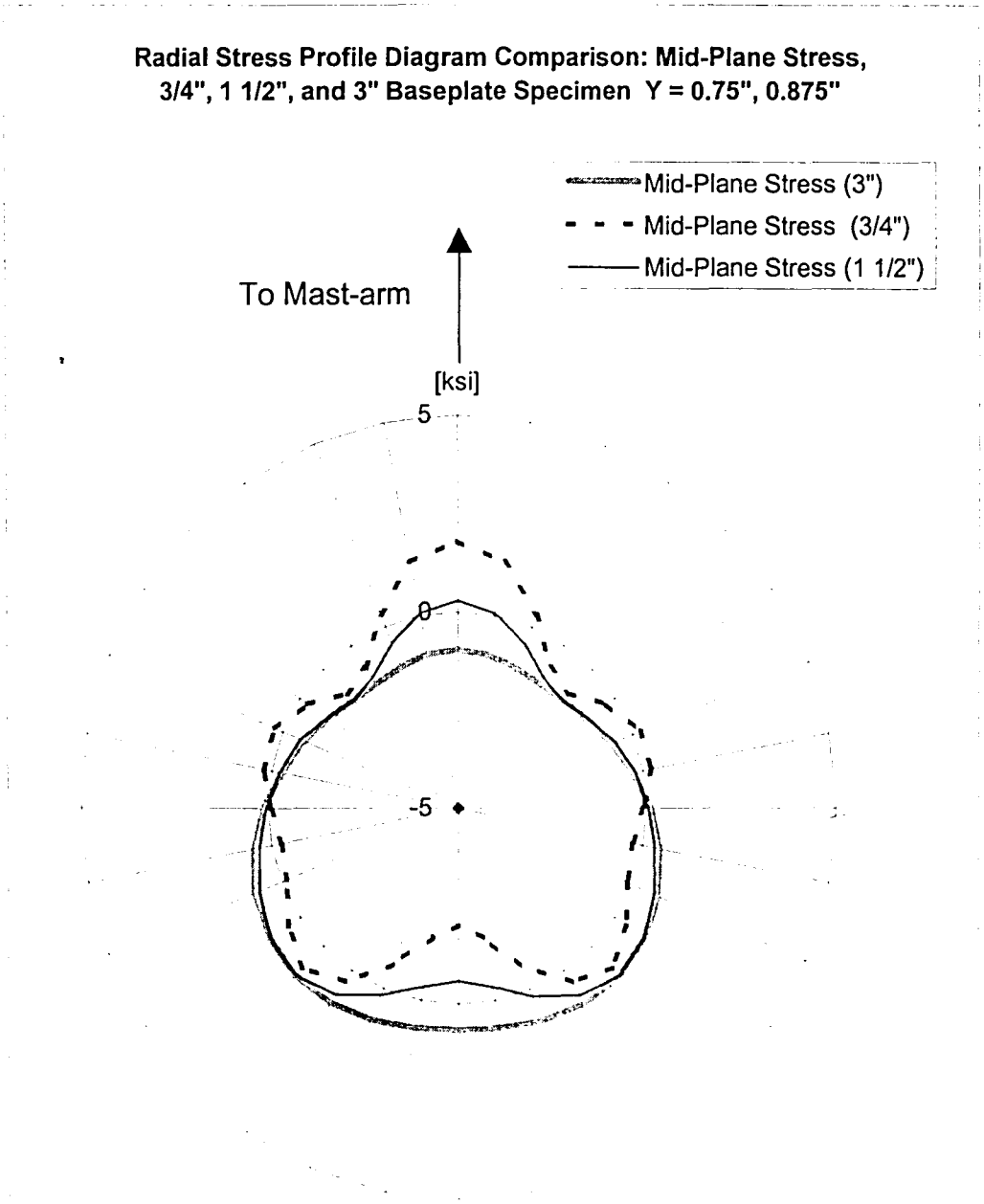

Figure 4.2.1.22: Radial Stress Profile Diagram Comparison: Mid-Plane Stress

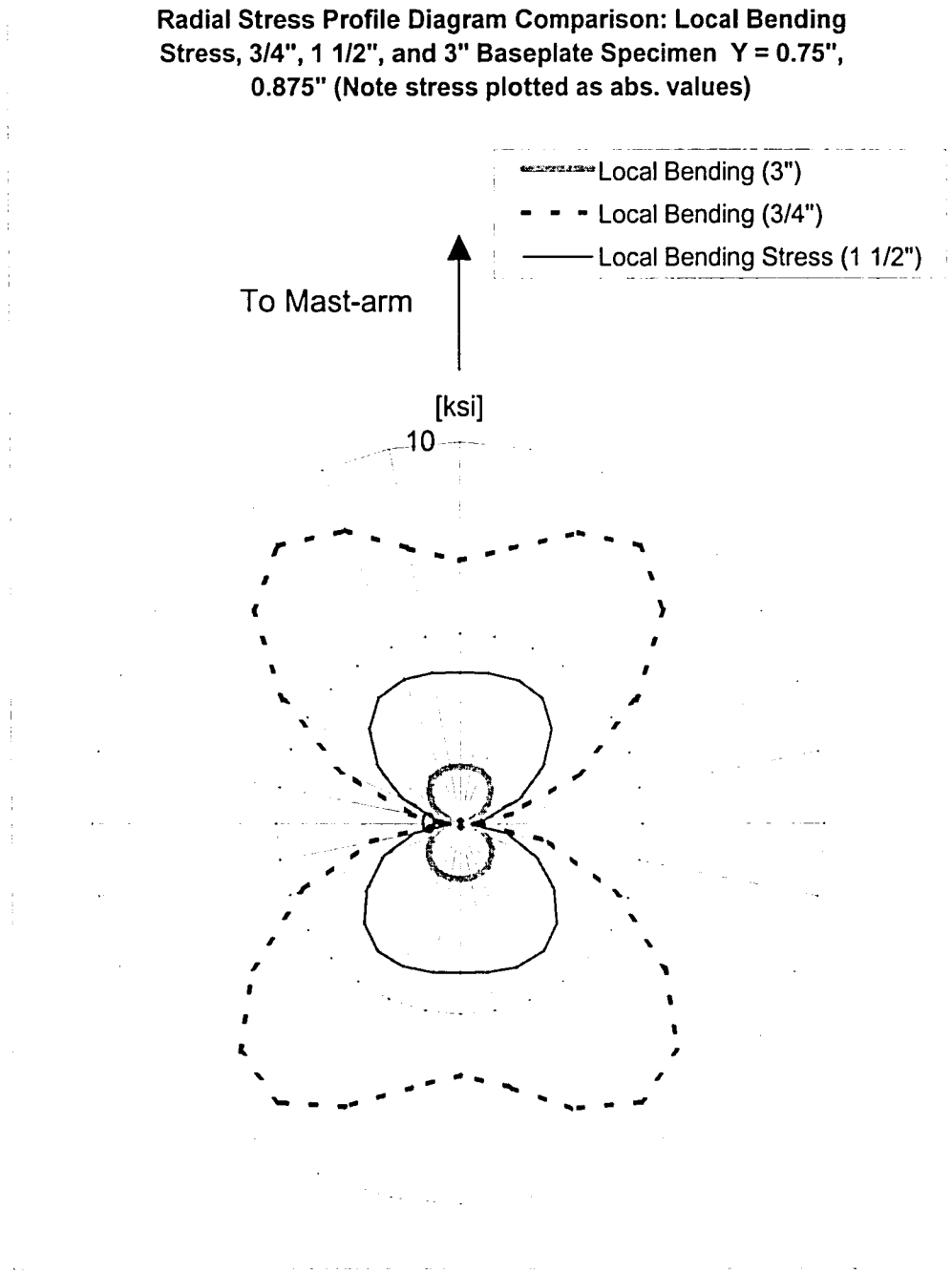

Figure 4.2.1.23: Radial Stress Profile Diagram Comparison: Local Bending Stress

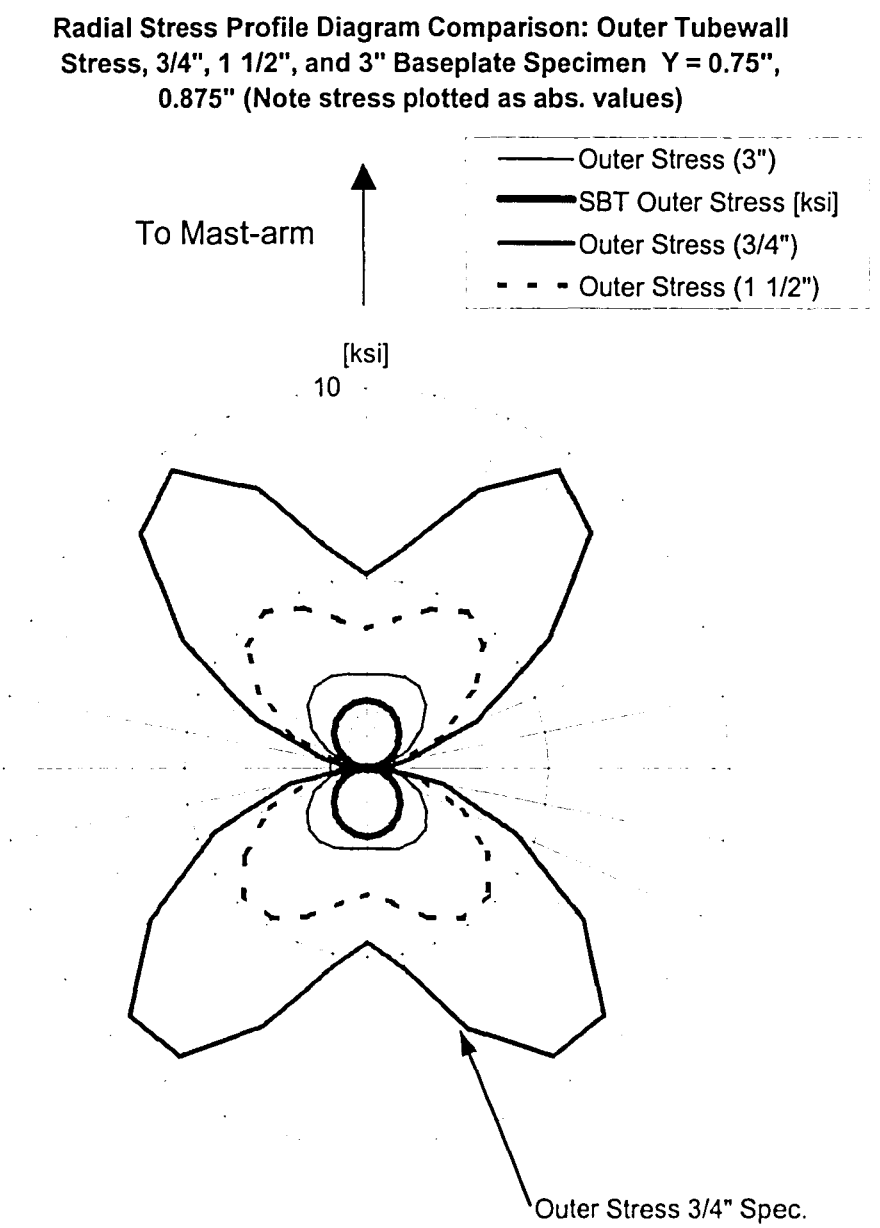

Figure 4.2.1.24: Radial Stress Profile Diagram Comparison: Outer Tubewall Stress

1 1/2" Baseplate Specimen Leveling Imperfection Tubewall Stress Radial Diagram; Left Tension Anchor Rod Up 3/32"

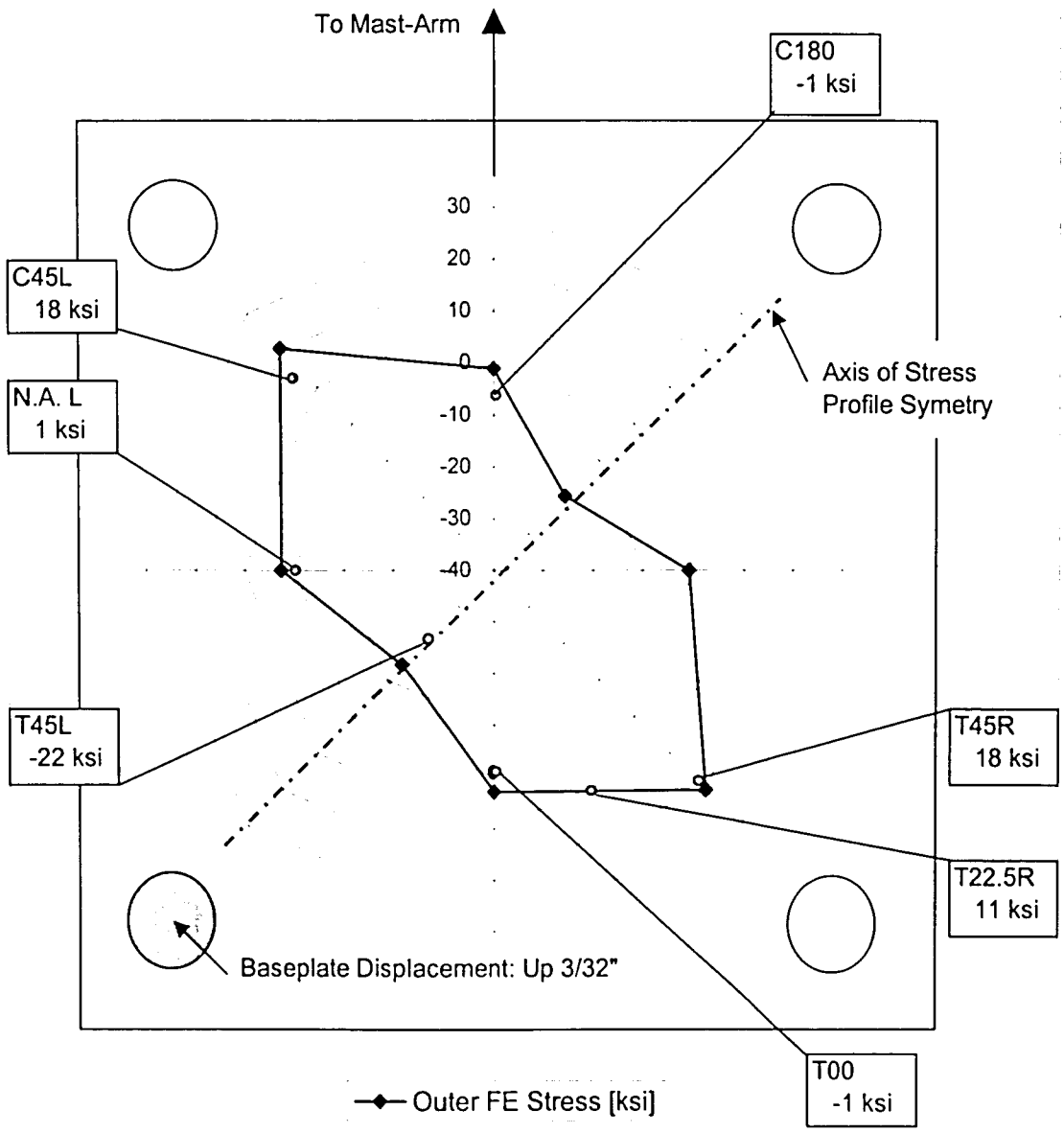

Figure 4.2.2.1: Baseplate Leveling Imperfection Tubewall Stresses

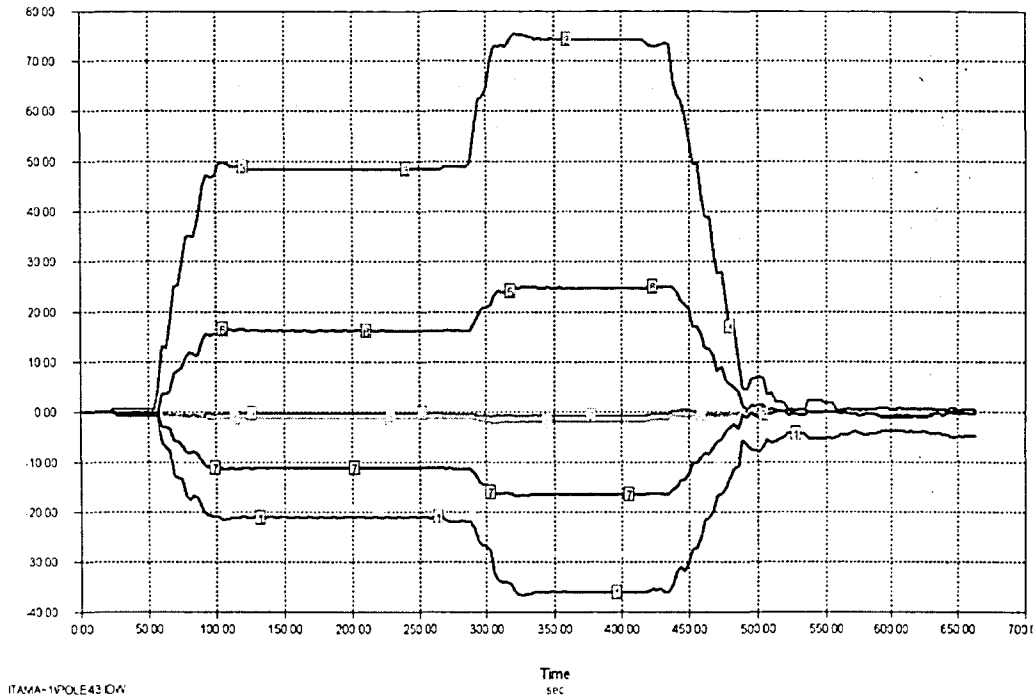

Figure 4.2.2.1A: Sample Data Record of Baseplate Leveling Test
(Please note that the chart's text size does not conform to L.U.'s Thesis requirements as the figure is intended for illustrative purposes only).

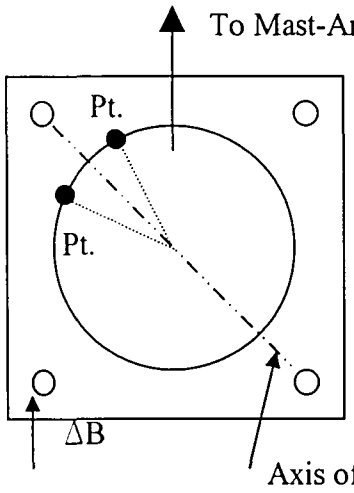

Symmetry 1: Symetry in Stress profile about diagonal imperfection displacement axis.

$$\sigma\Delta_{BP\_PT1} = \sigma\Delta_{BP\_PT2}$$

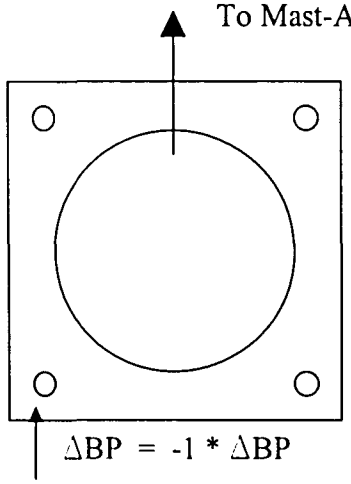

Symmetry 2: Anti-symmetry, equal and opposite stresses produced by equal and opposite enforced leveling imperfections.

$$\sigma\Delta_{BP\_up\_PT1} = -1 * \sigma\Delta_{BP\_down\_PT1}$$

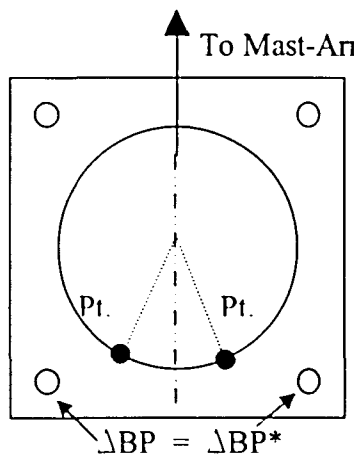

Symmetry 3: Symmetry of Loading Location about Mast-arm Axis.

$$\sigma\Delta_{BP\_PT1} = \sigma\Delta_{BP}{}^{*}\_PT2$$

Figure 4.2.2.2: Baseplate Leveling Imperfection Behavior Symetry Diagram

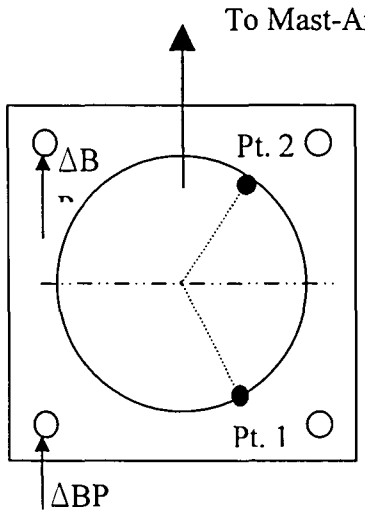

Symmetry 4: Symmetry of Loading about Neutral Axis.

$\Delta BP = \Delta BP^*$

$\sigma\Delta_{BP}\_PT1 = \sigma\Delta_{BP^*}\_PT2$

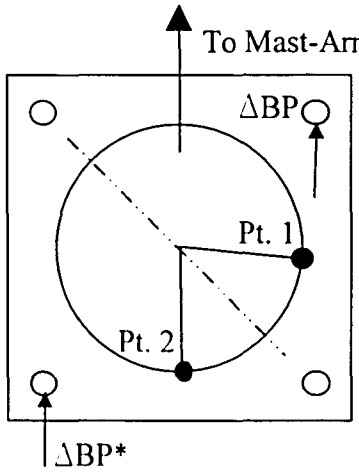

Symmetry 5: Symmetry of Loading Location about Diagonal Axis.

$\Delta BP = \Delta BP^*$

$\sigma\Delta_{BP}\_PT1 = \sigma\Delta_{BP^*}\_PT2$

Figure 4.2.2.2: (Continued) Baseplate Leveling Imperfection Behavior Symetry Diagram

Horizontal Plane of Enforced Vertical Nodal Displacements

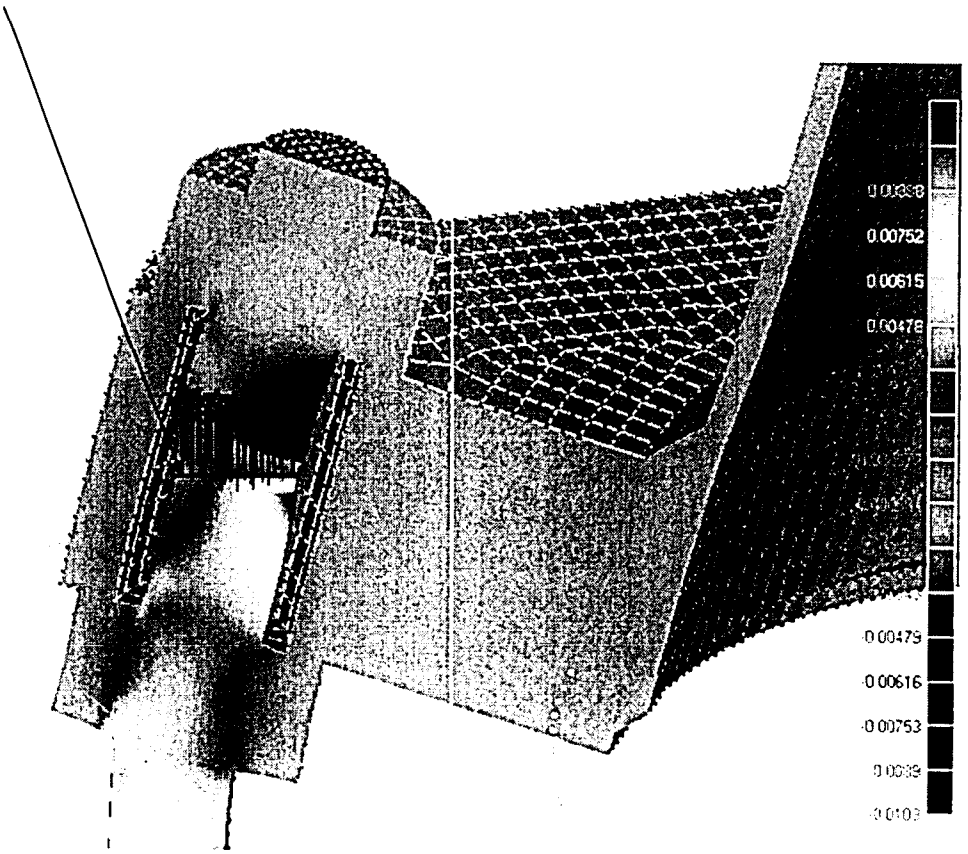

Figure 4.2.2.3: Baseplate Leveling Imperfection Loading Test Model. Section through anchor rod showing location of nodal enforced displacements.

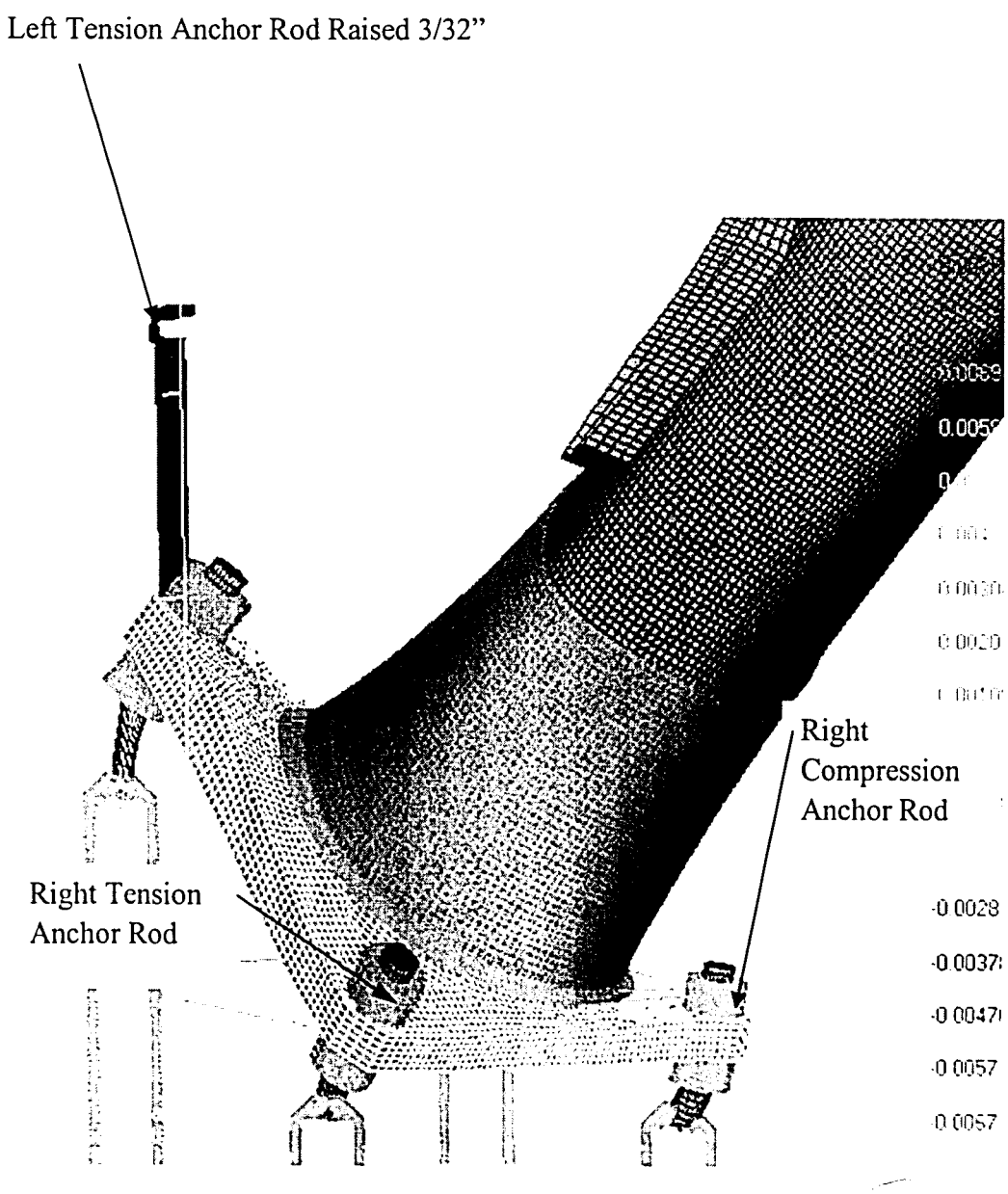

Figure 4.2.2.4: Baseplate Leveling Imperfection Model

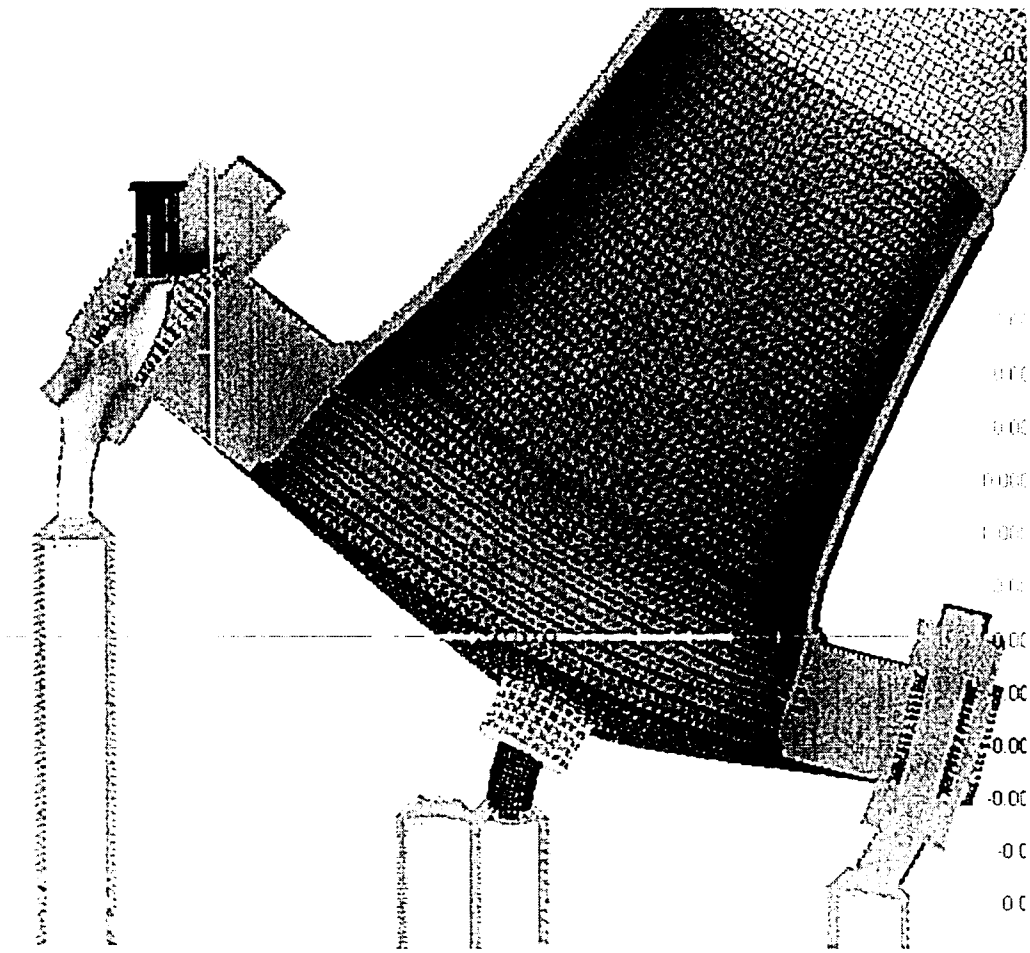

Figure 4.2.2.5. Section through diagonal axis, from the left tension to the right compression anchor rods of imperfection loading model.
Note the different flexibility behaviors at each side of the baseplate to tubewall connection.

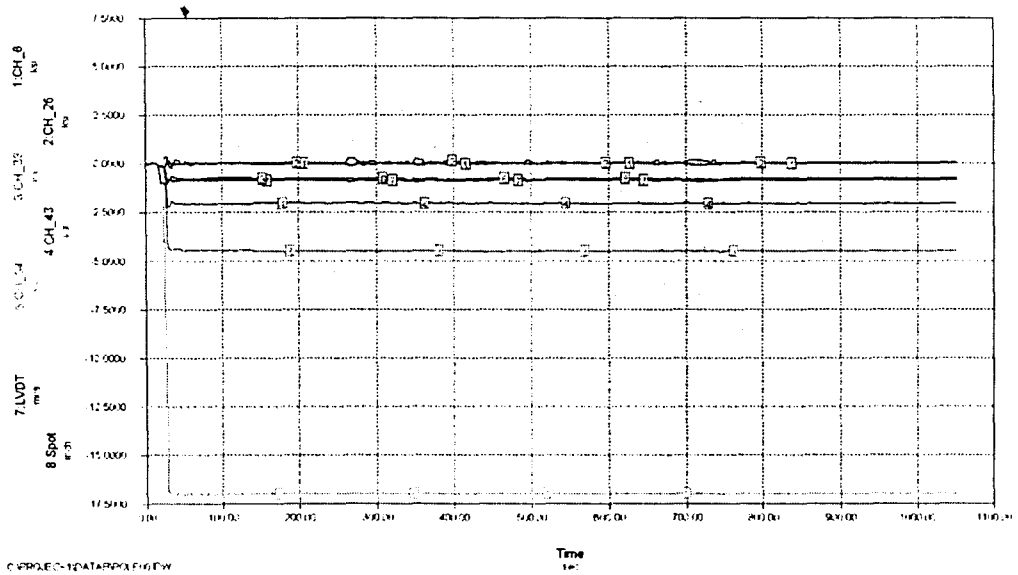

Figure 4.2.3.1: Sample Data Record of Mast-Arm Tension Bolt Removal Test
(Please note that the chart's text size does not conform to L.U.'s Thesis requirements as the figure is intended for illustrative purposes only).

Figure 4.2.3.2 Photo of Gap between Endplate and Flangeplate induced upon removal of Left Tension Mast-Arm Bolt

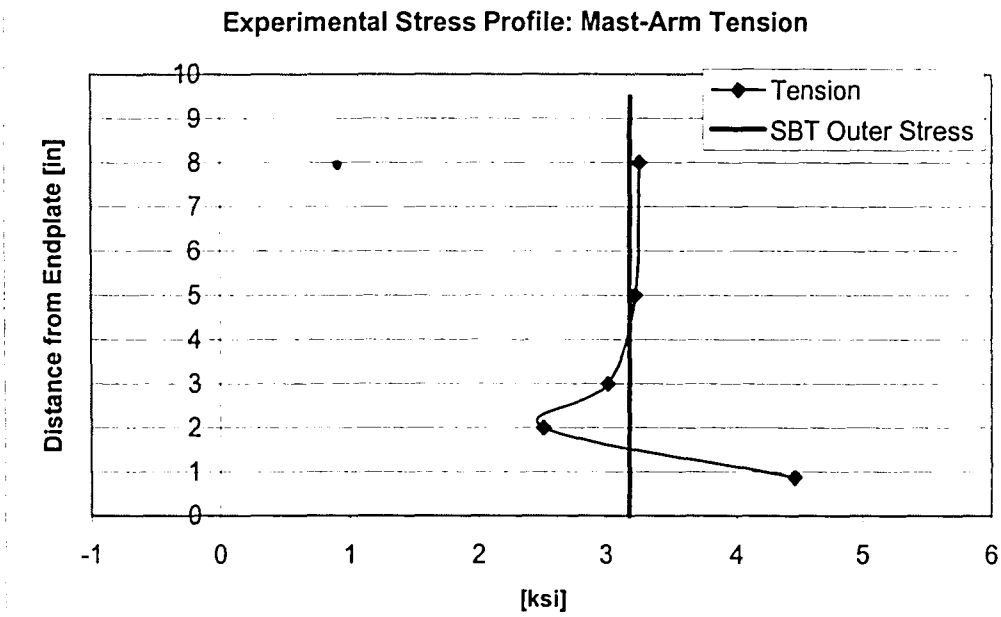

Figure 4.2.3.2: Experimental Stress Profile: Mast-Arm, Tension

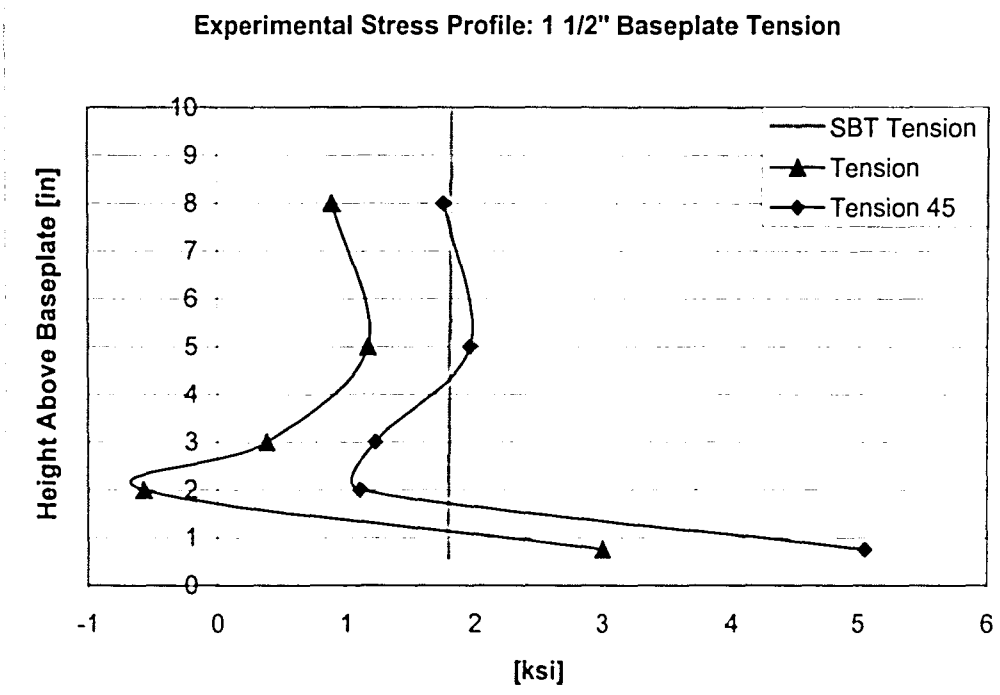

Figure 4.2.3.2: Experimental Stress Profile: 1 1/2" Baseplate Tension

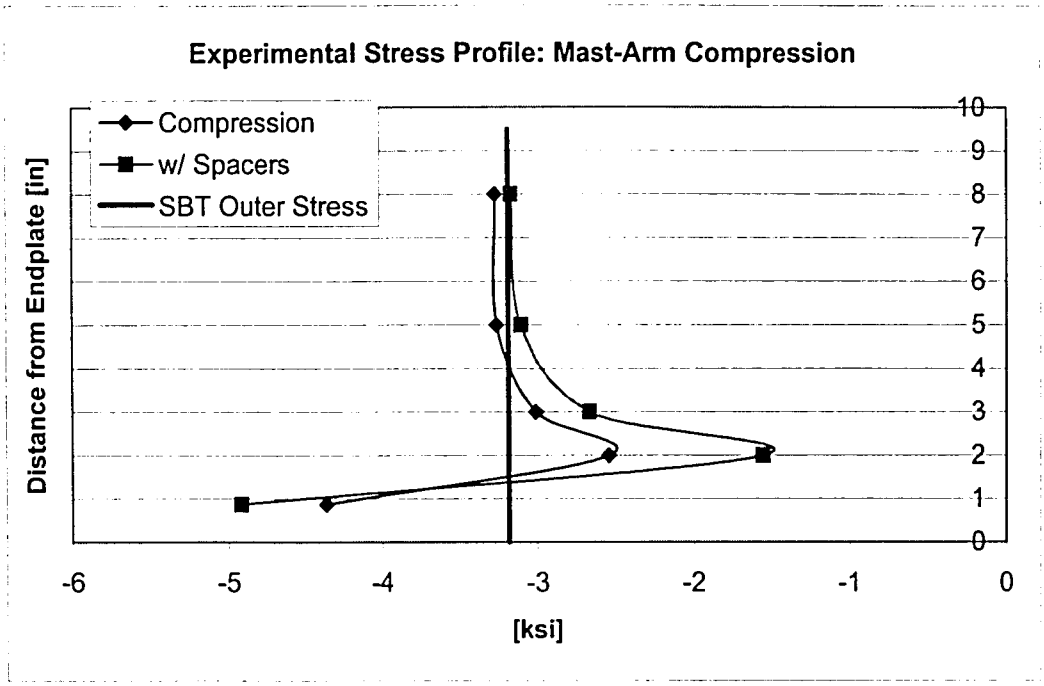

Figure 4.2.3.4: Experimental Stress Profile: Mast-Arm, Compression

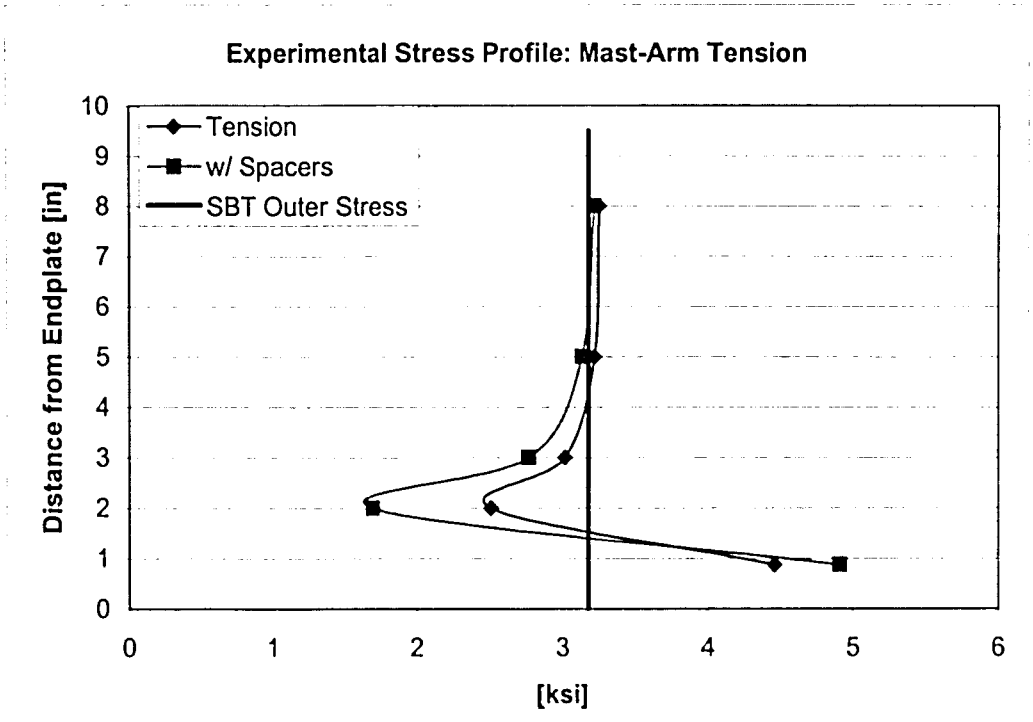

Figure 4.2.3.5: Experimental Stress Profile: Mast-Arm, Tension

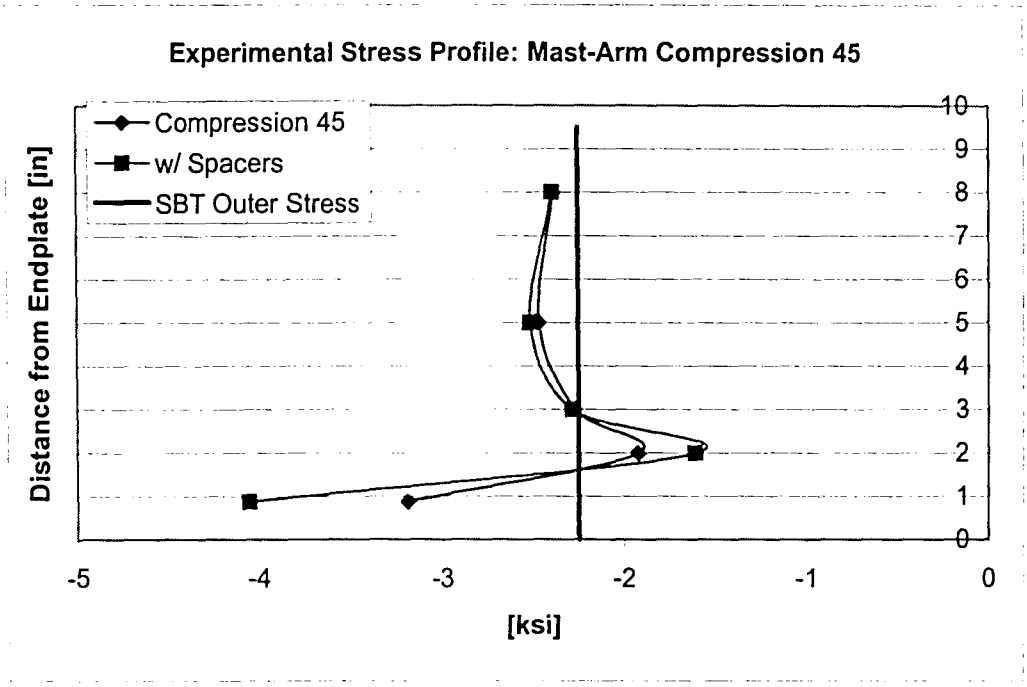

Figure 4.2.3.6: Experimental Stress Profile: Mast-Arm, Compression 45

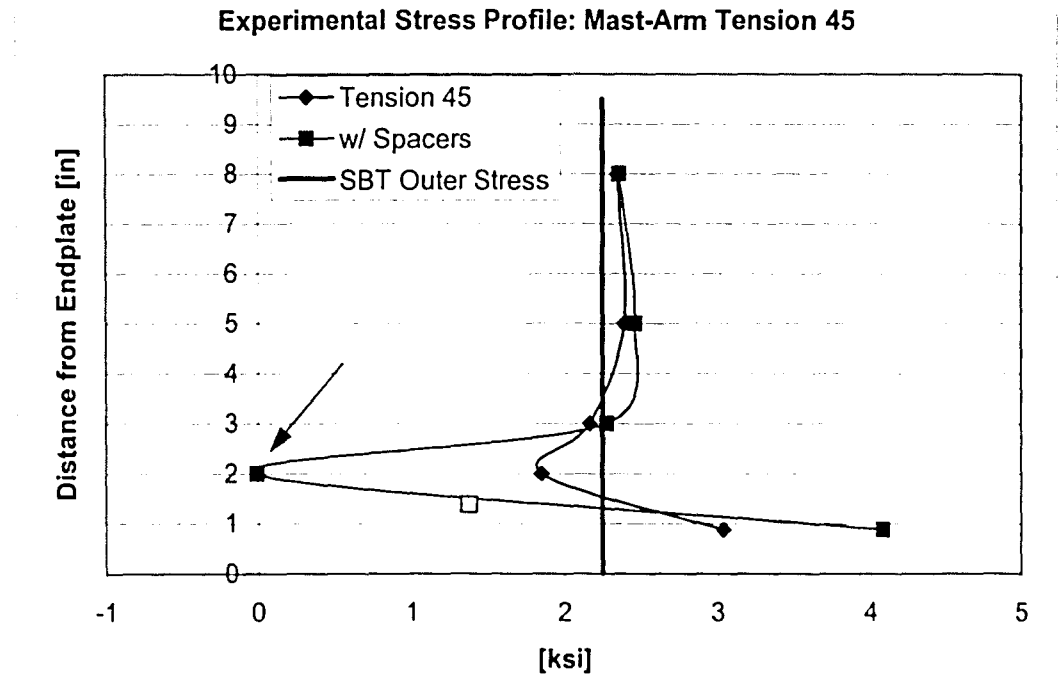

Figure 4.2.3.7: Experimental Stress Profile: Mast-Arm, Tension 45

* - Instrumentation Problem, Bad Gage

Chapter 5

Chapter 5, the final chapter of this report, functions as the final step in the objective of the study, to determine the effects of baseplate flexibility on the fatigue performance of welded socket joints in cantilevered signal structures. Chapter 5 begins with a summary of the finite element parametric study conducted and a discussion on the assumptions made within that process (Section 5.1). The next subsection (5.2) discusses the results of the four geometric variables beginning with baseplate thickness, baseplate side length, anchor rod spacing, and finally tubewall thickness. The final two sections of the report cover the conclusions and implications of the entire study. Subsection 5.3 focuses on the conclusions of parametric studies including implications of the results as they relate to design, with an emphasis on incorporating the effects of baseplate flexibility (as a measured quantity) into the current nominal stress fatigue design approach. Subsection 5.4 then discusses the conclusions of the entire study and recommendations for future research.

Section 5.1: Introduction to Parametric Study

As the title of the study suggests the end goal of this project is to examine baseplate flexibility's influence on fatigue performance. Prior to this section, the report has discussed the work performed regarding the experimental and finite element studies, the analysis and comparison of these results, the resulting stress behavior in the tubewall adjacent to the socket connection, as well as background information on cantilevered sign structures, including the results of previous fatigue

research. Given the information learned in the experimental and finite element studies, the results of past fatigue research, and the conclusion made in the calibration study of satisfactory agreement between finite element and experimental static data, a finite element parametric study has been organized and performed.

The details of this parametric study have been carefully considered based on the understanding of the structural behavior and the experimental data. Several rational assumptions still need to be made in order to transform finite element analysis results to fatigue performance. The following paragraph summarizes the parametric study and some of the more basic assumptions made. Afterwards, the following two paragraphs discuss some of the finer points including a discussion of the linear elastic assumption of the stress field and the selection of the most appropriate vertical location on the tubewall to take as the maximum fatigue stress. Section 5.1 concludes with a brief description of the parametric study plots used to illustrate the effect baseplate and tubewall flexibility has on fatigue stresses.

In summary of the study, and the assumptions made, four different basic baseplate to pole socket connection geometry alterations were studied. The parametric study variables included the baseplate thickness, side lengths, anchor rod spacing, and the tubewall thickness. The simple approach to the study was to use the same 1 ½" thick baseplate specimen geometry for all of the parametric study, altering the specific geometric variable to produce a series of nearly identical modeled geometries. This process of creating identical models except for the particular geometric variable is very significant. Because the weld profile

geometry, baseplate fixity conditions, and mesh refinement are consistent for the different models of the parametric study, comparison between the results of different variables cancels out the effects of stress concentration, fixity, and mesh refinement issues. That is not to say that the results of the individual parametric study models do not give reasonable results on an individual basis, as the calibration study has shown that the same identical modeling procedures do provide very reasonable stress results over a very large range of baseplate flexibilities. It is important to realize that many factors affect the baseplate flexibility and the structural behavior. Thus the maximum tensile stress results given by the parametric study for a 1 ½" thick baseplate with side lengths of 20 inches likely will not compare well to an actual structure with the same baseplate geometry, with different anchor rod spacing or pole diameter. Figure 5.1.1 displays the geometries of the different models analyzed in the different geometry variable studies, as well as lists the structural and as modeled geometric details common to all the models of the study.

A common approach to studying the performance of welded fatigue sensitive connection details is to examine the connection using linear elastic analysis. This approach is referred to as linear elastic fracture mechanics (Barsom and Rolfe, 1987). Due to the residual stresses created by the heating and cooling process of welding, locations near the weld metal will likely be plastic, including at the tips of the sharp flaws created in the welding process (Barsom and Rolfe 1987). These very local locations of plastic behavior though must follow the kinematic

constraints of the surrounding elastically behaving structure. Thus the strain field will be constant throughout the tubewall even at the plastic regions, due to an applied fatigue loading (Barsom and Rolfe, 1987). For this reason, an elastic analysis can be applied to determine the stress range at the connection, and elastic static load experimental testing results also apply to the fatigue behavior of the structure.

Thus given the validity of the linear elastic fracture mechanics approach, there are two ways that elastic stress can be related to fatigue performance. The first involves the threshold stress-intensity factor which is nearly identical to the stress-intensity factor as discussed in Section 1.5. The threshold stress intensity factor range (ΔK_{TH}) is given by:

$$\Delta K_{TH} = \Delta\sigma * (a)^{1/2} * f(g)$$

Where $\Delta\sigma$, is the stress range applied to the initial flaw size a and f(g) is a constant based on the loading, structural, and crack geometry. The threshold stress intensity factor range then represents the allowable intensity of stress range, or likelihood of fatigue cracking initiating at the flaw due to the stress range, geometry, and flaw size (Barsom and Rolfe 1987). The critical value for the stress intensity factor range is determined based on the material properties of the steel. Thus assuming the same crack size and geometry fatigue performance is directly a function of the maximum stress range applied to the welded detail. AASHTO specifications for sign structures specify infinite life design, in which maximum stress ranges at fatigue details should never exceed the critical threshold value of the stress

intensity factor. Thus the comparison of fatigue performance of two welded socket connection geometries of various baseplate flexibilities, simply reduces to a comparison of the maximum tensile stresses developed in elastic loading. These tensile stresses have been shown to be a drastically related to baseplate flexibility, thus fatigue performance is also related to baseplate flexibility. The other second way that that elastic stress can be related to fatigue performance is through the relationship between stress range and number of cycles using the well established nominal stress finite life approach by AASHTO:

$$N=A/S_R^3$$

One of the major decisions made in the parametric study was the vertical location of stress to be used in the study. Referring back to Section 4.2.1 and the associated vertical stress distribution visual aids, several observations can be made regarding the appropriate vertical location. To begin as discussed in Section 1.5, research consistently shows fatigue cracking to occur in the tubewall adjacent to the vertical fillet weld toe. The finite element outer tubewall stresses in the plots shows stresses are maximum at the weld toe edge, or very near to the edge. (Note the plotted stresses begin at the edge of the vertical weld toe). The finite element stresses are very linear just above the weld toe, with increasing height above the baseplate. This linear gradient according to the finite element analysis results, is quite severe in the thin and flexible baseplate specimens (16 ksi per inch), but is much less in the thicker less flexible baseplates (4-5 ksi per inch). Experimental and finite element data show very good correlation, especially in the valley location

of the profiles. Experimental data shows similar steep strain gradients. The characterization of this gradient is limited because the gage placement just above the weld toe, since only two gages would fit in that short linear region just above the weld toe. The use of a strip gage, with multiple strain sensors closely spaced together would be recommended to verify this steep finite element linear stress gradient, down to the edge of the vertical weld toe.

The main problem is that there may be some question as to whether the finite element results are accurate so close to or directly at the geometric edge of the vertical weld toe and tubewall. However, stresses used in the parametric study will be taken at the edge of the vertical weld toe. As shown in the vertical stress profiles there is not a major jump or serious discontinuity in the plotted stress at this location, instead the stress continues on the same linear gradient right to the edge of the weld toe. As noted in a concluding remark in the vertical stress profile discussion in Section 4.2.1, depending on the size and inertial properties of the upper fillet weld, outer tubewall stresses may not be perfectly linear over the small distance, approximately 1/10" or less above the weld toe. The stress directly at the weld toe is slightly reduced, as would be expected, as the weld profile inertia acts to inhibit the local deformations of the tubewall in the very small vertical region just above the weld toe. This effect is very minute, and thus it is felt that it is still appropriate to take the maximum stress at the weld toe edge. Justification of this point includes: the small magnitude of the difference, the fact that maximum stresses do often occur at the weld toe, and the lack of a better understanding of this

stress concentration effect, which is consistent for all of the models of the parametric study

Additionally the various stress gradients have been shown to be very different depending on the thickness and flexibility of the baseplate. Using stresses from a consistent distance away from the weld toe (for example ¾") would allow for possibly more reliable finite element data, further away from a modeled geometric discontinuity and with corresponding experimental data. In this approach the comparison could be made between the different models, to gauge the reduction or amplification of stress at the weld toe, assuming a consistent strain gradient. The consequence of performing the study with stresses from a consistent vertical distance away from the weld toe, would become apparent in the comparison of baseplate specimens with different flexibilities, and different stress gradients. Using a simple numeric example to illustrate this point, imagine two baseplate specimens with different flexibilities. The flexible specimen has an outer stress gradient of 16 ksi per inch, and the stiff specimen has an outer stress gradient of 4 ksi per inch. At a point one-quarter of an inch above the weld toe the stiff and flexible specimen have tubewall outer stresses of 3 and 7 ksi, and thus have outer stresses of 4 and 11 ksi at the edge of the weld toe. The reduction in fatigue critical tubewall stresses (which are at the weld toe) due to the stiffer baseplate compared to the more flexible baseplate, is not accurately accounted for by measuring stresses anywhere else other than at the edge of the weld toe, because of the variation in stress gradient. The concern that at the very edge of the weld toe, the good

agreement between the finite element and experimental data may not exist is a valid concern. As mentioned earlier the use of strip gage to experimentally measure the gradient directly above the weld toe, could further verify the finite element results and may provide additional assurance. However it is felt that the abundance strain data obtained and the good agreement with the finite element data is sufficient to suggest that the finite element stresses at the weld toe are appropriate. In addition, as mentioned before the primary purpose of the parametric study is to provide a relative comparison between different baseplate flexibilities, thus in this comparison process the effects on stress due to the finite element mesh, if any do exist, will be canceled out.

Prior to beginning the discussion of the results of the parametric study, the procedure used to organization the maximum fatigue stress data must be explained. Because the fatigue performance is typically based on simple limit state criteria, it is essential that the stress at a particular fatigue sensitive location must remain less than the critical value. This simple principle, was previously discussed in terms of threshold stress intensity factor, if the stress range and thus the threshold stress intensity factor range are above a critical value, fatigue crack initiation occurs. The same principle is used in the nominal stress approach to fatigue design, that a nominally calculated stress range due to prescribed fatigue loading must be less than the constant amplitude fatigue limit for the particular detail. Thus the most appropriate approach to the parametric study is to compare the maximum stress in the tubewall adjacent to the weld toe, relative to simple beam theory nominally

calculated maximum stresses. As discussed in Section 4.2.1, in the radial stress diagram section, and with other finite element study (which is not provided) two major remarks can be made about the maximum tensile stress. First the maximum tensile stress in the pole always occurs on the outer surface of the pole, as an outer tubewall stress. Second, the maximum outer stress always occurs at or near the weld toe, the radial position around the tubewall varies due to baseplate flexibility.

Thus for every model specimen in the parametric study the maximum tensile outer tubewall stress was determined at the weld toe and recorded. For additional information on the flexibility trends, outer stress data was also recorded at the direct tension, and 45 degree tension radial location at the weld toe, and baseplate displacement was also measured. The baseplate deformation was measured on the compressive side along the mast-arm axis of the baseplate 1" in from the edge. The plots present these trends in baseplate deflection and tubewall stresses over the different baseplate geometric variables. Stresses are now presented normalized by the maximum nominal stress, 1.76 ksi due to the standard 100 pound cantilever end gravity static load. This maximum nominal stress is consistent for all of the modeled geometries except the tubewall thickness finite element specimens. These tubewall thickness specimens, were normalized by their respective simple beam theory stresses as well, as indicated.

Section 5.2: Discussion of Parametric Study Results

Prior discussion has described the behavior of welded socket connections, particularly the effect of baseplate flexibility. The following section presents the

results of the parametric study. In each of the individual parametric studies, the geometry variables alter the flexibility of the welded socket connection. As indicated in previous discussions, there are many other aspects of the geometry that can alter the flexibility of the connection. Only the four with the most meaningful results have been selected. Several other key aspects of the structure geometry and their effects on flexibility are discussed in the next section. The four different baseplate and pole geometry variables are discussed in the following subsections: baseplate thickness Section 5.2.1, baseplate side length Section 5.2.2, anchor rod spacing Section 5.2.3, and tubewall thickness Section 5.2.4. As will be discussed in greater detail in the next section (5.3), the first three baseplate parametric geometry variables define the quantities of the simply supported beam calculation of stiffness. These quantities are span length and cross sectional inertial properties, depth and width.

The objective of this section is to simply present the results of each study. As the previous section concluded, the simple limit state for fatigue design typically involves producing nominal stresses less than a critical fatigue stress vale. Thus the main focus of each subsection will be showing the maximum fatigue stress plotted over the particular parametric geometry variable, as well as the baseplate displacement. This simple presentation will allow for comparison of maximum fatigue stress reduction between the four variables and be the basis for the discussion in Section 5.3.

Section 5.2.1: Baseplate Thickness

The first parametric baseplate geometry variable to be discussed is baseplate thickness, which has been discussed in the results of the previous experimental and finite element studies. The previous discussion has already concluded that baseplate thickness is a strong contributor to the structure's overall baseplate flexibility, and thus drastically raises fatigue stresses at the weld toe. The results of this particular parametric study, which may seem repetitive, are very significant and necessary as they provide a means to compare the baseplate thickness related flexibility influenced behavior that has been studied experimentally and analytically to the three remaining parametric geometry studies. The trends in stress behavior of the three remaining parametric studies are assumed to behave similarly to the thickness study. For this reason it is beneficial to examine the stress behavior a little bit more thoroughly than the following individual parametric studies.

Figure 5.2.1.1 shows the relationship between baseplate thickness and baseplate deflection. The analytical and experimental data again corresponds to the standard static cantilever end load test of 100 pounds. Note the deflection of the baseplate is measured on the compression side of the pole or the downlift side of the baseplate. The point, where both the finite element and experimental baseplate deflections were taken, is located on the mast-arm axis, approximately one inch away from the edge of the baseplate. In future studies of different baseplate geometries, baseplate deflection is taken at the same point, on the mast-arm axis, though at a consistent distance away from the line between the center of the

compression anchor rods. Note the relationship that exists between baseplate deflection and increasing baseplate thickness is not linear. Approximately at a 3" thick baseplate, increasing baseplate thickness provides very little decrease in baseplate deflection, as the deflection becomes nearly constant. Also note that the experimental deflection results are shown. Again in comparison, it is seen that the finite element results for the thinner specimens (the ¾" and 1 ½" thick baseplate), over predict the stiffness of the baseplate, most likely due to the leveling nut fixity conditions. These leveling nut fixity conditions were hand tightened experimentally and thus produced a baseplate fixity resulting in a more flexible baseplate than in the analytical model.

As discussed in Section 5.1, the parametric study is concerned with the stresses at the fatigue critical location, the vertical weld toe of the upper fillet weld, which corresponds to a height of 0.559" above the baseplate. However for the sake of comparison to existing experimental data, stress results will also be presented, which were located at a height of 0.75" above the top of the baseplate. This vertical location corresponds to hotspot experimental stress data, which for the ¾" and 1 ½" thick specimen data was measured 0.75" above the weld toe. The 3" specimen hotspot data, to be shown in the next three plots was recorded at 0.875" above the baseplate. Another inconsistency between the experimental and analytical data, is that all three upper fillet weld profiles of the experimental test specimens were slightly different. Though these effects do influence stress behavior, the overall trend due to increasing baseplate thickness should roughly be

the same for the experimental and analytical data. Note that the non linear trend in deflection with baseplate thickness is similar to the deflection of a beam, which is proportional to the cube of the beam depth.

Figures 5.2.1.2 – 5.2.1.2.4 compare the results of the finite element parametric study with corresponding experimental data, located slightly above the weld toe. In Figure 5.2.1.2, the maximum outer stress 0.75" above the baseplate is plotted over increasing baseplate thickness. Since this position varies radially around the pole, no corresponding experimental data has been included. The plot shows that for very thin baseplates, the maximum stress can be nearly seven times larger than the nominal stress, calculated by simple beam theory. Again the relationship between stress and baseplate thickness varies non-linearly. At a baseplate thickness of 2 ½" to 3", the trend in maximum stress becomes nearly constant. The stress amplification toward the very large baseplate thickness, representative of a perfectly fixed condition, is approximately 1.5. Thus due to stress concentration the stress measured is 50% greater than the nominal stress. Referring to Section 4.2.1, as shown in the radial diagram discussion, outer tubewall stress is typically quite constant from the 45 degree tensile radial position to the direct tension radial position. Thus the trends in the 45 degree radial location stress data, which does have corresponding experimental data should be very similar.

Figure 5.2.1.4 displays the trend in normalized stress at the 45 degree tensile radial location over increasing baseplate thickness. Note that the

corresponding experimental data, shows good agreement. The magnitudes of the normalized stress are very close to those presented in the Figure 5.2.1.2. However it is noted that the magnitudes particularly for the very thin and very thick baseplates are less than the maximum stress data presented in Figure 5.2.1.2. This is because the shape of the radial stress profile changes with increasing baseplate thickness. As discussed in Section 4.2.1, the location of maximum stress changes with increasing baseplate stiffness (thickness). Thus for thinner baseplates as shown in the two plots, the 45 degree radial location data, is slightly less than the maximum data, which occurs a small distance away radially. For the thicker baseplates shown in the plots, the radial distribution of stress begins to behave more like simple beam theory and hence, the maximum stress does begin to occur at or close to the distance furthest away from the neutral axis. Thus the 45 degree normalized stress data is less than the maximum normalized stress data, which occurs at or near the direct tension radial location. This concept of changing locations of maximum stress is also evident in the behavior of the normalized stress above the weld toe at the direct tension location. Note there is very little decrease in stress. This occurs due to the fact that for thinner baseplates, the outer stress is very small at the direct tension location, as it is located in the dip in outer stress, shown in radial stress distribution diagrams in Section 4.2.1. for the thicker baseplate shown in the plot, the direct tension radial location is the maximum outer stress, though stresses at the thicker baseplate specimens are much less due to the reduction in bending deformation of the stiffer baseplate.

Figures 5.2.1.5 - 5.2.1.7 show identical plots to those just discussed. The new plots show the trends in the various normalized stresses over increasing baseplate thickness, however at a different vertical location on the tubewall. As discussed and justified in Section 5.1, the vertical location the parametric study is concerned with is directly at the weld toe. The trends in normalized stress at the weld toe are exactly the same as those discussed previously which were just above the weld toe. Note that the corresponding behavior and magnitudes of the stress at the two different locations also adds justification for the selection of critical point in the parametric study. The similar behavior shows that as long as the geometry and location of stress data is consistent through out the parametric study analytical models, the relative behavior and trends with flexibility will be valid, and improvement in stress reduction can be represented by a ratio of two corresponding normalized stresses.

Section 5.2.2: Baseplate Side Length

The next aspect of baseplate geometry examined in the parametric study was baseplate side length. As shown in Figure 5.1.1, all pole and anchor rod geometry remained constant and a wide range of side lengths were examined. Thus an increase in baseplate side length corresponds to extra material to be deformed by the load. Increasing baseplate side length, while maintaining the poles outer diameter thus increases the width between the outer edge of the pole and the edge of the baseplate. Baseplate side length is somewhat different to the previous

baseplate geometry variable discussed. Baseplate thickness is a geometry variable that really has no consequence to any of the other main baseplate geometry variables. Unlike thickness, the side length of a baseplate does have a practical limit, compared to the other aspects of baseplate geometry, especially the pole base diameter. From a design point of view baseplate side lengths are controlled by the pole base diameter as to provide a certain minimum length of material between the edge of the baseplate and the edge of the pole baseplate cut-out. This distance typically varies between different designers or manufacturers, but affects the stiffness of the baseplate in a manner similar to baseplate thickness, as will be discussed in Section 5.3.

Figures 5.2.2.1 – 5.2.2.4 present the same normalized stress and baseplate deflection data as discussed in Section 5.2.1, though now in terms of increasing baseplate side length. As would be expected overall the trends in deflection and stress are quite linear, with increasing baseplate side length, similar to the deflection of a beam. The deflection of beam is linearly proportional to the thickness of the beam. Over the range of baseplate side lengths provided (17" to 26"), a very small linear varying reduction in baseplate deflection occurs of slightly less than one milli-inch, which is corresponds to a 25% reduction in original deflection. In a manner different from the previous discussion on baseplate thickness, the stress at the direct tensile location actually increases, with increasing baseplate side length. This increase, as shown in Figure 5.2.2.3, is very minor and linear but is unexpected as with increasing baseplate thickness and hence baseplate

stiffness the stress at the direct tension location had decreased. Also unexpected is the fact that the maximum normalized maximum stress as shown in Figure 5.2.2, is reasonably non-linear with respects to increasing baseplate side length. A straight line is shown to illustrate this non-linearity. This non-linear trend with increasing side length goes against the idea of a simply supported beam approximation of the baseplate cross section as will be discussed. It is important to note that the non linearity of the trend occurs in the very wide baseplates, which is not representative of typical baseplate geometry. These non-typical geometries obviously have more complex stress behavior, as the increasing side lengths may begin to alter the typical stress distribution trends seen in the baseplate thickness study. In addition these wide baseplates, with the extreme baseplate side lengths do not have a large influence on reducing the maximum stress. The maximum normalized stress or stress amplification due to the extreme baseplate side length is 2.7 compared to 1.6 due to the extreme baseplate thickness.

Section 5.2.3: Anchor Rod Spacing

The third aspect of baseplate geometry examined in the parametric study was anchor rod spacing. As shown in Figure 5.1.1, all pole and baseplate geometry remained constant for all three of the different anchor rod configurations studied. When considering possible geometry alterations to the typical baseplate geometry, alterations to the anchor rod spacing is very limited, as well as very interrelated to the other aspects of baseplate geometry, as discussed in the previous subsection.

Anchor rod spacing can not be considerably reduced in most typical baseplate geometries as to allow adequate clearance with the pole for tightening the leveling nuts. Anchor rod spacing can only be increased if the baseplate's side lengths are wide enough. Typically, the pole would likely be larger also, which would dictate that the anchor rod spacing must be increased. In this study a 20" baseplate was examined, with a smaller pole base diameter which was typical for the 17" baseplate. This large baseplate allowed for 3 different anchor rod positions. This geometry used in the parametric study is not entirely realistic, though useful in giving insight to the influence of this parameter. Though the anchor rod spacing configurations studied provide more than an adequate or practical range of anchor rod spacings for the study, as anchor rod spacings are very limited.

Figure 5.2.3.1 plots baseplate deflection over increasing anchor rod spacing. As previously discussed baseplate deflection is taken along the mast-arm axis, at a consistent point located 0.41" away towards the edge of the baseplate and from the line from the center of the compression anchor rods. This point corresponds to the original experimental set up, which measured the baseplate deflection 1" from the edge of the baseplate, due to the pole geometry. The trend in baseplate deflection provides somewhat of unexpected results. As seen in the Figure, the baseplate deflection increases linearly with increasing anchor rod spacing. This linear trend is surprising at the trend was expected to exhibit a similar non-linear response to anchor rod spacing as was shown to occur due to baseplate thickness. In a simply supported or doubly fixed end beam the deflection is proportional to the span

length cubed. Thus it was believed that the response to increasing anchor rod spacing would produce much more drastic trends in baseplate deflection and stress.

The baseplate deflection is shown to be increased by less than 1 milli-inch over the range of spacings studied. Upon closer inspection it is seen that the trend in baseplate deflection is not completely linear, as the rate of increase in deflection per additional anchor rod spacing does increase very slightly with increasing anchor rod spacing. As shown in Figures 5.2.3.3, stresses at fatigue critical stress locations at the weld toe, at both the direct tension and the tension 45 radial locations increase with increasing anchor rod spacing. This is very expected as the baseplate becomes more flexible as the distance from the pole to the anchor rods increases, thus greater baseplate deformations occur at both locations which corresponds to increasing stresses.

Figure 5.2.3.2 displays the trend in the normalized maximum outer tubewall stress at the weld toe over increasing anchor rod spacing. Note that the trend is nearly perfectly linear with increasing anchor rod spacing. Also note that the over the plotted anchor rod spacing (from 14.19" to 17") the increase in maximum tubewall stress is only 0.49 times the nominal stress, or less than 0.9 ksi. This difference in maximum stress is much less than the difference in maximum stress due to the range of baseplate thicknesses observed, and is slightly greater than that for the baseplate side length study. As will be discussed later, it is somewhat unexpected that anchor rod spacing has such a gradual and linear effect on stress and baseplate displacement.

Section 5.2.4: Pole Tubular Thickness

The intent behind the study of tubewall thickness in the parametric study was intended to determine whether a thicker tubewall could reduce the amount of baseplate deformation and thus reduce the amplification of the tubewall stress relative to the corresponding nominal values. It is very critical to understand the concept behind the nominal stress design approach, as it relates to changing the nominal dimensions of the pole base. Using a thicker tubewall pole section in a design will always increase fatigue resistance, simply because the section is larger and nominal stresses are smaller. A more common situation occurs in fatigue testing and analysis, is a situation where two identical details with different nominal dimensions, receive the same nominal stress. Considering this situation, with pole socket connections, the pole with the larger nominal dimensions is applying more load to the baseplate and the welded connection, than the smaller nominal dimension pole specimen, with the same connection detail and baseplate geometry. The baseplate which is receiving more load does not have an appropriately scaled up baseplate, thus the deformations and flexibility behavior which is not considered in the nominal design approach, are greater in the specimen. Due to these larger deformations, stresses are also greater, and thus the fatigue resistance is decreased.

Figure 5.2.4.1 shows the relationship between baseplate deflection and increasing pole tubewall thickness. Note that the same 100 pound cantilever end loading is applied to all of the structures, regardless of the dimensions of the pole.

As would be expected with increasing pole tubewall thickness, the baseplate deflection increases. Figure 5.2.4.5 first shows the relationship between the maximum stress over increasing tubewall thickness. Note here the maximum stress is normalized in name only, instead all of the stress results for the different pole cross section geometries are normalized by one consistent nominal stress. Thus the plot shows the point just discussed, that for the same loading, stress decreases with increasing pole thickness. This in contrast to Figure 5.2.4.2, which plots the true normalized maximum outer stress at the weld toe over increasing baseplate thickness. Note here the stress results were normalized with their respective nominal stresses. This effectively applies the same exact nominal stress to every pole specimen, to allow for comparison. Thus the effects of increasing tubewall thickness can be thought of in two ways. First that with increasing tubewall thickness more load is applied to the baseplate. The second way to illustrate the effect of increasing tubewall thickness is that the baseplate becomes increasingly deficient to resist the deformation due to the increased loading of the stiffer pole. In both cases, the behavior is primarily controlled by the baseplate flexibility. Greater deformation and hence greater stress amplifications occur in the thicker tubewall specimens. thus this indicates the thicker tubewall has little to no effect in stiffening the baseplate, and only acts to apply more load to the baseplate, than a detail with smaller nominal pole dimensions.

Section 5.3: Fatigue Design Recommendations

The results of this study find baseplate flexibility to be very important to the behavior and design of welded socket connections used in cantilevered sign structures. Previous research on the subject, including fatigue testing which fatigue specifications are based, has limited understanding of the influence of baseplate flexibility. Through experimental and analytical study emphasizing behavior the influence of baseplate flexibility has been clearly shown.

The term fatigue performance, which appears in the study's title, relates to understanding the behavior such to be able to design welded socket connections to be more effective in resisting fatigue. Fatigue problems exist in cantilever signal support structures. These problems can partially be accounted for by the poor understanding of the influence of baseplate flexibility on the stress behavior in the tubewall, especially at fatigue sensitive locations, such as the vertical weld toe of the upper fillet weld. The solution to the problem is to incorporate flexibility into the specifications, with appropriate commentary such that designers can understand the importance of baseplate stiffness. Efficient, economic, and safe designs can not be made without considering baseplate flexibility.

In order to incorporate baseplate flexibility into the nominal stress fatigue design approach two possible methods were developed and will be discussed. These two methods follow the results of the parametric study. The results of the parametric study are believed to provide a good representation of baseplate flexibility induced behavior. However it is recommended that, the study is limited as it only examines one typical baseplate socket connection geometry. As will be

discussed in the next section, the previous parametric study would need to be greatly enlarged examining a wide range of typical geometries, including different weld profiles, pole, anchor rod, and baseplate dimensions. Again it is strongly felt that the trends in baseplate flexibility will be very similar for different geometries. The two possible approaches to incorporating baseplate flexibility into the fatigue design process will be discussed, using the limited though representative results of the parametric study. The analytical flexibility amplification ratio method will be discussed in Section 5.3.1 and the beam approximation flexibility amplification ratio method will be discussed in Section 5.3.2.

Section 5.3.1: Analytical Flexibility Amplification Ratio Method

A simple method to incorporate the effects of flexibility into the nominal stress approach to fatigue design is the flexibility amplification ratio method. This method provides a simple ratio which can be used to account for the increased fatigue resistance of "stiffer" baseplate geometry or the decreased fatigue resistance of "more flexible" baseplate geometry. (The following discussion will clarify this relative comparison of flexibility). This simple approach relies entirely on analytical results, similar to the parametric study discussed in Section 5.2. These analytical results would certainly need to examine additional baseplate and pole geometry, in order to provide an envelope of normalized nominal stress. These additional analytical results needed, should also include experimental load testing as necessary to establish the relevance of the finite element modeling. Once the

details of the flexibility amplification ratio method were finalized, fatigue testing could be performed to verify the method.

The major advantage of this method is its' simplicity. It is most convenient to consider only one aspect of baseplate geometry as a variable in baseplate flexibility. Thus the only logical choice for a baseplate geometry variable, is baseplate thickness. As shown in the parametric study in Section 5.2, baseplate thickness has the greatest influence on tubewall stress. There are many options as how to implement this method, but it would seem that the multiple options can be divided into two approaches. The first approach involves allowing designers to have the option of using many different baseplate thicknesses. This option would present the designers with wide range of normalized stress envelope data and a simple procedure to calculate flexibility amplification ratios. In addition this approach would make clear the concept and importance of flexibility in a way that the next approach might not. The second approach involves the creation of multiple categories or ranges of baseplate thickness and giving flexibility amplification ratios for each category of or range of baseplate thicknesses. This second approach is more of "black box" type approach, and may not as effectively emphasize the importance of baseplate flexibility to fatigue design. These two approaches to implementing the amplification ratio method, incorporating baseplate flexibility into the nominal stress approach to fatigue design will be discussed in the following discussion.

The first approach as mentioned, provides the designer the ability to select any baseplate thickness and determine a corresponding flexibility baseplate thicknesses. A plot similar to Figure 5.2.1.5, as discussed in Section 5.2 would be provided. This plot provided to the designer, would provide envelope values of normalized maximum outer tubewall stresses plotted over increasing baseplate thickness. These envelope values would represent the maximum stresses of various baseplate thicknesses, including the effects of all practical baseplate geometry, such as weld profile stress concentration effects, pole base diameter, pole tubewall thickness, baseplate side lengths , anchor rods spacing, etc. In addition as discussed in Sections 5.2.4 and 5.4.4, restraints on the tubewall thickness must be made, though current pole tubewall thicknesses used in industry appear to be sufficient to avoid problems related to baseplate flexibility as discussed. These envelope values of normalized stress are nothing more than representations of the maximum fatigue critical stresses as amplifications of the nominal stress.

Given these envelope values of normalized maximum stress as functions of increasing baseplate thickness, values corresponding to the design baseplate thickness must be compared with the envelope normalized maximum stress corresponding to the baseplate thickness which was used to derive the E' fatigue detail category. Unfortunately due to a lack of understanding of the baseplate flexibility issue and a shortage of available fatigue data on welded socket pole to baseplate connections this is somewhat of a grey area. In fact it is not unreasonable to consider the available fatigue data to be insufficient to provide a reasonable

fatigue resistance for just one specific baseplate thickness. As will be discussed in Sec 5.4.4 and 5.4.5, these design methods are also very valuable in the process of obtaining the necessary fatigue data library, by reducing the number of different tests performed on different geometries. However given the baseplate and endplate flexibility conditions of the research performed by Fisher (Fisher and Slutter, 1981), and the 1.5" thick endplate specimens tested with a "washer spacers" by Koenigs and the University of Texas (Koenigs, 2003), (Section 1.5), it is reasonable to associate the 1.5" thick baseplate with the Category E' fatigue detail, and a constant amplitude fatigue limit of 2.6 ksi. Thus in order to calculate the baseplate flexibility amplification ratio, the envelope normalized stresses of the design and fatigue test cases are compared and applied to the constant amplitude fatigue limit to give a modified fatigue stress range limit for design, as shown in Figure 5.3.1.1. The premise of the design calculations is that in the fatigue test a nominal stress was determined for which fatigue life was infinite. However due to baseplate flexibility the actual stress applied to the welded connection was not necessarily the same value as the constant amplitude fatigue limit. In fact this variation of the actual stress applied to the welded connection drastically varies with baseplate thickness as shown in Figure 5.2.1.5, to the degree that it must be included in order to produce effective economical fatigue designs. By setting the actual stress applied to the fatigue test and the design structure equal, the modified stress range for design SR_{DES} can be determined as a ratio of the envelope normalized maximum stress for the design structure N_{DES} and the fatigue test

structure N_{FT}. The stress range for design SR_{DES}, is nominally calculated and represents the limiting stress range accounting for the relative variation of baseplate flexibility. (Note notation does not refer to N as number of cycles).

$$N_{DES} * SR_{DES} = \sigma_{ACT\_DES} = \sigma_{ACT\_FT} = N_{FT} * CAFL \text{ , and thus}$$

$$SR_{DES} = (N_{FT} / N_{DES}) * CAFL$$

As simply illustrated in the example in Figure 5.3.1.1 all that a designer needs to do is rearrange these simple equations to produce the flexibility amplification ratio, in which to adjust the constant amplitude fatigue limit to accommodate the flexibility of the baseplate. As seen in the figure the thinner 1" thick baseplate requires that the designer select a pole section that will have a nominal stress less than 1.7 ksi, which is less than the constant amplitude fatigue limit given currently in the specifications. Using the thicker 2" baseplate increases the design stress range to 3.7 ksi which is greater than the current CAFL.

The second approach to incorporating the flexibility amplification ratio method is to simplify the first approach discussed above. The second approach transforms the first approach into a tabular format, such that it only examines a few different ranges of baseplate thickness. This method removes most of the participation of the designer and takes away some of the underlying information regarding the baseplate flexibility. A sample table which could be used to implement this second approach is shown in Figure 5.3.1.2. Note three ranges of baseplate thickness were selected, those greater than or equal to 1", those greater than or equal to 1.5" and those greater than or equal to 2.5". Note that the second

column in the Figure would not necessarily be provided to the engineer but is shown to document how the other values were determined. At each of these baseplate thickness cutoffs, the envelope value of normalized maximum stress would be determined, as was discussed previously. This value corresponds to the values plotted in Figure 5.2.1.5 as discussed above, and as an envelope value would represent the maximum due to other geometric variations as determined by further analytical results, as discussed previously. Using the simple equations relating the actual stress on the design structure and the actual stress on the fatigue specimen, the appropriate flexibility amplification ratio can be determined. Previously this ratio was described as (N_{FT} / N_{DES}). This flexibility amplification ratio is applied to the CAFL, to produce a modified fatigue limit stress range for design. This stress range for design represents the most conservative flexibility amplification ratio, for the baseplate thickness range. This method is also very simple and could be expanded to include more baseplate thickness ranges, as the most economic design will always be using the cutoff baseplate thickness value.

Section 5.3.2: Beam Approximation Flexibility Amplification Ratio Method

The results of the parametric study have already, (particularly the format used to present the normalized stress data) proved to be very useful in the implementation of the flexibility amplification ratio method, used to incorporate the effects of baseplate flexibility into the nominal stress fatigue design approach. The parametric results can also be manipulated slightly to suggest another plausible method to incorporate the effects of baseplate flexibility into the fatigue design

process. This particular method is based on a beam approximation approach, and provides a rational explanation of the flexibility based behavior. The primary concept behind this method is to correlate the flexibility of a beam in bending to the stress amplification in the tubewall due to baseplate flexibility. Thus the designer is provided a tangible analysis method, based on simple statics, rather than a list or plot of abstract values. In order to correlate the behavior of the baseplate to a beam section finite element analysis must be used. As discussed in Section 5.3.2, additional finite element analysis will be necessary to develop an envelope of the stress behavior, which examines the baseplate flexibility effect simultaneously with other baseplate geometries. The results of the parametric study discussed in Section 5.2, are a good base and likely very indicative of the influence of baseplate flexibility considering slightly different geometries. These results again will be the basis for the discussion of the beam approximation method. Note that the same concept utilizing a beam approximation, has been discussed in the literature review, with regards to research on baseplate design, authored by Hag-Elsafi, Alampalli, and Owens (1999).

Figure 5.3.2.1 illustrates schematically the main concept behind the beam approximation method of incorporating baseplate flexibility into the fatigue design process. Note that as shown in the top left of the figure, a baseplate can very much be thought of as four inter locking beams surrounding the base of the pole, connected at the four anchor rods. And thus without a great deal of imagination, the uplift and downlift sides can be thought of as either a simply supported beam or

a doubly fixed end beam. The fixity conditions of the assumed beam are obviously a combination of those two fixity cases. Additionally the loading of the assumed beam is likely to be a combination of evenly distributed and concentrated loading. The distribution of loading on the assumed beam very likely may be quite different depending on the flexibility of the baseplate, as can be inferred by reviewing the discussion of radial distribution of stress in Section 4.2.1. However the exact loading is not imperative, to the method. The assumed beam dimensions are shown in the figure. The depth, is represented by T, and is simply the thickness of the baseplate. The width of the beam approximation, noted as B is obtained by subtracting the base pole diameter from the baseplate side length and dividing by two. The span given by S, is calculated by subtracting the anchor rod spacing by the diameter of the leveling nut.

The maximum deflection at mid-span of this assumed beam is shown for the four different cases. Most notably the deflection for a simply supported beam is given by $(5/384)*(w*L/E)*(L^3/I)$. Note the w*L term is replaced by P, the concentrated load depending on the loading assumption. Thus the w*L term can really thought of to be a constant value, that does not change with increasing span length. (If the span length, L, is increased, the distributed load, w, will decrease.) As shown in the second page of Figure 5.3.2.1 a quantity termed the geometric flexibility can be determined. As shown in the figure displacement is force divided by stiffness and flexibility is the inverse of stiffness. As shown in the first page of Figure 5.3.2.1 the general form of the midspan deflection of the assumed beam is:

$\Delta = (12*S^3/B*T^3)*(1/E)*(\text{Loading Constant Fraction})*(w*L \text{ or } P)$

Removing unnecessary constants including the loading constant fraction and Young's modulus, E, the geometric flexibility can be defined as:

$s_{geom.} = 12\ S^3 / B*T^3$

Given simple beam behavior displacement should vary linearly with this parameter, with the slope being determined by the loading, the material constants, and the distribution of loading and fixity on the beam.

Figure 5.3.1 shows the results of the parametric study, plotting baseplate deflection over increasing geometric flexibility of the assumed beam (times 10^{-2} for plotting purposes only). The results of each individual parametric study examining baseplate thickness, side length, and anchor rod spacing are shown. The relationship is quite linear considering that the assumption of simple beam theory is not entirely expected. Note that by far the baseplate thickness covers a wider range of flexibility. This is not a result of poor planning of the parametric study, but indicative of the geometry itself. The other parameters especially anchor rod spacing can't reasonably or practically be increased to the same degree that baseplate thickness. Figure 5.3.3 shows the same plot, in a close up, over the small range of flexibility included in the baseplate side length and anchor rod spacing parametric studies. Note the good agreement and linear behavior in baseplate deflection between the three different parametric study. Figures 5.3.2 and 5.3.4 show corresponding plots of maximum normalized stress over increasing geometric flexibility of the beam approximation. Note again that there is good agreement

between the data. The baseplate side length somewhat diverges from the linear trends of the other two parametric studies. This may be expected as the large side lengths studied were very much out of the range of typical baseplate dimensions. Additionally in both Figures 5.3.2 and 5.3.1 a non linear trend begins to develop in the very flexible baseplate thickness specimen studied. This is very reasonable as the thickness was small enough such that the weld profile which was constant for all models, may have began to limit the linear increase in baseplate deflection, as its' stiffness began to make a larger percentage of contribution, to the overall stiffness of the structure.

As seen in Figures 5.3.1 and 5.3.2 the dominant trait influencing the geometric flexibility is the baseplate thickness. Thus in order to further simplify the approach of incorporating the baseplate flexibility into the fatigue design process, it may be more convenient to consider the stress relationship over the quantity $1 / T^3$, instead of the geometric flexibility which is, $12 S^3 / B*T^3$. Figures 5.3.6 similar to the previous four plots, show the trend in baseplate deflection, and normalized maximum stress over increasing values of $(1 / T^3)$. Note again that the behavior is mostly linear, again the outlier in which the major non-linear trend begins is due to the most flexible baseplate studied. Also note that the results of the non-thickness parametric studies, are mostly below the thickness plot. This is because increasing the baseplate side lengths only introduced increasing stiffness to the typical baseplate geometry. The study of anchor rod spacing used a 20" baseplate (compared to the 17" typical baseplate), which counteracted the

effects of increasing anchor rod spacing, which added flexibility to the geometry. The final model with the maximum anchor rod spacing was the most flexible, and thus is the only non-thickness geometry to shows up above the thickness parametric study plot.

The plots of normalized maximum stress with increasing geometric stiffness and inverse of baseplate thickness cubed, both are shown to be very linear, considering that the assumed beam sections in the baseplate are not really beams. And thus the behavior of the baseplate is more complex, though quite adequately captured by the assumption. Another key point is that the non linearity trend in stress begins at very flexible, thin baseplates. Over the realistic range of baseplate flexibilities and thicknesses the trend in maximum stress is very linear. A linear approximation can capture the stresses over this realistic range very well. In addition this linear approximation would force the designer to include the extra stress at the unrealistically flexible and thin baseplate geometries, thus compelling the designer to use a thicker or stiffer baseplate.

Figures 5.3.5 and 5.3.8 show the normalized maximum outer tubewall stress at the weld toe plotted over increasing geometric flexibility and the inverse baseplate thickness cubed. Note the good agreement between the linear approximation and the actual plotted values of the baseplate thickness parametric study. The baseplate thicknesses of the specimens of the parametric study are indicated to aid in understanding the flexibility of the structure. Note that good agreement with the linear approximation exists at the 1 ½" thick baseplate

specimen. With increasing baseplate flexibility and decreasing baseplate thickness less than the 1 ½" thick baseplate the linear approximation conservatively predicts the maximum stress.

As discussed in Section 5.3.1 additional finite element studies would be required to completely examine all of the different baseplate geometries. It is confidently felt that the parametric results, which only consider one single typical baseplate geometry, are indicative of the flexibility effect for all common baseplate geometries. Also discussed in the previous section was the concept of the flexibility amplification ratio method. The same procedure is used in the beam approximation flexibility amplification ratio method as discussed previously. The primary difference between the two method, is the procedure used to determine the N_{DES}, the normalized maximum tubewall stress at the weld toe, or the amplification the particular baseplate design geometry imparts over the nominally calculated stress range. In the beam approximation method, design stress amplifications can be calculated based on the geometric properties of the baseplate or the assumed beam section.

One simple design example is shown in both plots. Given the geometric properties of the baseplate, the normalized maximum stress, N_{DES}, for design can be calculated. Note both methods adequately predict this value. The N_{FT} , the amplification factor, which multiplied by the nominal fatigue stress range, would give the actual stress on the fatigue specimen, can either be determined with the beam approximation formula for NDES, or could be a constant value prescribed by

the specifications. Both of the beam approximation methods, using the geometric flexibility and the inverse of baseplate thickness cubed, provide an increased design stress range, SR_{DES} of 3.8 and 3.7 ksi. This design stress range would be the nominal calculated stress range that the designer would use to size the pole diameter.

5.4: Conclusions

The main result of the study, "Investigation of Influence of Baseplate Flexibility on the Fatigue Performance of Welded Socket Connection, in Cantilevered Signs Structures", has been defining the structural behavior and influence of baseplate flexibility in these connections. Prior to the beginning of this study the behavior of welded socket joints of cantilevered signs structures was marginally understood. Through an extensive experimental testing program, the validity of finite element modeling of the structure was studied and verified. Additional experimental tests were performed to examine different behavior relating to the baseplate flexibility and fatigue. Given the understanding of this behavior, and the verified finite element procedures a preliminary parametric study was conducted, using typical structure geometry. This study gives very representative results of the flexibility induced behavior though further analytical work is required to cover the wide range of possible baseplate geometry.

The results of this parametric study and the previous components of the study show very clearly that the baseplate flexibility must be considered in order to produce fatigue designs that are efficient, economic and safe. Based on the limited

but representative parametric study results two procedures to be used in conjunction with the existing nominal stress fatigue design approach are presented. These two procedures to be added to the nominal stress approach, adequately provide a consistent, simple, rational method to safely and economically design the baseplate and pole geometry, of the welded socket connections in cantilevered sign structures. These procedures have another considerable benefit in that they can be used to considerably reduce the magnitude of fatigue testing effort required to provide necessary updated sign structure fatigue testing data, as will be discussed further in Subsection 5.4.5.

Subsection 5.4.1 discusses the conclusions and summary of the flexibility induced structural behavior of socket welded cantilever sign structures. Subsection 5.4.2 discusses the results of some interesting additional experimental testing, which have some serious implications to fatigue design and testing. Subsection 5.4.3 discusses some general conclusions on the finite element modeling of these structures and some of the major issues determined influencing model calibration. Subsection 5.4.4 discusses the results of the parametric study and the proposed fatigue design methods to be added to the nominal stress fatigue design approach.

5.4.1: Structural Behavior Conclusions

- In summary of the structural behavior observed in local to welded socket connections in cantilevered sign structures, the nominal stress or simple beam theory predicted stress behavior does not occur in magnitude or distribution. Structural behavior was adequately discussed in Section 4.2.1. An experimental

testing program consisting of the static vertical load testing of three specimens each with different baseplate thicknesses, as well as an extensive analytical study was used to study the structural behavior. Fatigue cracking almost exclusively occurs at the vertical weld toe of the upper fillet weld in the pole tubewall (Fisher, 1981; Koenigs, 2003). Thus the study was primarily concerned with baseplate flexibility's influence on stresses in the tubewall adjacent to the baseplate. In general the behavior of the structure increasingly deviates from the nominal stress magnitudes and distribution with increasing baseplate flexibility.

- The vertical distribution of axial stress in the pole is characterized as distinctive peak and valley stress plot. This peak occurs at the weld toe and includes the inner, outer, and local bending tubewall stresses, and increases with increasing baseplate flexibility. For typically sized baseplates this maximum stress can be as much as four times the nominal stress depending on the baseplate flexibility. This maximum is also clearly shown to exist separately from the stress concentration effects of the connection. At the direct tensile or compressive locations, the outer and local bending stresses are of opposite sign expected, for example the outer stress at the traditional direct tensile side of the pole is compressive. In between the peak stress at the weld toe to the valley stress point, which is fairly consistently located 1 ½" above the weld toe a very linear vertical stress gradient exists. This linear stress gradient can be quite steep for flexible baseplates. The valley stress especially at 45 degree radial locations on the tubewall can represent a sign change in stress. Continuing upwards all stresses

begin to converge towards nominal stress magnitudes and distributions. At 45 degree radial locations stresses decrease in their convergence towards simple beam theory predicted values. But at the direct tensile and compressive radial locations, stresses increase in their convergence towards simple beam theory values. Convergence on the compressive side of the pole occurs at approximately 7-8" above the baseplate. Where as convergence is usually interrupted by the hand access hole induced behavior on the tension side of the pole.

- In addition to the vertical distribution of stress the radial distribution of axial stress does not behave accordingly to simple beam theory either. Maximum outer stress in the pole tubewall, especially in flexible baseplates occurs positioned in line with the anchor rods, or at the 45 degree radial positions. In flexible baseplates, the outer stress also considerably decreases at the direct tensile and compressive radial locations, where simple beam theory would predict the maximum stress. Local bending stresses rapidly increase from the neutral axis to the 45 degree radial locations, and then very gradually reaches a maximum at the direct tensile and compressive radial locations. Mid-plane stress is also at a maximum at the 45 degree radial locations, with the expected sign convention, compressive local to the compressive anchor rods, etc.

- There are two separate flexibility related parameters that simultaneously affect the structural behavior of welded socket connection behavior in cantilever sign structures. Both cumulatively make up the flexibility effect. The first and dominant is the local bending deformation effect, which alters tubewall stress

through local bending stress. This behavior is simply the result of local out of plane deformation of the tubewall and baseplate. Section 4.2.1 adequately describes and illustrates this behavior. The local bending behavior in the tubewall varies throughout the tubewall due to the different local baseplate flexibilities as result of being further away from the leveling nut imposed baseplate fixity. The second component is the mid-plane effect. This behavior involves the influence of flexibility on load path. As the baseplate at the direct tensile and compressive radial locations is considerably more flexible than that adjacent to the anchor rods, the axial load in the pole is diverted away from the direct locations and goes directly to tubewall locations near the anchor rods. This is indicated by the fact that the mid-plane stresses near the anchor rods have the correct sense of stress, compressive adjacent to the compressive anchor rods.

5.4.2: Additional Experimental Testing Conclusions

- Supplemental experimental testing was performed, in addition to the static vertical load testing which was a key part of the study. The static vertical load testing was primarily used to understand the structural behavior of the connection and to study and verify the finite element modeling used in the parametric study. These additional tests, though not the main focus of the study are also important. These tests involve the flexibility effect in less general way and look at more complex loading and constraint behavior. The results of these additional tests are strongly related to fatigue as well as the flexibility effect.

- Baseplate leveling imperfect induced loading was the first additional test discussed (See Section 4.2.2). The main reason to study this type of loading is that as experienced in the laboratory in the experimental set-up, it is difficult to perfectly level all the leveling nuts. Thus by tightening the leveling nuts it is very possible to lock in a tensile stress, into the tubewall adjacent to the weld toe. By performing a simple test, in which an enforced baseplate displacement or leveling perfection is introduced to the structure, the values of stress induced can be measured. A leveling imperfection measured at the center line of the anchor rod of 3/32" was enforced by a hand tightening leveling nuts as to lower and raise the baseplate. A simple finite element loading was used to simulate the experimental testing and good data agreement was obtained. It was noted that due to the loading of the very symmetric structure, the stress distribution exhibited may different types of symmetry. However due to the influence of local fixities of the leveling nuts, this symmetry was roughly observed, and the data was somewhat scattered. Through multiple testing at different locations, and the use of the symmetries a very good estimate of the tensile stress induced due to the loading were achieved. For example a 1 ½" baseplate was experimentally shown to experience an induced stress of 23 ksi due to an enforced baseplate leveling imperfection of 3/32".

- Though the study primarily focuses on the behavior in the pole to baseplate welded socket connection, much of the behavior and conclusions completely or partially apply to the mast-arm to endplate connection. Mast-arm experimental testing was performed without corresponding finite element study, and is discussed

in Section 4.2.3. The experimental results of statically loading the mast-arm with vertical load, as performed on the pole, showed very similar stress behavior adjacent to socket connection. In addition to the static load testing of the mast-arm under typical completely bolted conditions to the pole, experimental testing was performed under incomplete bolting conditions which are know to occur in the field. The first of these bolting conditions examined the difference in stress when the mast-arm was bolted using washers as spacers to prevent contact between the endplate and the flange-plate of the built up box of the pole. This is the same condition used in mast-arm fatigue testing. Experimentally the stresses measured just above the weld toe showed a greater than 10% increase with the washer spacers preventing contact. In addition the mast-arm was statically tested with non load carrying tension mast-arm bolt. Experimentally the maximum difference in tensile stress due to the absent bolt condition was observed to be a 60% increase in the normal bolted condition stress.

5.4.3: General Finite Element and Calibration Conclusions

- Using a combination of parabolic solid, shell, and beam elements, in a finely meshed model, which simplifies the complex leveling nut baseplate connection and the anchor rod concrete constraints, it is possible to fairly accurately model the behavior of cantilevered sign structures.

- Data agreement in general was very good, as multiply discussed in Section 4.1, 4.2.1, and Chapter 3. Some strain data measured at gage locations just off the weld toe would be classified as fair, with slightly poor strain data agreement at the

direct tensile and compressive radial locations, just above the weld toe. Though at the 45 degree radial locations, strain data was in good agreement, at the gage locations positioned just above the weld toe. Their seemed to be a slight problem in data agreement with the 3" thick baseplate specimen at the gage locations just above the weld toe at the direct tensile and compressive radial locations. The other strain data, at gage locations not directly above the weld toe was very good at all locations measuring inner stresses. The problems in data agreement are attributed to the very high strain gradient resulting in experimental error. In addition error in data agreement also is caused by simulating the hand tightened leveling nuts, with their different local fixities with a simple solid element model.

- Calibration study efforts showed that there wasn't a simple modeling solution to correct some of these minor problems in data agreement. Two trial solutions did show an ability to influence tubewall stress. The weld profile including the concavity of the weld metal was shown to influence stresses, as a stress concentration effect. Due to the mild variability in the weld profile, the approach taken was to model the weld profile as close to the most accurately measured values as possible. In addition the way that the leveling nuts were modeled seemed to be of concern, as several different option showed an ability to considerably alter tubewall stresses. More complex contact and pre-stress elements were not included in the finite element study. It is believed that these more complex elements, which would require estimates of initial gap, and prestress force, are not necessarily the solution to the data agreement problems.

5.4.4: Parametric Study and Design Conclusions

- The research has shown that baseplate flexibility has considerable implications to the fatigue design procedure of cantilevered sign structures, as discussed in Section 5.1-5.3. Unlike other fatigue details the magnitude of stress in socket welded baseplate and endplate connections in cantilevered sign structures are nearly influenced by one single geometric parameter, the baseplate flexibility. One primary assumption of the nominal stress design approach that the pole is considered fixed at the baseplate. Baseplate flexibility, especially when considering the practical limitations on the different aspects of baseplate geometry primarily is dependent on baseplate thickness. Stress at fatigue sensitive locations in the tubewall increases drastically with increasing baseplate flexibility. The trend is too great to not be considered in the fatigue design of cantilevered sign structures.

- Results of the parametric study show the major influence of baseplate flexibility is baseplate thickness, followed by anchor rod spacing, then the baseplate side lengths (which is primarily a measure of the width between the outer edge of the pole and the edge of the baseplate. The parametric study shows good linearly increasing trends between the maximum tubewall stress and 1) increasing geometric flexibility (which is quantified based on an assumed beam approximation as discussed) and 2) the inverse cube of the baseplate thickness cubed ($1/T^3$).

- These two trends can be used to establish two proposed methods to incorporate baseplate flexibility into the nominal stress approach to fatigue design. These two trends discussed in detail and illustrated by quick examples are termed the analytical flexibility amplification ratio method and the beam approximation flexibility amplification ratio method. Behind both add-ons to the nominal stress design method is a simple concept of equating the actual maximum stress experienced by the fatigue test and design detail. Normalizing the analytically determined maximum stress in the tubewall (normalized with the maximum nominal stress for that location), effectively represents the maximum stress by an amplification factor (N not to be confused with the number of cycles) times the nominally calculated stress. These values for N using direct analytically obtained plots of different baseplate geometries, or the linear relationships existing between maximum stress and geometric flexibility and ($1/T^3$), can allow a rational determination of maximum stress for any baseplate geometry. Thus the actual stress on a fatigue test specimen can be simplified as the amplification factor (N_{FT}) times the nominal stress range, which can be considered the CAFL. Similarly the actual stress on the design structure connection can be given as the product of the amplification factor (N_{DES}) and the design stress range (SR_{DES}). Thus equating these two products the nominally calculated stress range for design modified to accommodate differences in flexibility is simply the ratio the fatigue test amplification factor over the design amplification factor multiplied by the constant amplitude fatigue limit (of E' fatigue detail, 2.6 ksi). This proposed method is very

conservative and assumes infinite life. Another possible approach would be to consider finite life, in which the ratio applied to the CAFL would be cubed. Fatigue testing would be necessary to evaluate this less conservative approach.

- This indicates a very serious problem in fatigue test data, as no matter what method could be used to incorporate baseplate flexibility into the fatigue design process, reliable fatigue data that includes accurate and consistent baseplate flexibility conditions will be required. The next section discusses recommendations on future research. To summarize the future needs for fatigue research of socket welded connections in cantilevered sign structures, similar finite element and additional parametric study must be conducted to draft a specification incorporating baseplate flexibility, similar to those methods presented. Then a fatigue testing must be performed to confidently determine the fatigue resistance of a common baseplate geometry, to be used as a base reference, and more limited testing of more and less flexible baseplate specimens would need to be performed to verify the specification. Thus these new design methods also can be extremely valuable in reducing the amount of fatigue testing required.

- Stand-off length, the length between the top of the concrete foundation and the bottom of the leveling nut was shown both through experimental testing and analytical finite element modeling, to not be a factor in altering tubewall stresses.

- Tubewall thickness was shown to have no beneficial effect of stiffening the baseplate, and thus reducing tubewall stresses. Instead increasing tubewall thickness or base diameter increases the amount of load deforming the baseplate.

Thus in order to obtain the same fatigue resistance between two differently sized poles, the larger pole must have it's baseplate enlarged to resist the extra load of the larger pole.

- Anchor rod spacing was shown to have a minor and linear effect on tubewall stress and baseplate displacement, especially when compared to the same results for increasing baseplate thickness. Considering the beam mid span deflection both variables are proportionate to deflection by a cubic function, $1/T^3$ and L^3. Thus a greater and less linear trend between baseplate deflection and tubewall stress was expected for the anchor rod spacing, as was the case for baseplate thickness. Given the practical constraints in possible thicknesses and anchor rod spacing, it is important consider the numeric effect of these ranges. Aside from economic considerations, an increase in baseplate from 1.25" to 2.5" is very possible. Where for anchor rod spacing going from 17" to 14" spacing is a reasonable range. For the thickness and anchor rod spacing ranges the respective changes in dimension are 2 and 1.21. When these two factors are cubed this idea of a practical range really becomes apparent, as the thickness range is 8 times stiffer and the anchor rod spacing reduction is 1.8 times stiffer.

5.4.5: Future Experimentation Conclusions

- The results of the study, in particular the parametric study have some very strong implications to the fatigue design and testing of welded socket connections in cantilevered sign structures. Neglecting to consider the results and conclusions of this study, by not advancing the research, would be neglecting safety in some

existing flexible baseplate designs, and neglecting economy in stiffer baseplate designs. Currently no consistent approach addresses the design of the baseplate, the results of this study provides a basic outline of a simple procedure to design both the nominal dimensions of the pole and size the baseplate. Additionally since the endplate to mast-arm connection has been shown to be a less severe case due to the added endplate stiffness created by the contact pressure on the endplate, the results for the pole connection could easily be extended to the mast-arm connection given the appropriate attention. The simple design approaches which incorporate baseplate flexibility also have the benefit of providing a considerable reduction in required fatigue testing. The following recommendations for future study, follow in a rational order as to most effectively make use of limited resources for sign structure research.

- The first phase of recommended future research would focus on the finite element analysis performed, especially the parametric study as discussed in Section 5.1, 5.2, and 5.3. As discussed many times, the results of the parametric study represent well the trend in flexibility of only one standard baseplate base diameter and baseplate side length geometry. These results and trends with flexibility are indicative of the behavior of slightly different geometries, though they still need to be considered. Thus a fairly large task of expanding this parametric study to envelope the stress behavior of different typical baseplate geometries is needed.

- With this newly acquired envelope of stress behavior of increasing baseplate flexibility and thickness, the same procedures introduced previously to incorporate baseplate flexibility could then be used with this new stress envelope data. The two main methods discussed in Section 5.3.1 and 5.3.2 respectively are the analytical flexibility amplification ratio method and the beam approximation flexibility methods. The analytical method is very simple and relies entirely on finite element data, and can be broken down into a tabular form, effectively creating ranges of baseplate thickness with corresponding flexibility modified limiting fatigue stress ranges. At this time additional factors of safety could be adopted into the procedure chosen if deemed necessary. As shown in Section 5.3.1 and 5.3.2, this envelope data using either method would provide a relationship between baseplate geometry and the resulting amplification factor. Thus for any baseplate geometry the finite element base guidelines would be able to provide a amplification factor, either for design (N_{DES}) or fatigue testing (N_{FT}).

- The final phase of the recommended future research would be fatigue testing, and would have two separate objectives, which would be necessary to incorporate baseplate flexibility into the fatigue design process. The first objective would be to confidently define the constant amplitude fatigue limit of the "standard" baseplate geometry. A recommendation of the approximate baseplate geometry would be a 17" baseplate, with 1 ½" thickness and a 13" outer pole diameter, as it would seem that this may be similar to the geometry previously focused on by previous testing. Given this well defined standard the

flexibility amplification (N_{FT}) of the fatigue testing specimen can be determined by the baseplate geometry as shown in Section 5.3. Then given the possible new constant amplitude fatigue limit and the N_{FT} and N_{DES} the modified stress range for design could be determined as shown in Section 5.3. Using a limited amount of fatigue testing the newly drafted fatigue specification could then be verified. Thus a considerable amount of fatigue testing could be avoided. Without the use of finite element based analysis it would be very difficult to test all of the required numbers of different baseplate geometries, as in fatigue testing it necessary to duplicate tests on the same geometry.

Figure 5.1.1

Parametric Study Model Geometry Worksheet

1. Baseplate Thickness

	Baseplate Thickness [in]	Baseplate Side Length * [in]	Anchor Rod Spacing [in]	Tubewall Thickness [in]	Inner Base Diameter [in]
1	0.625	17	14.1875	0.23	6.32
2	1				
3	1.5				
4	2.25				
5	3.5				

2. Baseplae Side Length

	Baseplate Thickness [in]	Baseplate Side Length [in]	Anchor Rod Spacing [in]	Tubewall Thickness [in]	Inner Base Diameter [in]
1 *	1.5	17	14.1875	0.23	6.32
2**		17			
3**		18.5			
4**		20			
5**		22			

3. Anchor Rod Spacing

	Baseplate Thickness [in]	Baseplate Side Length ** [in]	Anchor Rod Spacing [in]	Tubewall Thickness [in]	Inner Base Diameter [in]
1	1.5	20	14.1875	0.23	6.32
2			15.25		
3			17		

4. Tubewall Thickness

	Baseplate Thickness [in]	Baseplate Side Length * [in]	Anchor Rod Spacing [in]	Tubewall Thickness*** [in]	Inner Base Diameter [in]	Tubewall Thickness **** [in]
1	1.5	17	14.1875	0.23	6.32	0.23
2				0.18		0.18
3				0.28		0.23
4				0.28		0.28
5				0.33		0.23

* Square Side Length. With 1"x1" Isoscoles Triangle Clipped Corners (unless noted otherwise)

** No clipped corner

*** Pole Tubewall thickness from 0 up to 11" above top of baseplate

**** Remaining Pole Tubewall Thickness of Pole

Chart 5.1.1 Continued on Next Page.

Figure 5.1.1 (Continued)

Parametric Study Model Geometry Worksheet (Continued)

All Models:

Material Properties

E [ksi]	29000

Global Geometry/Loading

Pole Height [in]	210
Mast-Arm Length [in]	526
Cantilever End Load [pound]	100

Pole Geometry

Pole Outer Base Diameter [in]	13.1
Taper [in/ft]	-0.1425

Anchor Rod

Diameter [in]	1.08
Stand-off Length [in]	1.625"
Restrained Length (with surface constraints applied) [in]	15

Leveling Nuts * * Complete circular leveling nut, no "partial" leveling nuts

Diameter [in]	2.16
Height	1.25

Socket Connection Geometry

Upper Fillet Weld Height [in]	0.56
Upper Fillet Weld Width [in]	0.42
Lower Fillet Weld	Included
Gap between Pole Baseplate Cutout and outer tubewall	Included

Hand Access Hole

Hand Access Hole **	Included

** See discussion of typical hand access hole geometry

Figure 5.2.1.1 * Weld Toe located 0.559" above top of baseplate (Y=0.559")

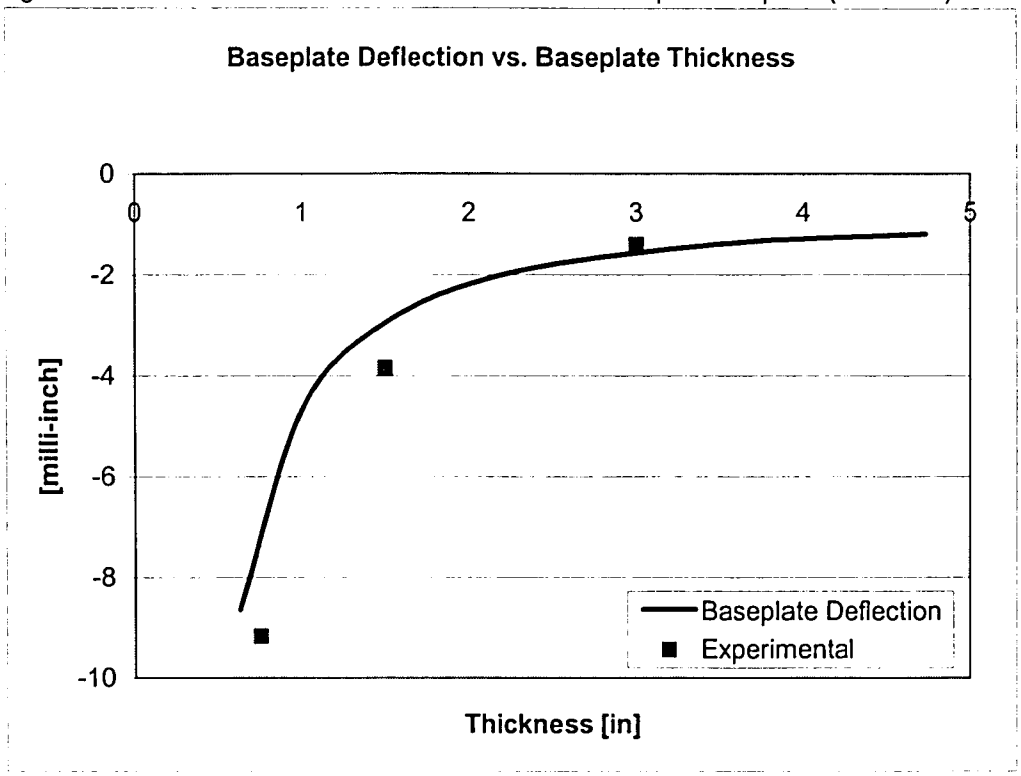

Figure 5.2.1.2 ** Stress Normalized with Maximum Nominal Stress (1.76 ksi)

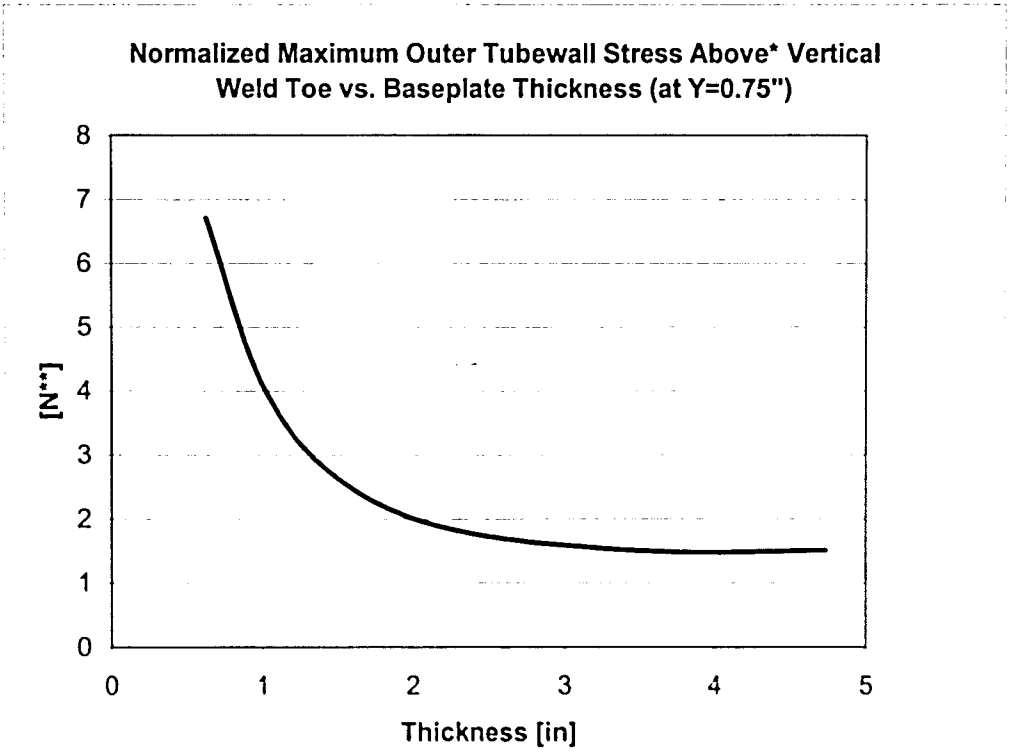

Figure 5.2.1.3 * Weld Toe located 0.559" above top of baseplate (Y=0.559")

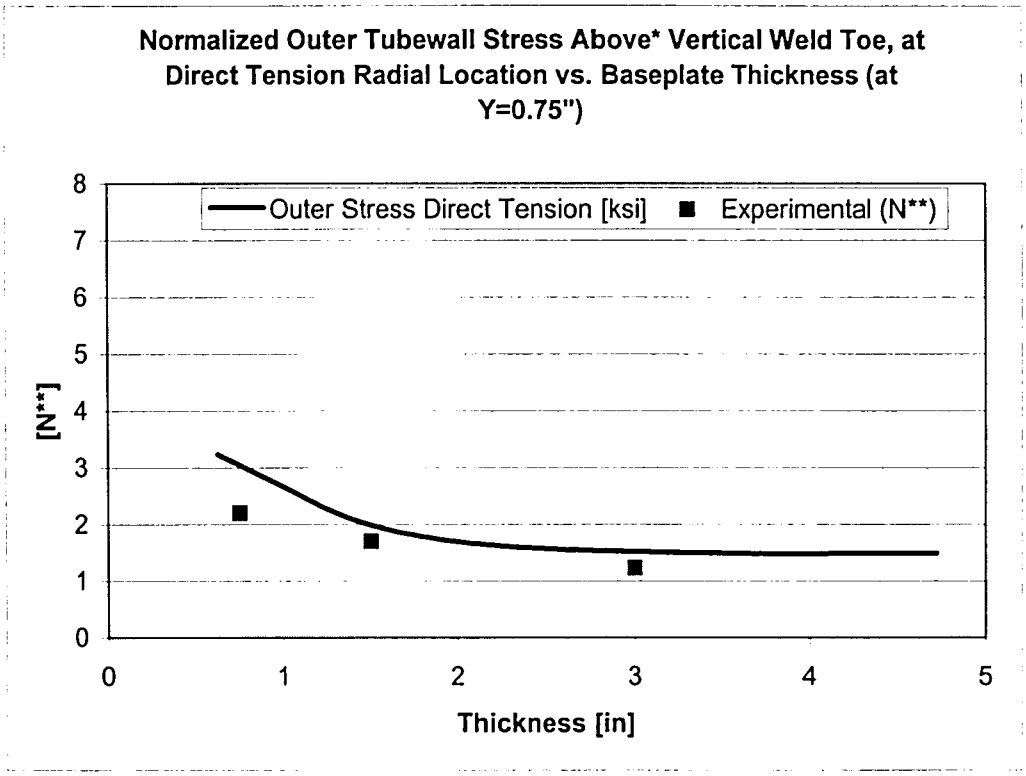

Figure 5.2.1.4 ** Stress Normalized with Maximum Nominal Stress (1.76 ksi)

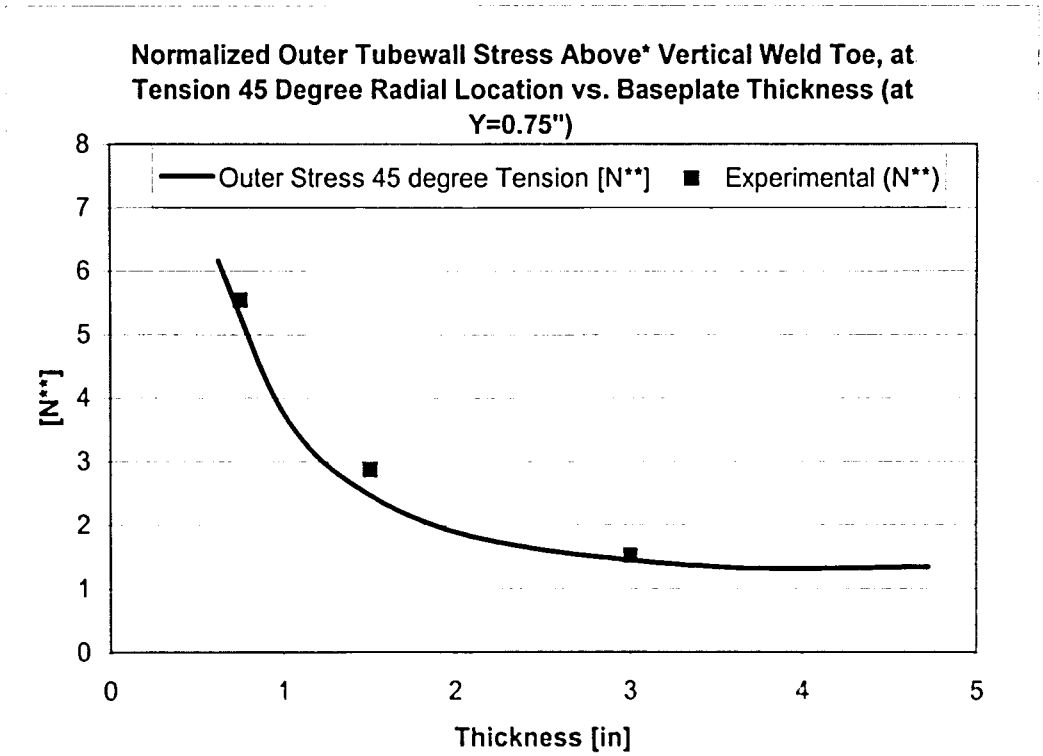

Figure 5.2.1.5 * Weld Toe located 0.559" above top of baseplate (Y=0.559")

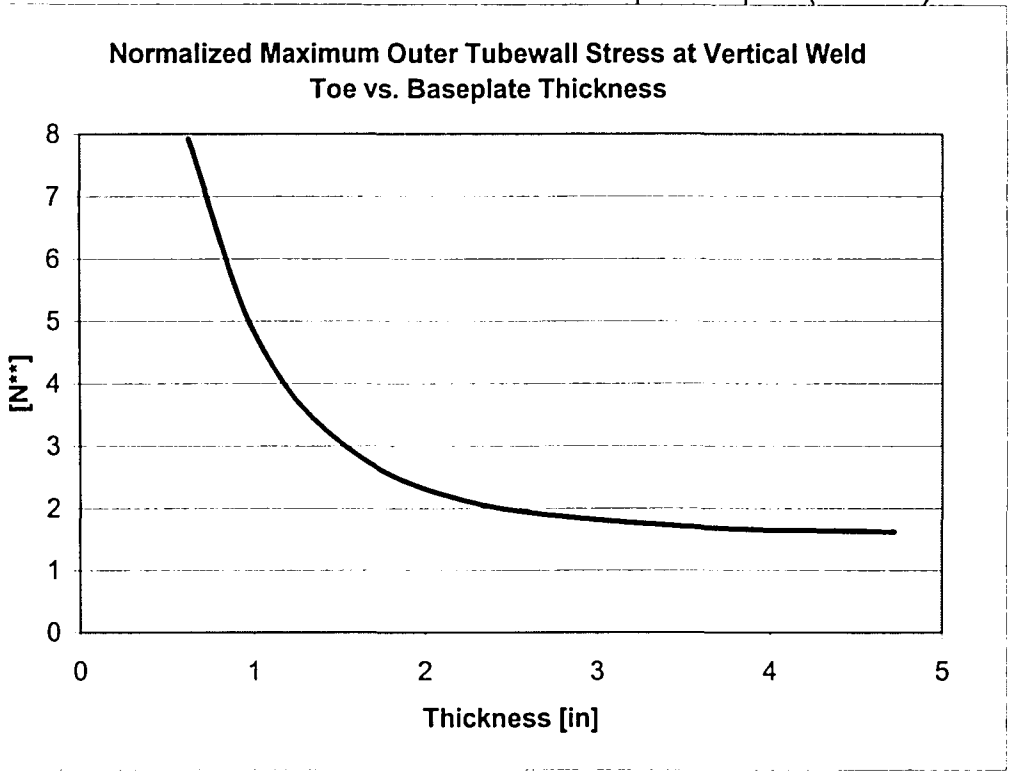

Figure 5.2.1.6 ** Stress Normalized with Maximum Nominal Stress (1.76 ksi)

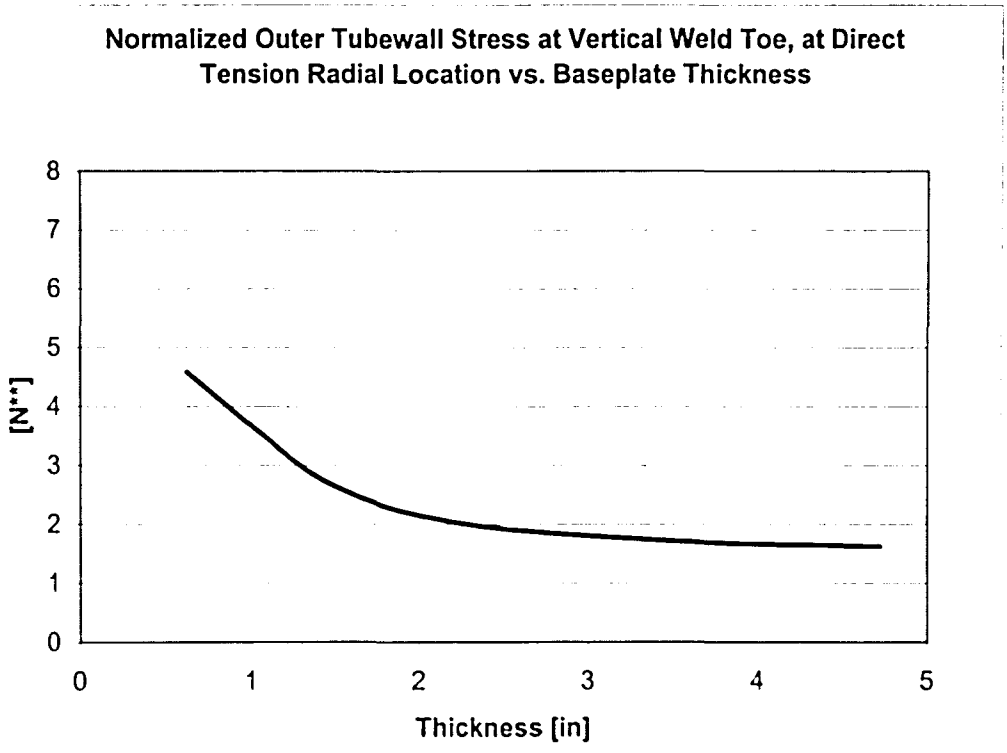

Figure 5.2.1.7 * Weld Toe located 0.559" above top of baseplate (Y=0.559")

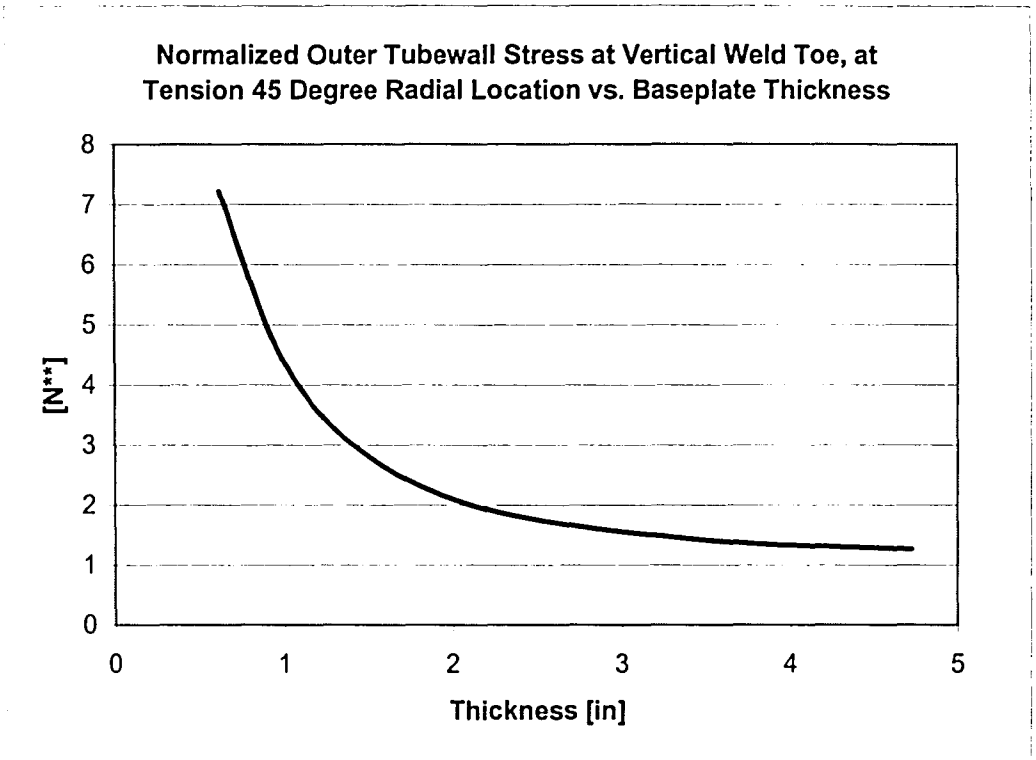

** Stress Normalized with Maximum Nominal Stress (1.76 ksi)

Figure 5.2.2.1 * Weld Toe located 0.559" above top of baseplate (Y=0.559")

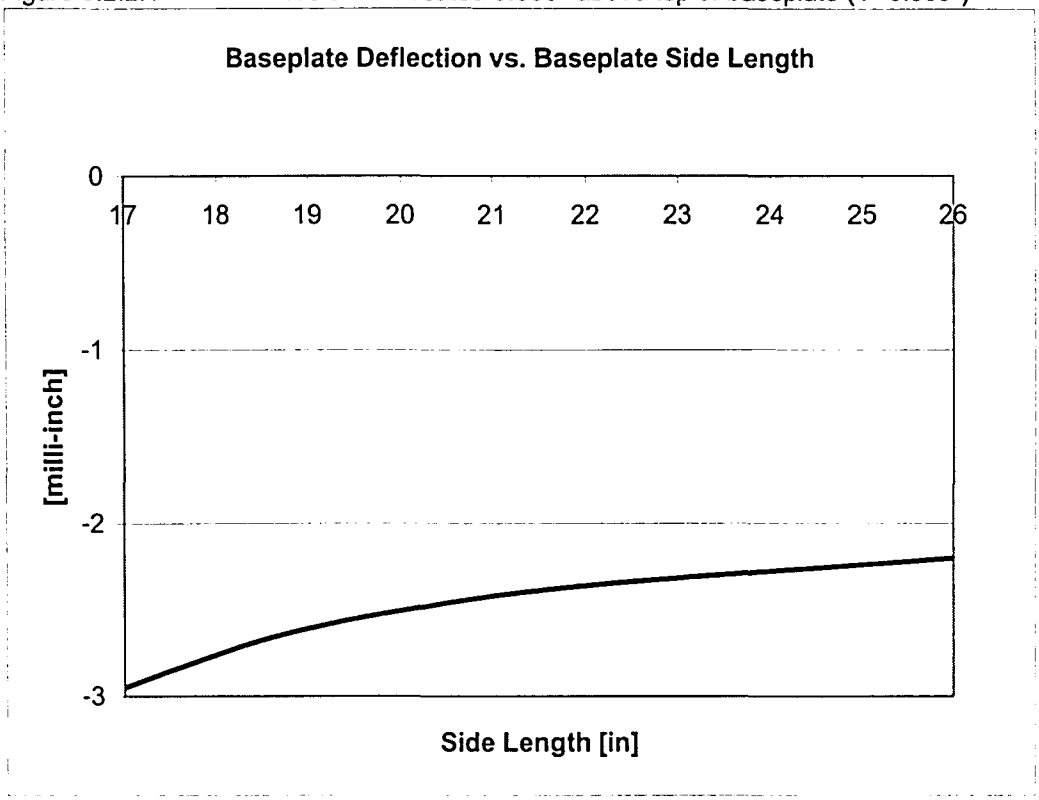

Figure 5.2.2.2 ** Stress Normalized with Maximum Nominal Stress (1.76 ksi)

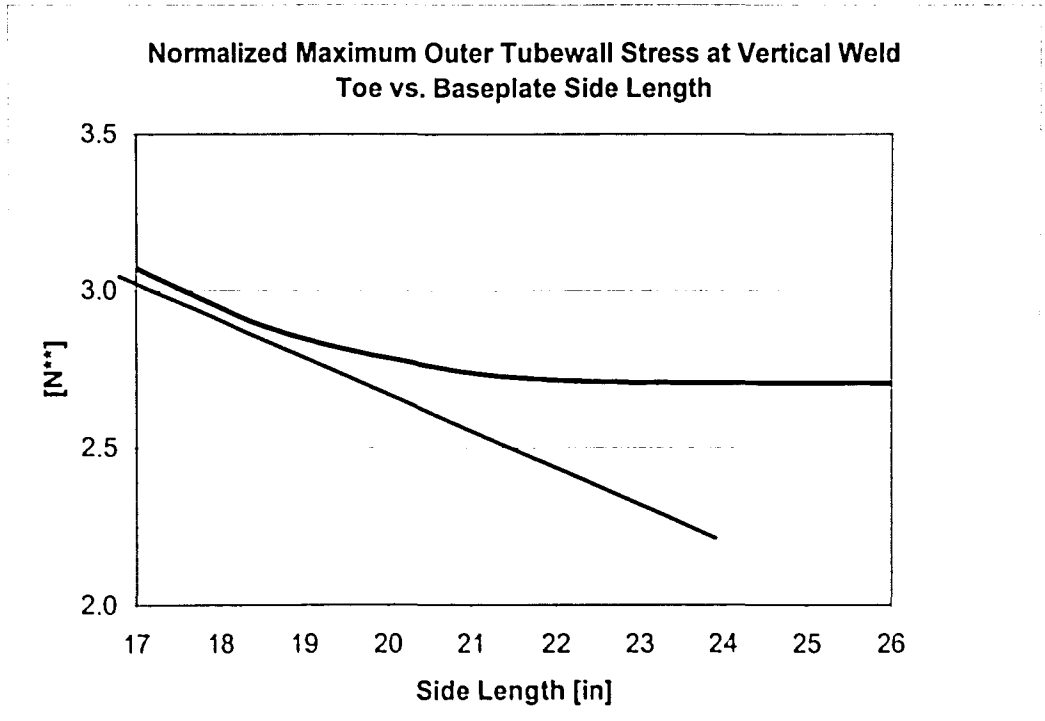

Figure 5.2.2.3 Weld Toe located 0.559" above top of baseplate (Y=0.559")

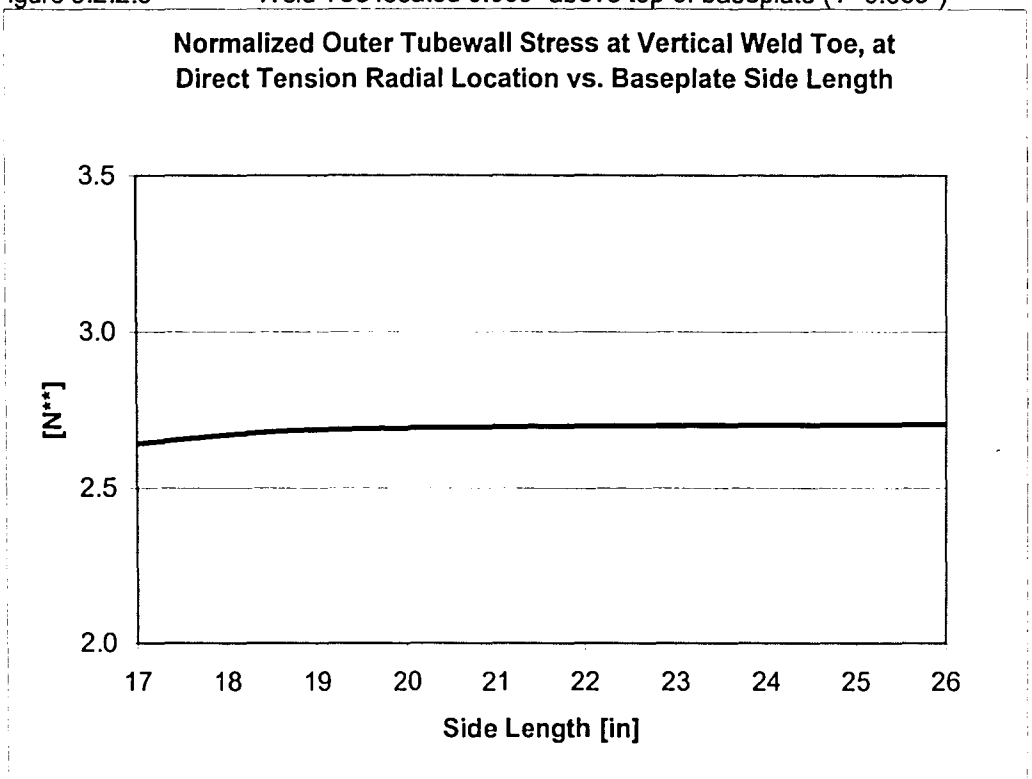

Figure 5.2.2.4 ** Stress Normalized with Maximum Nominal Stress (1.76 ksi)

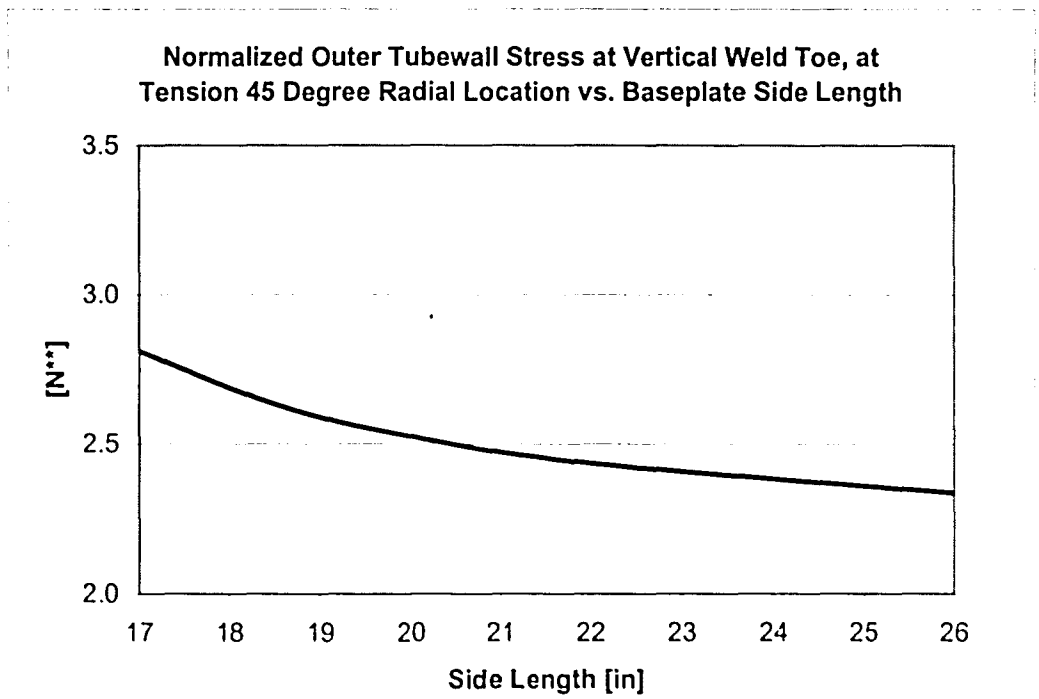

Figure 5.2.3.1 * Baseplate Deflection measured along mast-arm axis and at constant position relative Anchor Rod Center Line

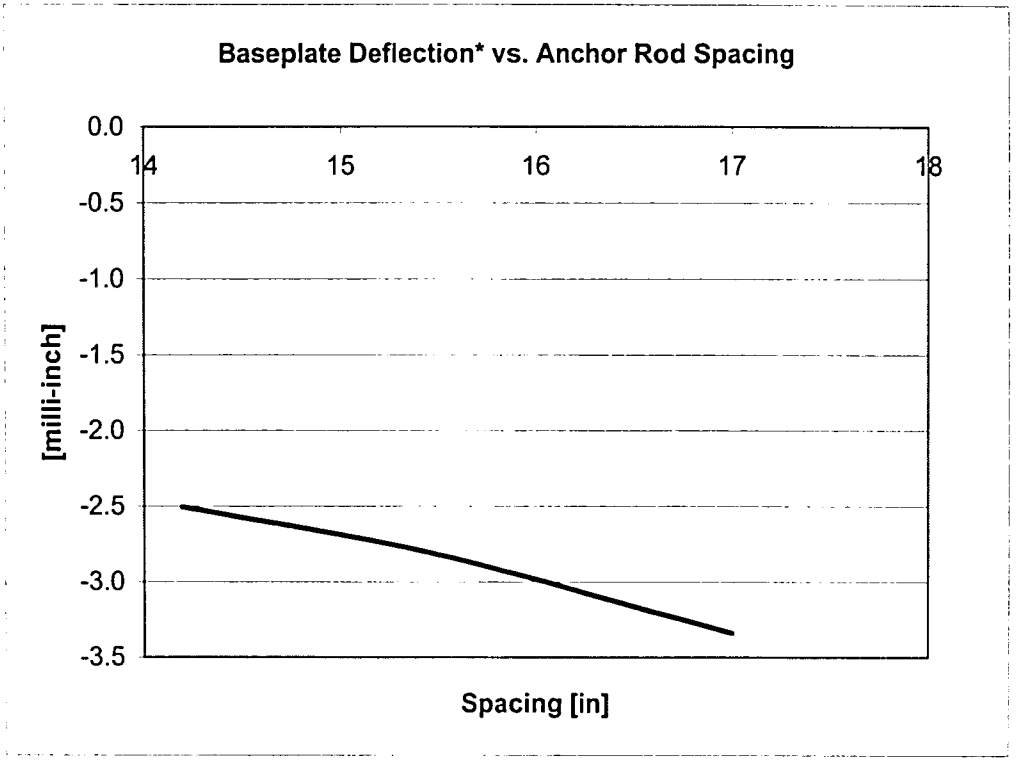

Figure 5.2.3.2 ** Stress Normalized with Maximum Nominal Stress (1.76 ksi)

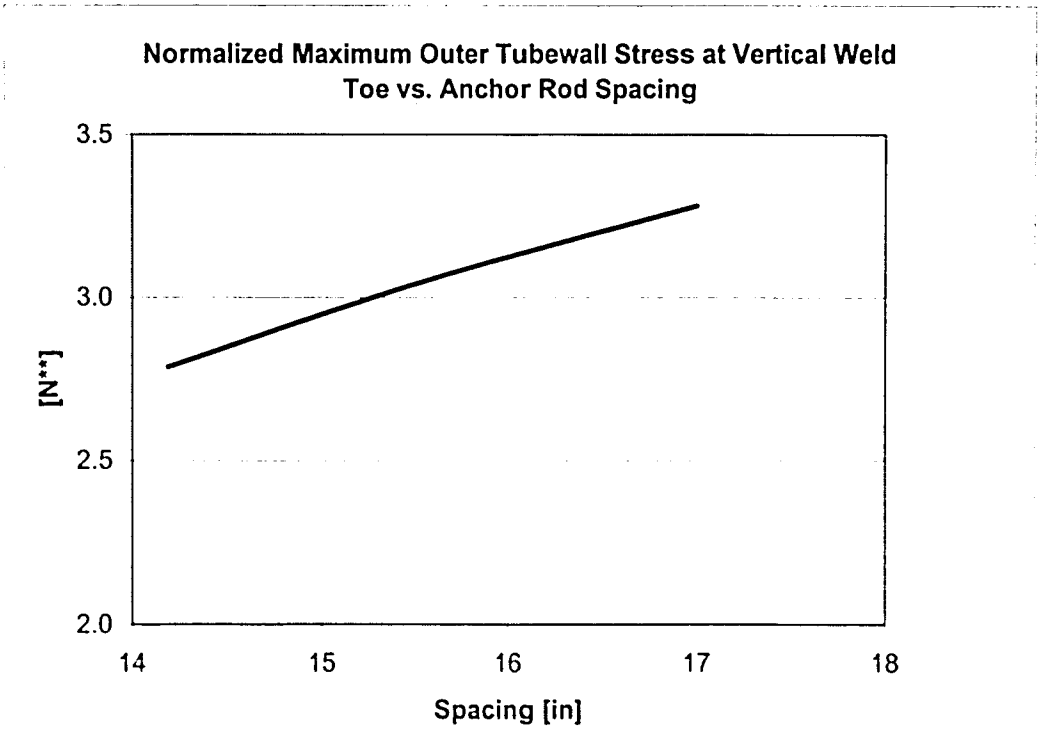

Figure 5.2.3.3 Weld Toe located 0.559" above top of baseplate (Y=0.559")

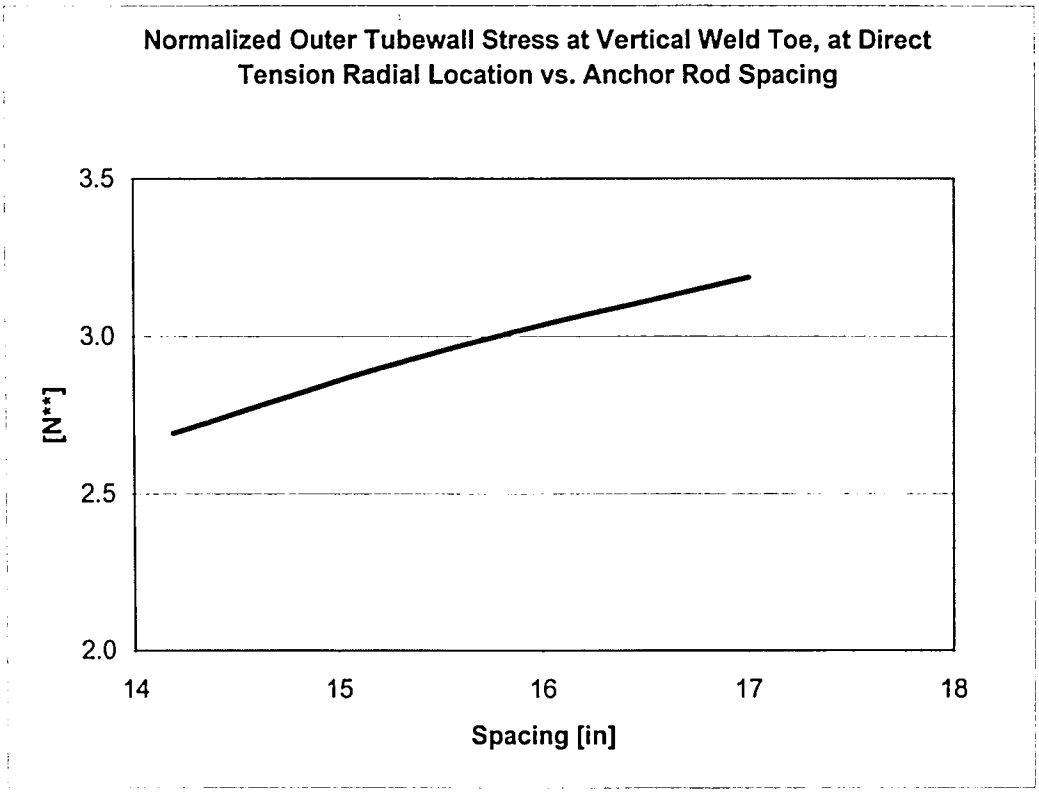

Figure 5.2.3.4 ** Stress Normalized with Maximum Nominal Stress (1.76 ksi)

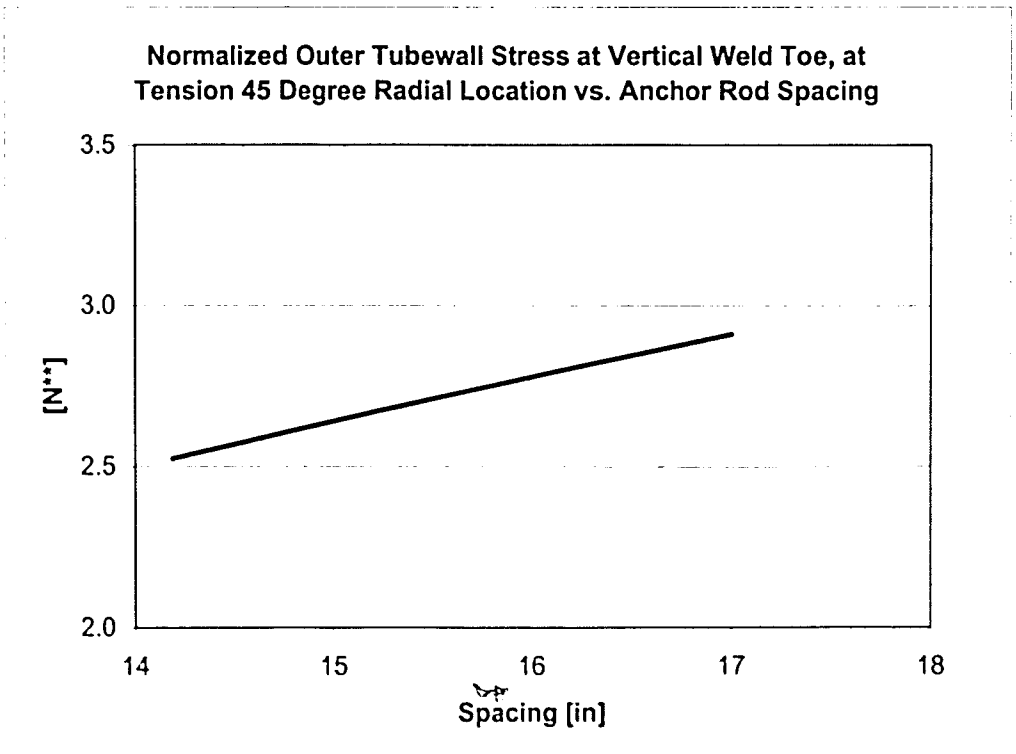

Figure 5.2.4.1 ** Stress Normalized with Maximum. Nominal Stress Values

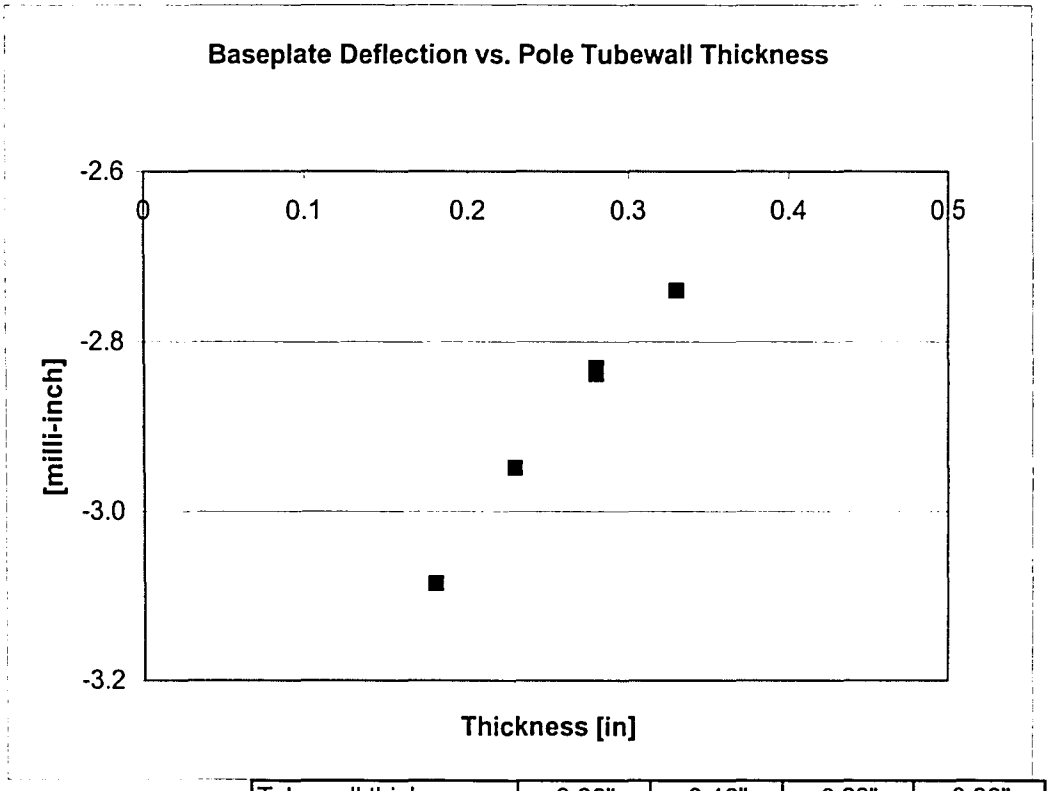

Figure 5.2.4.2

Tubewall thickness:	0.23"	0.18"	0.28"	0.33"
Max. nominal stress:	1.76 ksi	2.23 ksi	1.46 ksi	1.26 ksi

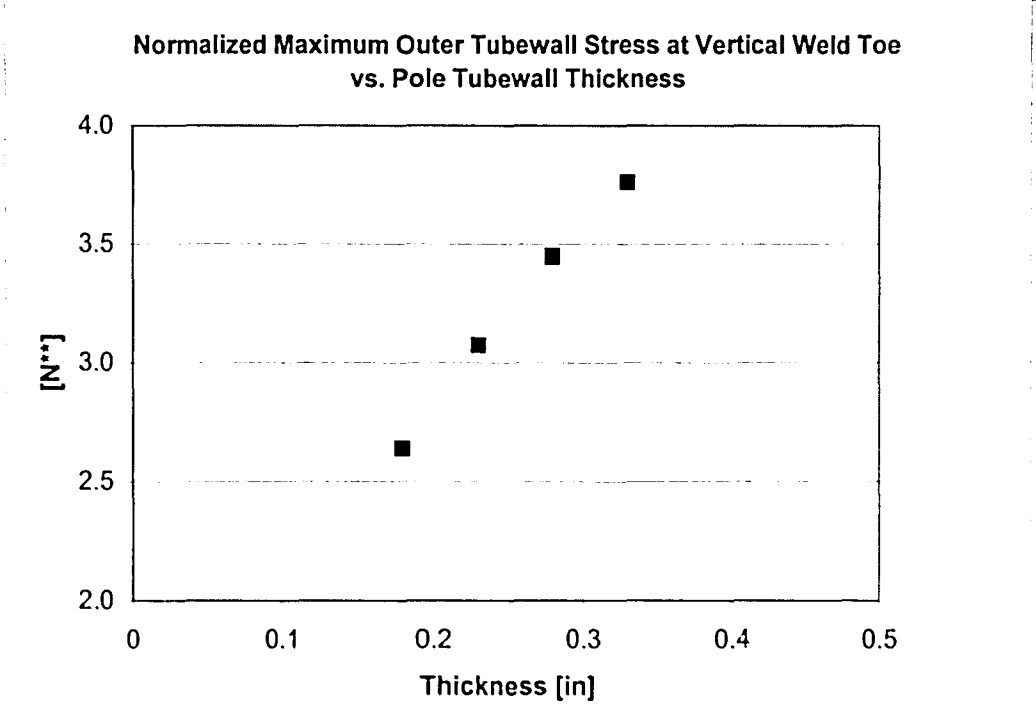

Figure 5.2.4.3 ** Stress Normalized with Maximum. Nominal Stress Values

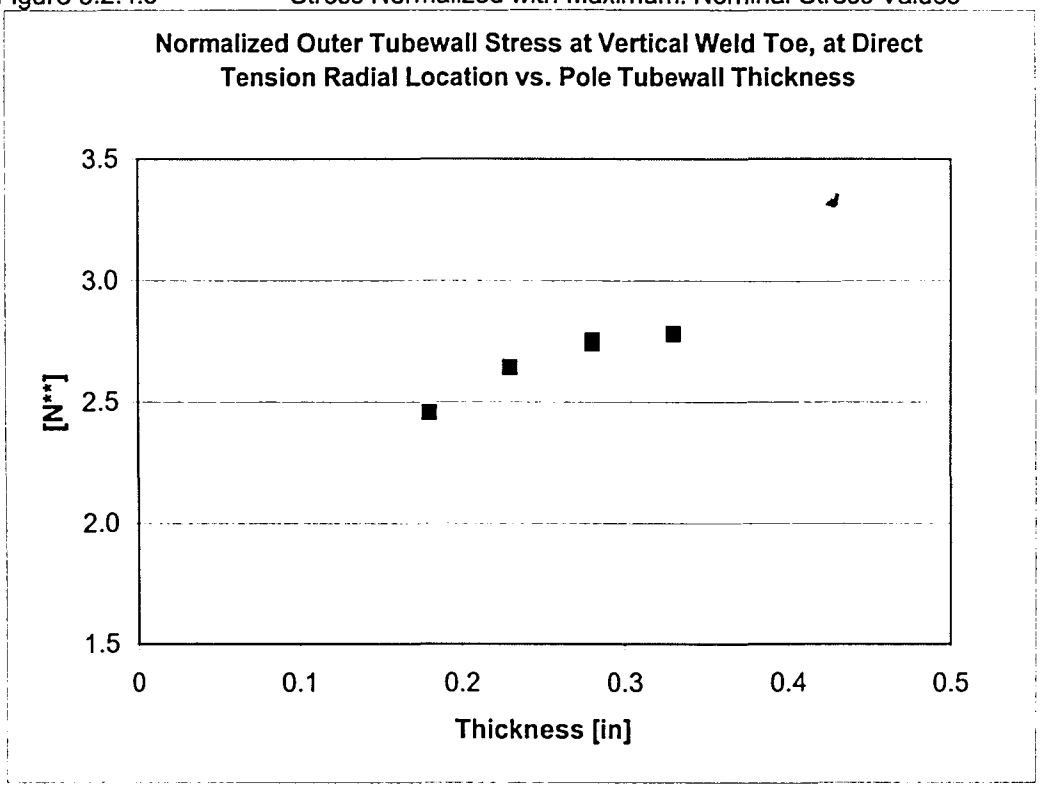

Tubewall thickness:	0.23"	0.18"	0.28"	0.33"
Max. nominal stress:	1.76 ksi	2.23 ksi	1.46 ksi	1.26 ksi

Figure 5.2.4.4

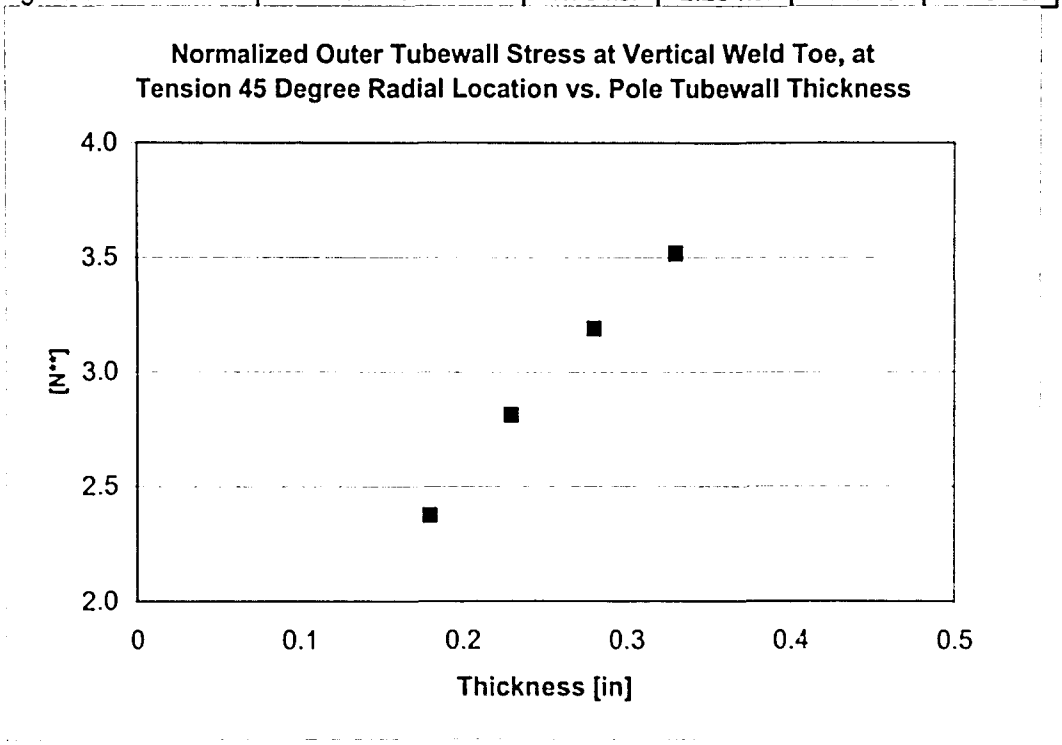

Figure 5.2.4.5

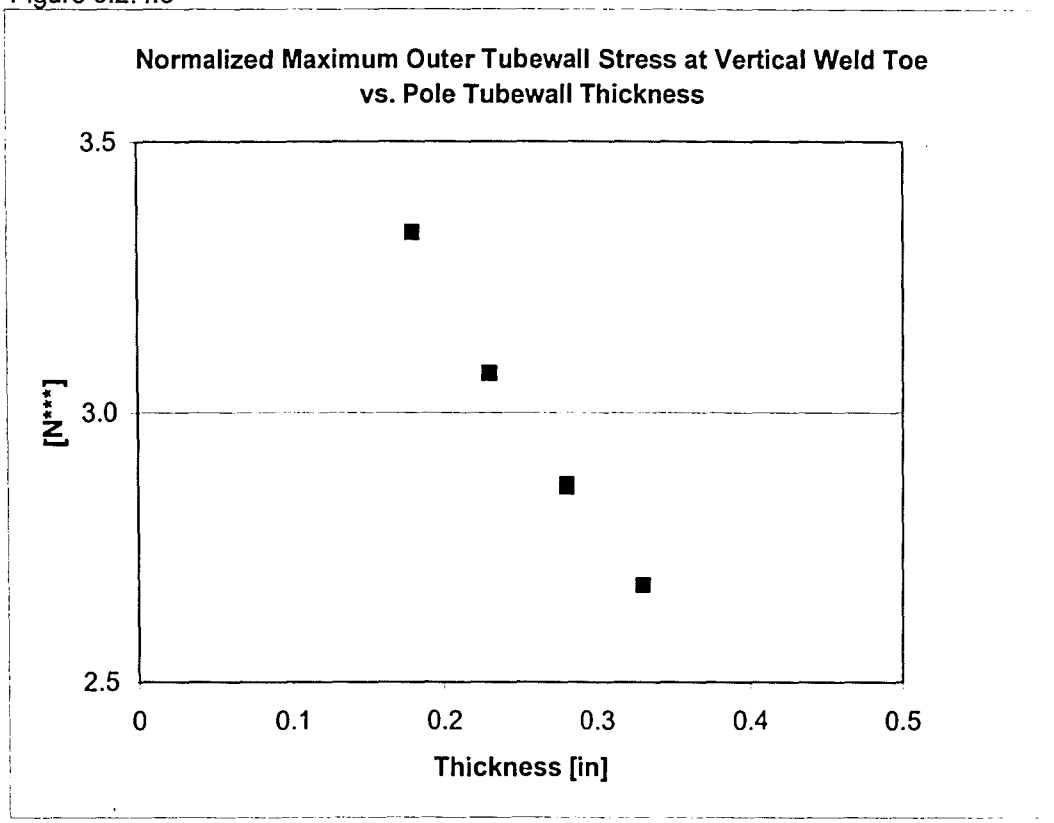

*** All stress normalized with consistent value, the nominal stress of the 0.23" thick tubewall specimen. (1.76 ksi)

Figure 5.3.1 * Flexibility refers to geometry of beam approximation, as explained

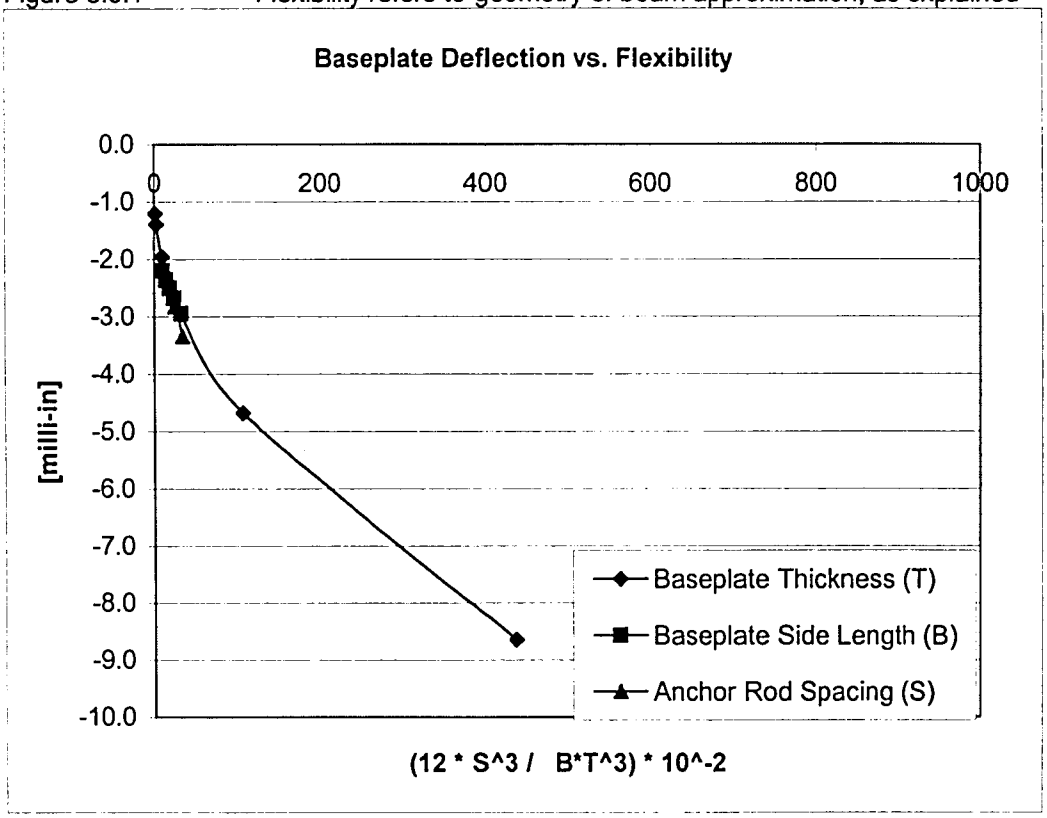

Figure 5.3.2 ** Stress Normalized with Maximum Nominal Stress (1.76 ksi)

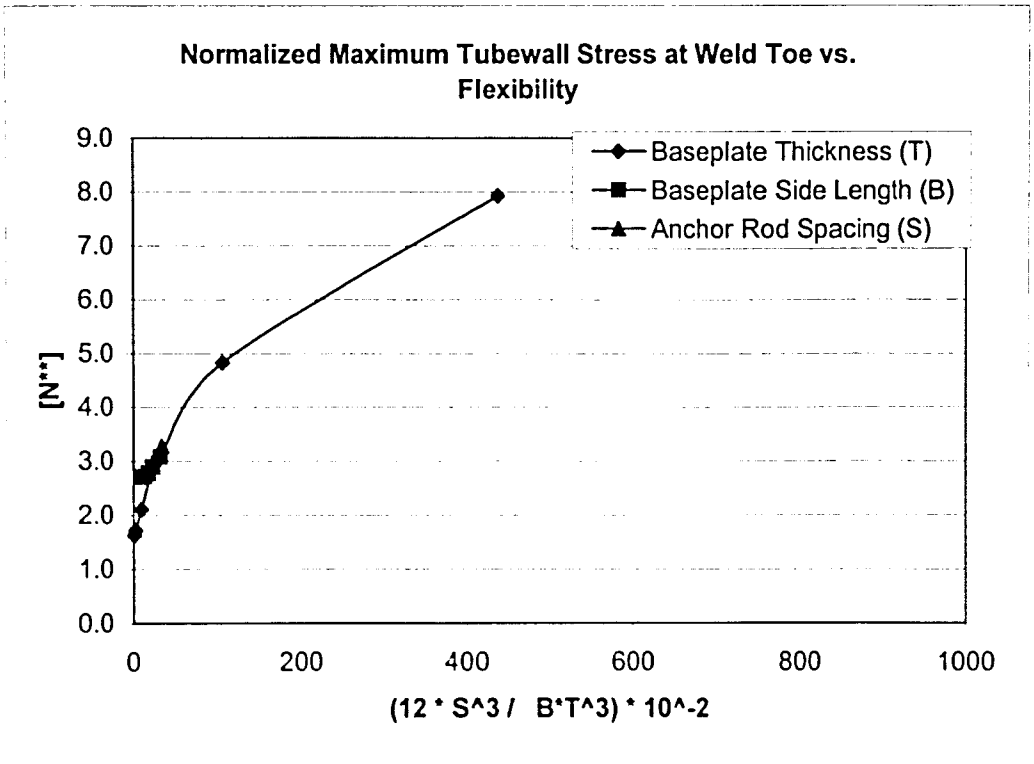

Figure 5.3.3 * Flexibility refers to geometry of beam approximation, as explained

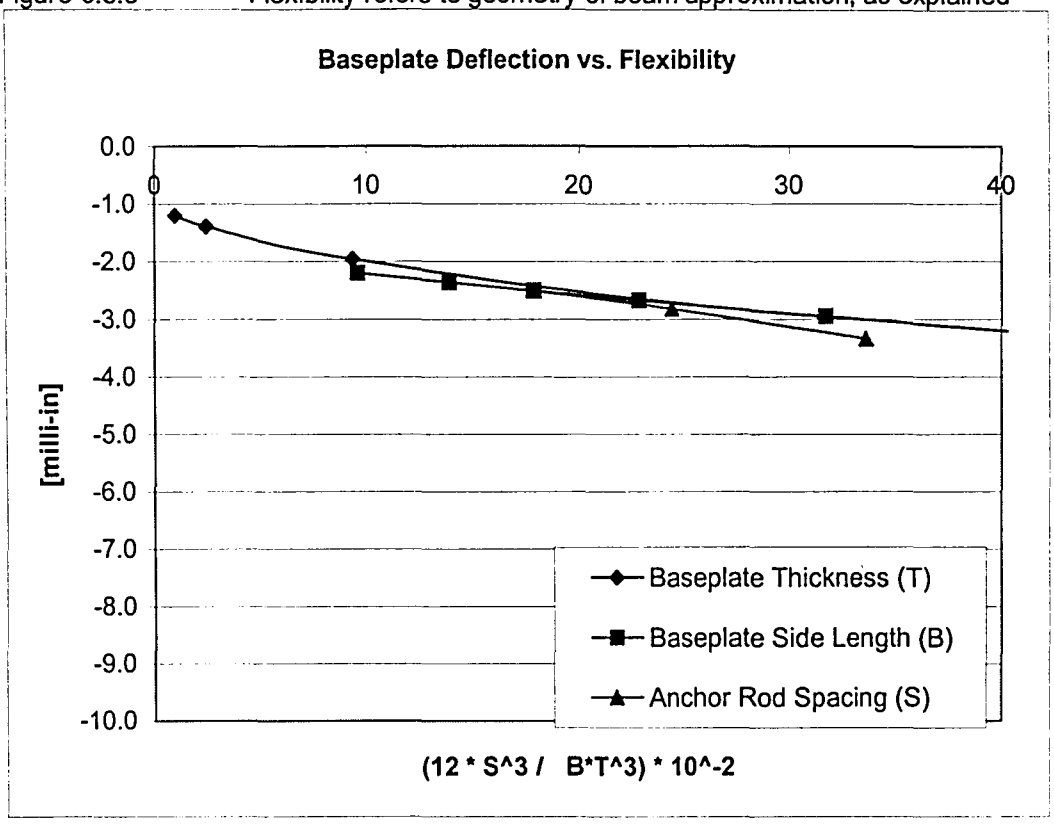

Figure 5.3.4 ** Stress Normalized with Maximum Nominal Stress (1.76 ksi)

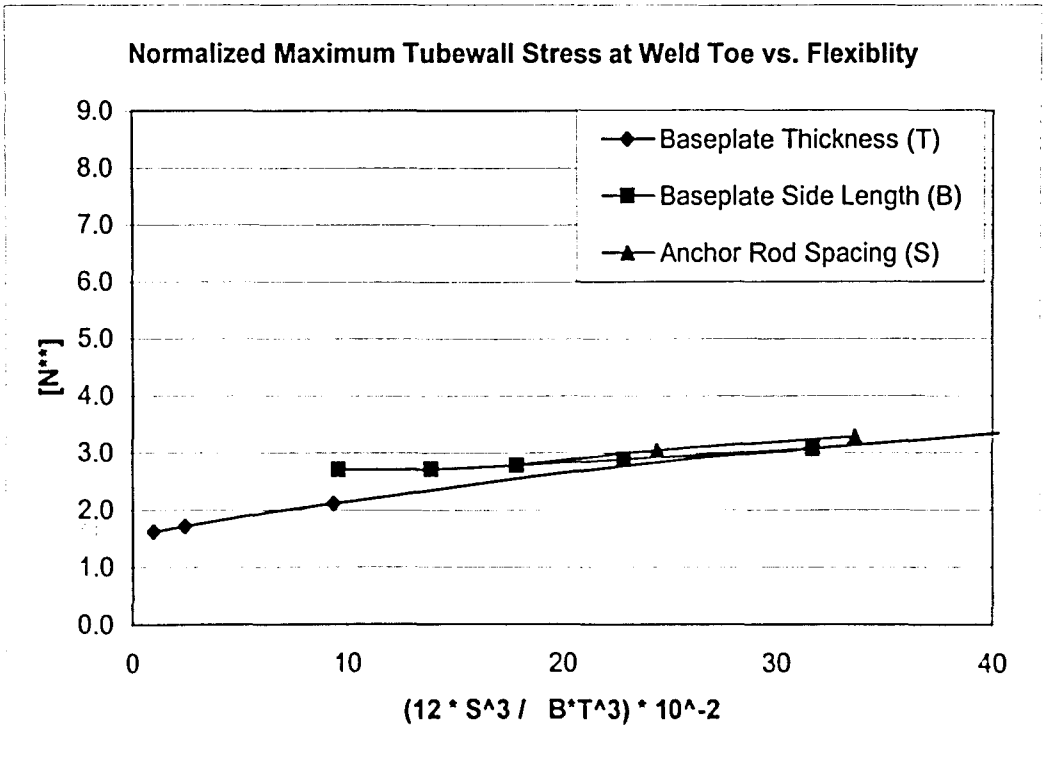

Figure 5.3.5 * Flexibility refers to geometry of beam approximation, as explained

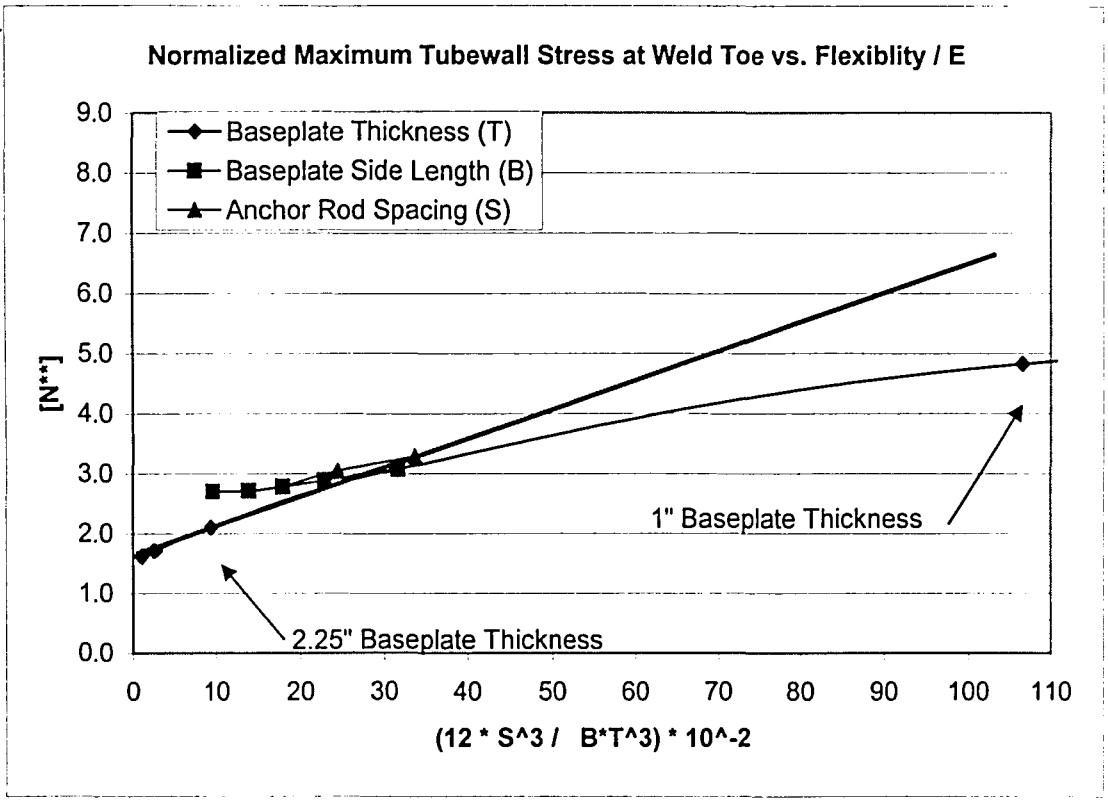

** Stress Normalized with Maximum Nominal Stress (1.76 ksi)

$$N_{DES} = 1.75 + 5.25/100 * (12 * S^3 / B*T^3)*(10^{-2})$$

Example Problem: What is the maximum fatigue stress due for a 16" baseplate with pole base diameter 12", baseplate thickness of 2.25", anchor rod spacing of 15" and leveling nut diameters of 2".

T = 2.25"
B = (16-12)/2 = 2" (12 * S3 / B*T3)*(10-2; 11.57
S = 15 - 2 = 13"

N_{DES} = 2.2

As discussed in Section 5.3.1

$SR_{DES} * N_{DES}$ = Actual Fatigue Testing Stress Applied = CAFL * N_{FT}

Thus given NFT = 3.1,

SR_{DES} = 3.1 * 2.6 ksi / 2.2 = 3.7 ksi

Figure 5.3.6

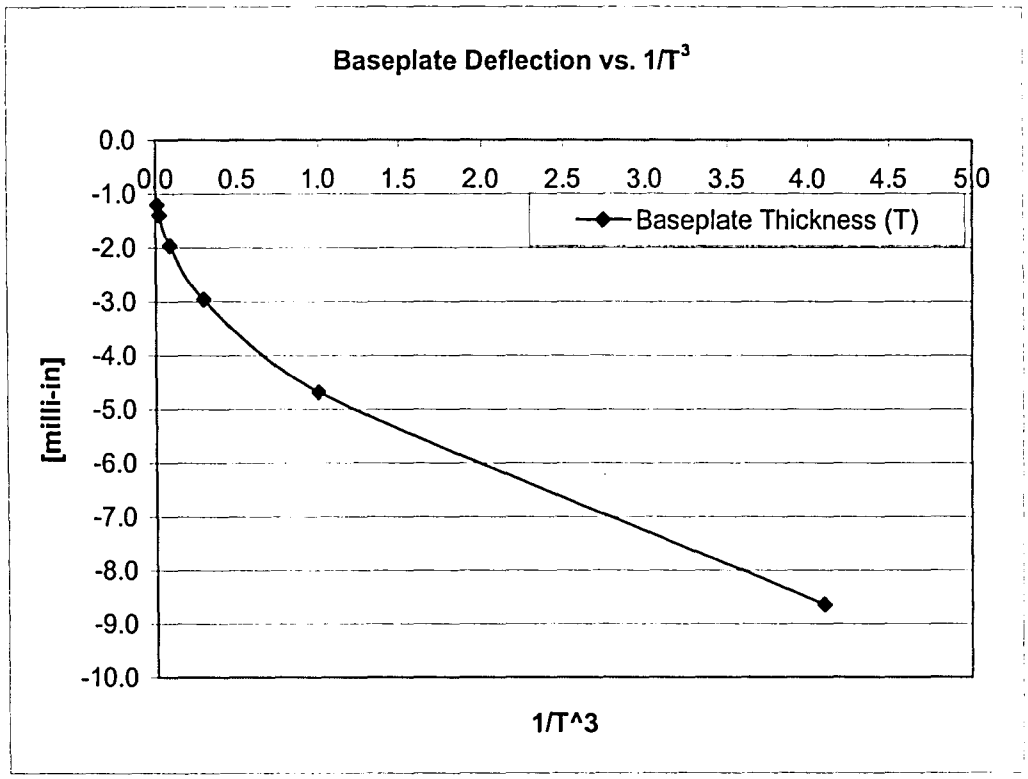

Figure 5.3.7 ** Stress Normalized with Maximum Nominal Stress (1.76 ksi)

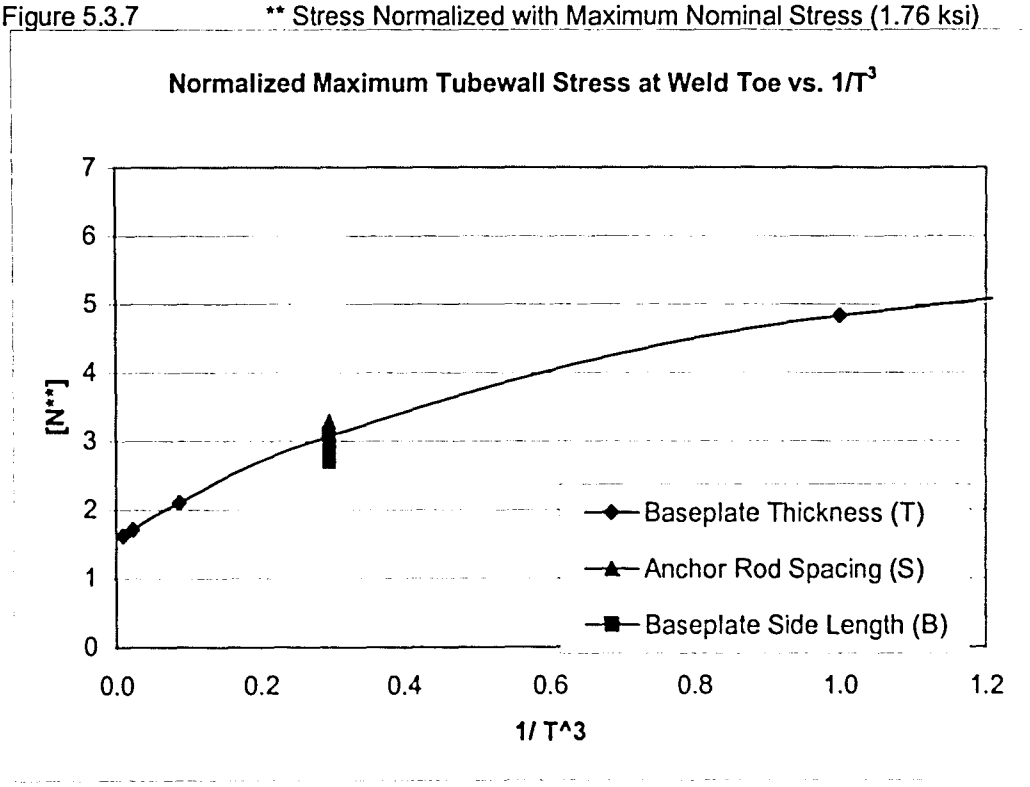

Figure 5.3.8 ** Stress Normalized with Maximum Nominal Stress (1.76 ksi)

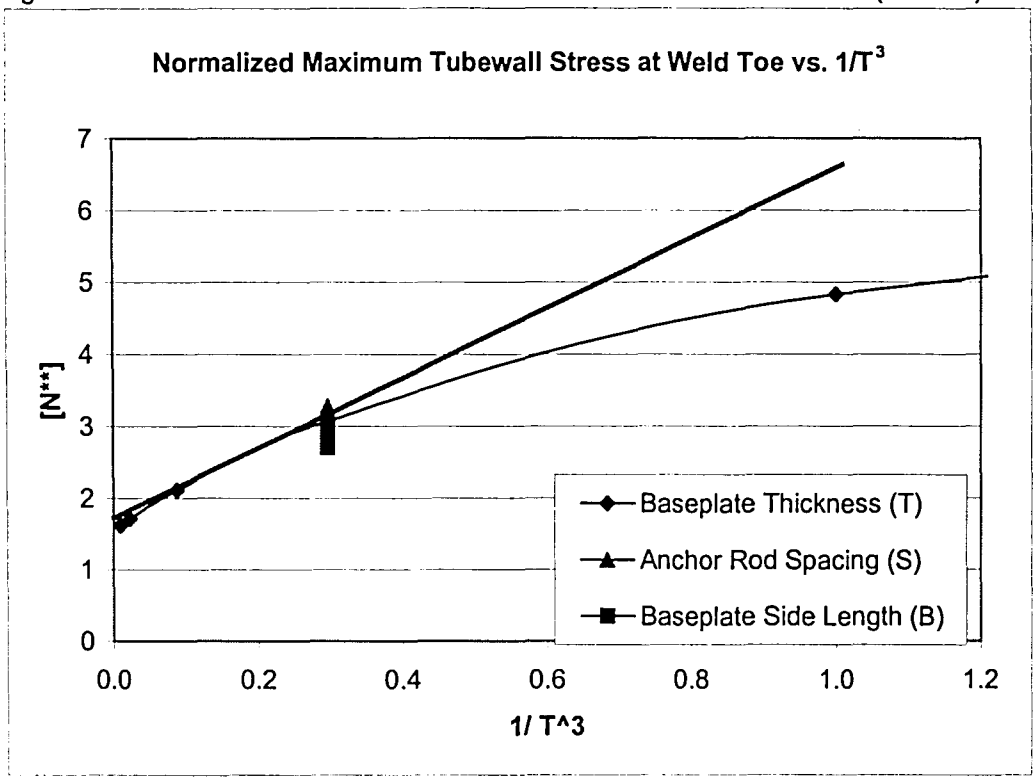

$$N_{DES} = 1.75 + 4.75\ (1 / T^3)$$

Example Problem: What is the maximum fatigue stress due for a 16" baseplate with pole base diameter 12", baseplate thickness of 2.25", anchor rod spacing of 15" and leveling nut diameters of 2".

$T = 2.25"$ $(1 / T^3) = .088$

$N_{DES} =$ 2.1

As discussed in Section 5.3.1

$$SR_{DES} * N_{DES} = \text{Actual Fatigue Testing Stress Applied} = CAFL * N_{FT}$$

Thus given NFT = 3.1,

$$SR_{DES} = 3.1 * 2.6 \text{ ksi} / 2.1 = 3.8 \text{ ksi}$$

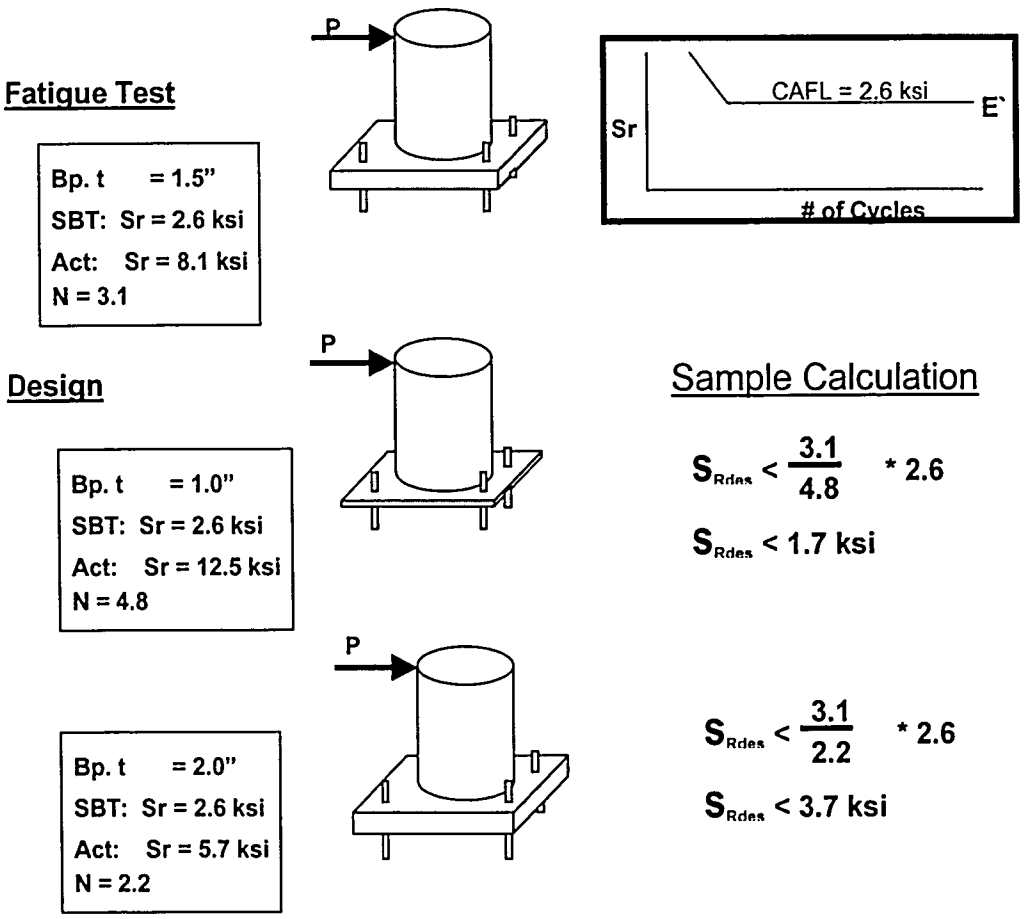

Figure 5.3.1.1: Flexibility Amplification Ratio Example

Baseplate Thickness [in]	N_{DES}, Normalized Maximum Stress Envelope Value	Flexibility Amplification Ratio	Modified Constant Amplitude Fatigue Limit [ksi]
≧ 1.0"	4.8 (@ Bp. Th. = 1")	0.65	1.7 ksi
≧ 1.5"	3.1 (@ Bp. Th. = 1.5")	1.00	2.6 ksi
≧ 2.5"	2.0 (@ Bp. Th. = 2.5")	1.55	4.0 ksi

Figure 5.3.1.2: Tabular Form of Flexibility Amplification Ratio Method

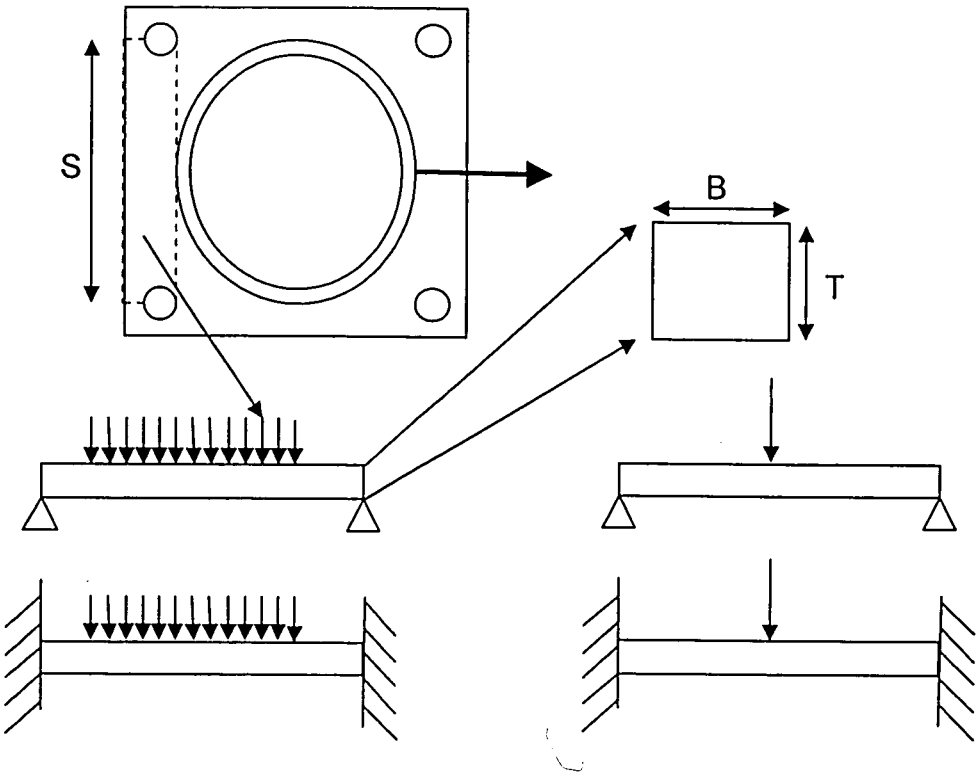

$\Delta =$ (5/384)* (w*L/E)*(L3/I) (1/48)* (P/E)*(L3/I)

(1/384)* (w*L/E)*(L3/I) (1/192)* (P/E)*(L3/I)

Depth: T, The thickness of the Baseplate
Width: B, (Side Length – Base Diameter)/2
Span: S, (or L) Anchor Rod Spacing – Diameter of Leveling Nut

Figure 5.3.2.1: Diagram Illustrating Beam Approximation

$\Delta = F / K$; where K is stiffness, and s is flexibility

$s = 1 / K$

Given the assumed beam geometry from the previous page

Δ = (12*S3/B*T3)*(1/E)*(Loading Constant Fraction)* (w*L or P)

Removing the loading fraction and Youngs Modulus the geometric flexibility becomes:

Figure 5.3.2.1: (Continued) Diagram Illustrating Beam Approximation

References Cited

1. Abaqus/Standard Users Manual. Version 6.1. Hibbitt, Karlson & Sorensen. Pawtucket, Rhode Island. 2000

2. American Association of State Highway and Transportation Officials. AASHTO Standard Specifications for Structural Supports for Highway Signs, Luminaires and Traffic Signals. 4th Edition. Washington, D.C: AASHTO, 2001.

3. Barsom, John M. and Rolfe, Stanley T. Fracture and Fatigue Control in Structures. Second Edition. Englewood Cliffs, New Jersey: Prentice Hall, 1987.

4. Connor, Robert; Hodgson, Ian; Hall, John; and Bowman, Carl. "Laboratory and Field Investigation of Cantilevered Signal Support Structures in the City of Philadelphia." ATLSS Report #04-22. October 2004.

5. Cook, Robert D.; Malkus, David; Plesha, Michael; and Witt, Robert. Concepts and Applications of Finite Element Analysis. New York: Wiley and Sons, 2002.

6. Fisher, John W.; Slutter, Roger G.; and Miki, Chitoshi. Fatigue Behavior of Steel Light Poles. State of California Department of Transportation. December 1981

7. Hetenyi, M. The Handbook of Experimental Stress Analysis. New York: Wiley and Sons, 1950.

8. Kaczinski, M. R.; Dexter R. J.; and Van Dien, J. P. NCHRP Report 412: Fatigue Resistant Design of Cantilevered Signals, Sign and Light Supports. TRB, National Research Council, Washington, D.C., 1998.

9. Owens, F. T.; Hag-Elsafi, O.; and Alampalli, S., A Simplified Design Procedure for End-Plates and Base Plates of Cantilevered Traffic Structures. Special Report 131, Transportation and Development Bureau, New York State Department of Transportation, July 1999.

Biography

John Henry Hall III was born in Brooklyn, Connecticut on December 4,1979, to John and Diane Hall. After graduating from the Woodstock Academy in 1998, he attended Clarkson University, where he received his Bachelor of Science in Civil Engineering. John then enrolled in the masters graduate program at Lehigh University in August of 2002.

Permanent Address: bigjhh3rd@hotmail.com

END OF TITLE